Republic of Iraq
Ministry of Higher Education and Scientific Research
University of Babylon
College of Materials Engineering
Department of Polymer Engineering and Petrochemical Industries

Preparation and Characterization of Hybrid Nanocomposite of Epoxy Coating for Thermal and Electrical Application

A dissertation
Submitted to the Council of the College of Materials Engineering/ University of Babylon in Partial Fulfillment of the Requirements for the Degree of Doctorate of philosophy in Materials Engineering/ Polymer

By
Anwar Qasim Saeed Joody
Supervised by
Prof. Dr. **Zoalfokkar Kareem Mezaal Al-obad**

2022 A.M 1444 A.H

سورة النور اية35

Supervisors Certification

I certify that this dissertation entitled **(Preparation and Characterization of Hybrid Nanocomposite of Epoxy Coating for Thermal and Electrical Application)** had been carried out under my supervision at the University of Babylon / Collage of Materials Engineering / Department of Polymer Engineering and Petrochemical Industries in Partial Fulfillment of the Requirements for the Degree of Doctorate of philosophy in Materials Engineering/ Polymer

Signature:

Name: ***Prof. Dr.*** **Zoalfokkar Kareem Mezaal Al-obad**

(Supervisor)

Date: / / 2022

Dedication

To the sustainer who raining me with his blessings .To the merciful who I rely upon in my life. .....To GOD

To our great prophet Mohammad and his relatives (peace and blessings of Allah be upon them) without them, every step in my life will seem meaningless.

To my the infallible and courageous Imam Ali Ibn Abi Talib (peace be upon him)

To my Family**.....**

To my father, God may have mercy on him, and make him live in peace.

To whom you offered my happiness and comfort over her happiness, To my soul (Mom)

To all my brothers and sisters;(my preferred sister Raja)

To my wonderful husband;(Tammar)

To my pure and innocent my children; My heart (Jummana and Laith ... love you so much)

To my Homeland

To My Teachers

To my Friends

With my respect and gratitude

Anwar Qasim

Acknowledgment

First of all, I would like to express my utmost thanks to our almighty God Allah who blessed me with this opportunity, encompassed me with his mercy

I would like to express my deepest sense of gratitude to my supervisor Prof.Dr Zoalfokkar Kareem Mezaal Al-Obad for his continuous advice and encouragement throughout the course of this work. I thank him for the guidance and great effort he made in supervising this scientific field.

Additionally, I would like to thank my virtuous teacher Prof. Ammar Emad Al-Kawaz for his continuous help during this work.

Sincere thanks are also expressed to the staff of the college of Materials Engineering especially in Polymers laboratories (Atheer Hussein ,Ban Jwad, ,Ali Yhea And Fadaa Ather ,Yaser Ammar) for the encouragement during this work.

I would like to express my deepest gratitude for my friends who've been agood company throughout these years.

I would like to thank my family who showed great support and patience throughout the years and endured everything to make me the person who I am today and I hope I can payback even if small part if it one day.

Anwar Qasim

Abstract :

Epoxy and epoxy based composites are preferred insulating materials for several electrical applications, such as printed circuit boards, generator ground wall insulation systems, and cast resin transformers, Although epoxy resins are extremely valuable materials in coatings and adhesion applications, thermal conductivity of these polymer resins is in a low range from 0.1 to 0.3 W/m·K.

It make epoxy insurable use in heat dissipation application . The addition of inorganic nano particles into the epoxy material can significantly improve the thermal conductivity and mechanical properties of the nanocomposite. this the easiest way to reach the aimed technological goals such as heat dissipation.

In this study, it is developed a new corrosion protective coating with heat dissipation and electrical insulation that can be used to protect turbines in automobiles, ships, or planes, as well as in the electric and electronic industry such as Automotive electronic control units (ECUs) , using epoxy as matrix phase and MgO, h-BN and 1:1 MgO/H-BN hybrid nanoparticles as strengthening phase and it is compared the mechanical, thermal, electrical properties and Potentiodynamic Polarization of nanocomposites coating. Heat dissipation and electrical insulation were provided by magnesium oxide (MgO) and hexagonal boron nitride (h-BN), MgO offers a number of appealing properties, including affordable ,harmless and good electrical insulation Meanwhile, BN appears to be on the verge of developing high temperature conductive adhesives for heat dissipations coating applications with better electric insulation than graphene nanoparticles.

Nanocomposites coating were prepared using Dip coating with different concentrations of nanoparticles (NP) MgO , BN or hybrid (with ratio1:1) with weight percent (0, 1, 3, 5 and 7 Wt %).

The characteristics of the polymer nanocomposites were investigated using (FTIR,XRD, FESEM, AFM, Thermal and Electrical measurements, Tensile Test, Impact test, Fracture Toughness test, Shor D hardness, Pull-Off Adhesion test and Potentiodynamic Polarization test and Coating Thickness measurement .

In FESEM images, MgO NP has a coarse size but BN shows a finer size, The addition of 7 wt % hybrid nanoparticles improved the tensile strength , about 19 % as compared of pure epoxy and another non hybrid nanocomposites .The addition of 7% hybrid nanoparticles enhanced (Tensile Strength ,Modulus of Elasticity ,Shor D Hardness, The Impact Strengths, The Compact Tension Fracture Toughness K_{IC} ,The Single Edge Notched Bending K_{IIC}, Pull off Adhesion Strength) about (19 % ,37%, 10,%56% ,68%,41% and 69%) Respectively ,as compared to pure epoxy and another non hybrid nanocomposites .The addition of 7% hybrid nanoparticles enhanced the efficiency of inhibition about 87% as compared to pure epoxy and another non hybrid nanocomposites . The 1:1 MgO/h-BN hybrid is chosen as an appropriate filler to prepare nanocomposites coating with the best efficiency of inhibition . In addition, the application of hybrids in thermally conductive and electrical insulation coatings are also worth investigating due to good electrical insulation and mechanical strength of MgO nanoparticles and high thermal conductivity of h-BN nanoparticles.

Table of Contents

Abbreviations	
Abbreviation	Definition
TC	Thermal conductivity
BN	Boron Nitride
MgO	Magnesium Oxide
FTIR	Fourier-transform infrared spectrometer
SEM	Scanning electron microscope
AFM	Atomic force microscope
nm	nanometers
PNCs	Polymer nanocomposites
Al_2O_3	Aluminum Oxide
SiO_2	Silicon dioxide
ZnO	Zinc Oxide
TiO_2	Titanium
$Al(OH)_3$	Aluminum hydroxide
$Mg(OH)_2$	Magnesium hydroxide
$CaCO_3$	Calcium bicarbonate
$BaTiO_3$	**Barium titanate**
Al	Aluminum
Au	Gold metal
Cu	Copper metal
Aln	Aluminum Nitride
SiC	Silicon Carbide
CNTs	Carbon nanotubes
$MgCO_3$	magnesium carbonate
$Mg(OH)_2$	magnesium hydroxide
GIS	gas insulated systems
h-BN	Hexagonal boron nitride
DGEBA	Diglycidyl ether of bisphenol A
TMMs	heat management materials
HVAC	Metal heating, ventilation, and air conditioning
LED	light-emitting diode
TIM	thermal interface materials

ECU	automobile electronic control units
LDPE	Low density poly ethylene
CTPB	carboxyl-terminated polybutadiene liquid rubber
GNP	graphene nanoplatelets
BNNTs	boron nitride nanotubes
ASTM	American Society for Testing and Materials
MWCNTs	multi-walled carbon nanotubes
CTI	comparative tracking index
DMA	dynamic mechanical analysis
HDPE	high-density polyethylene
ABS	acrylonitrile butadiene styrene
LCE	liquid crystal epoxy
GO	graphene oxide
RT	room temperature
CT	compact tension
SENB	Single Edge Notched Beam
EP	epoxy
FE-SEM	field emission scanning electron microscopy
NaCl	Sodium chloride

List of Symbols		
q	the rate of heat transfer	W
J	the heat flux	W/m2
K	the thermal conductivity	W/(m.K)
A	the cross sectional transfer area	m2
T	temperature	oC
L	Length	m
Tg	Glass transition temperature	oC
Td	Decomposition temperature	
R	electrical resistance	Ω
λ	thermal conductivity	W/M.K
ρ	Electrical resistivity	Ω.cm
K_{IC}	Compact tension fracture toughness	MPa m^1/2
K_{IIC}	Single Edge Notched Beam fracture toughness	MPa m^1/2
F	load	N
σ	Stress	Mpa

Δ σ	Change in Stress	Mpa
ε	Strain	No unit
Δε	Change in strain	
E	modulus	Gpa
T	thickness	mm
W	Width	mm
Gc	Impact strength	J/m^2
Uc	Energy of impact	J
X	pull-off adhesion strength achieved at failure	MPa
D	diameter	mm
M	Mass	Kg
I	efficiency of inhibition	%

List of Figures		
Figure No.	**Subject**	**Page No.**
Chapter one		
1.1	Application fields of epoxy-based coating	3
Chapter Two		
2.1	Polymer nanocomposites with (a) shape, (b) dispersion, (c) morphology, and (d) external stimulus	6
2.2	Schematic illustration for the solution blending method	7
2.3	Effect of shearing on the dispersion of the nanoparticles during melt blending	8
2.4	Schematic illustration for the in situ polymerization	9

List of Tables

Chapter One

Introduction

1.1 Introduction

At present, the rapid development of highly integrated and high-power microelectronic devices,5G semiconductor chips, and integrated circuits has led to the continuous reduction in product size and increment in product power[1,2].

The electronic equipment and its associated components produce a large amount of heat during operation, so the heat generated will be in certain locations, resulting in the problem of local overheating [3,4].Therefore, the problem of rapid heat accumulation and heat dissipation becomes increasingly more prominent, seriously affecting the stability and service life of electronic products, and is also one of the most important difficulties at present[5,6].There is evidence that the performance of electronic products decreases by 10% when the temperature increases to 2 ◦C [7].Hence, it is extremely urgent to prepare thermal management materials (TMMs) with excellent comprehensive properties[8].Thermal interface materials (TIMs) for the thermal management system of key components, which is usually made of polymer composites, can fill the space between the two surfaces, thus increasing the effective contact area. TIMs have a significant improvement in interface heat transfer, because the λ of air between two surfaces is particularly low (0.026W/m·K). Consequently, TIMs play an important role in the heat dissipation of electronic devices.

This leads to a continuous demand of thermal conductive coatings and adhesives, with high electrical insulation capability. This demand is originated by the constant miniaturization, integration and functionalization of electronics and the appearance of new applications such as flexible electronics, light emitting diodes, etc. In this sense, heat management has special interest in electronic components since they can be deserved for greater power output, improved efficiency and lengthening of half-life time and prevention of premature failures of

devices[9]. These kinds of thermally conductive polymers find also usage in other applications like aerospace industry, heat exchangers and corrosion-resistant coatings and therefore the research in these materials is in constant development [10]. As shown in figure (1.1).

Thermal energy is defined by the existence of microscopic vibrations of particles. The temperature, describing the state of a body, is a physical property quantifying those microscopic thermal vibrations of the particles. Heat is directly related to the thermal conductivity (TC), and has been defined as the thermal energy transfer from a specific point to its surroundings due to the temperature gradient[11]. Thus, temperature is produced by particles vibration and heat evaluates how much of this energy is transferred, how fast and in what direction. epoxy and epoxy based composites are preferred insulating materials for several electrical applications, such as printed circuit boards, generator ground wall insulation systems, and cast resin transformers. Excellent adhesive properties, resistance to heat and chemicals, good mechanical properties and very good electrical insulating properties make epoxy a favored insulating material [12].

Although epoxy resins are extremely valuable materials in coatings and adhesion applications, thermal conductivity of these polymer resins is in the low range from 0.1 to 0.3 W/m·K.The addition of inorganic filler particles into the epoxy material can significantly improve the TC and can also affect the mechanical properties of the composite. However, this constitutes the easiest way to reach the aimed technological goals such as heat dissipation[13].

Polymeric nanocomposite has been attracting more attention as a new insulating material because homogeneous dispersion of nanosized inorganic fillers can improve various properties significantly. They possess promising high performances as engineering materials if they are prepared and fabricated

properly[14]. Therefore, studies have focused on how nanotechnology can improve the thermal conductivity without deteriorating existing electrical properties[15].

Among inorganic fillers, hexagonal boron nitride (BN) is structurally analogous to graphite and has similar thermal conductivity[16,17] ,and was several advantages over those based on graphite because of BN is a nonelectrically conductor[18].

In addition, thermally conducting but electrically insulating MgO nano particles [19]. the MgO represents a prospective filler. Especially, due to wide band gap (7.8 eV) and high volume resistivity (10^{17} Ω·m). It is the highest value of volume resistivity from commonly used nanoscale oxides[20]. were used as hybrid fillers to improve the thermal conductivity of epoxy composites.

Figure 1.1: Application fields of epoxy-based coating [21].

In this study, an attempt was made to investigate the fundamental properties of the nano magnesium oxide MgO ,nano boron nitride BN and hybrid of(1:1 MgO /BN) materials using it as a filler material in epoxy resin. The dielectric characteristics of epoxy nanocomposites are known to be influenced by the interfacial interactions between the nanoparticles and the base polymer matrix. As a result, an attempt was made to comprehend the differences in properties of epoxy nanocomposites having various percentages of nanofiller. Furthermore, the mechanical and thermal properties of insulating materials.

1.2 Aim of The Research

This work aims to prepare nanocomposite coating for electrical insulating and thermal conducting applications .

1.3 Objective

- Using MgO, BN and hybrid as Nanoreinforcement.
- Study the effect of nanoparticles MgO, BN and hybrid on the mechanical, morphological, structural, thermal ,electrical and corrosion properties of epoxy nanocomposites material.
- Prepare epoxy nanocomposite reinforced with different weight percent of MgO , BN, and (1:1 of MgO/BN) hybrid Nps with (1, 3,5,7%wt %).
- Study the mechanical properties ,fracture toughness (C.T and SENB,tensile, impact, hardness and pull off adhesion) for prepared nanocomposites.
- Study the physical (FTIR) and morphological(SEM, AFM) properties for nanocomposites.
- Study the structural properties for nanocomposites by XRD.
- Study thermal and electrical properties for prepare nanocomposites.
- Study Potentiodynamtic polarization properties for prepare nanocomposites.

Chapter Two
Theoretical Part
and
Literature Survey

2.1 Nanocomposite

A nanocomposite is a multiphase solid substance with one, two, or three dimensions of fewer than 100 nanometers, or a structure with nanoscale repeat distances between the distinct phases that make up the material (nm). According to the matrix type, nanocomposite materials are divided into three types [22,23]:

1- Composite with metal matrix.

2- Composite with ceramic matrix.

3- Composite with polymer matrix.

2.1.1 Polymer Nanocomposite

Polymer nanocomposites are a novel type of polymer composite that can be used instead of regular polymer composites [24]. PNCs are a mixture of two or more materials in which the matrix is a polymer and the dispersed phase has at least one dimension less than 100 nm [25] . Mechanical strength, toughness, and stiffness, electrical and thermal conductivity, enhanced flame retardancy, and a higher barrier to moisture and gases are all examples of improved performance of those materials. As illustrated in Figure (2.1), nanocomposites have unique design possibilities that provide significant benefits in the creation of functional materials with desired qualities for specific applications[26].

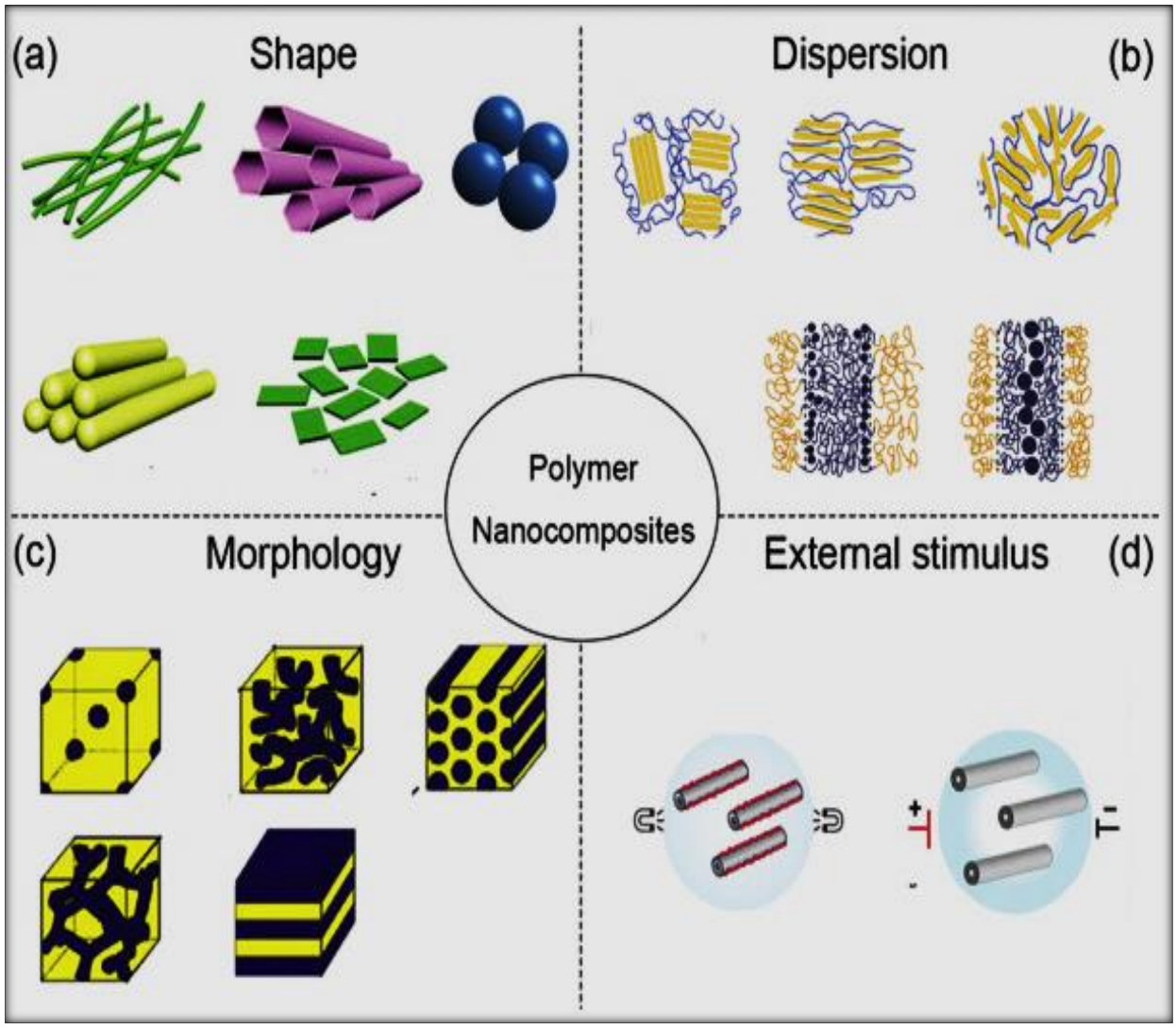

Figure 2.1: Polymer nanocomposites with (a) shape, (b) dispersion, (c) morphology, and (d) external stimulus [27].

2.1.2 Polymer Matrix Nanocomposite Processing Techniques

Chemical or mechanical methods can be used to create polymer matrix nanocomposite. The primary issues that arise during the construction of polymer nanocomposite are uniform and homogenous dispersion of nanoparticles in the polymer matrix[23].

Polymer nanocomposites can be made in a variety of ways, however there are three typical approaches to make nanomaterials [28]:

1- Solution method.

2- Mixing the molten.

3- In-situ polymerization method.

❖ In Solution Method:

The nanoparticles were disseminated in the solvent before being introduced to the polymer solution, allowing them to spread evenly throughout the polymer and evaporating the solvent. As illustrated in Figure (2.2):

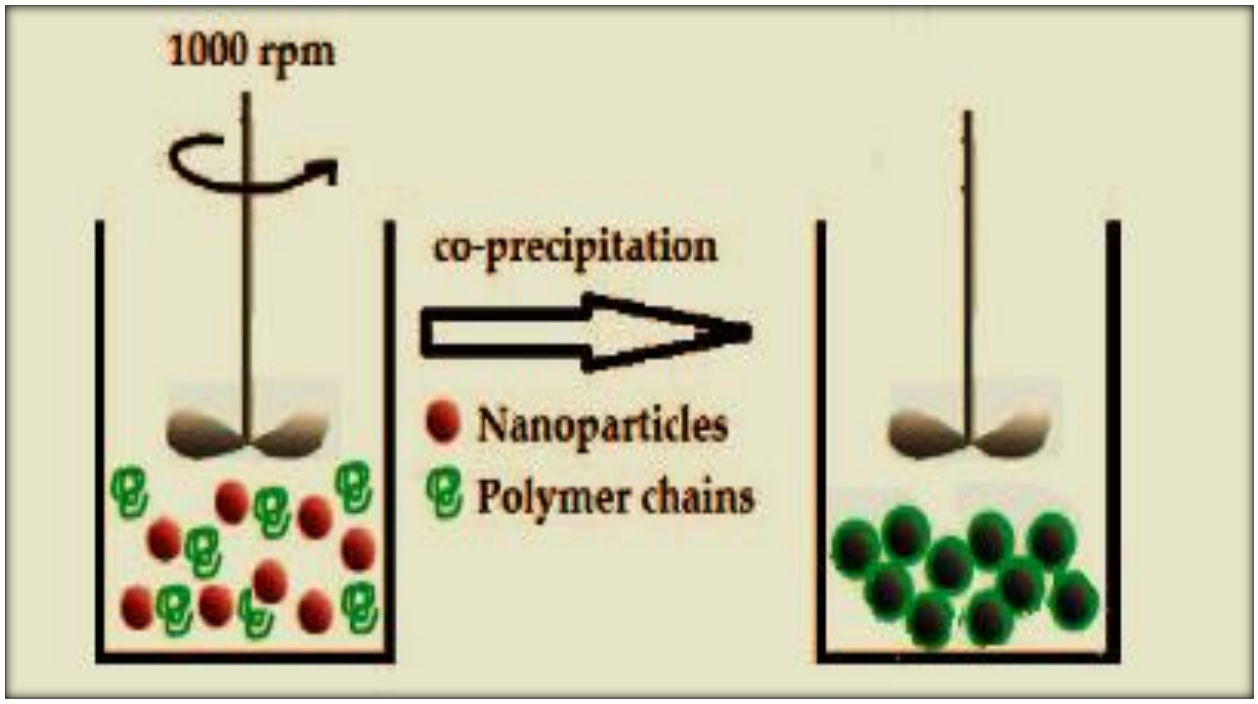

Figure 2.2: Schematic illustration for the solution blending method [29] **.**

❖ Melt Compounding Method:

This method includes adding nanoparticles to a polymer at a temperature above its melting point, then forming the final material. As illustrated in Figure (2. 3) [30]:

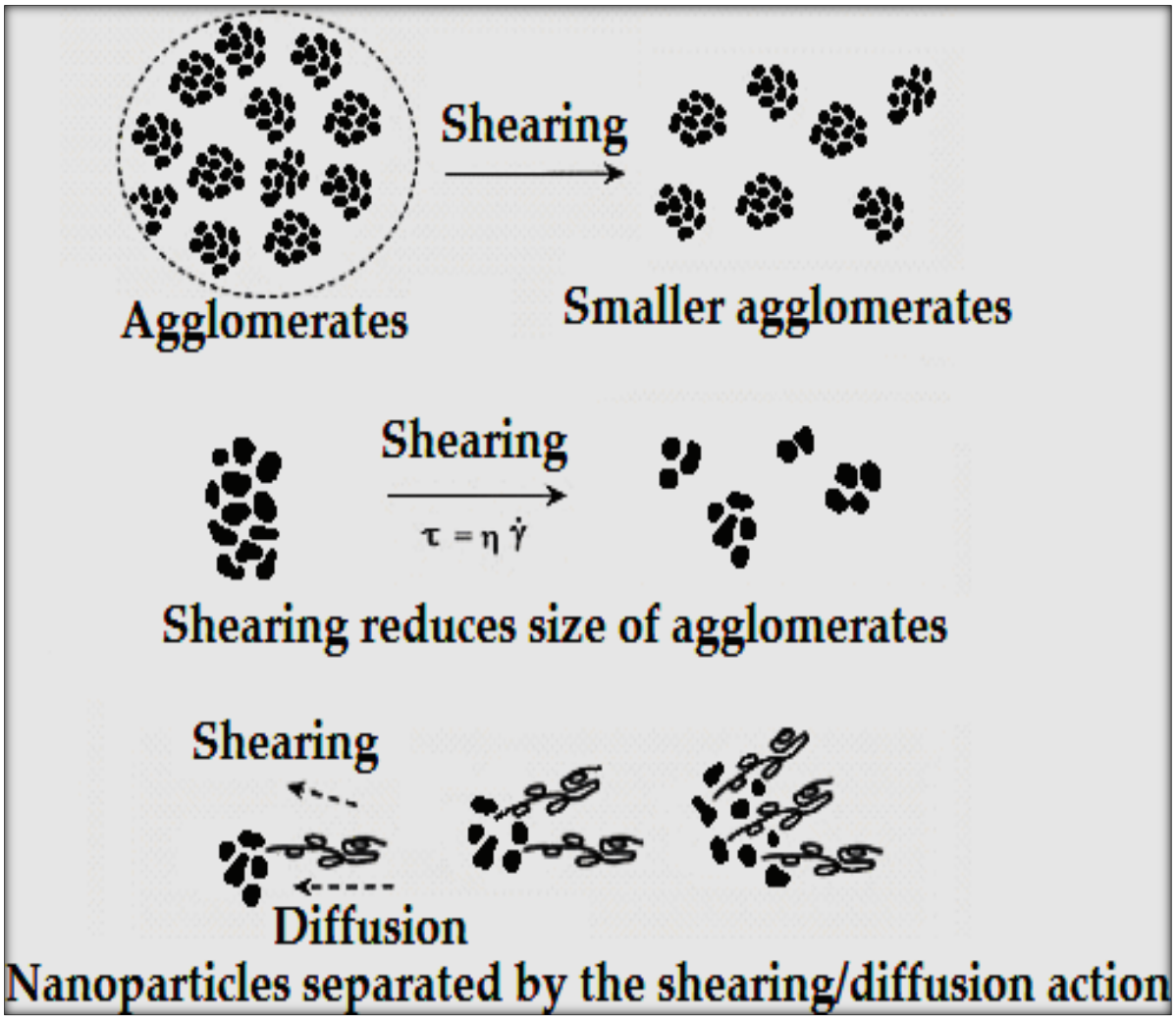

Figure 2.3: ***Effect of shearing on the dispersion of the nanoparticles during melt blending***[31].

❖ In - Situ Polymerization:

This method is for making nanocomposites by including nanoparticles into the polymerization process. It's a good way to get a homogeneous filler dispersion in the polymer [32,33]. Figure (2.4) shows the approach for making polymer nanocomposites using this technique.

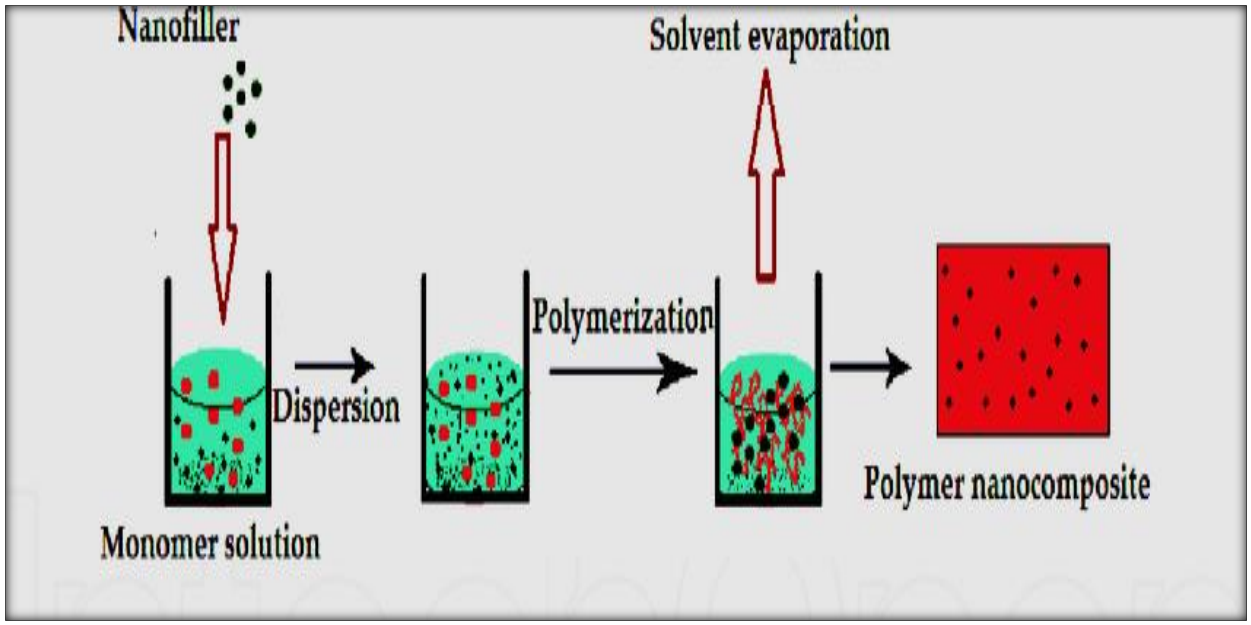

Figure 2.4: Schematic illustration for the in situ polymerization method[34].

2.1.3 Properties of Polymer Matrix Nanocomposites

The qualities of nanocomposites are determined not only by the properties of individual components, but also by the parameters listed below [35]:

1. A method for making nanocomposite materials.
2. The many types of filler materials and how they are oriented
3. The degree to which two phases are mixed
4. Nanoparticle properties and morphology
5. Size and shape of nano filler materials

Nanosized particles must be correctly dispersed and distributed in the matrix material to produce increased nanocomposites properties; otherwise, particles would agglomerate and the properties of nanocomposites will deteriorate. These aggregates operate as defects, limiting the nanocomposite's property enhancement. To obtain optimum property enhancement, the nanoparticles should be uniformly disspertion throughout the matrix,as illustrated in Figure (2.5) [36].

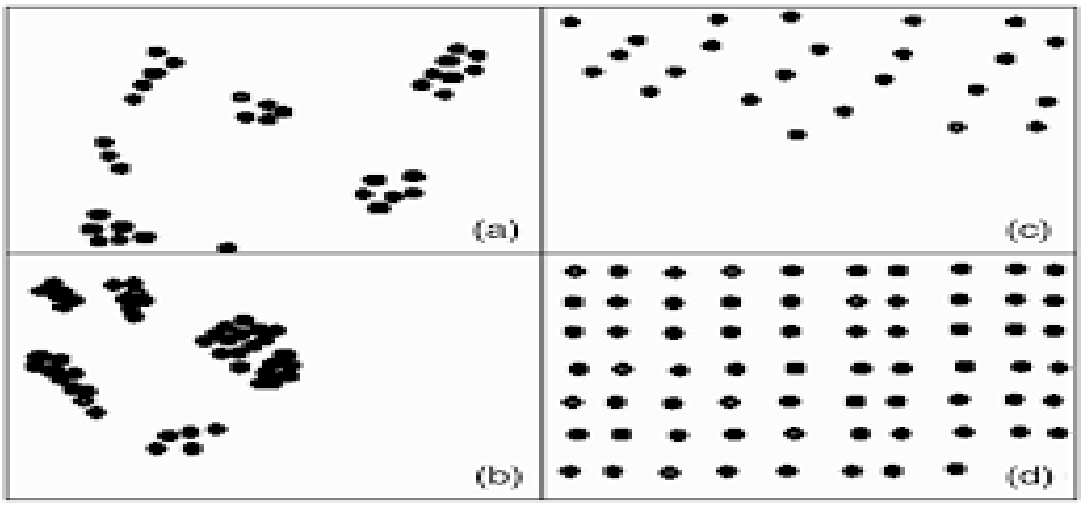

Figure 2.5:Distribution and dispersion of nanoparticles in the matrix[37].

Nanoparticles have a large surface area, and the overall surface area of a nanoparticle dictates the amount of the interface phenomenon that influences nanocomposites' attributes, as illustrated in Figure (2.6) [38].

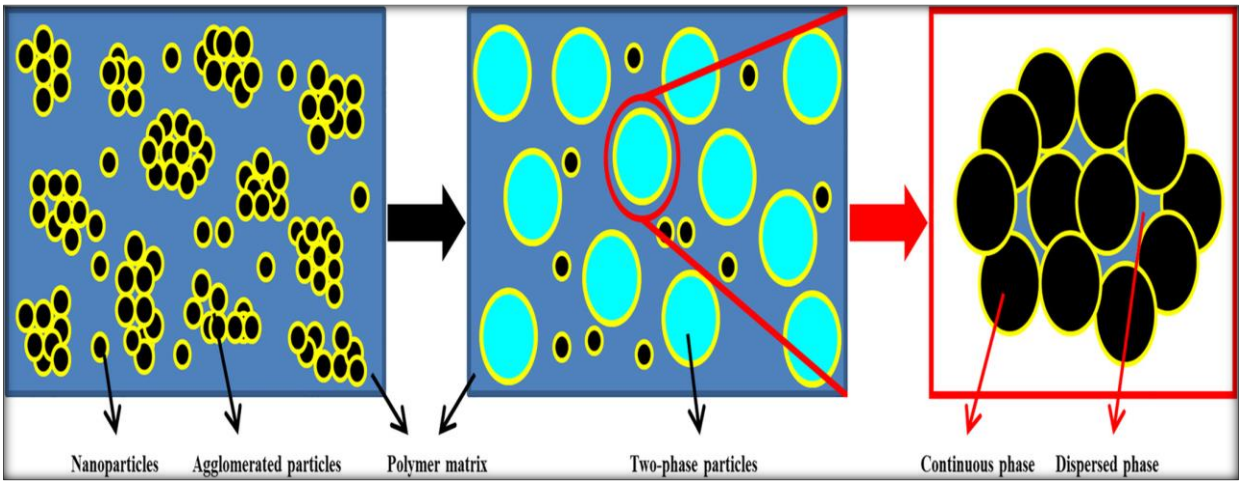

Figure 2.6: Interphase region between filler and polymer matrix [39].

2.2 Classification and Types of Fillers

Fillers that are commonly employed to reinforce polymer materials can be classified into three types based on their size. Micron sized particles, also known as conventional sized filler, are the earliest type of filler. The size of these particles can range from 1 μm to 100 μm, The second type of particle is known as submicron-sized particles. Their size ranges from 100 nm to 1 μm. The first two

types are sometimes grouped together and referred to as micro particles. The group of nanometer sized particles is the third type of particle. These particles should be less than 100 nm in at least one dimension. Nanofillers can be one-dimensional (nanotubes, fibers, rods), two-dimensional (clay, plane-like particles), or three-dimensional nanospheres, (spherical particles). Fillers are defined by their shape and size, as well as their aspect ratio. The chemical structures, forms, dimensions, sizes, and intrinsic qualities of the numerous substances employed as fillers vary significantly. Fillers are categorised as either inorganic or organic chemicals, with further subcategories based on chemical family[40]. In the creation of thermosetting composites, the use of nanostructured fillers in epoxy systems has become increasingly important. Carbon-based fillers, inorganic fillers, metal fillers, and hybrid fillers are the four different types of thermally conductive fillers. as seen in the Table (2.1) [41].

Table 2.1: Different types of filler[42]**.**

Chemical family	Examples
Inorganics	
Oxides	Al_2O_3, SiO_2, MgO, ZnO, TiO_2, glass
Hydroxides	$Al(OH)_3$, $Mg(OH)_2$
Silicates	Talc , mica, nanoclays, asbestos
Salts, compounds	$CaCO_3$, $BaSO_4$, $BaTiO_3$
Metals	Al, Ag, Sn, Au, Cu
Nitrides, carbides	AlN, BN, Si_3N_4, SiC
Organics	
Carbon	Carbon fibers, carbon black, graphite fibers and flakes, carbon nanotubes, nanodiamonds
Natural polymers	Cellulose fibers, wood flour, flax, sisal
Synthetic polymers	Polyamide, polyester, aramid

2.2.1 Hybrid fillers

Multiscale fillers, such as hybrid fillers, are utilized to enhance polymer matrix materials. The main benefit of hybrid fillers is that the inherent qualities of each filler are combined to obtain the necessary mechanical properties in the final composite. Hybrid fillers have a unique architecture capable of reinforcing the filler matrix interface and contributing considerably to the mechanical characteristics of epoxy composites, in addition to improving electrical[38,39] , thermal [45] and corrosion resistance [41,42] .Hybrid fillers are often employed in thermally conductive composites because combined fillers of different sizes or types can generate a better thermally conductive network. By constructing bridges between fillers and increasing filler packing density, a hybrid filler system can aid in the formation of a vast thermally conductive network. Another benefit of a hybrid filler system is that it can help lower overall filler loading and hence system viscosity. A tiny amount of carbon nanotubes (CNTs) (1 vol%) in an aluminum nitride (AlN)/epoxy system with a 25 vol% AlN loading demonstrated similar thermal conductivity to an epoxy composite with 50 vol% AlN. a hybrid filler system can not only increase packing density and minimize system viscosity but also improve thermal conductivity [48] .

2.3 Thermoset

A thermosetting polymer, often known as a thermoset, is a polymer made by irreversibly hardening and curing a soft solid or viscous liquid pre polymer (resin). Curing is caused by heat or appropriate radiation, and it can be accelerated by applying high pressure or mixing with a catalyst. Heat is often generated through the reaction of the resin with a curing agent, rather than being applied externally (catalyst, hardener). Curing causes chemical processes that result in substantial cross-linking between polymer chains, resulting in an insoluble and infusible

polymer network[49], Prior to curing, the beginning material for thermosets is usually pliable or liquid, and it is frequently designed to be molded into the final shape. It can be used as an adhesive as well. In contrast to thermoplastic polymers, which are frequently produced and distributed in the form of pellets and moulded into the final product form by melting, pressing, or injection molding [45,46]. thermoset polymers cannot be melted for reshaping once hardened as seen in figure(2.7).

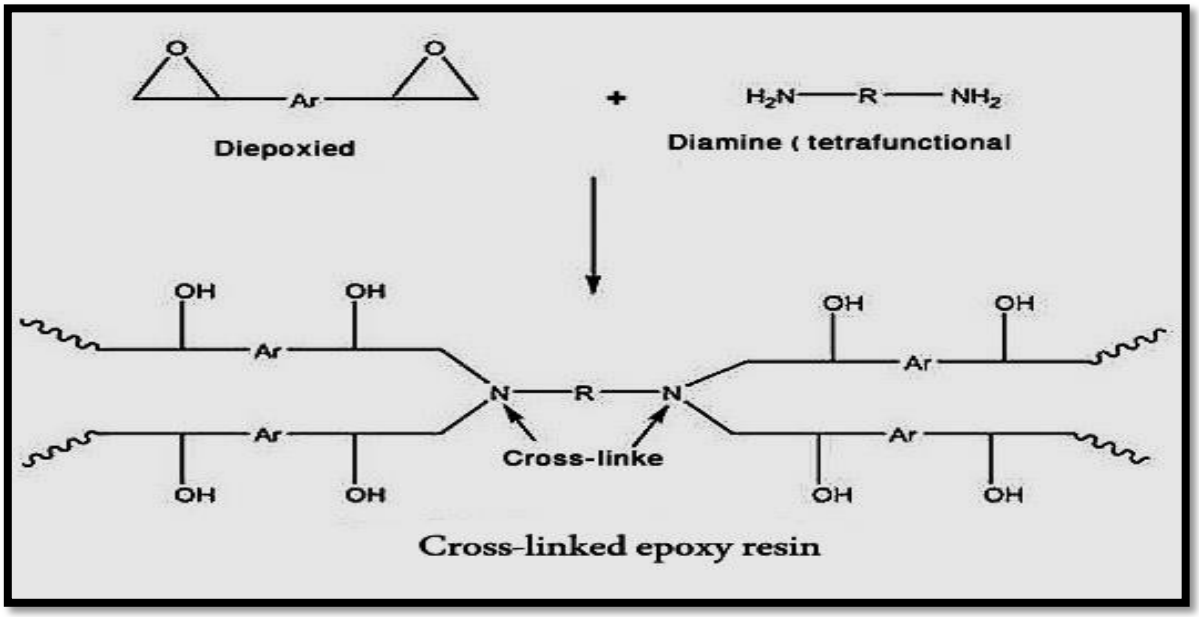

Figure 2.7: Synthesis and structures of thermoset and linear adhesives by addition polymerization[51]**.**

When cured with a curing agent, thermosetting resins such as epoxy, unsaturated polyester or phenolic resins become rigid. The system can be thought of as a three-dimensional cross-linked network. Figure (2. 8) shows how it may appear in a plane[52].

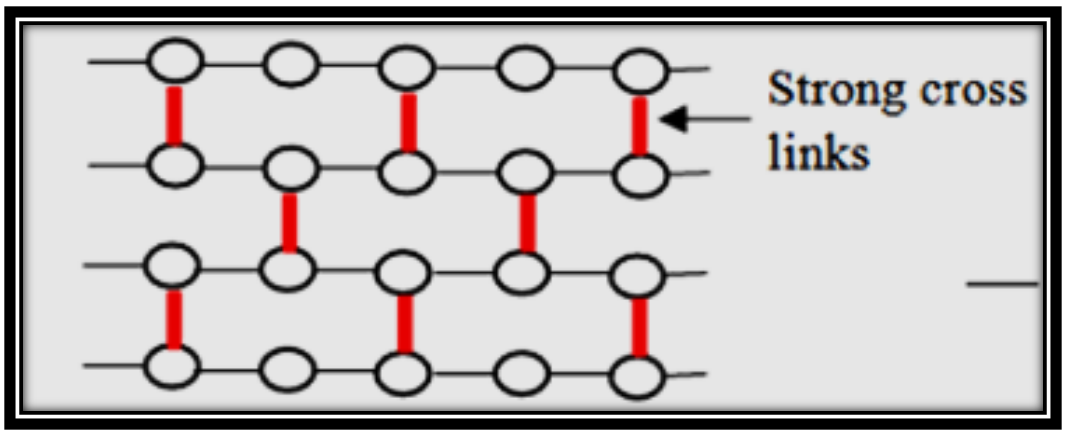

Figure 2.8: Schematic representation of a thermosetting polymer[53].

2.4. Epoxy

Epoxy resins are pre-polymers with a low molecular weight that contain more than one epoxide group of the form [54] :

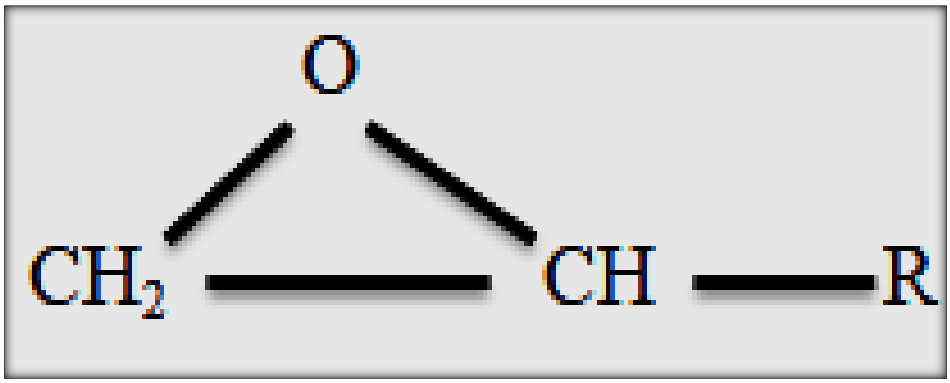

Figure 2.9: The Chemical Structure of the Epoxy Group [55].

Because of their high modulus and strength, excellent chemical resistance, and ease of processing, epoxy resin is one of the most important thermosetting polymers materials. It has been widely used as a high performance material, adhesive, coating, matrix of composite materials, and electronic encapsulating materials[31,32]. where a number of researchers looked at the mechanical properties of particle reinforced epoxy composites by use of inorganic filler to improve the thermal and mechanical properties of epoxy systems [53–56].

2.4.1 Applications Fields of Epoxy Resin

Coatings, electrical, automotive, marine, aerospace, sealing liquids, laminates, adhesives, tool fabrication, pipes and vessels in the chemical industry, food packing, construction and building material, and light weight structural components are just a few of the many applications for epoxy resins (2.10). Epoxy resins have become a viable material for high performance applications in the transportation industry, mainly in the form of composite materials, due to their low density and outstanding adhesive and mechanical qualities. Epoxy composite materials can be found in many elements of the body and structure of military and civil aircrafts, and the number of uses is growing in the aerospace sector. Epoxy resins are widely utilized in commercial and military applications due to their high mechanical/adhesion properties, solvent and chemical resistance, and ability to cure over a wide temperature range. Epoxy resin systems are thermosets commonly utilized in electrical engineering applications such rotating machines, switchgear systems, generator ground wall insulation systems and insulators[57–59] .

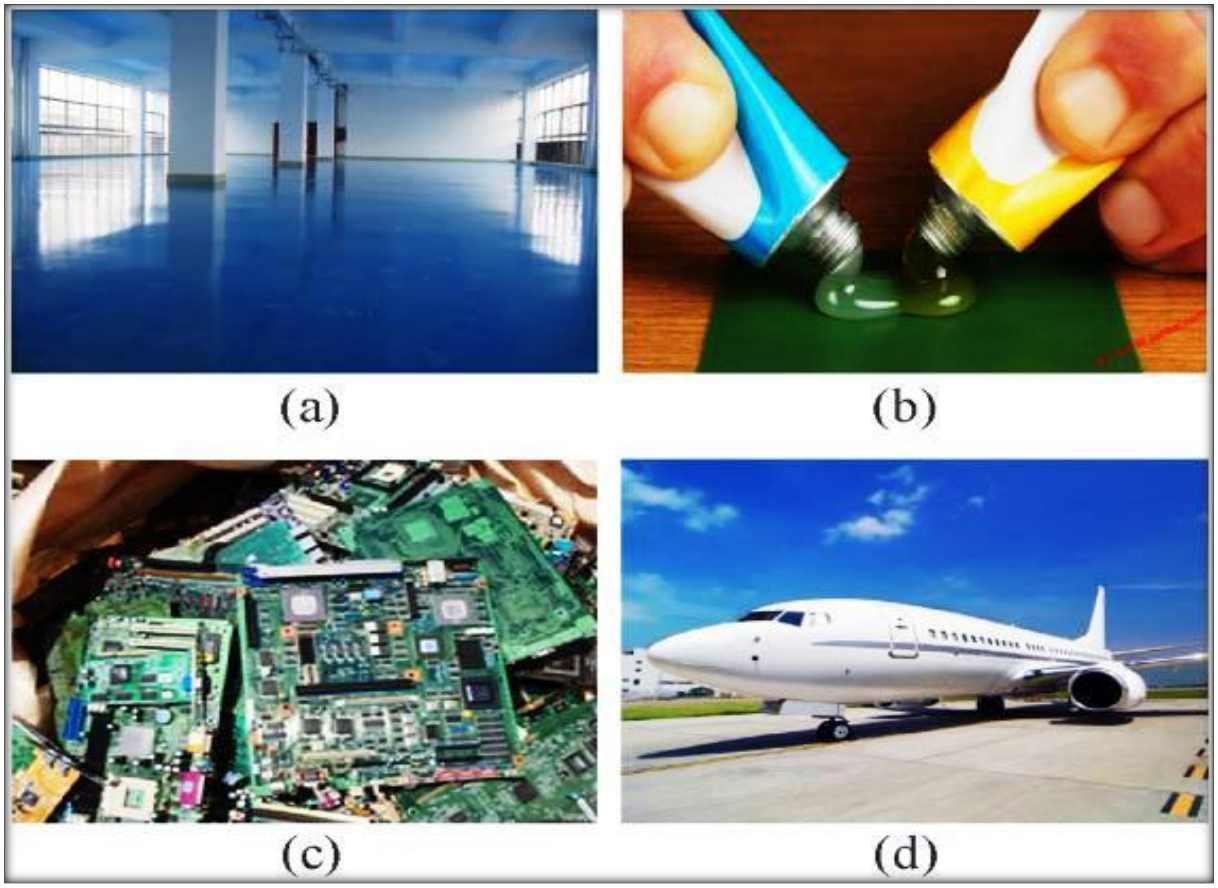

Figure 2.10: Applications of Epoxy Resins Used in (a) Paints and Coatings, (b) Adhesives, (c) Electronic materials, and (d) Aerospace Industry[65].

2.5 Epoxy/Inorganic Filler Nanocomposites

The stiffness, flame retardancy, barrier and scratch resistance, optical properties, and electrical properties of the polymer inorganic filler nanocomposites are all exceptional. Because of their improved structural properties, these nanocomposites are currently attracting study attention. In most cases, these materials are made up of two phases: inorganic strengthening material and a polymer matrix. Nanometer-scale particles (1-100 nm) dispersed throughout the polymeric matrix make up the inorganic material. Because nanoparticles have a large surface area per unit volume, phase interactions between the polymeric matrix and nanoparticles are improved[66]. In the electric and electronic industries,

epoxy resin has been widely used as a packing material [67]. Because of its cheap cost effectiveness, low viscosity, and excellent thermal stability [68],[69]. Inorganic thermally conductive fillers are commonly utilized to make thermally conductive insulating composites because they have high thermal conductivity TC and electrical insulation characteristics. BN, AlN, SiC, Al_2O_3, MgO, and other inorganic fillers are examples. Boron nitride has a substantially higher thermal conductivity (TC) than other inorganic fillers[70].

2.6. Magnesium Oxide (MgO) Nanoparticles:

Magnesium oxide is a refractory substance that is white in color. It has the empirical formula MgO, and its lattice is made up of Mg^{2+} ions and O^{2-} ions bound together by ionic bonds (Figure 2.11). The calcination of magnesium hydroxide $Mg(OH)_2$ or magnesium carbonate $MgCO_3$ produces magnesium oxide. The surface area and pore size of produced magnesium oxide, as well as the ultimate reactivity, are all affected by the thermal treatment utilized during the calcination process. Temperatures used can be divided into three groups: 700°C to 1000°C for caustic calcined magnesium oxide, 1000°C to 1500°C for lower chemical activity magnesium oxide, and calcination over 1500°C for reduced chemical activity type of refractory magnesium oxide, which is mostly used for electrical and refractory applications[66,67].

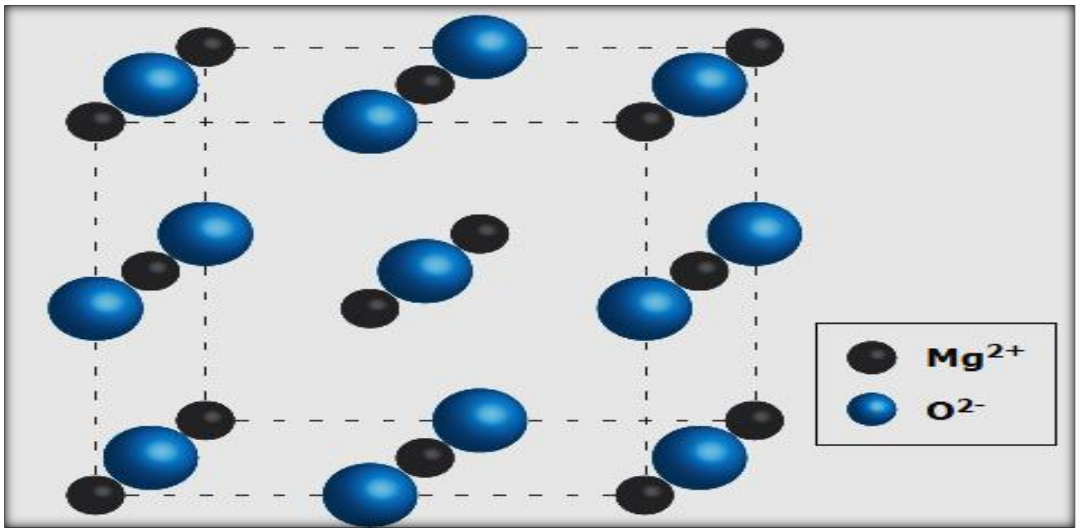

Figure 2.11:Structure of magnesium oxide[72].

2.6.1 Properties of magnesium Oxide Nanoparticles

Magnesium oxide has physical qualities that make it available for a various of applications. When looking at the surface structure of MgO, it is clear that it possesses the simplest oxide structure. It has a density of about 3.579 g/cm^3. At T=100°C, the thermal conductivity of sintered magnesium oxide is defined as 36 W/m·k .Magnesium oxide has extremely high melting and boiling points due to its refractory qualities (melting point: 2800°C, boiling point: 3600°C). The purity of magnesium oxide determines the value of electrical resistance. Magnesium oxide has a dielectric constant ranging from 3.2 to 9.8 at 25°C and 1 MHz, and dielectric loss values for the same conditions are approximately 10^{-4} [68- 70].

2.6.1.1 Applications of Magnesium Oxide Nanoparticles

Magnesium oxide has a wide range of applications in a variety of industries. It is a valuable fireproofing element in construction materials due to its refractory characteristics. MgO is highly valued as a refractory material, or a solid that

remains physically and chemically stable at high temperatures. It possesses a high thermal conductivity as well as a high electrical resistance, which are both beneficial. A prominent application is in the heating components of kitchen electric stoves. The refractory sector is by far the greatest consumer of MgO and another used in agricultural, chemical, construction, environmental, and other industrial uses[76]. Magnesium oxide (MgO) is a common crucible refractory material Also in corrosion prone applications [58]. MgO is used for medicinal applications[59]. Insulators[77] fertilizers [78], water treatment [79], protective coatings [80], and other applications are among the others. There is currently a movement to utilize nanoscale fillers [81]. Nanotechnology [82], could be utilized to make nanoscale magnesium oxide [78,79].

2.6.1.2 Epoxy /MgO Nanocomposite:

Rotating machineries, gas insulated systems (GIS), transformers, and cable joints all use epoxy resin as an insulant[80,81]. In addition to electrical stress, the insulating structure in the power apparatus is subjected to heat stress during operation. Chemical modifications to the insulating material are also possible depending on where it is used. This implies that the insulating material undergoes multi stress ageing during operation. In order to improve the reliability of power apparatus, it is now necessary to design and create insulation structures with desired electrical, thermal, and mechanical properties. It has been discovered that adding a small percentage of nanoparticles to the base polymer material improves properties such as breakdown strength, dielectric loss, and dielectric constant, as well as reducing weight and improving chemical, mechanical, thermal, and electrical discharge resistance [82-85]. Epoxy nanocomposites have recently gained favor, particularly when magnesium oxide is used as a filler, due to the nanocomposites material's lack of space charge [89].

2.6.2 Boron nitride (BN) Nanoparticles

Boron nitride (BN) is a refractory substance comprised of boron and nitrogen that contains 43.6 percent boron and 56.4 percent nitrogen by chemical composition. It possesses good lubrication and abrasion resistance, as well as good thermal conductivity and electrical insulation. Diverse boron and nitrogen atom configurations yield different structures. Depending on the pressure and temperature, it can crystallize in a variety of shapes (hexagonal, rhomboedral, diamond-like cubic) [90]. However, as demonstrated in Figure (2.12), among the BN types, the hexagonal form corresponding to graphite is the most stable and softest [91]. Hexagonal boron nitride is sometimes known as white graphite (h-BN) because of its extremely high thermal conductivity, it is a one of a kind substance [87,88], and electrically insulating behavior [94] and has recently gotten a lot of press because of its excellent heat dissipation performance. It's comparable to graphene, which is utilized to make thermal management materials (TMMs)[90,91]. It's also utilized to improve overall thermal conductivity in polymeric nanocomposites. The resurgence of interest in h-BN has been sparked by the advent of two-dimensional materials, which has been heralded by graphene [92, 93]. The arrangement in layers of hexagons of alternating boron and nitrogen atoms, similar to graphene structure, characterizes this configuration Strong covalent bonding with a spacing that is nearly identical to graphene characterize the hexagonal layer plane. As B and N atoms align alternatively in a vertical orientation, the layers composing the three-dimensional structure are held together by van der Waals forces, as stated in[99] . Because of its structural similarities to graphene, this material has gotten a lot of attention in recent years, since its layered structure has been used to create various nanostructures such boron nitride nanotubes, nanosheets, nanohorns, and nanoparticles of various forms[100].

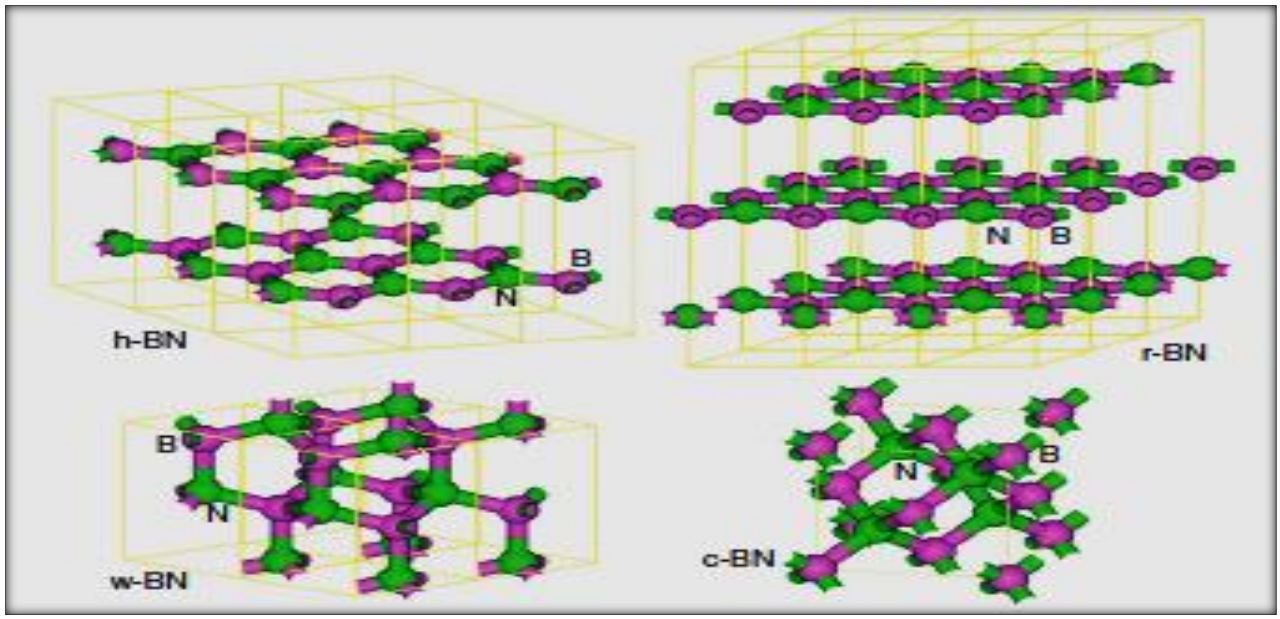

Figure 2.12: Structure models of hexagonal BN, rhombohedral BN, wurzite BN, and cubic BN[101]**.**

2.6.2.1 Application Areas of Boron Nitride Nanoparticles

The boron nitride nanoparticles are incredibly fine powder. Boron nitride nanoparticles can be used in a variety of applications due to their hardness, thermal, and electrical properties. It's easy to see why boron nitride is so important in the industrial world. Because of its high hardness and thermal stability, low dielectric constant, corrosion and oxidation resistance, high mechanical strength, and great thermal conductivity [102]. Boron nitride nanoparticles are used in subsurface exploration, drilling, and high-speed cutting tools. Metal forming and metal drawing lubricant releasing agents made of boron nitride nanoparticles are utilized. These nanoparticles can be molded into a variety of shapes and employed as high-voltage, high-temperature, insulation, and cooling components. Boron nitride nanoparticles can be found in transistors, plasma arc insulators, high-voltage high-frequency electricity, automatic welding high-temperature coating and rocket engine components. Another application for boron nitride nanoparticles is as a

catalyst in high-temperature and high-pressure processes. Boron nitride nanoparticles are widely employed as a ceramic composite, a thermally conductive filler for polymers, and a high temperature lubricant. The aerospace industry uses boron nitride nanoparticles because they can be employed in heat shielding materials. So, boron nitride nanoparticles have exceptional performance, a wide range of applications, and a lot of potential, and they play an essential role in a variety of technical sectors [101]. The higher chemical inertness of BN over carbon nanostructures makes it a compelling candidate for use as a carbon nanostructure replacement in biological applications [103]. Boron nitride has a high heat conductivity and is commonly utilized in the manufacture of thermally conducting epoxy composites [99,101].

2.6.2.2 Epoxy/boron nitride Nanocomposite

Because of its superior electrical insulation, ease of processing, and low cost, epoxy resin is a suitable molding compound for encapsulating heat-dissipating electronic components. To improve the resin's thermal conductivity, high thermal conductive fillers are applied. Various types of fillers, such as metal particles (copper, iron, and zinc) and ceramic particles (aluminum nitride), have been used in numerous investigations. Metallic fillers have a number of drawbacks over ceramic fillers, including high density and oxidation susceptibility. Due to their excellent thermal conductivity, BN and aluminum nitride are among the most effective ceramic fillers for these composites. Aluminum nitride, on the other hand, is vulnerable to moisture, but BN is not[106]. Hexagonal boron nitride (h-BN), often known as white graphite, is a platelet-shaped synthetic ceramic with a high aspect ratio and layers of hexagonal crystals. The platelets have a great thermal conductivity inherent to them[106] . Furthermore, as compared to Al_2O_3, SiO_2, and AlN, h-BN is electrically insulating and has great chemical and thermal stability,

with a dielectric constant of around 4[107]. These characteristics make h-BN a suitable filler for high thermally conductive composite production.

2.7 **Coating**

polymer coatings on conducting substrates have always piqued researchers' interest. Surface decoration, optical activity change, heat and corrosion protection are all possible applications for the coatings. Improvement of interfacial laminar shear strength and toughness of brittle composites are two more major applications. polymer coatings are once applied to substrates by hand or mechanically. Manual or mechanical application of coatings, on the other hand, has inherent drawbacks and has resulted in additional problems[108] .

The coating process can be classification in to:

A. Spin coating

Spin coating is a technique for depositing a homogeneous coating of organic compounds on flat surfaces in thin films [105,106] . Deposition, spin up, spin off, and evaporation are the four steps of spin coating, as shown in Figure (2.13).

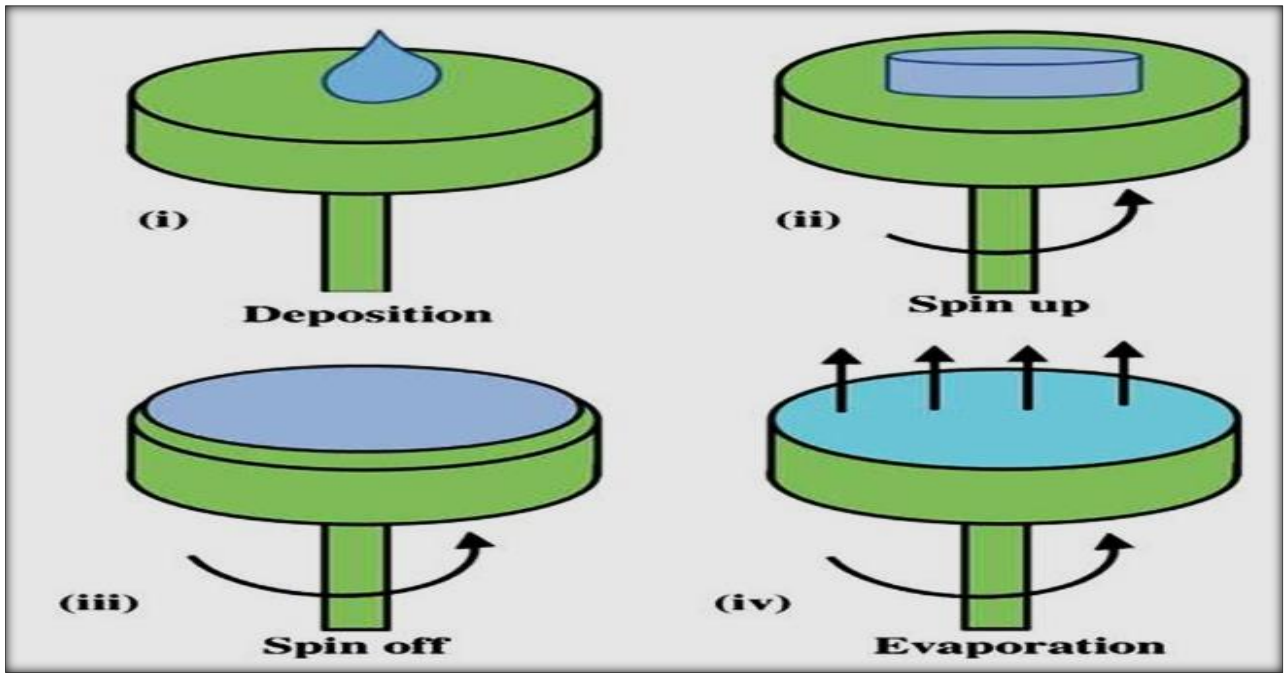

Figure 2.13: Stages of spin coating on substrate[109]**.**

The material is placed on the turntable in the first stage, after which it is spun up and spun off in series, with the evaporation stage occurring throughout the operation. Centrifugal force distributes the applied solution on the turntable. The layer thins as the spinning speed increases. The applied layer is then dried after this procedure. Because of the quick rotation, uniform evaporation of the solvent is achievable. Evaporation or simply drying removes the high volatile components of the solution from the substrate, while the low volatile components of the solution stay on the surface. The viscosity of the coating solution and the rotational speed control the thickness of the deposited layer[111] . The size of the substrate is one of the major drawbacks of spin coating. Because film thinning becomes more difficult as the size grows, high-speed spinning becomes more challenging. As a result, spin coating's material efficiency is quite low. In general, during the procedure, (95-98%) of the material is tossed off and discarded, while just (2-5%) of the material is dispensed onto the substrate[112] .

B. Spray Coating

Spray coating is commonly utilized in the industry to coat complex-shaped polymeric substrates. Atomizers are a type of atomizer that is used to generate electricity. The core of a tool that generates a spray of liquid is the atomizer nozzle. Atomizer nozzles are used for spraying and applying paint, fuel injection systems [113]. as shown in Figure (2.14).

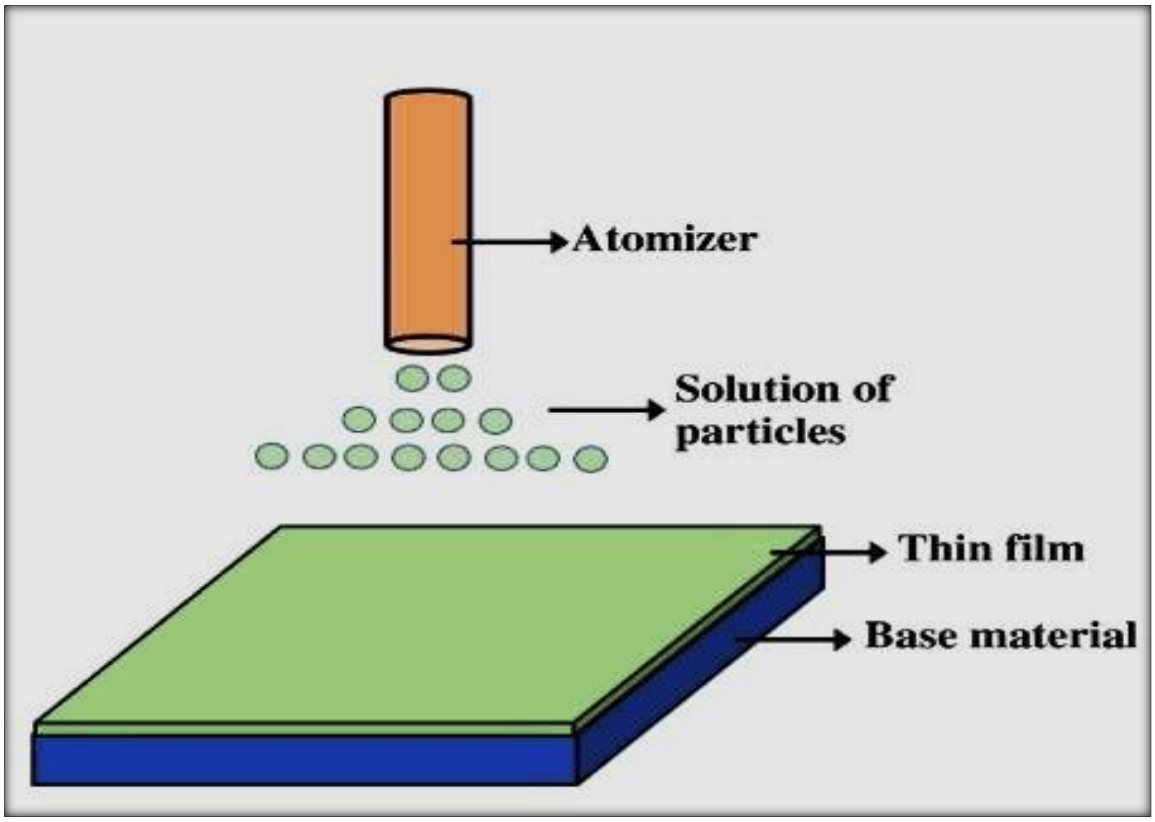

Figure 2.14: Spray coating on substrate[109] **.**

C. Dip Coating

The substrate is coated by immersing it in a liquid during the dip-coating process[111]. Figure (2.15) depicts a typical schematic depiction of the dip-coating process. Dip-coating is a common alternative to spin coating for producing thin films from sol-gel precursors for research purposes, where many chemical and nanomaterial engineering research projects use the dip coating technique to create thin-film coatings. and technique is typically used for applying films to flat or cylindrical substrates [114].

There are five phases to the dip-coating procedure:

1- Immersion: At a steady pace, the substrate is immersed in the coating material's solution (preferably jitter-free).

2- Start-up: The substrate has been suspended in the solution for some time and is now being hauled up.

3- Deposition: As the thin layer is dragged up, it deposits itself on the substrate to avoid jitters, the withdrawing is done at a constant speed. The thickness of the coating is determined by the speed (faster withdrawal gives thicker coating material).

4- Drainage: Any excess liquid will run off the surface.

5- Evaporation: The solvent in the liquid evaporates, leaving a thin layer behind. Evaporation begins during the deposition and drainage processes for volatile solvents like alcohols [112].The phases of a continuous process are carried out one after the other. The final state of a thin film's dip coating is determined by a number of factors. Many factors, including the functionality of the initial substrate surface, submersion time, withdrawal speed, number of dipping cycles, solution composition, concentration and temperature, and environment humidity, can be controlled to produce a wide range of repeatable dip coated film structures and thicknesses. Even on bulky, complex shapes, the dip coating process can produce homogeneous, high-quality films[117].

Nanoparticles are often used as a coating material. Dip coating applications include:

1- Multilayer sensor coatings

2- Implant functionalist

3- Hydro gels

4- Sol-gel nanoparticle coatings

5- Self-assembled mono layers

6- Layer-by-layer nanoparticle assemblies.

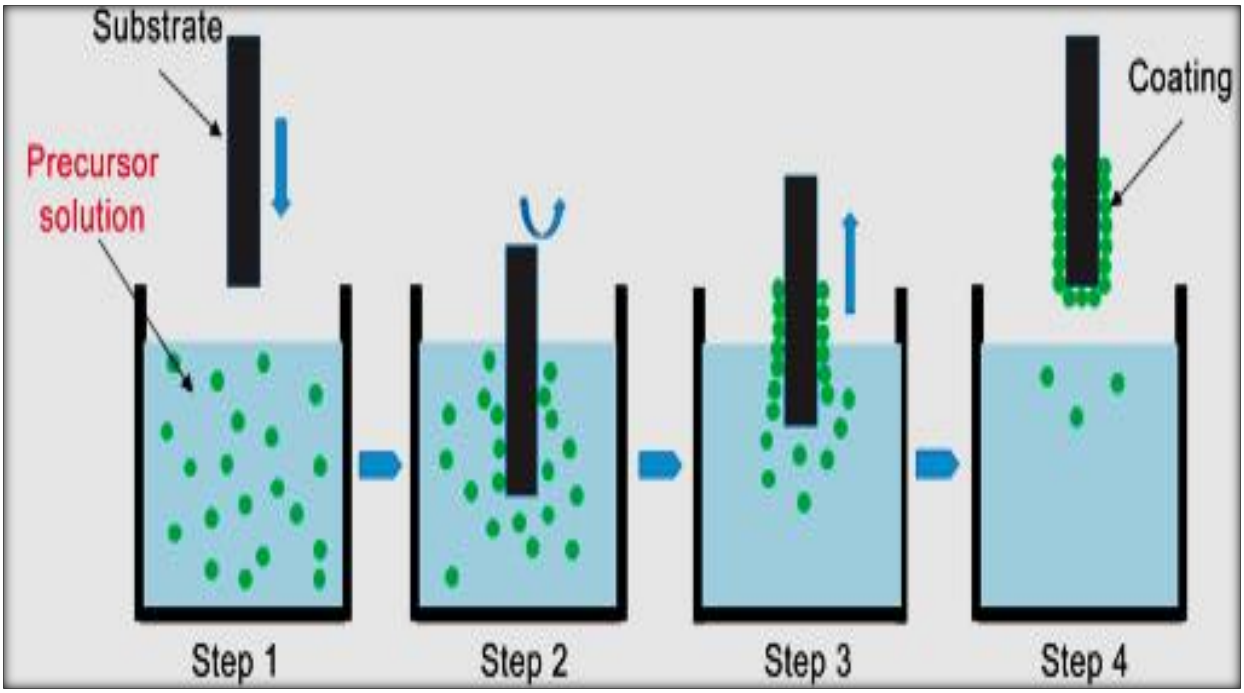

Figure 2.15: A schematic view of the steps in dip coating[118].

Dip coating has a number of distinct advantages. These benefits are illustrated by a quick glance at some of the most typical applications:

1- Metal heating, ventilation, and air conditioning (HVAC) component dip coating: the ability of dip coating to offer comprehensive coverage to surfaces with difficult geometries is perhaps its most important benefit. In the HVAC and air pollution control industries, metal blower wheels, for example, are utilized in centrifugal fans. The blades on the wheel, often known as a'squirrel cage,' are important to the fan's basic function but make spraying or powder coating a nightmare. Consider how difficult it would be for a technician to coat hundreds of crevices on the wheel with a uniform thickness and in a timely manner. A dip coat, on the other hand, glides over the entire surface with relative ease, producing uniform coverage.

2- Tool Handle Dip Coatings: When it comes to giving their handles a soft, graspable touch, manufacturers have two options: injection molding a sleeve or adding a dip coating. Dip coating achieves the same result as injection

molding, but in a far more straight forward and cost-effective industrial method.

3- Metal Warehousing Rack Dip Coatings: Because of their open shape, metal warehouse racks are frequently dip coated. Spraying racks would be inefficient, and it would be a waste of money to invest in a powder coating plant to coat these materials. Dip coating methods offer similar benefits in the manufacturing

4- Dip coating lines are also highly efficient, low-waste systems, because any surplus paint simply drops back into the dip tank, where it will be reused in the next cycle of application. When it comes to spray painting lines, a large amount of the paint gets up on the walls and floor around the coated item. [111].

2.8 Failure Modes in Adhesive Bonds :

There are several different modes of failure in Adhesive Bonds of as following:

2.8.1 Adhesive Failure

Failure of a bonded joint between the adhesive and the substrate as shown in Figure (2.16),is Primarily due to a lack of chemical bonding between the adhesive and the bonding substrate. Can be indicative of poor surface preparation or contamination or incorrect adhesive selection for the substrate materials. This failure mode can be mitigated by several methods. Preparation of the substrate's surface by using abrasives or bead/shot blasting to roughen will give better adhesion and bond strength[119] . Cleanliness of the substrate is also of importance, due to the possibility of machining fluids, lubricants, and leftover materials (e.g., powder) causing adhesion issues. For most applications, degreasing with chemical methods—such as detergents and solvents can lead to

successful adhesion. For materials with lower surface energy, more specialized treatments (e.g., plasma or corona discharge) can enhance bond ability [120].

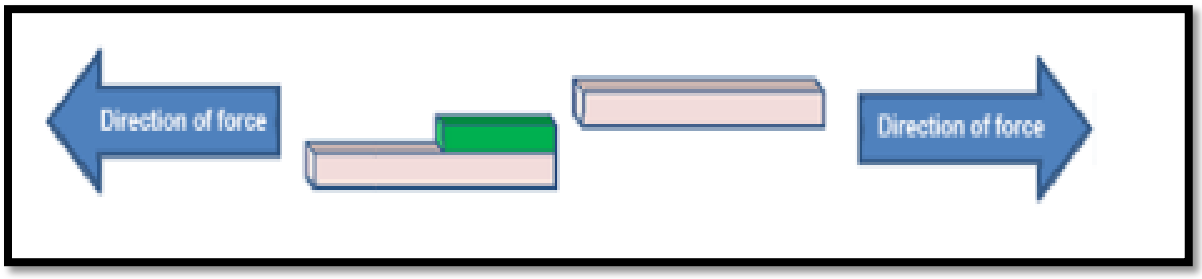

Figure 2.16 : Adhesive Failure[119]

2.8.2 Cohesive Failure

Cohesive failure is a breakdown of intermolecular bonding forces in a given adhesive substance as shown in Figure (2.17). This type of failure occurs in the bulk layer of the adhesive [120].This is most common failure when the adhesive is too weak for the intended application. As shown below, the adhesion to the substrates is greater than of the structural integrity of the adhesive. This can occur with soft adhesives like certain urethanes and silicones. It can also occur if the adhesive bondline is applied too thick [121].

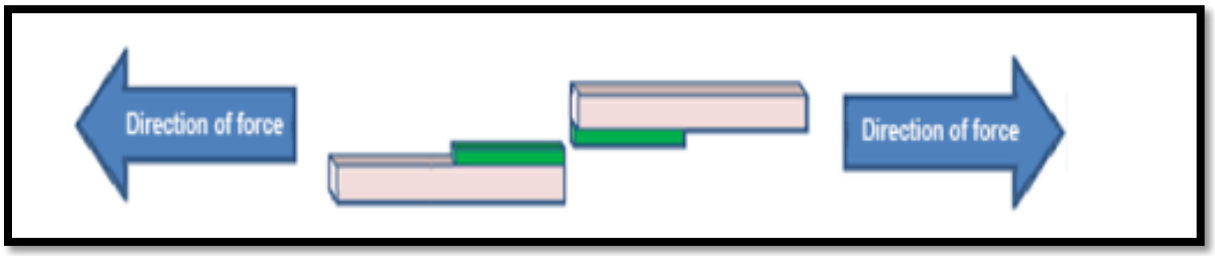

Figure 2.17: Cohesive Failure[119]

2.8.3 Substrate Failure

Interlaminer fracture in composite structures as shown in Figure(2.19) , usually between the first and second plies adjacent to the bond line, can be common in composite laminates especially those with brittle epoxies [57,58].

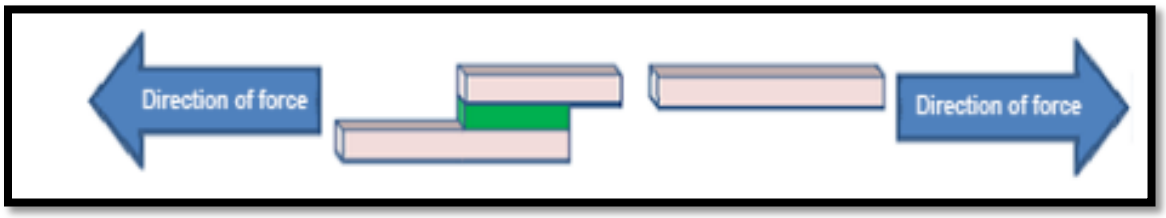

Figure 2.18: Substrate Failure[119] .

2.9 Introduction of Thermal and Electrical Characterizations:

2.9.1 Thermal Conduction Mechanisms

In general, heat transfer can be conducted in three basic ways: Thermal conduction, thermal convection, thermal radiation[122] . Thermal conduction refers to the process of heat energy transfer caused by the existence of temperature differences in objects. Thermal convection is a process in which heat flows through a fluid medium to stabilize the temperature uniformly. Thermal radiation refers to the phenomenon that the object holds temperature and emits energy in the form of electromagnetic waves. The heat transfer mechanisms of gases, liquids, and solids are different.

The essence of heat conduction refers to the process that the thermal motions of molecules in a substance collide with each other to transfer energy. In solid materials, due to the difference in temperature, the kinetic energy of the particles at the nodes in the crystal is different. The heat energy inside the crystal is transferred

from the part with high kinetic energy to the part with low kinetic energy. In conductive material, there are a large number of free electrons that are constantly making irregular thermal motions, and the general lattice vibration energy is low, so free electrons play a major role in heat conduction. In insulated conductors, the main form of thermal conduction is the lattice vibration of atoms and molecules near their equilibrium positions. The normal-mode energy quantum of lattice vibration is called the phonon[123] . The phonon has no mass and obeys Bose–Einstein theory[124] . Polymers usually have no free electrons, and their thermal conduction mainly relies on phonon transport. However, the polymer has characteristics of the random entanglement of molecular chains and high relative molecular mass, so it is difficult to crystallize completely. These factors can lead to phonon scattering and hinder phonon transfer. Therefore, the λ of most polymer composites were relatively poor (0.1–0.5 W/m·K) [125,126].

At present, the synthesis of intrinsic thermally conductive polymers and the preparation of filled thermally conductive polymers are the two main methods for obtaining high TCPCs. Intrinsic thermally conductive polymers mainly change the molecular chain structure of the polymer to obtain an ordered structure, thereby enhancing the λ of composites. The filled thermally conductive polymer is stuffed with high-thermal-conductivity inorganic fillers or metal fillers in the polymer matrices to obtain high TCPCs. Compared with the low fabrication efficiency, cumbersome synthesis process, and high cost for the synthesis of intrinsic thermally conductive polymer composites, the fabrication of the filled thermally conductive polymers shows the advantages of easy operation, low cost, and suitability for industrial production. It has already become the mainstream development direction of TCPCs[127] .

The addition of high-thermal-conductivity fillers to polymer matrices can effectively improve the λ of composites. However, the thermal conductivity mechanism of TCPCs will become very complicated because it is related to the filler type, filler structure, filler distribution, filler content, interface thermal resistance, and intrinsic thermal conductivity of the fillers. Currently(thermal conduction path theory, percolation theory, and thermoelastic coefficient theories) are the accepted explanation of the thermal conductivity mechanism of TCPCs [128].

The thermal conduction path theory is, when the thermally conductive fillers are added to the polymer matrices, the thermally conductive fillers form continuous networks inside the polymer matrices, and heat is conducted along the filler network[129] . This theory feels easy to accept.

Percolation theory is similar to thermal conduction path theory. Percolation theory refers to, when the filler load is low, the fillers are evenly dispersed in the polymer matrices to form a "sea-island structure" without forming continuous networks, and the λ of the composites slowly increases. When the thermally conductive fillers reach the percolation threshold, the thermally conductive fillers are connected to each other to form a "sea-sea structure", and the λ increases sharply [130].As the critical point is not obvious, this theory is controversial. Many experimental results prove the correctness of this theory . The changing law of λ is related to the coefficient of elasticity in classical elastic mechanics.Therefore, the researchers regard λ as the thermally elastic coefficient of phonons in the propagation process .

These are **the thermoelastic coefficient theories.** In other words, λ has nothing to do with the transmission path, but depends on the overall performance

of the composites. The transfer efficiency of phonons increases with the improvement in λ and thermoelastic coefficient of composites[131].

2.9.2 Thermal conductivity:

The performance, longevity, and dependability of electronic devices are all dependent on thermal dissipation. Thermal dissipation has become a difficult challenge with the downsizing, integration, and functionalization of electronics, as well as the advent of novel applications such as three-dimensional chip stack, flexible electronics, and light emitting diodes, among others. As a result, new highly thermally conductive materials are required to address this problem[132,133].

Thermal conductivity, like radiation and convection, is a heat transport process. Convection is the direct particle contact that transfers energy inside liquids and gases. Radiation is the transfer of energy by energetic particles or waves emitting and absorbing energy. Thermal conductivity is the main method of heat transfer within solid materials. A material's thermal conductivity is a quality that determines how well it can conduct heat. When the temperature difference between the opposite sides of the cube is 1K, this physical constant is defined as the amount of heat that flows through a unit cube of a material in a unit of time. In solids, heat may be transported by charge carriers (such as electrons and holes) or by phonons (energy quanta of atomic lattice vibrations). The contribution of phonons dominates the thermal conductivity of insulators and semiconductors, but the electronic component substantially surpasses the phonon contribution in metals. The principal mode of heat conduction in most polymers is by phonons.
The heat conduction rate is represented by Fourier's equations (2.1) and (2.2) for one-dimensional, steady-state heat flow:

$$q = KA\frac{\Delta T}{L} \quad \text{…(2.1)}$$

Or

$$J = \frac{q}{A} = -k\frac{dT}{dX} \quad \text{...(2.2)}$$

where q is the rate of heat transfer (W), J is the heat flux (W/m^2), and k is the thermal conductivity W/(mK); A is the cross sectional transfer area (m^2), T is the temperature differential (^oC), and L is the length of the conduction path (m). The Debye equation can be used to calculate the thermal conductivity (TC) of polymers (typically denoted by a Greek letter or a Latin lowercase k).

$$K = \frac{Cp\ vl}{3} \quad \text{...(2.3)}$$

where Cp is the specific heat capacity per unit volume, υ is the phonon velocity, and l is the phonon mean free path. For most polymers, l is extremely small due to scattering with other phonons, defects, and grain boundaries. Therefore, most polymers have a low TC in the range of 0.1 to 0.5 W/(m·K) which is insufficient for many applications requiring substantial heat conduction [134].

2.9.3 Thermal Conductivity of Polymers

The thermal conductivity of both polymers and fillers affect the thermal conductivity of polymer composites. However, because the thermal conductivity of polymers is typically low compared to that of the filler it is frequently overlooked in the design of thermally conductive polymer composites. Because the thermally conductive fillers are separated by the polymer matrix which functions as a thermal barrier and becomes rate limiting in the thermal conduction pathway at low filler loadings the thermal conductivity of polymers is especially essential. In order to

get a high thermal conductivity, inorganic fillers that are thermally conductive must be used. The thermal conductivity of polymer composites is strongly influenced by the filler type, loading level, filler size, and filler shape as illustrated in Figure (2.19), [134].

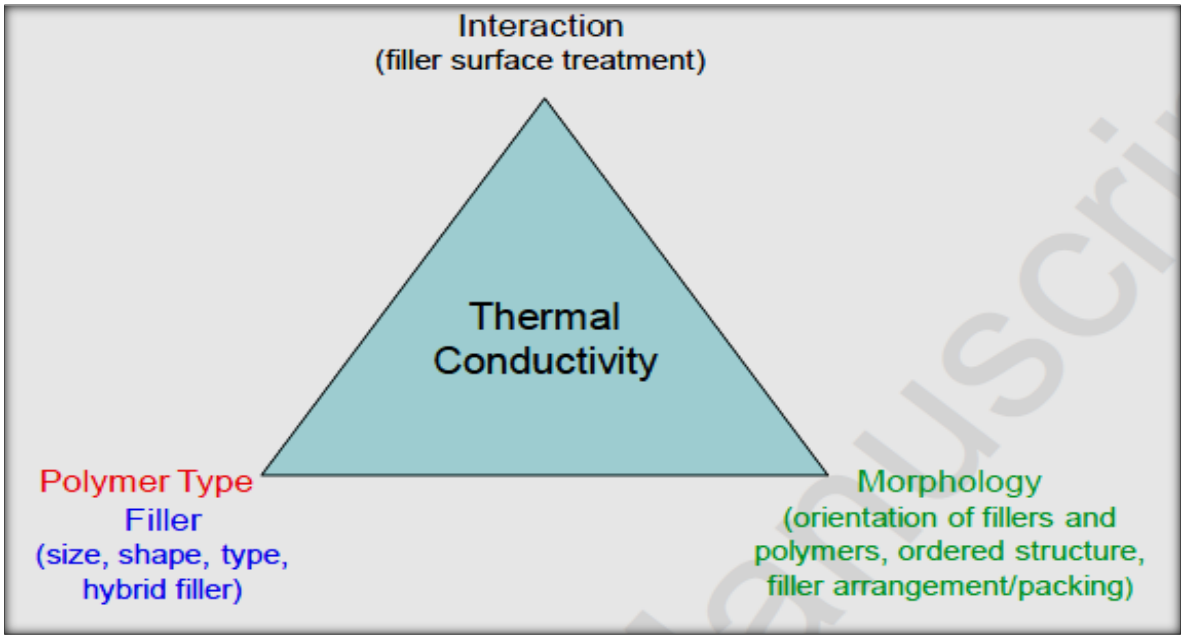

Figure 2.19: Effect of the structure ,properties of polymer , fillers and the morphology of the composites on the thermal conductivity[134].

High thermal conductivity is required for a variety of applications in electrical and electronic industry . This is much more significant for polymers supplemented with various sorts of fillers. The inclusion of highly heat conductive fillers or molecule orientation can both improve thermal conductivity in polymers[85, 86]. In the production of systems with better mechanical, thermal, electrical, and other properties, it is normal practice to reinforce polymers with various types of organic or inorganic fillers [84]. One of the most actively explored nanodielectric systems is epoxy resin(ER) enhanced with nanoparticles [84]. Magnesium oxide (MgO) was chosen as a filler material because it reduces

the amount of space charge in the polymer, as well as being a high electrical insulation material with a high TC [87, 88] Boron nitride (BN) is a material having a high thermal conductivity, low dielectric permittivity, and high dielectric breakdown strength [139] .

2.9.4 Applications of Thermally Conductive Polymer Composites

New thermally conductive materials are in high demand these days, because rising cooling needs in growing industries. Polymer composites have the following characteristics when compared to other thermally conductive materials such as metals, ceramics, and carbon compounds[134] :

a) The selection of proper fillers can affect electrical insulation and conduction.

b) Processing integrated pieces or complex geometry is simple.

c) Light weight.

d) Corrosion resistant.

e) If a flexible polymer is utilized, it must conform to the geometry of the nearby rough surfaces.

f) Vibration damping owing to polymer composites' toughness.

LED devices, electronic assembly and packaging, battery and solar energy are just a few of the new application areas for thermally conductive polymer composites, as shown in the sections below:

❖ LED devices

When compared to traditional lighting, light-emitting diode (LED) lighting has a longer lifespan and is more energy efficient (30 percent). In LED gadgets, however, 70% of the energy is converted to heat. Increasing the TC of thermal interface materials(TIM) is a constant need[140]. As shown in figure(2.20), a final heat management option for LED heat sinks could be adequate thermally conductive polymer composites combined with proper design [82- 87].

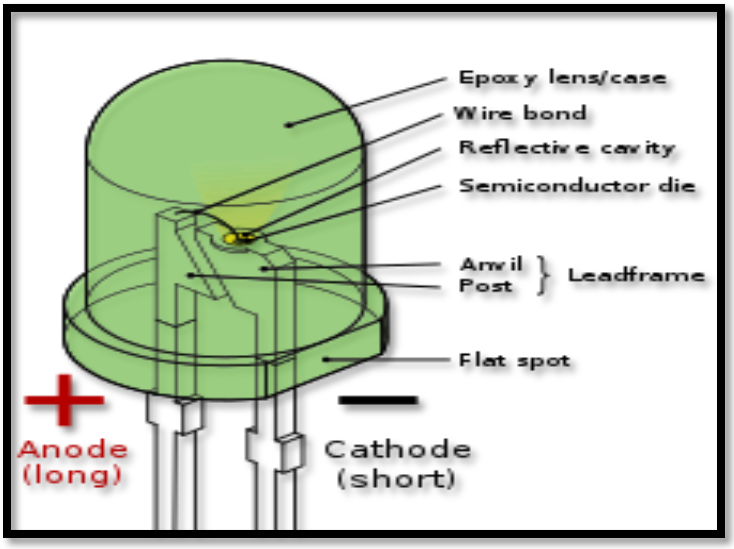

Figures 2.20:Parts of a conventional LED **[87].**

❖ Electronic Packaging

The goal of thermal management in electronics is to keep all of the system's components within their functioning temperature range. As a result, a thermally conductive path for heat dissipation and the elimination of hot spots in electronic devices is required [142] . Single chip packages, 3D chip stack packages, and automobile electronic control units (ECU) will be the focus of the debate on

thermally conductive polymer composites in electronic assembly and packaging[134]. as shown in Figure (2.21) .

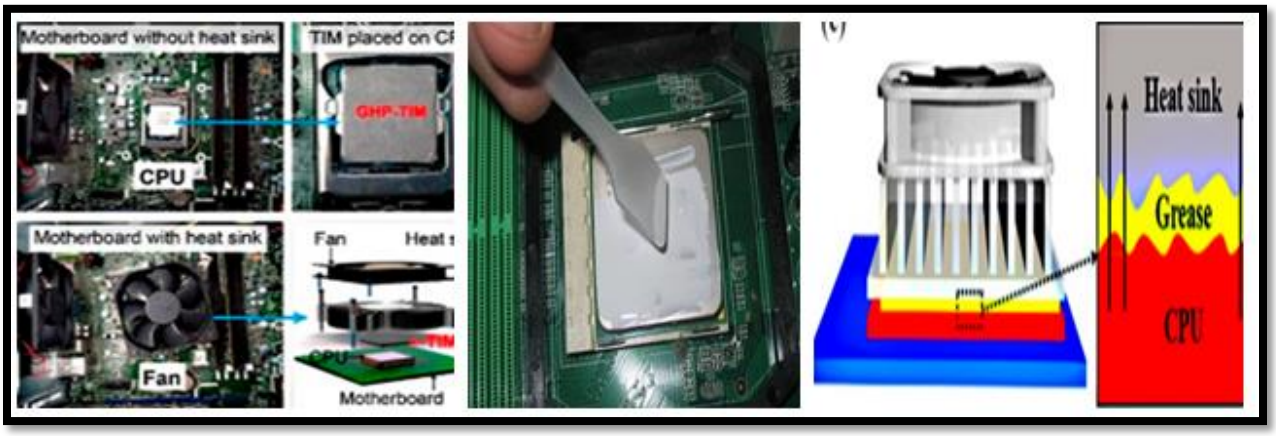

Figure 2.21: 3D chip stack assembly [134].

❖ Automotive electronic control units (ECUs)

The ECU is responsible for coordinating and combining a variety of complex processes, including mixture generation, combustion, and exhaust gas treatment. ECUs are intended to have more functionality, be smaller and lighter, and have a higher power density in order to reduce pollutant emissions. As a result, thermal management within the chip and its surrounding package is more difficult than ever. Another issue to consider is the effect of extreme under-hood vehicle ambient temperatures on the electronics utilized in ECU assembly. When exposed to high temperatures for an extended period of time, the performance of thermal grease, thermal pads, and phase change materials (PCMs) may decrease. As a result, the key difficulty for polymer composites in ECU applications is raising TC while retaining other attributes in a hostile environment [134] as seen in Figure (2.22).

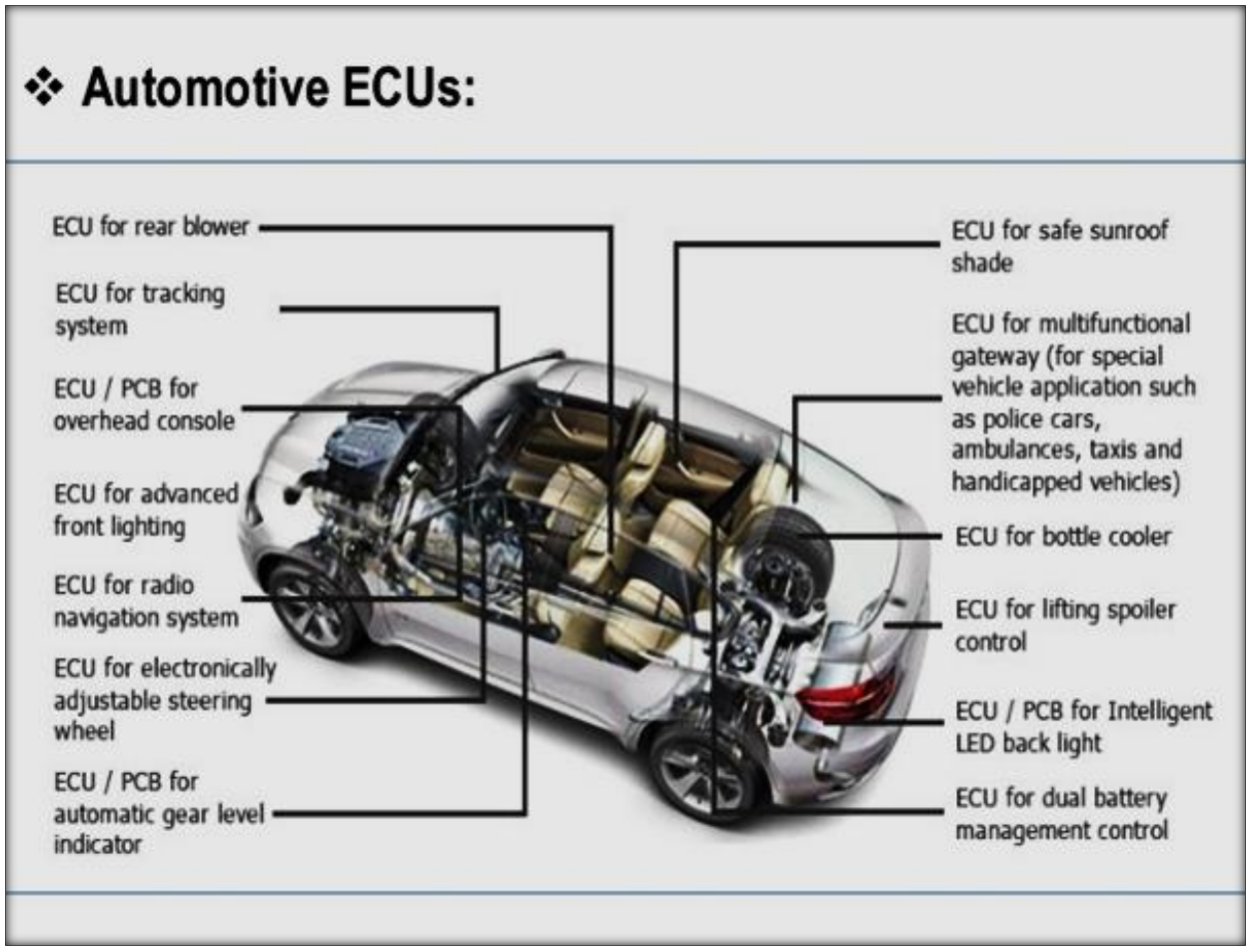

Figure 2.22: ECU engine control unit car [134].

❖ Batteries

Thermal management is becoming one of the most important issues in the expanding use of batteries as they become more powerful and used in more diverse applications. When cells are utilized at a high discharge/charge rate or at a high ambient temperature, the heat generation rate can surpass the heat dissipation rate. The cell may experience thermal runaway, as well as internal pressure buildup, which could cause the cell to rupture. Due to this safety concern, highly thermally conductive materials are required to keep a battery pack at an ideal average temperature. In this situation, phase-changing materials and coolants can be

employed to help the battery pack dissipate heat [143]. However, because to the lack of cost effectiveness and the complexity of structures, they are not particularly feasible to apply to real systems. Thermally conductive polymer composites may open up new possibilities for battery pack thermal system design, as shown in Figure (2.23) [134].

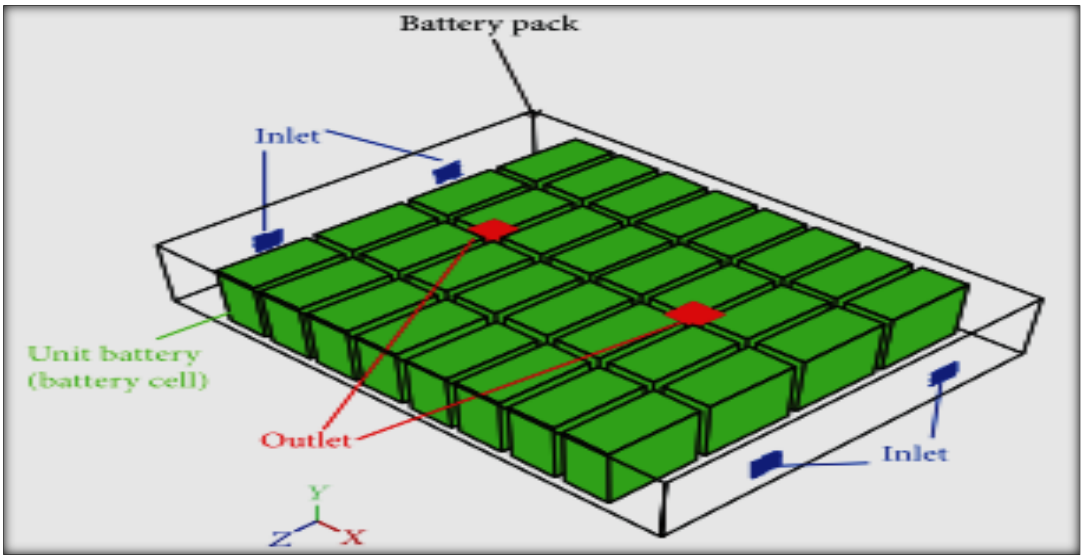

Figure 2.23: Baseline battery pack [144].

❖ Solar

Solar's popularity as a renewable and sustainable energy source has exploded in recent years. Because photovoltaic (PV) cells have a low conversion efficiency, most of the absorbed solar energy is converted to heat energy within the cell [145]. The solar conversion efficiency of PV cells decline as the operating temperature of the cells rises. For crystalline silicon-based cells, increasing the temperature by 1 °C reduces the relative conversion efficiency by roughly 0.4-0.5% and around 0.25 percent for amorphous silicon cells [146]. It is desirable to remove accumulated heat from the PV surface in order to boost the conversion

efficiency of PVs, especially for concentrated PV systems [147]. as seen in Figure(2.24).

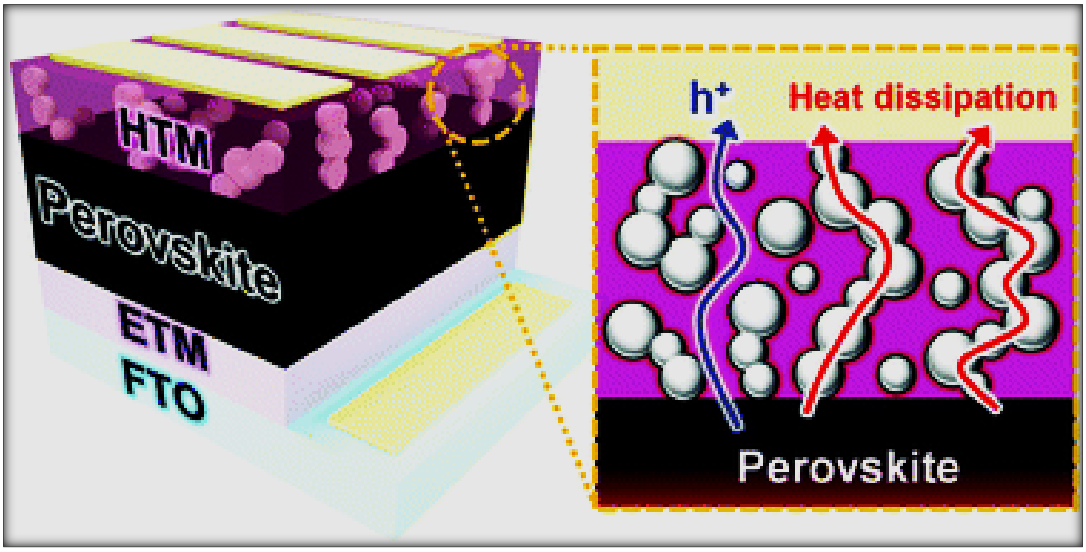

Figure 2.24: heat dissipation effects on the stability of planar perovskite solar cells[148].

One of the most difficult problems is transferring heat from the cell to the outside. Because of their low manufacturing costs and light weight, organic and perovskite thin film solar cells are a developing cost-effective photovoltaic technology. The poor device stability of organic and perovskite solar cells (PSC) is the fundamental impediment to commercialization. Encapsulation of solar photovoltaic devices is one of the most effective solutions to address this stability issue and extend device life by using materials and structures with good oxygen and moisture barrier performance [149].

2.10 Electrical Resistivity:

Electrical resistivity (also known as specific electrical resistance or volume resistivity) is a material attribute that determines how well it resists electric current. A substance with a low resistivity allows electric current to flow freely. The Greek

letter is widely used to indicate resistance (rho). The ohm-meter is the unit of electrical resistivity (Ω·m) [150] .A material with low resistivity is one that allows electricity to flow freely through it. A material with a high resistivity has a tough time allowing electricity to flow through it. The Greek letter stands for electrical resistance (r). The Greek symbol (s) stands for electrical conductivity, which is defined as the inverse of resistivity. As a result, a high resistivity equals a low conductivity, and a low resistivity equals a high conductivity[150]. The Simple model of electricity flowing through a substance under an applied voltage is shown in figure (2.25). The white circle represents an electron travelling through the material from left to right, while the black circles indicate the substance's atoms. Collisions between the electron and the atoms cause the electron to slow down resulting in electrical resistance[150].

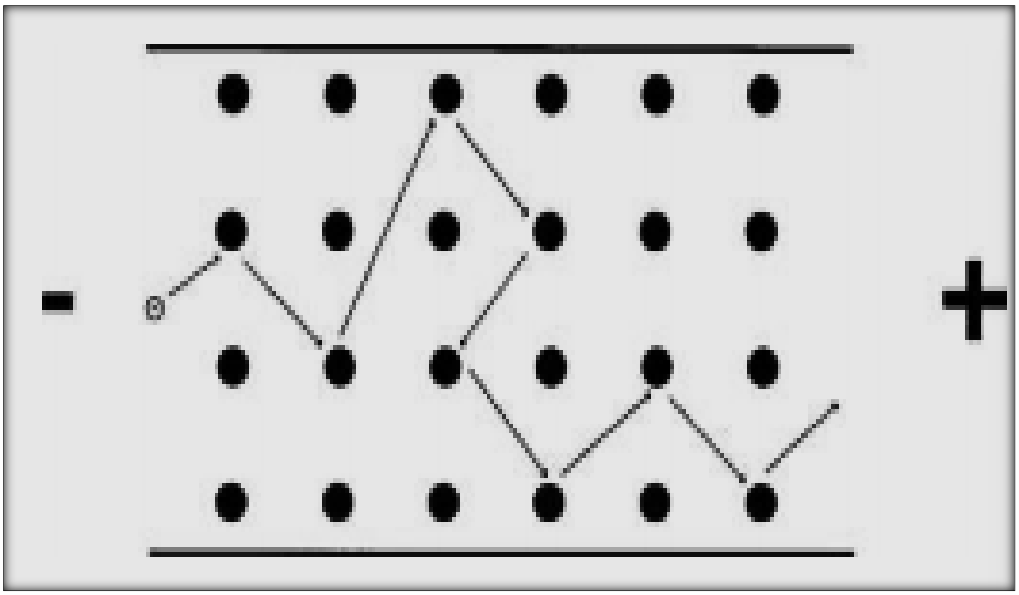

Figure 2.25:Simple model of electricity flowing through a material under an applied voltage.

In an ideal situation, the studied materials' cross-section and physical composition are homogeneous across the sample, and the electric field and current

density are parallel and constant everywhere. When this is the case as seen in Figure (2.26).

the electrical resistivity (Greek: rho) can be determined as follows[150]:

$$\rho = R \frac{A}{L} \quad \text{....(2.7)}$$

where

R is the electrical resistance of an uniform material specimen (Ω).

L is the specimen's length (m).

A is the specimen's cross-sectional area (m^2).

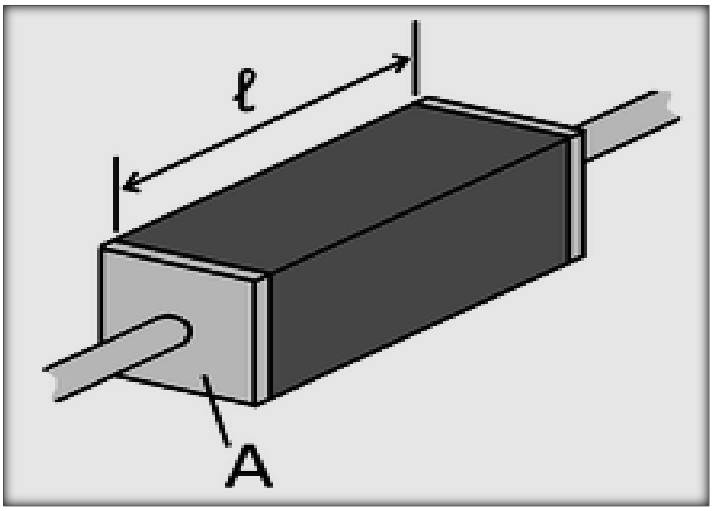

Figure 2.26: A piece of resistive material with electrical contacts on both ends[151]**.**

2.11 Literature Review

In 2016, Wang et al.[152] studied the effect of MgO on breakdown strength of LDPE with (0.5%,1%,2%,3%,4% wt%) filler loading. The data confirmed that the breakdown strength increased when 2% wt of MgO was added, but then began to gradually decrease when 3% wt and 4% wt of MgO were added, though the

breakdown strength in these nanocomposites was still higher than the breakdown strength of the unfilled LDPE.

In 2016, Chen et al[153] used TiO_2 and SiO_2 nanoparticles with (0, 0.5 %, 2 %, 4% wt) filler loading, the relation between dielectric properties of nanoparticles and their impacts on dielectric breakdown strength of epoxy was examined. The dielectric characteristic was customized by encapsulating a silica surface on TiO_2. The results revealed that, compared to raw TiO_2, adding TiO_2 and SiO_2 core-shell nanoparticles to epoxy resin significantly increased the dielectric breakdown strength.

In 2017, Gong, Ying ,et al[154] investigated the effect of BN/ carboxyl-terminated polybutadiene (CTPB) liquid rubber on the toughness and electrical insulating capabilities of modified epoxy with (10%, 20%, 30%, and 40% wt%) BN loading. The CTPB-epoxy had a stronger impact strength and a lower dielectric constant and loss than pure epoxy, according to the findings. Furthermore, epoxy treated with 20 phr CTPB was reinforced with boron nitride (BN). The heat conductive BN/CTPB/epoxy had a reduced dielectric permittivity and dissipation factor in all frequency ranges from 10^2–10^7 Hz, a stronger dielectric breakdown strength, and improved mechanical toughness when compared to the BN/epoxy under the same filler loading. As a result, the generated BN/CTPB/epoxy composites might be used in electrical insulation applications.

In, 2017,K. Elanseralathan et al [155] studied the effect of nano fillers such as titanium dioxide (TiO_2), zinc oxide (ZnO) with filler concentrations (1 % ,2 %wt) on the breakdown strength of epoxy nanocomposites. The waveform used for the tests was high voltage AC at power frequency. The results showed that 2% wt

nanofillers improved electrical treeing resistance whereas 1% wt worsened it compared to pure epoxy.

In 2017 Li, Y., Zhang,etal [156] studied the mechanical, electrical conductivity, and thermal characteristics of exfoliated graphene (GNP)/epoxy nanocomposites in situ with different filler concentrations (2 % ,3 % ,4 % ,5% wt). The end result was positive. Mechanical reinforcement (160 %increase in flexural modulus at 4% wt GNP) electrical conductivity (102 S/m at 3% wt GNP) and thermal conductivity (0.70 W m^{-1} K^{-1} at 5% wt GNP were all satisfactory.

In 2017, Dass, K et al [157] investigated the influence of silicon carbide (SiC), aluminum oxide (Al_2O_3), and zinc oxide (ZnO) nanoparticles on the mechanical performance of epoxy based nanocomposites with filler content (1 % ,2 % ,3 % ,4 % wt) .The results showed that increasing the filler content increases the hardness and flexural strength of epoxy composites filled with nano (SiC, Al_2O_3, and ZnO) particulates. The tensile strength of these nanocomposites increases as the filler percentage increases from 1 to 2% wt but if the filler amount increases further the tensile strength declines.

IN 2018 , Farimah Tikhani et al [158] Investigated the effect of silica nanoparticles on curability of epoxy ,Three kinds of silica nanoparticles with non-porous curved-rod, non-porous spherical, and mesoporous spherical microstructures were synthesized and characterized by Fourier-transform infrared spectroscopy, scanning electron microscopy (SEM) and Brunauer–Emmett–Teller analyses. Epoxy nanocomposites containing 0.1, 0.3, 0.5 wt.% of nanoparticles cured nonisothermally in differential scanning calorimetry (DSC) at different heating rates and the glass transition temperature (Tg) for fully-cured samples was estimated. Cure Index unravelled the effect of nanoparticle morphology and

porosity on epoxy crosslinking. Good cure was unconditionally the case for systems containing 0.3 wt.% of mesoporous spherical nanoparticles due to appropriate dispersion of porous nanoparticles, as captured by SEM. By contrast, dependency of curing on heating rate and nanoparticle loading in the case of non-porous spherical and curved-rod particles was evidenced by partially agglomerated domains. The state of nanoparticle-polymer interaction was also inferred in view of network formation in the presence of nanosilica particles of various morphology and porosity, which was nicely monitored by the use of Cure Index.

In 2018 , Sushil. S et al [159] investigate the effect of SiO_2 nanoparticals on the tensile and flexural properties of /epoxy polymer. Dispersion of SiO_2 nanoparticles in the epoxy polymer was achieved by ultrasonication. SiO_2/epoxy nanocomposites contain varying amount of nano size silicon dioxide (SiO_2) up to 8 wt.%. The investigated properties of SiO_2/epoxy nanocomposites increases with the increasing nanoparticles dispersion up to 4 wt.% SiO_2 nanoparticles and deterioration in the mechanical properties is realized above 4 wt.%. This may be due to the significant increase in agglomeration and settlement of the SiO_2 nanoparticles during the long curing time. The tensile strength increases by 30.57 %, flexural strength by 17 % and flexural modulus by 76 % for 4 wt. % dispersion of SiO_2.

In 2019, Jen, Y. M [160] studied the thermomechanical characteristics and electric resistance of epoxy polymers after adding multi walled carbon nanotubes (MWCNTs) and graphene nanoplatelets (GNPs). The overall concentration of the two carbon fillers was held constant at 0.4 wt%, and seven filler ratios (10:0, 1:9, 3:7, 5:5, 7:3, 9:1, and 0:10) were used between the two fillers (MWCNTs:GNPs). The addition of two nanofillers improved storage moduli, glass transition temperatures, and electric conductivity according to the findings. On the contrary,

The thermomechanical characteristics of composites with a MWCNT:GNP ratio of 1:9 show the greatest improvement.

In 2019, Zhaoliang Xing, et al [161] investigated the effects of surface hydrophobicity on the tracking resistance of MgO/epoxy nanocomposites with nanofiller percentages of (0.1, 1, 2, 6, and 10 wt %), respectively. The results showed that MgO/epoxy nanocomposite samples had increased tracking resistance. The comparative tracking index (CTI) was enhanced from 400 V for the neat epoxy samples to 475 V for the 10 wt percent nano MgO doped samples, which is defined as the greatest voltage that the sample can withstand, indicating superior anti-tracking ability.

In 2019,Nagachandrika Peddamallu, et al [162] studied the effect of magnesium oxide nanoparticles on the mechanical properties of epoxy nanocomposites. the MgO ratio was added were(0.5%, 2%, and 4% wt%), The results showed an increase in the content of MgO in the epoxy resin. Tensile and flexural properties were greatly improved for nanocomposite compared to epoxy. The dynamic mechanical analysis (DMA) results showed an increase in the storage modulus and reduction of tan δ of epoxy nanocomposites. The glass transition temperature (T_g) and activation energy increased with an increase in the filler content.

In 2020 ,Tony Zhou,,et al [163] investigated the effects of boron nitride and polymer blends on the thermal and mechanical properties of acrylonitrile butadiene styrene (ABS) composites containing boron nitride. (10, 20, 30, 40, 50, 60 wt %). When compared to an ABS matrix, adding both high density polyethylene (HDPE) and maleic anhydride to the acrylonitrile butadiene styrene (ABS) matrix resulted in a 40% increase in impact strength without a reduction in thermal conductivity. The effective medium theory model is used to help explain how strong filler

alignment helps achieve high thermal conductivity, greater than 5 W/m K for 60 wt % boron nitride.

In 2021, Fan, J et al [164] investigated the impact of graphene oxide (GO) with varied oxidation degrees on the cryogenic mechanical characteristics of GO/epoxy nanocomposites. As the graphene oxide ratio (0.05,0.1,0.2,0.3 wt%) rose, it was discovered that GO had greater dispersion in the matrix and improved interfacial interactions with epoxy resin. When a result, as the GO oxidation degree increased the tensile characteristics of GO/epoxy nanocomposites improved at room temperature (RT) and liquid nitrogen temperature (LNT), eventually reaching the maximum performance with the right GO oxidation degree. The tensile strength of GO/epoxy nanocomposites with a modest GO loading of 0.10 wt percent was 78.0 MPa at RT and 123.2 MPa, respectively, 31% and 14% greater than pure epoxy.

IN 2021 ,H. Mohit, et al [165] investigated the effects of of titanium carbide (TiC) nanoparticles and coir fiber as hybrid reinforcements on the physical, mechanical characteristics, and thermal stability of Coir fiber/TiC epoxy composites. The hand layup technique was applied for the fabrication of composites by reinforcing a fixed quantity of coir fiber (0, 5, and 10 wt%) and TiC nanoparticles (0, 5, and 10 wt%) in the proportion of bio-epoxy Sr 33 (100, 95, and 90 wt%) and synthetic epoxy (100, 95, and 90 wt%) resin. The cured specimen were subjected to flexural, tensile, impact, shore hardness, and chemical resistance tests. The fracture surface of the epoxy composites was investigated from a scanning electron microscope (SEM). From the outcomes, it was found that the reinforcement of coir fiber in epoxy polymer showed better than the neat polymer in most of the considered properties. The incorporation of TiC nanoparticles in coir fiber/epoxy composites exhibited some improvement in the mechanical characteristics (tensile strength by 4.99% and flexural strength from 115.05 to 124

MPa) and thermal stability (up to 402.71 °C) of the developed composites, which have a resistance under different loading conditions.

In 2022, Nitesh et al [166] investigated the effects of MWCNT/TiO_2 on properties of pure epoxy ,In this study, TiO_2 nanoparticles are decorated on multi-walled carbon nanotubes (MWCNTs) by exploitation of opposite zeta potential of MWCNTs and TiO_2 nanoparticles without degrading the hexagonal interatomic structure of MWCNTs, resulting in a new MWCNT/TiO_2 hybrid nanofiller with improved morphology and tensile performance (MT hybrid nanofiller). To understand the multiphase nanocomposite in terms of mechanical performance under various loads, the recently developed MT hybrid nanofiller (from 0.25 wt percent to 1.50 wt percent) is loaded in crosslinking epoxy matrix (storage modulus, loss modulus, tensile strength, and modulus). The outcome revealed the addition of TiO_2 nanoparticles to MWCNTs alters the fracture process in the mirror zone and creates a new fracture surface, altering the behavior of multiphase nanocomposites under diverse stress conditions.

In 2022, JinWang et al [167] investigated the effect of epoxy-based composite has been produced by introducing a long-range ordered carbon/graphene/MgO ternary foam (CGMF). The heat conduction shortcut provided by the vertically aligned structure of CGMF endows the composites with excellent thermal conductivity of 4.87 $Wm^{-1}K^{-1}$ at 12.96 vol% filler loading. Meanwhile, the barrier of MgO and PVA to the electron transmission in CGMF results in the composite with high electrical resistivity which satisfies the requirement of electrical insulation.

In 2022, Namdev, A. et al [168] investigated the impacts of carbon fiber and graphene nanoplatelets (GNP) reinforced hybrid composites with weight percents

(0, 0.25, 0.50, 0.75, and 1 wt%) on mechanical, thermal, and physical properties The results demonstrated that a 0.5 wt percent GNP filled carbon fiber/epoxy composite with increased tensile and flexural strength, interlaminar shear strength, and Vickers hardness when compared to other composites. Impact strength was highest at 0.25 wt% GNP-filled epoxy hybrid composite. The greatest tensile and flexural strength values were achieved at 0.5 wt% GNP, 11 and 8% greater than plain fiber composites, respectively. In terms of thermal properties, the 0.5 wt percent GNP composite has the maximum heat deflection temperature and thermal conductivity.

In 2022, Ali, N. H et al [169] investigated the influence of reinforcing hybrid fibers/particles on the mechanical and physical properties of polymer hybrid compounds. According to the findings, fibers have become a viable alternative to mineral materials. Synthetic fibers (carbon fibers, electronic glass, Kevlar fibers) and natural fibers (bamboo fibers, Jute fibers, sisal fibers) with various particles (alumina, graphene, titanium oxide, and silicon carbide) were the most widely used and effective, resulting in significant improvements in the mechanical and physical properties of polymer materials.

2.12 Summary:

The following notes can be prepared based on the literature review:

1. A group of researchers is looking at the impact of nanomaterials (Al_2O_3, TiO_2, ZnO, GO,AIN) on the thermal and electrical properties of epoxy.

2. A group of researchers is investigating the impact of nanomaterials (Al_2O_3, TiO_2, MgO, ZnO, GO, SiO_2) and their mixtures on the mechanical properties of epoxy and other polymers.

3. The influence of nanomaterials (MWCNTs) and graphene nanoplatelets (GNPs) on the thermomechanical characteristics and electric resistance of epoxy polymers is being investigated by a group of researchers.
4. Some studies concerned on the influence of reinforcing hybrid fibers/particles on the mechanical and physical properties of polymer hybrid compounds.

Substantial efforts, such as surface modification [170]. alignment by electrical field and magnetic field [171].Adding inorganic fillers with high thermal conductivity, such as Al_2O_3,[157,158]. AlN [159,160]. carbon nanotubes (CNTs), [176]. graphene[162,163]. etc., is thought to be an effective way to improve the polymer matrix's thermal conductivity .However, in order to attain high heat conductivity of the polymer composites, very high filler loading (>50 wt percent) is commonly used, resulting in high cost, heavy weight, and considerable mechanical integrity degradation of the polymer materials [179].

5. The impact of hybrid(MgO and BN nanoparticles) on the morphological, structural, thermal, electrical, tribological, and mechanical properties of epoxy is considered in this work.

2.13 The Originality of The Study :

The use of hybrid additives [180], [181], [182]. to generate high thermal performance polymer composites with minimal loading content. Due to their capacity to build effective thermal networks that benefit from the synergistic effect, the simultaneous use of multi-component fillers with diverse morphologies, dimensions, and sizes is an alternative technique to improve the thermal conductivity of composites [183]. This research adds to our understanding of how to make very thermally conductive and electrically insulating composites. To

achieve high heat conductivity and superior electrical insulation, hybrid adhesives incorporating two types of fillers with various shapes and sizes have been recommended. Due to the ability of a mixture of conductive fillers to increase the filling density, which allows small particles to occupy the space between adjacent large particles, thermally conductive networks can be generated with less filler. In this study, it is developed a new corrosion protective coating with heat dissipation, electrical insulation and strength that can be used to protect parts in automobiles, ships, or planes, as well as in electrical engineering, including insulating materials for power equipment, electronic packaging and encapsulations, computer chips, satellite devices, and other areas where good heat dissipation is required,and it is compared the mechanical, thermal, tribological, and electrical properties of coating resins using epoxy resin. Heat dissipation and electrical insulation were provided by magnesium oxide (MgO) and hexagonal boron nitride (hBN), as described in chapter (4). MgO offers a number of appealing properties, including a bulk thermal conductivity larger than alumina, as well as being affordable and harmless. Meanwhile, BN appears to be on the verge of developing high-temperature conductive adhesives for coating applications with better electric insulation than graphene nanoparticles, It is a thermally conductive, electrically insulating coating that withstands aggressive chemicals, exhibits exceptional performance. superior protection against corrosion in various harsh environments, it is resistant to high temperatures.

Chapter Three
Experimental Work

3.1 Introduction

This chapter describes the experimental work particularlymaterials selection, properties of the materials, samples preparation methods, and methods of testing used. It provides a full overview of the experimental approach, which includes procedures for preparing materials and samples as well as a detailed description of the test instruments employed.

3.2 The Used Materials

3.2.1 Epoxy Resin

Epoxy Sikadur 52(lp) was purchased from Iraq Sikadur company , Hilla, Iraq with the properties as shown in Table (3.1).

Table 3.1 :Properties of Epoxy

Property	Data
Form	Liquid
ratio of mixing	Component A (Resin): Component B(Hardener) = 2:1 by volume
Viscosity	≈ 330 mPa s at +20 ^{0}C
Color	Clear, pale yellow
Odour	Mild
Density	≈ 1.06 Kg/I
Tensile Strength	≈ 27 N/mm^2 (7day/30 ^{0}C) (ISO527)

Compressive Strength	≥ 70 N/mm2 (7day/30 0C) (ASTMD695)
Tensile Adhesion Strength	≥ 7 N/mm2 At 25 0C (2days) ≥ 10 N/mm2 At 25 0C (14days) (ASTMC882)

3.2.2 Magnesium Oxide Nanoparticles .

Magnesium Oxide nanoparticles were purchased from US Research Nanomaterial, Inc. Limited, Houston TX, USA with properties listed in Table(3.2).

Table 3.2: The Properties of Magnesium Oxide Nanoparticles

Property	Data
Purity	99 %
Grain Size	(100) nm
Color	White Nano powder
True density	3.58 g/cm^3

3.2.3 Boron Nitride Nanoparticles(BN NP$_S$)

Boron Nitride nanoparticles were purchased from Shanghai Civi Chemical Technology Co., Ltd., China with properties listed in Table (3.3).

Table 3.3: The Properties of Boron Nitride Nanoparticles .

Property	Data
Purity	99.8%

Crystal form	Hexagonal
Grain Size	50-100 nm
Color	Gray White powder Nano grade
True density	2.29 g/cm^3

3.2.4 Ethanol alcohol:

Ethanol alcohol with the qualities mentioned in Table(3.4), was acquired was from the local Iraqi market.

Table 3.4: Ethanol Alcohol Properties.

Property	Data
Purity	99.9%
boiling point	70 ^{0}C
Color	Transparent liquid
density	789 Kg/m^3

3.2.5 Acetone alcohol:

Acetone alcohol with the qualities mentioned in Table 3.5 was purchased from the local Iraqi market.

Table 3.5: Acetone Alcohol Properties.

Property	Data
Purity	99.9%

boiling point	56 ^{0}C
Color	Transparent liquid
density	784 Kg/m^3

3.2.6 Sodium chloride(NaCl) solution:

Sodium Chloride with the qualities mentioned in Table(3.6), was purchased from the local Iraqi market.

Table 3.6: Sodium chloride Properties.

Property	Data
Chemical formula	NaCl
Molar mass	58.443 g/mol
Appearance	Colorless cubic crystals
Odor	Odorless
Density	2.17 g/cm^3
Melting point	800.7 °C
Boiling point	1.465 °C

3.3 Preparation Procedures

3.3.1 Preparation of pure Epoxy Samples

The epoxy resin was mixed with hardener (with ratio 2:1) by using a mechanical stirrer for 5 minutes. The mixture was put in under vacuum at room temperature for 30 minutes to eliminate bubbles. Then the mixture was poure into the silicon mold, which was previously prepared, then left it for 7 days at room

temperature to complete curing. Figure (3.1) explains the steps of preparation samples of pure epoxy .

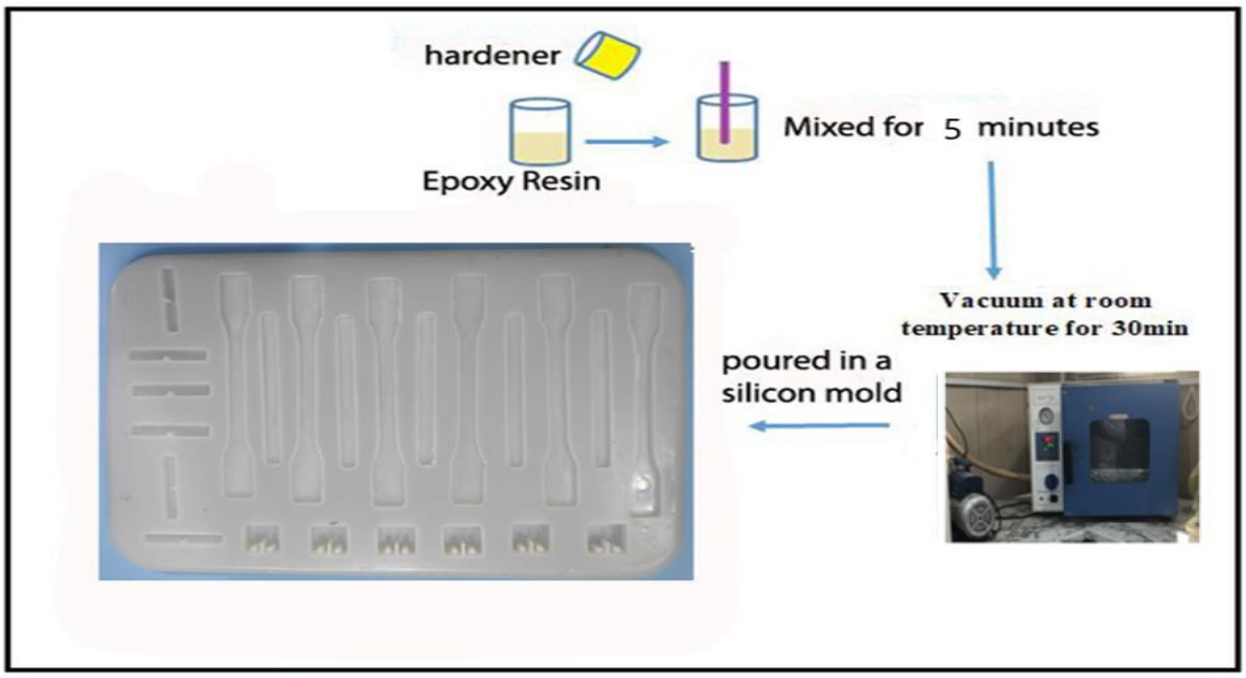

Figure (3.1): The Steps of preparation samples of pure epoxy .

3.3.2 Preparation of Nanoparticles

- Magnesium oxide Nanoparticles (MgO).
- Boron Nitride Nanoparticles (BN).
- Hybrid Nano Nanoparticles (H).

Nanoparticles were prepared using different concentrations of nanoparticles (NP) MgO , BN or hybrid (with ratio1:1) with weight percent (0,1,3,5 and 7%Wt). The dispersion of NP in ethanol was carried out using Magnetic stirrer for 5 minutes, Then the mixture was put in ultrasonic-Probe Model (SJIA-1200W) for 45 minutes at 25 °C, mode 20 ϕ and 10 % (watt) for good dispersion of nanoparticles.

Figure 3.2 :Image of Ultrasonic Cell crusher

3.3.3 Preparation of Nano composites

- Epoxy / Magnesium oxide Composites (EP/MgO).
- Epoxy / Boron Nitride Composite (EP/BN).
- Epoxy / hybrid Nano Composite (EP/H).

Following the preparation of Nanoparticles the NP solution added into resin then using mechanical mixing for one hour with heating in oven at 70 °C for evaporate solvent and in order to get good mixing .After that , the mixture was weighed before using the degassing system under vacuum for 10 min at 70 °C for evaporate the solvent, then Re-weighing mixture to insure of evaporating solvent after using the degassing system under vacuum. Then the hardener (with ratio 2:1) was added and was mixed for 5 minutes using a mechanical stirrer. The prepared mixture put in the degassing system under vacuum at room temperature for 30 minutes to eliminate bubbles, and then the mixture was poured into the silicon

mold, and left it for 7 days at room temperature to complete curing. Figure (3.3) describes the procedures used to prepare the sample.

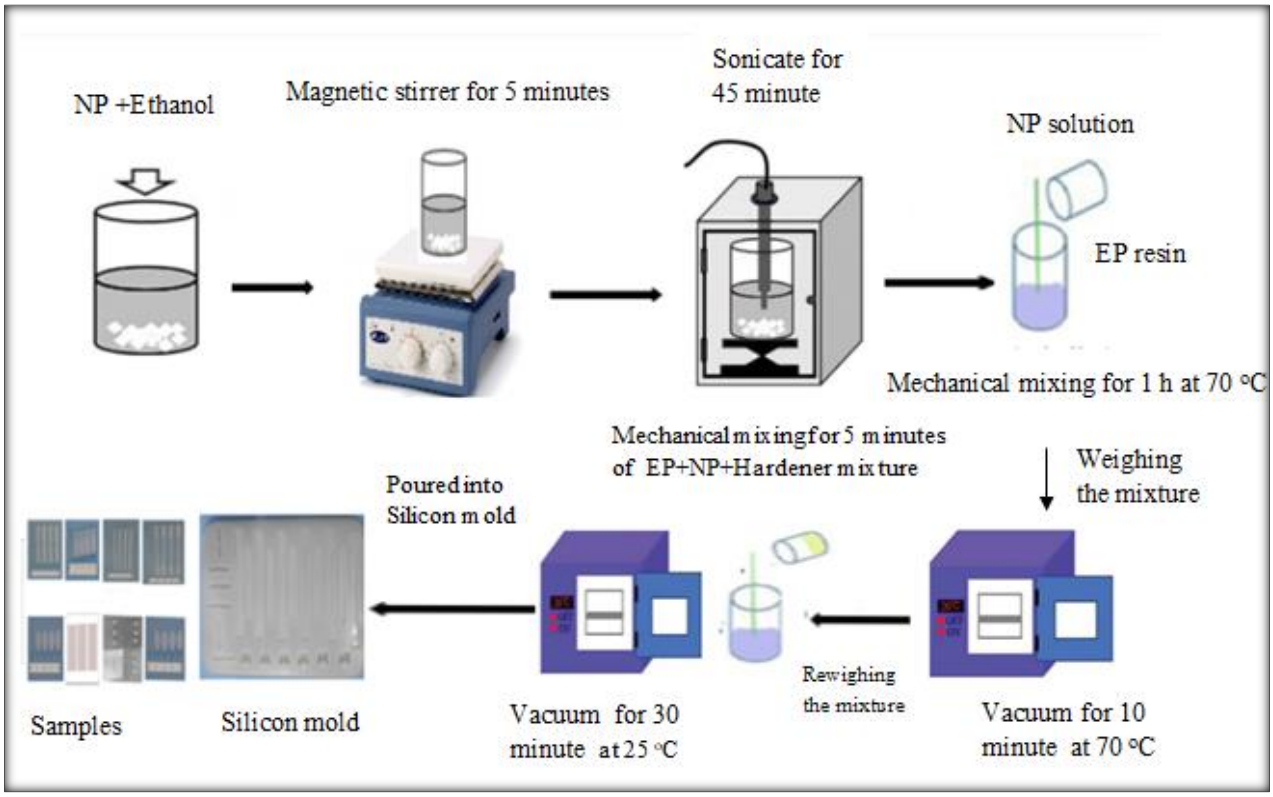

Figure 3.3: The Procedure to Prepare Epoxy/ MgO or BN ,and Hybrid Nano Composite.

After completing the process of casting samples in the silicone molds and completing curing of the samples, the surfaces of the samples were prepare where the grinding paper was used to modify the external surfaces of the samples and prepare them for mechanical ,thermal ,electrical,corrosion, morphological tests as shown in Figure (3.4) .

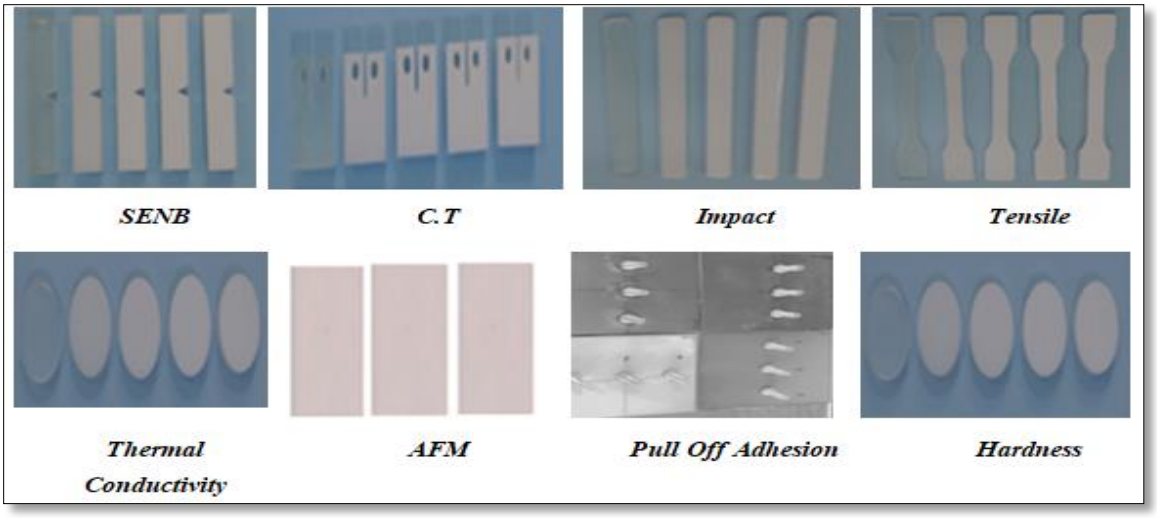

Figure 3.4: Samples After Finishing.

Thirteen samples were tested, as shown in Table 3.7.

Table 3.7: Samples composition.

Sample no	Sample Code	Sample Composition
1	EP	Epoxy without additives
2	EP/MgO1	Epoxy/1% Magnesium Oxide
3	EP/MgO3	Epoxy/3% Magnesium Oxide
4	EP/MgO5	Epoxy/5% Magnesium Oxide
5	EP/MgO7	Epoxy/7% Magnesium Oxide
6	EP/BN1	Epoxy/1% hexagonal Boron Nitride
7	EP/BN3	Epoxy/3% hexagonal Boron Nitride
8	EP/BN5	Epoxy/5% hexagonal Boron Nitride
9	EP/BN7	Epoxy/7% hexagonal Boron Nitride
10	EP/H1	Epoxy+(1:1) Hybrid(0.5%wt.MgO+0.5%wt. of h-BN NP)
11	EP/H3	Epoxy+(1:1) Hybrid(1.5%wt.MgO+1.5%wt. of h-BN NP)
12	EP/H5	Epoxy+(1:1) Hybrid(2.5%wt.MgO+2.5%wt. of h-BN NP)
13	EP/H7	Epoxy+(1:1) Hybrid(3.5%wt.MgO+3.5%wt. of h-BN NP)

3.3.4 Preparation of an epoxy nanocomposite coating

After physically polishing the steel substrates with 400, 800, and 1200 grit sandpaper, they were washed with alcohol and degreased with acetone.

The substrates were then dried in the open air. The nanocomposite coatings were uniformly cast on the steel surface using dip coating after being prepared. Dip coating method involves immersing a substrate vertically into a solution with dispersed nanoparticles and retracting it slowly [111]. Normally, the retracting speed is controlled (typically between 1 and 10 mm/min) to promote epoxy/Nanoparticles coating adhesion to the substrate layer as the solvent evaporates as denoted in Figure(3.5).The dip coating cycle is normally repeated several times to obtain reasonably homogenous and continuous transparent film of several micrometers thick. Maximum film thickness is between 200Mm and 250 Mm[184].

Samples were kept at room temperature for 7 days to cure completely. Nano composite coatings with different nanofillers (MgO, BN, and 1:1 of MgO /BN hybrid filler) were manufactured in a similar manner and termed epoxy/MgO, epoxy/BN and epoxy/hybrid, respectively. Furthermore, using the previous method, a neat epoxy coating was manufactured, and finally, the substrate was ready for coating tests[185].

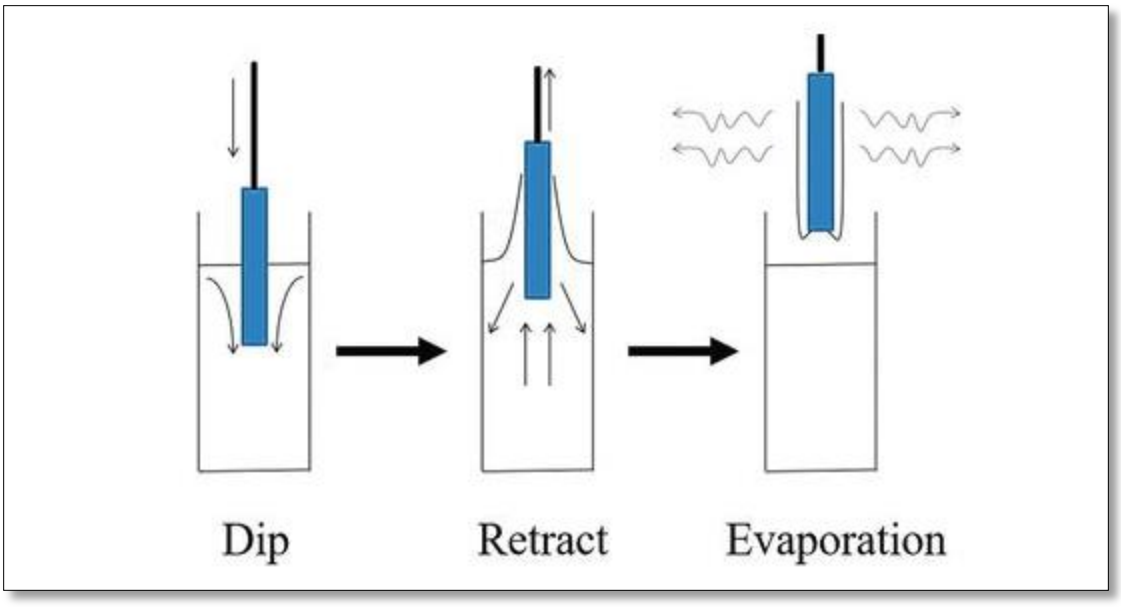

Figure 3.5: A schematic view of the steps in dip coating[185]

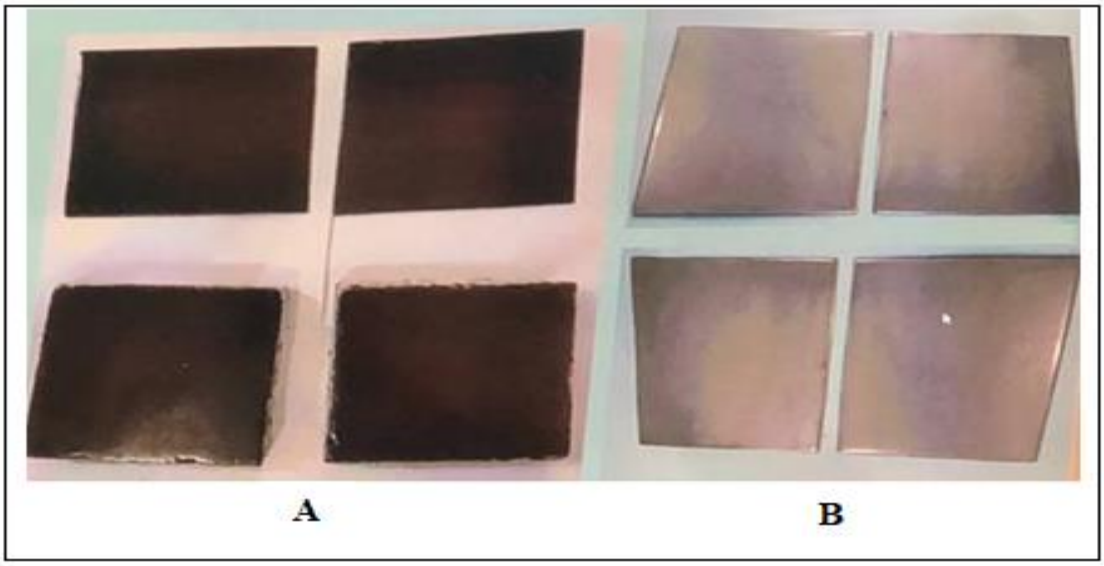

Figure 3.6:Image of Steel substrate (A)before coating (B) after coating.

3.5 Tests

The preparation samples tested using different techniques as shown in Figure (3.7).

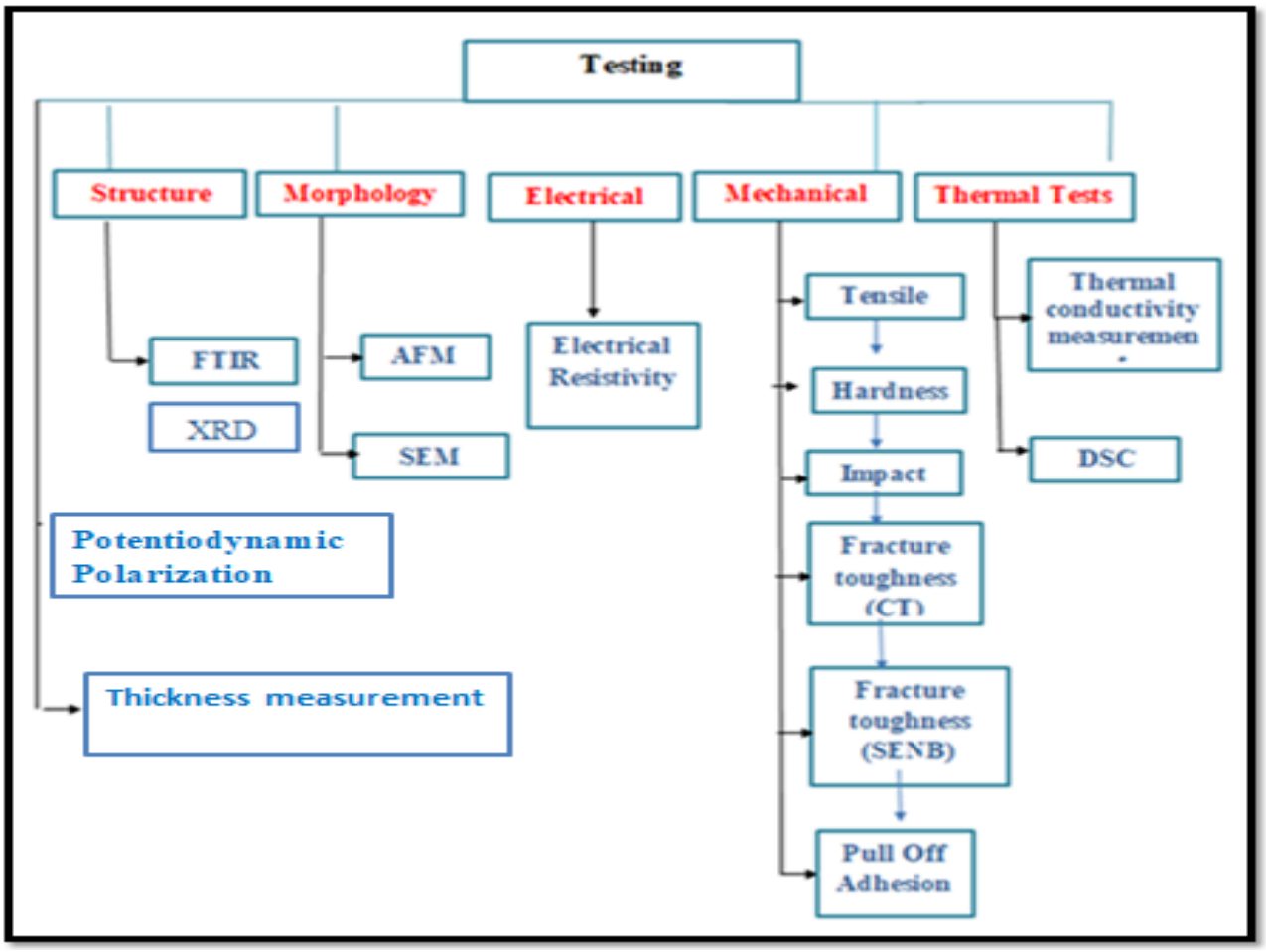

Figure 3.7: Procedure of testing the samples.

3.6 Characterisations

3.6.1 Infrared Fourier Transform Spectrometer (FTIR) Test

Fourier transforms infrared technique used to characterize the prepared samples using instrument type (IR Affinity-1) made in (Kyoto Japan) are located in the laboratory of the Department of polymer Engineering and Petrochemical Industries/Materials Engineering College/University of Babylon . To measure a

sample, use KBr to calibrate the device, They next make a powder out of the test sample and mix it with KBr at a (99%) mixing rate. FTIR spectrum provides a diagram between the permeability or absorption and the number of waves that show the chemical groups of the material. This test is carried out according to ASTM E1252[186]. For epoxy and epoxy/ NPs in order to know the bond between the polymer and fillers, if it is a chemical or physical bond.

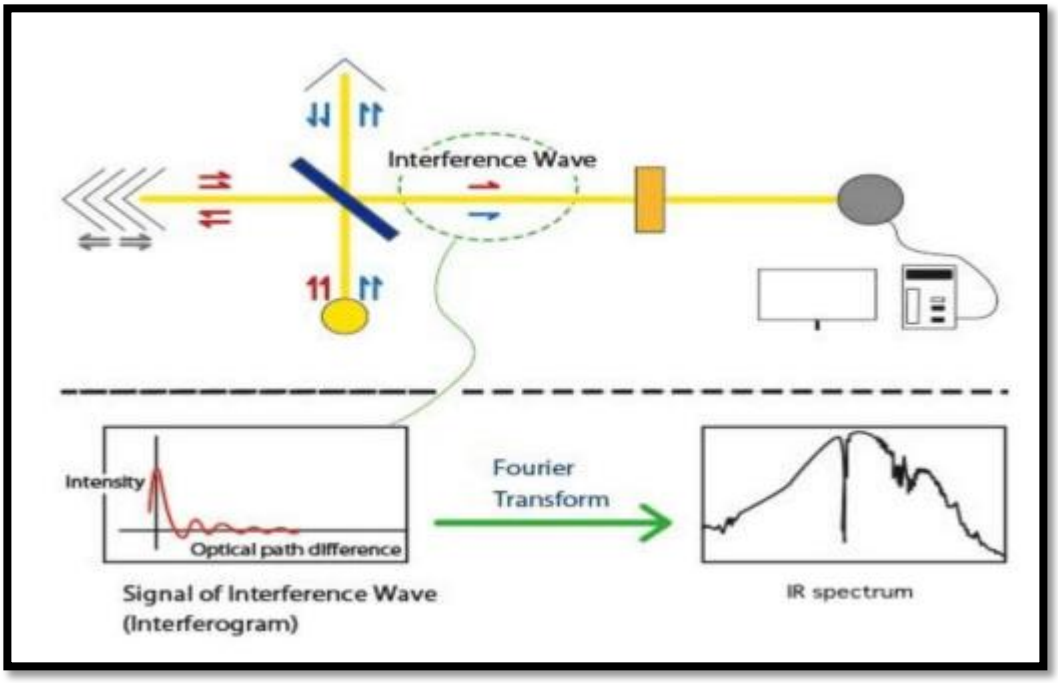

Figure 3.8: Instrument setup for FTIR spectroscopy

3.6.2 X-Ray Diffraction (XRD) Test

It is a rapid analytical technique, primarily used for phase identification of crystalline materials and also can provide information on unite cell dimensions. It is generated in cathode ray tube by heating a filament to produce accelerated electrons toward the target by applying high voltage.

Characterization of Magnesium Oxide and Boron nitride nanoparticles and the structural investigations of nanoparticles were made by X-ray diffraction (XRD) measurement at room temperature by using XRD- system type (XRD- 7000, X- Ray

Diffractometer , using Cu Kα radiation (λ = 1.5405 Å), and a scanning speed of 5θ˚/min from (10ºto 80º)of 2θ to which was located in the laboratories of the Department of Ceramic Engineering /College of Materials Engineering at Babylon University.as shown in figure (3.9)

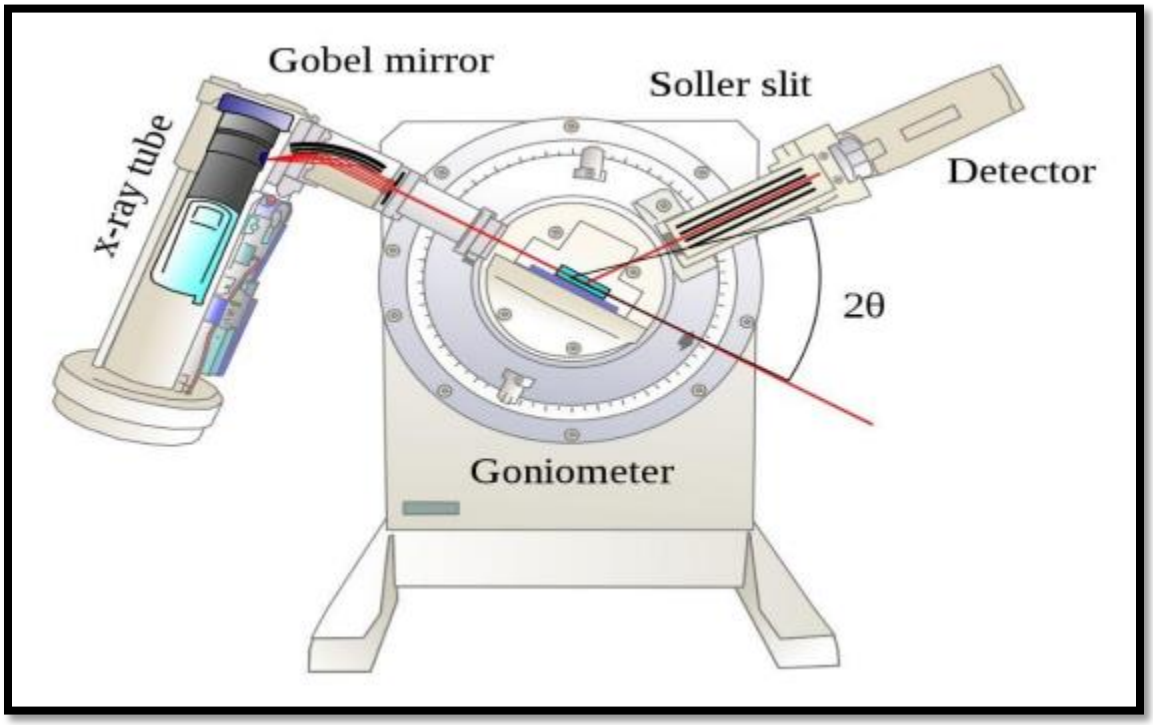

Figure 3.9: A schematic of X-ray diffraction (XRD)

3.7 Mechanical Test

There are many mechanical tests (Tensile, Fracture Toughness(CT,SENB) , Impact , Hardness and Pull Off adhesion) that were used to study the mechanical properties of pure epoxy, and epoxy/MgO, epoxy/BN and epoxy/hybrid nanocomposites .

3.7.1 The Tensile Test:

Tensile samples were manufactured in accordance with ASTM D638 type2 [187].Three specimens of each percent were tested Microcomputer-controlled

electronics universal testing devices developed in China type (WDW-5E). are used for tensile testing and are located in the laboratory of the Department of polymer Engineering and Petrochemical Industries/Materials Engineering College/University of Babylon, see figure (3.11). All of the samples were tested at room temperature with a load cell of 5KN and a speed of 2mm/min. The load was applied until the sample failed, and a stress-strain curve was acquired. The tensile strength and modulus were calculated by using the following equation:-

$$\boldsymbol{Tensile\ Strength} = \frac{\boldsymbol{F}}{\boldsymbol{A}} \quad (3.1)$$

$$\boldsymbol{Tensile\ Modulus} = \frac{\boldsymbol{\Delta\sigma}}{\boldsymbol{\Delta\varepsilon}} \quad (3.2)$$

Where

F = load (N).

A = area of samples (mm^2).

$\Delta\sigma$ = $\sigma 2 - \sigma 1$ the stress (MPa) of samples.

$\Delta\varepsilon$ = ε 2- ε 1 the strain of samples.

E = Tensile modulus.

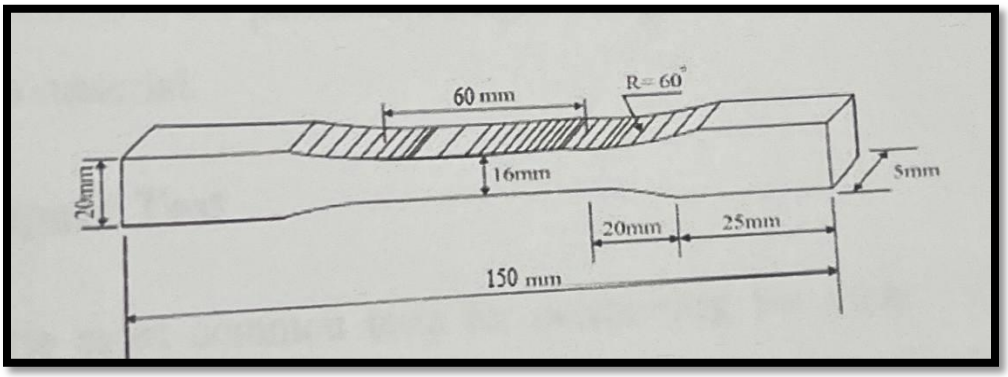

a

b

Figure (3.10) : (a) Schematic tensile specimen (b)Prepared tensile specimens

Figure 3.11: Tensile test Device

3.7.2 Impact Test

Pendulum impact test represents one of the most common tests for determining the impact resistance of plastics. Specimens were prepared according to the ISO 180-1 [188] . Three specimens of each percent were tested, The Figure (3.12) shows standard and experimental un-notched samples.

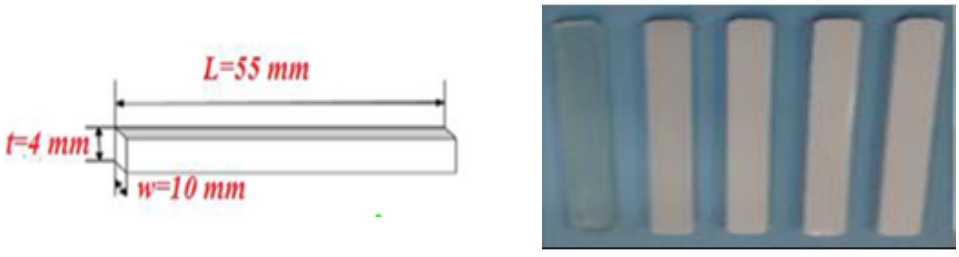

(a) (b)

Figure 3.12: (a) Schematic of impact specimen, (b) experimental impact specimens.

In this test, the specimen was fixed in a cantilever position. The specimen is struck by the arm of a pendulum. The energy absorbed by the specimen in the breaking process is defined as the breaking energy[189]. The breaking energy was measured using a joule unit. Model WP 400 charpy type made in German, pendulum impact tester was employed and located in the laboratory of the Department of polymer Engineering and Petrochemical Industries/Materials Engineering College/University of Babylon, as indicated in Figure (3.13).

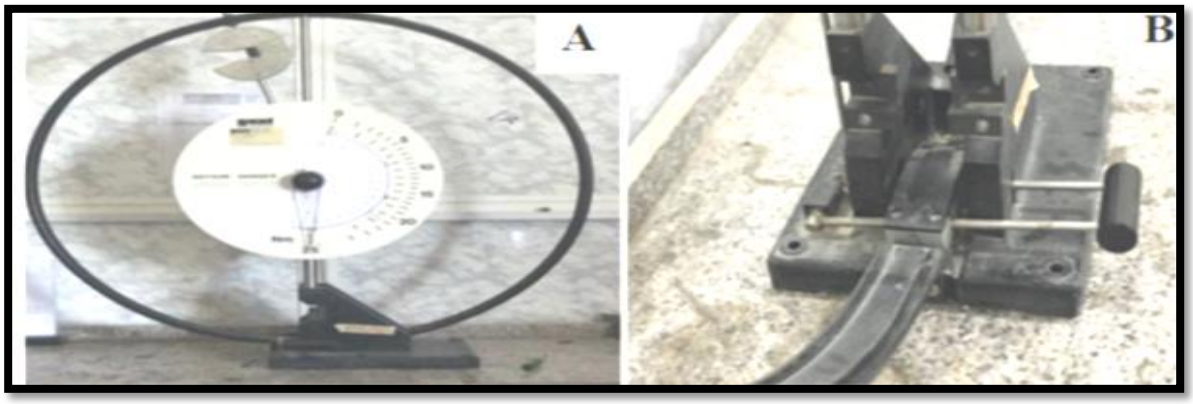

Figure 3.13: Pendulum Impact of (A) Machine for the Test, (B) Specimen Fixation

Fixation of the impact strength in this test were determined by calculating the needed energy for fracture. The following equation is used to determine impact strength: [190].

$$\boldsymbol{Gc = Uc/A} \qquad (3.3)$$

Where:

Gc; Impact strength (J/m^2)

Uc; Energy of impact (J)

A; is an abbreviation for cross-sectional area (m^2).

3.7.3 Hardness

It is well known that the hardness of the materials is determined by their resistance of penetration at the outer surface. Coatings for electronic devices need a high hardness to maintain the surface's appearance and protect the device. Because hardness is a desired attribute for coating resistance and endurance[191].

The samples' hardness was measured using a Model of Shore D hardness device developed in Germany (TH 210 FJ), which is located in the laboratory of the Department of polymer Engineering and Petrochemical Industries/Materials Engineering College/University of Babylon, as seen in the Figure (3.14). With ASTM D2240[192], the Shore instrument is similar to a compass in that it has a needle that is perpendicular to the sample. For each sample, an average result of three readings must be collected in various locations and at various points to achieve some degree of accuracy[193] .

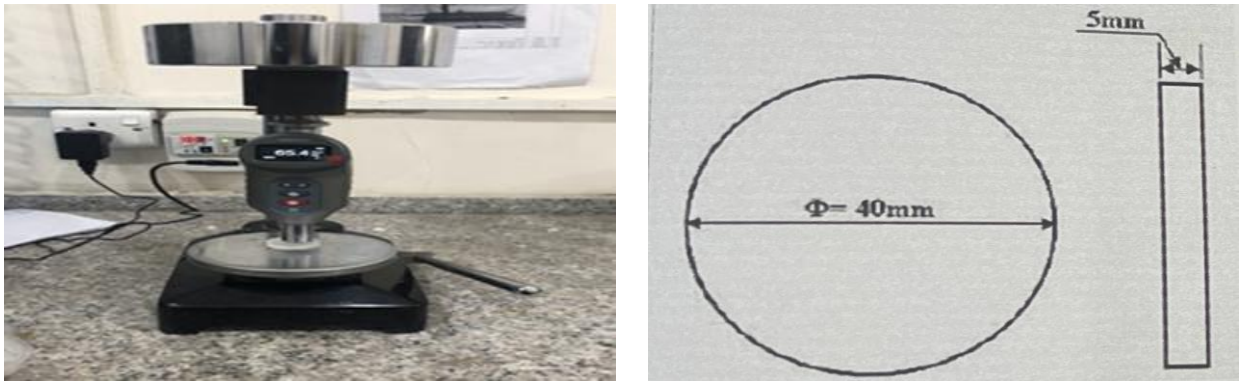

a b

Figure 3.14:(a)Exhibits Hardness Shore D apparatus, (b)Schematic Hardness specimen

3.7.4 Fracture Toughness Tests

For tests of Fracture Toughness (Compact Tension CT) and Single Edge Notched Beam SENB) after completing the preparation process of the samples an incision was made in the center of the original slit of the sample called a

sharp crack introduced by the razor where it was placed on the sample using a certain weight and a force called force of the hand to create an incision as shown in Figure (3.15), used to create an incision that is a stress center with a length of (2mm).

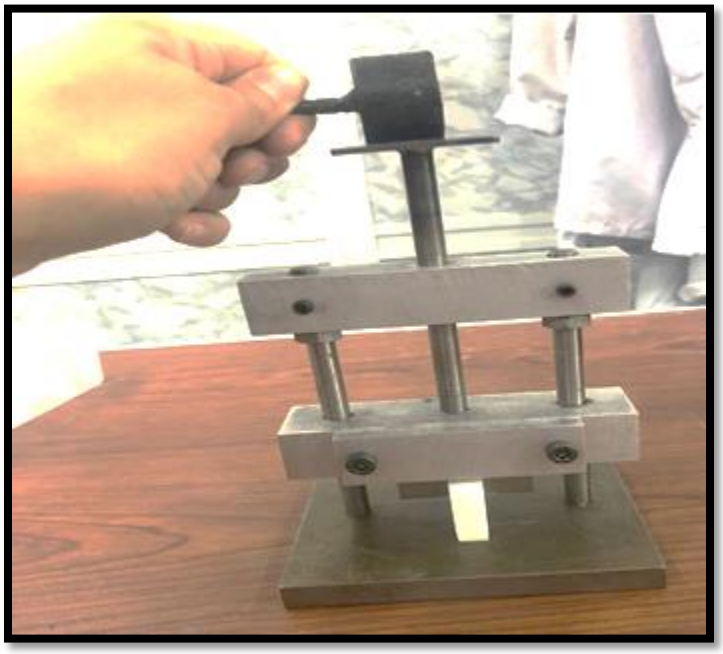

Figure 3.15:Method of Creating Incision for Samples of (SENB and C.T)

3.7.4.1 Compact Tension(C.T) Test

Fracture toughness test was conducted at room temperature according to the ASTM D5045 [194], [195].This type of universal testing machine (WDW/5E) samples was used for the testing, as shown in Figure (3.16A). standard sample geometries, as shown in Figure (3.17). To study the fracture toughness properties, the testing speed was chosen to be 10 mm/min with a 5 kN load cell. The stress intensity factor, K_{IC}, under the plane strain conditions was calculated using the following equation:

$$K_{IC} = \frac{P_{MAX}}{B(W)^{1/2}} f(\frac{a}{w}). \quad (3.4)$$

where

$$f\left(\frac{a}{w}\right)=\frac{\left(2+\frac{a}{W}\right)\left[0.886+4.64\left(\frac{a}{\pi}\right)-13.32\left(\frac{a}{W}\right)^{2}+14.72\left(\frac{a}{w}\right)^{3}-5.6\left(\frac{a}{\pi}\right)^{4}\right]}{\left(1-\frac{a}{w}\right)^{3/2}} \quad (3.5)$$

Where, P is the maximum load, B: the specimen thickness, W: the width, a: the initial crack length, X = a/w ,where (0 < x < 1).

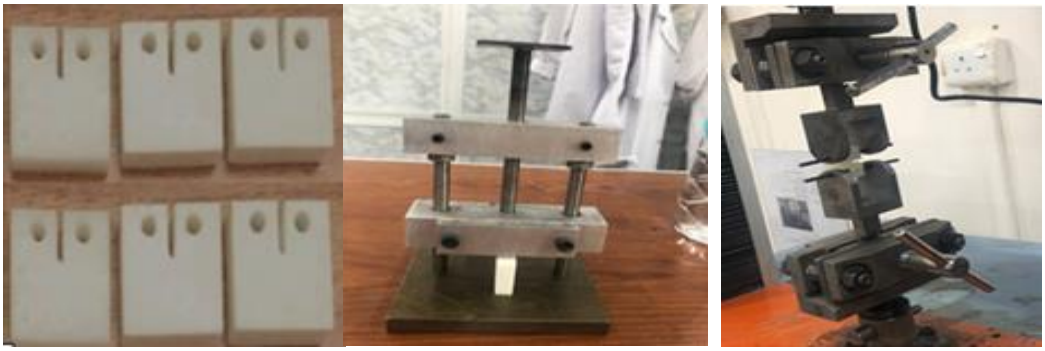

(a) (b) (c)

Figure 3.16:Display (a) Samples Used for Tests, (b): Create Crack, (c):Test

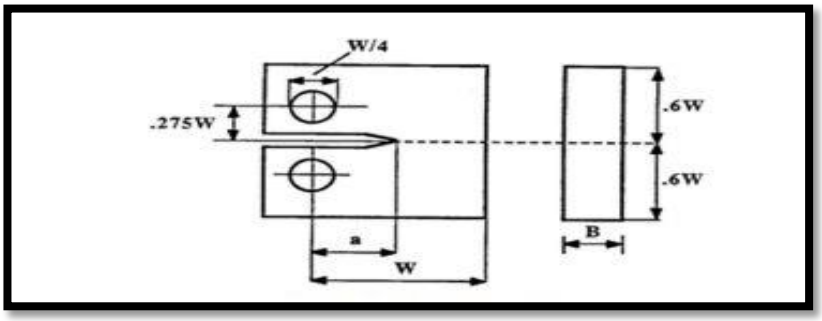

Figure 3.17: Standard Sample Geometries of Compact Tension test[196].

3.7.4.2 Single Edge Notched Beam Test Specimen Fracture Toughness

Single Edge Notched Beam (SENB) test was carried out to investigate the toughness of nanocomposite specimens. They were tested using a universal testing machine type (WDW/5E). Samples were being used for the testing such as shown in the figure(3.19 A). Standard Sample Geometries as shown in Figure(3.19), The cross-head speed was held constant and was chosen (10mm/min), span length was

(40 mm) according to ASTM D5045 [181,182]. The stress intensity factor (K_{IC}) was obtained using the relationships as shown below[199].

$$K_{IC} = \left(\frac{P}{BW^{\frac{1}{2}}}\right) f\left(\frac{a}{w}\right) \quad \textbf{(3.6)}$$

where (0 < x < 1), P is the critical load for split propagation, B is the specimen thickness, W is the specimen width, a is the crack length, and f (x) is a non-dimensional shape factor with x = a/W.

$$f(x) = 6x^{1/2}\,\frac{[1{,}99 - x(1-x)(2{,}15 - 3{,}93x + 2{,}7\,x^2)]}{(1+2x)(1-x)^{3/2}} \quad \textbf{(3.7)}$$

(a) (b) (c)

Figure 3.18: Image of (a): samples used for tests, (b): create crack,(c):test.

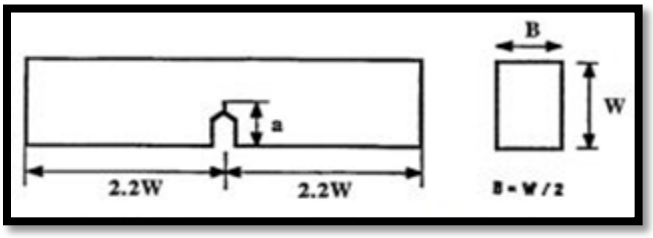

Figure 3.19 : Standard Sample Geometries of SENB Test .

3.7.5 Pull Off adhesion Test:

Adhesion is a complex property that depends on many different factors such as the properties of the coatings and substrates,surface roughness,type and content of addhesive material interfacial interactions or environmental conditions [200] .

The pull-off adhesion strength of coating systems was tested using the ASTM D4541 standard. There are several steps that were taken before coating and testing all steel substrates were grinding by sand paper. All grinding steel surfaces were cleaned using acetone to remove grease or oil contamination of the surfaces before application of each coating system. The substrates were coated with epoxy coating and epoxy with nanoparticles. The general pull-off adhesion test is performed by scoring through the coating down to the surface of the steel substrate at a diameter equal to the diameter of the loading fixture (dolly, stud) and securing the plate with an adhesive [184, 185].

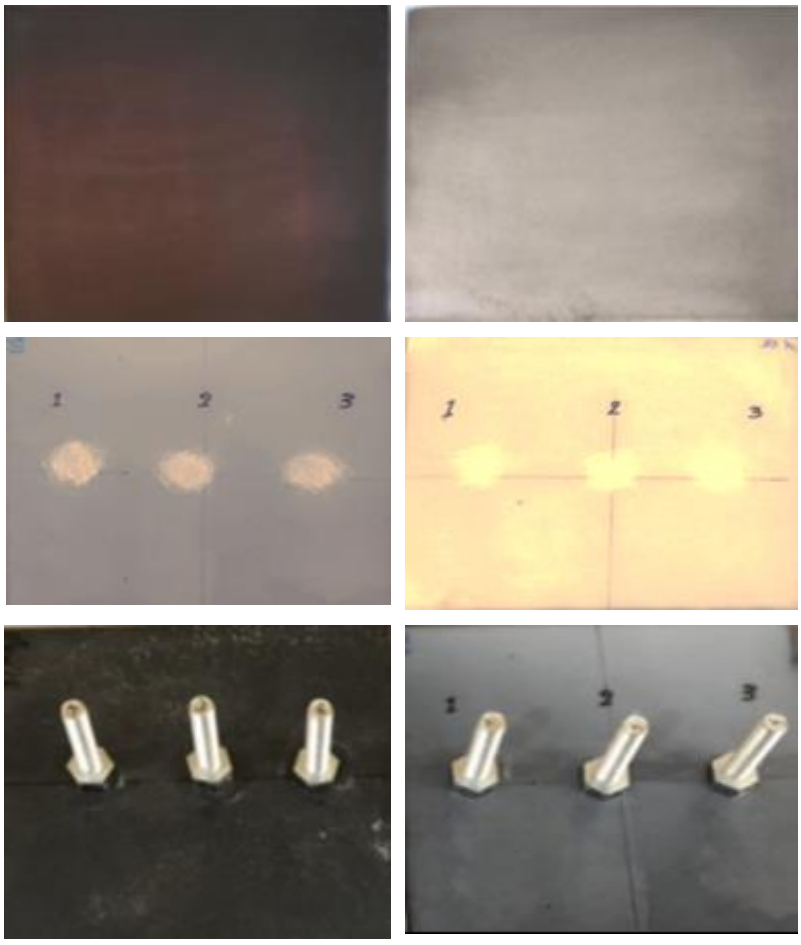

Figure 3.20: Image of pull off adhesion samples.

The nature of the failure was qualified in accordance with the percent of adhesive and cohesive failures and the actual interfaces and layers involved. After the adhesive was cured, a testing apparatus was attached to the loading fixture and aligned to apply tension normally to the test surface. When a plug of material is detached, the exposed surface represents the plane of limiting strength within the system.

The pull-off adhesion strength was computed based on the maximum indicated load the instrument calibration data and the surface area stressed. Pull-off adhesion strength calculated using the following formula:

$$\mathbf{X = 4F/\pi d^2} \qquad \textbf{(3.8)}$$

where:

X = The pull-off adhesion strength achieved at failure in MPa.

F = The maximum force applied to the test surface at failure in (N).

D = The diameter of the loading fixture in(mm)

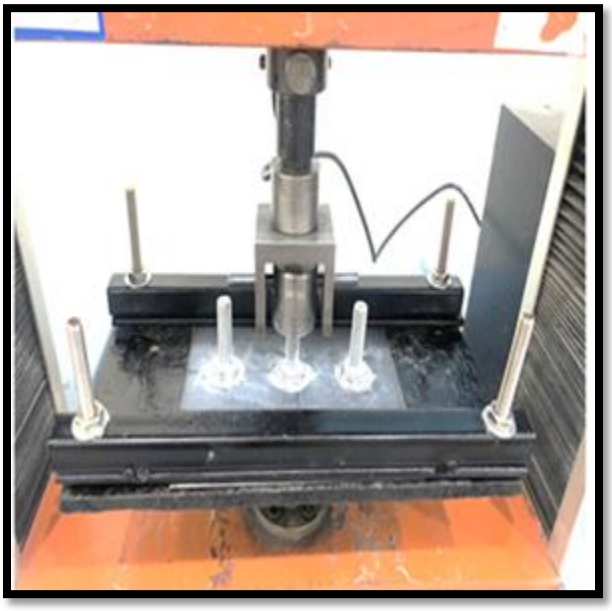

Figure 3.21: Image of the Pull-Off Adhesion test device.

3.8:Mophological test

3.8.1 Field Emission Scanning Electron Microscopy (FE-SEM):

The dispersion of (MgO , BN and (1:1of MgO / BN) hybrid nanoparticals, in the epoxy matrix (EP) samples, was tested by the model (SUPRA 55-VP-48-06) analytical field emission scanning electron microscopy (FE-SEM)[203]. It was used to evaluate the morphology of polymer nanocomposites at Tehran University in Iran. All samples were sputtered with gold from the surface to the edge to produce considerable electrical conductivity. The apparatus is depicted in Figure (3.22).

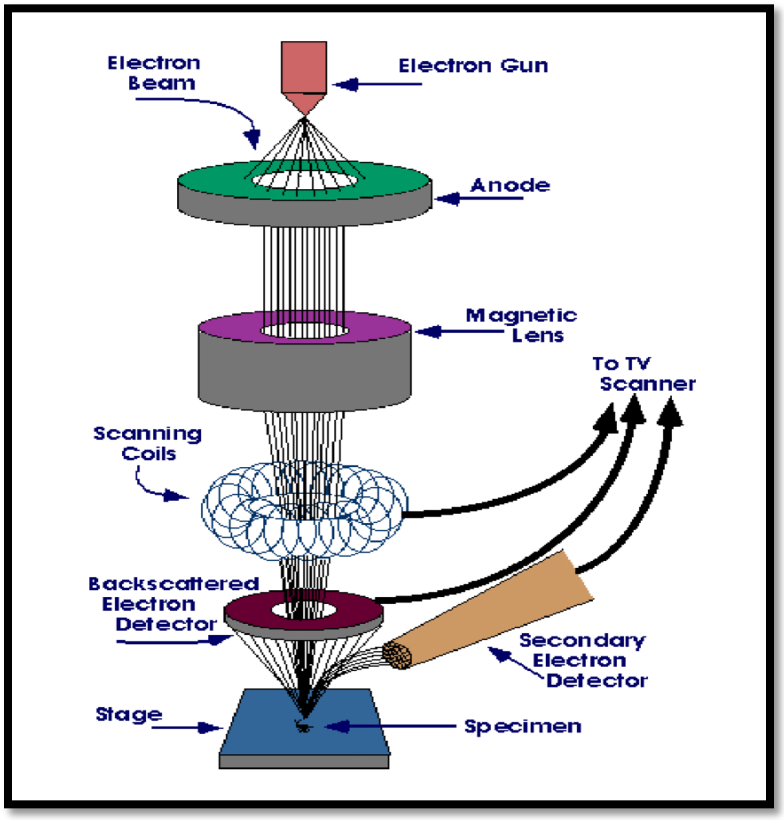

Figure 3.22: The principle of FESEM

3.8.2 Atomic Force Microscopy (AFM) Test

Topography and other properties of surfaces can be determined using an atomic force microscopy (AFM) technique. The principle of AFM is based on mechanical

contact between the surface of the sample and the tip so the measurement of particles in the nanoscale is strongly affected by surface sample-tip interaction. The morphological investigations were conducted for pure and nanocomposite materials by tapping model AFM (AA3000) in the laboratory of the Department of polymer Engineering and Petrochemical Industries/Materials Engineering College/University of Babylon. As illustrated in Figure (3.23).

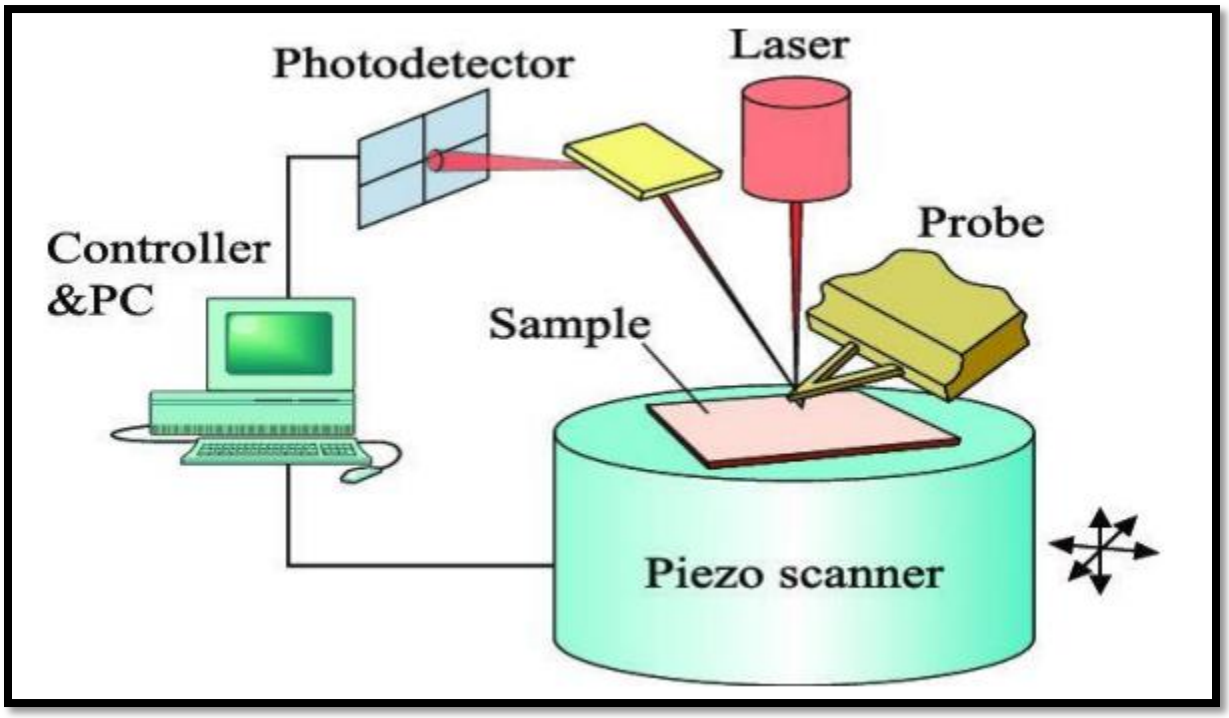

Figure 3.23: The Schematic drawing of AFM.

3.9 Thermal Testes:

3.9.1 Thermal conductivity Test

The effect of (MgO, BN) and (1:1of MgO / BN) hybrid NP on the thermal characteristics of epoxy at 100 ^{o}C is investigated using the thermal coefficient tester model (YBF-3) with top and bottom copper plates, which was located in the

laboratories of the Department of Ceramic Engineering /College of Materials Engineering at Babylon University, The test was carried out in accordance with ASTM E1530-99[204]. The samples were be manufactured at 50 mm in diameter and 10 mm in thickness as seen in Figure (3.24). Furthermore, Figure (3.25) shows thermal conductivity apparatus.

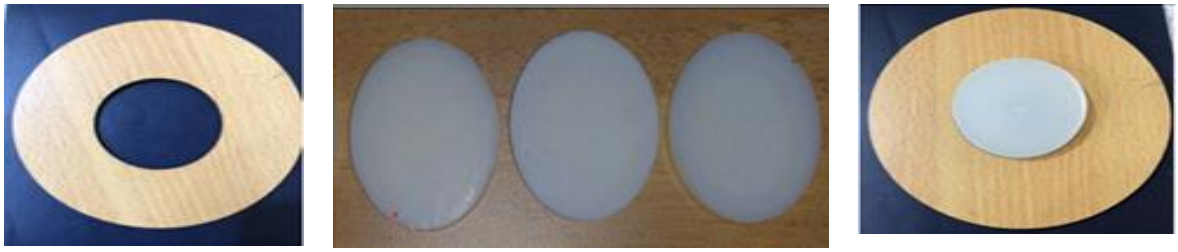

Figure 3.24:Thermal conductivity samples.

Figure 3.25: Thermal conductivity apparatus.

The test process is illustrated below:

1- Place the sample between the top and lower copper plates, ensuring good contact without being too tight or too loose.
2- Setting the temperature controller to 100 ^{o}C and switching to automatic control.
3- Switch off the heater and begin recording (T1), (T2) every two minutes until (T2) is relatively stable (the function is less than 0.01 mV) and (T2) stays constant.
4- Remove the sample and adjust the position of the top plate so that it makes an excellent contact with the bottom plate, then heat the lower copper plate disk to a temperature that is about 10 ^{o}C higher than the copper plate.
5- Remove the upper copper plate, exposing the entire lower surface to the environment and allowing it to cool naturally.
6- Take a temperature reading each 30 seconds.
7- Using the following formula(1) to calculate the thermal conductivity(λ)of the samples:

$$\boldsymbol{K} = (\boldsymbol{m} * \boldsymbol{c} * \frac{\boldsymbol{hB}}{\boldsymbol{\pi}} * (\boldsymbol{RB})^{2} * (\boldsymbol{v1} - \boldsymbol{v2})) * (\boldsymbol{2hp} + \boldsymbol{Rp})/(\boldsymbol{2Rp} + \boldsymbol{2\ hp})(\ \Delta\mathbf{V}/\ \Delta\boldsymbol{t}) \qquad \textbf{(3.9)}$$

Where

Where: K: thermal conductivity coefficient (w/m.k).

m: mass of copper plate (0.824 kg).

c: specific heat capacity of copper plate is 3.805*102 (kj/kg.k).

hp, Rp: thickness and radius of copper plate are(7.01mm,65 mm respectively).

R: radius of specimen is 10mm.

v1,v2: voltage of thermocouple 1,2 at heating.

Δv: difference in voltage at cooling.

Δt : difference in time at cooling.

3.9.2 Differential Scanning Calorimeter (DSC) Test :

The test was carried out in accordance with ASTM D3418-03[205], using the SH1MADZ-4 DSC-60 apparatus, which was located in the laboratory of the Department of polymer Engineering and Petrochemical Industries/Materials Engineering College/University of Babylon, as shown in Figure (3.26). Pure epoxy and epoxy/MgO NPs, epoxy/BN NPs, and epoxy/hybrid NPs were evaluated in powder form and a heating rate of 10 ^{0}C/min with a heating range of 25 to 300 ^{0}C .

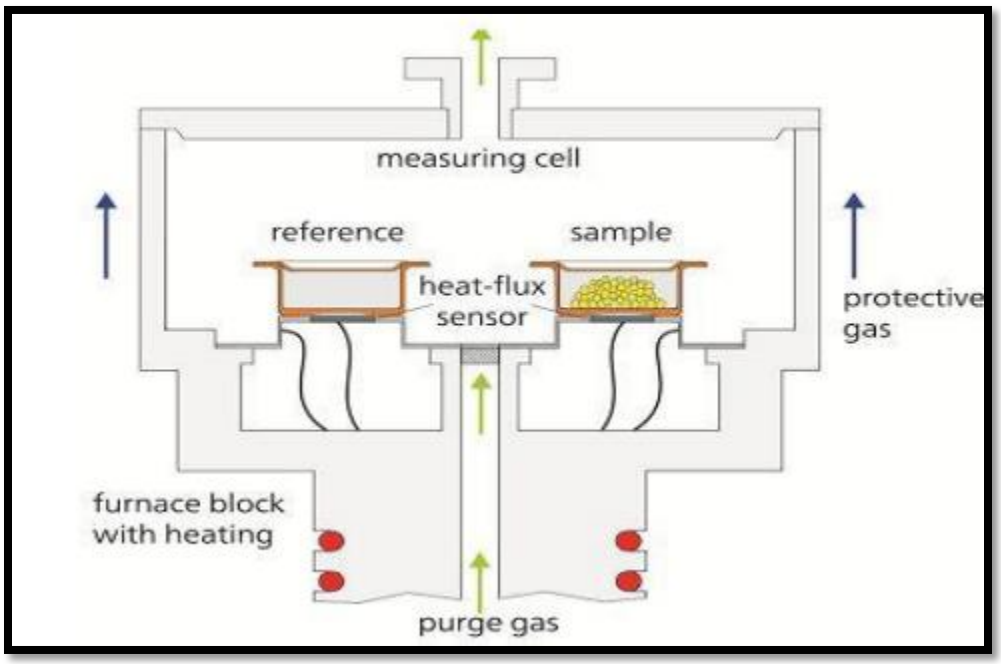

Figure 3.26: schematic of Differential Scanning Calorimetry (DSC)

3.10 Electical Testes:

3.10.1 Electrical Resistivity :

At room temperature samples electrical resistivity was measured using a Precision Ohmmeter model (ATS12) insulation tester in accordance with ASTM D257-14 [206], which was located in the laboratories of the Department of Polymer Engineering and Petrochemical Industries/College of Materials Engineering at Babylon University. It was used to measure the impact of fillers loading on the

electrical properties of epoxy. Pieces of 12 * 12 * 2.3 mm^3 were essayed between two stainless steel electrodes. The test process is illustrated below:

1. Connecting the apparatus to the electrical cercal.
2. The device's poles will be connected to the inspection cell.
3. Inserting the sample into the cell.
4. The number of (R) that appears on the device's screen will be recorded.
5. Calculating the (ρ) is from the equation :

$$\boldsymbol{\rho = (R.A)/(L)} \qquad (3.10)$$

Where

ρ: The electrical resistivity (Ω.cm)

R: The electrical resistance (Ω) that appears on the device's screen will be recorded

A:The cross section area(cm^2)

L : The length (cm).

Figure 3.27: Electrical Resistivity apparatus.

3.11. Electrochemical Test(Corrosion Test):

3.11.1. Solutions

The solution employed in this study was a blank solution within a NaCl prepared by dissolve 3.5g of NaCl in one liter water aqueous solution[207].

3.11.2 Potentiodynamic polarization

The corrosion behavior of all specimens was observed. Following the casting of nanofiller on the substrate, all specimens were tested in a 3.5 NaCl solution as an electrolyte. The corrosion rate was calculated using the tafel extrapolation method. This cell had three electrodes: one for the specimen and two for the counter and reference electrodes, which represented the platinum and saturated calomel electrodes, respectively. All of the electrodes were connected and immersed in the electrolyte. The thermometer was employed to maintain the solution's temperature at 25 $^{\circ}$C. The voltage of each specimen was measured in an open circuit at the start of the specimen test. Figure 3.28 depicts a thepotentiostatic instrument (type X MTD-2MA) (3.28). It's in the Metallurgical Department of the College of Materials Engineering at the University of Babylon. The test was carried out by potential stepping at 0.4 mV/s as a scanning rate from a starting 250 millivolts below the open cercuit potential. The scan was sustained up to 250 mV above the open-circuit voltage. The efficiency of inhibition (I) was calculated from the polarization curves using Eq. (3.11) according to [ASTM G102] [208] to evaluate the efficiency of an epoxy/MgO, epoxy/BN, and epoxy/hybrid nanocomposite for controlling the dissolving of steel.

$$I\,\% = \frac{icoor - icoor(film)}{icoor} * 100 \qquad 3.11$$

where:

icorr and icorr (film) and are the abbreviations of the values of the corrosion current density measured by (μAcm^{-2}) for bare and coated steel, respectively.

Figure 3.28: Potentiodynamic polarization test device

3.12 Coating Thickness Measurements:

A digital gage TT260 type as in Figure 3.30 was used so as to measure the thickness of the coating layer for all coated specimens (in the Lab of Metallurgical Engineering Department, /College of Materials Engineering, University of Babylon). The accuracy of this device is ± 0.1 μm. Three different measurements were taken for each specimen, and the average thickness was calculated.

Figure 3.29 Digital coating Thickness-TT260

Chapter Four
Results
and
Discussions

4.1 Introduction

This chapter illustrates the results obtained through the results of physical, morphology, mechanical,thermal,electrical,tribological tests of the preparing samples from (Mgo,BN,hybrid) nanoparticals, with different concentrations of nanoparticals in order to improve the thermal conductivity,electrical resistivety , mechanical, tribological properties of prepared samples . This chapter includes the following axes:

1. Studying the structural properties by XRD and FTIR technique.
2. Studying the morphological properties by AFM and SEM techniques .
3. Studying the mechanical properties of the prepared samples , which included measuring the tensile strength, young modulus ,elongation ,Impact strength, fracture toughness (K_{1C},K_{11C}),Pull Off Adhesion and hardness .
4.Studying the thermal properties by DSC and thermal conductivity measurement.
5. Studding the electrical properties by electrical resistivity measurement.
6.Studying the tribological properties by potentiodynamic polarization test.

4.2 Structural Results

4.2.1 FTIR results

Infrared FTIR was used for the characterization of nanoparticles and epoxy nanocomposites as seen in Figures (4.1) and (4.2) and Table (4.1) in appendix A. Figure (4.1) shows the FTIR spectra of pure epoxy, pure MgO NP and pure BN NP and Figure (4.2) display FTIR spectra of epoxy/MgO , epoxy/BN and epoxy/hybrid nanocomposites.

In Figure (4.1 a) shows the FTIR spectra of pure epoxy where band at 3500 cm^{-1} refers to O-H stretching ,band at 3057 cm^{-1} refers to Stretching of C-H of the oxirane ring,band at 2965- 2075 cm^{-1} refers to StretchingC-H of CH_2 and CH aromatic and aliphatic,band at 1604 cm^{-1} refers to Stretching C=C of aromatic

rings ,band at 1509 cm^{-1} refers to Stretching C-C of aromatic band at 1459.95 cm^{-1} refers to C-H bending bond,band at1212,1033 cm^{-1} refers to Stretching C-O of oxirane group,band at925 cm^{-1} refers to Stretching C-O-C of ethers,band at831 cm^{-1} refers to stretching C-O-C of oxirane group and band at 772 cm^{-1} refers to Rocking CH_2. In Figure (4.1 b) shows the FTIR spectra of pure MgO where band at 1381.03 cm^{-1} refer to C=O and band at 408.9 cm^{-1} refer to Mg-O .

In Figure (4.1 c) shows the FTIR spectra of pure BN where band at1388.75cm^{-1} and band at 802.39 cm^{-1} refers to B-N.

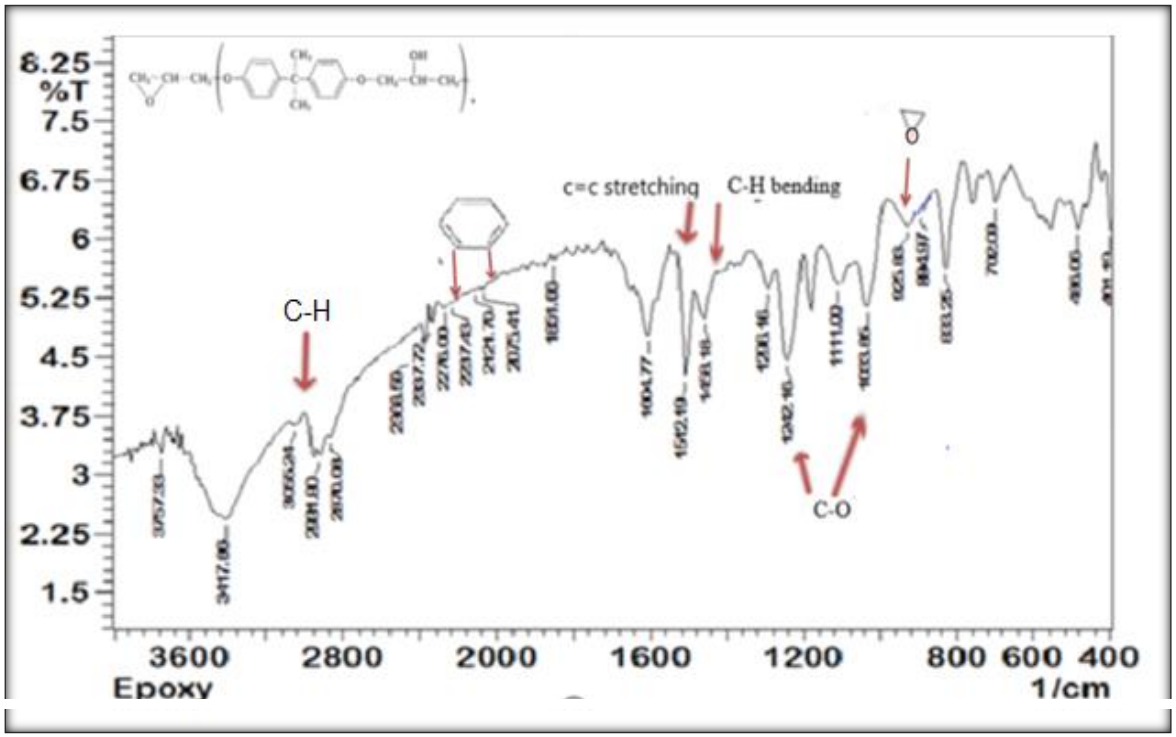

(a)

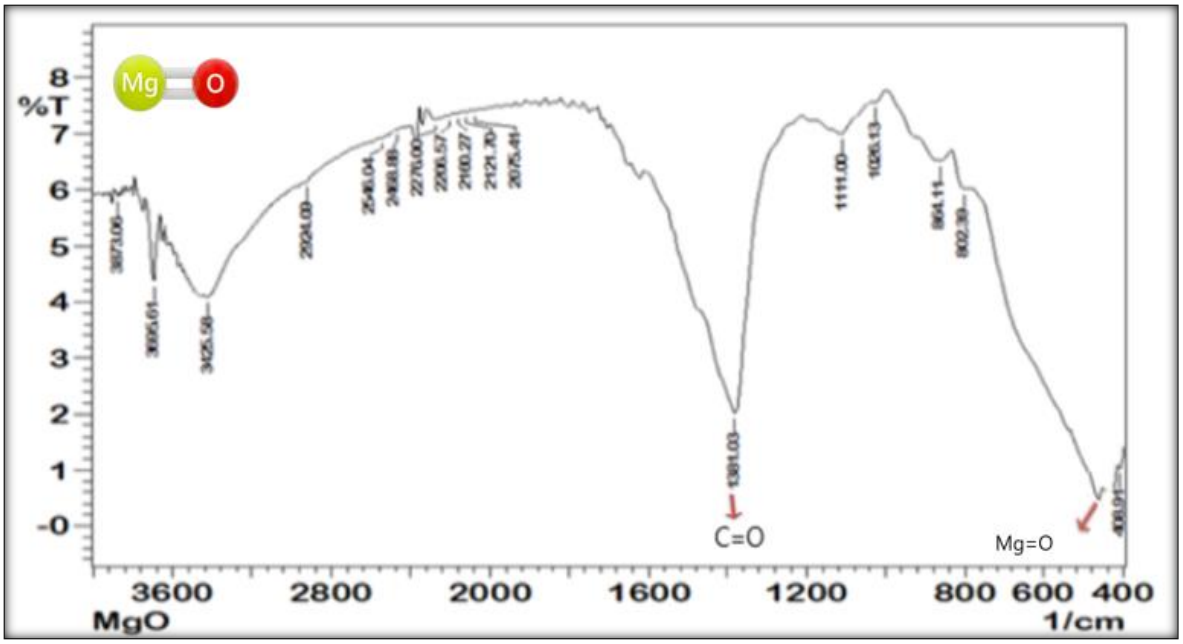

(b)

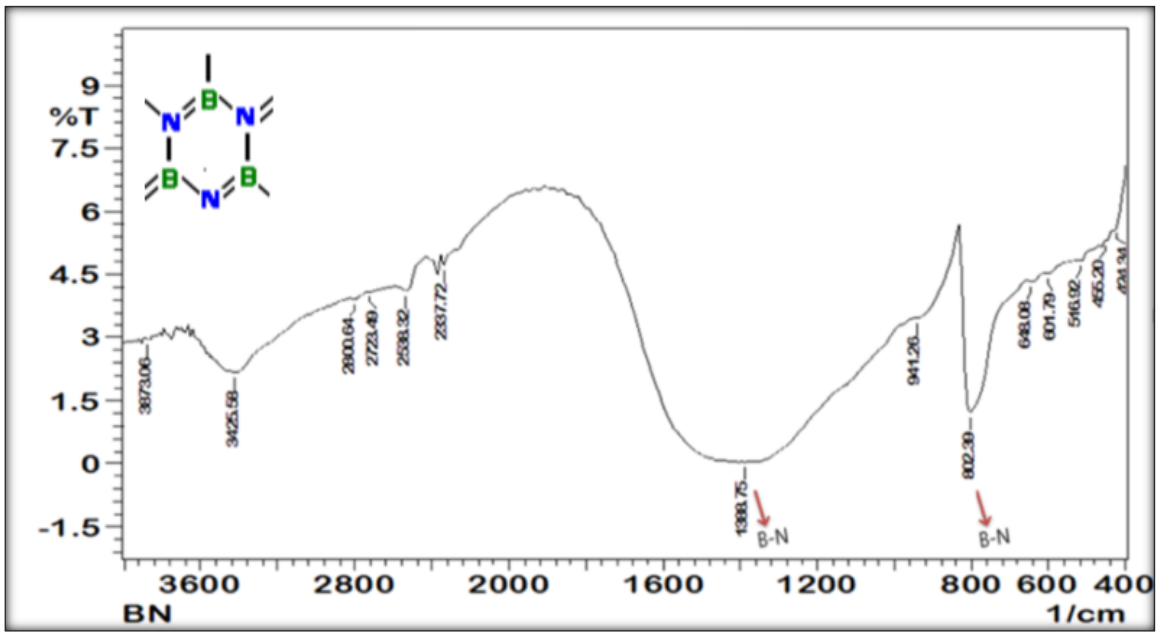

(c)

Figure 4.1: FTIR spectra of, (a):pure epoxy ,(b) pure MgO,(c) pure BN.

In Figure (4.2) display FTIR spectra of epoxy/MgO , epoxy/BN and epoxy/hybrid nanocomposites. Some of the bands and their corresponding

stretching frequencies are listed in table 4.1in appendix A .FTIR results, also show that there is no chemical reaction, no displacement of peeks and no new peek.

There is only the physical interaction between the active surface of nanoparticles and the polar matrix of epoxy polymer, This is because of the similarity of the structure in all weighing percent % of filler loading.

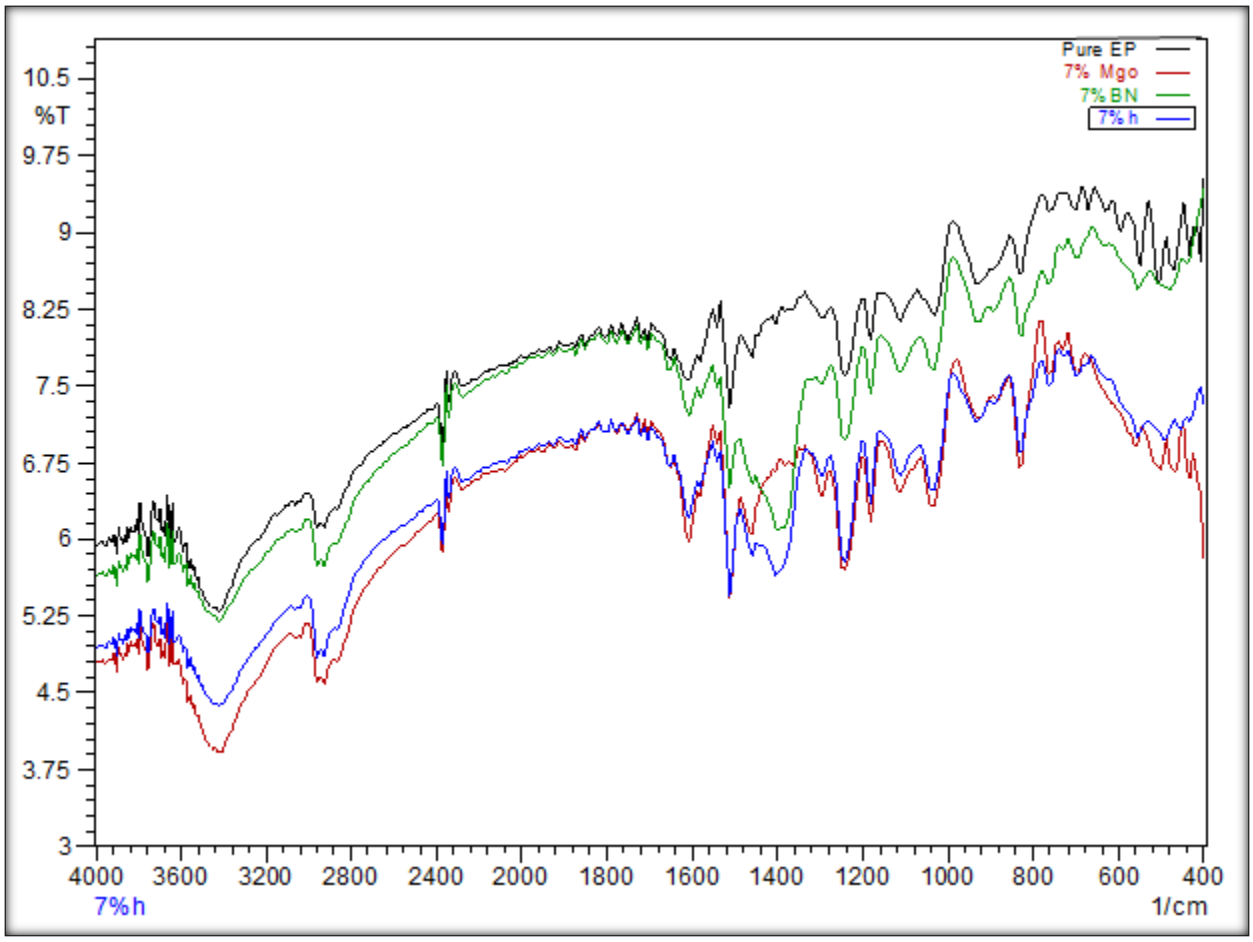

Figure 4.2: FTIR spectra of pure epoxy and epoxy with 7 wt% of (MgO, BN,hybrid) nanoparticles

4.2.2 XRD results

The XRD pattern of the MgO and BN NPs is shown in Figure 4.3 and 4.4 . All of the reflection peaks in this Figures can be easily indexed to pure cubic phase of MgO and to pure hexagonal phase of BN.

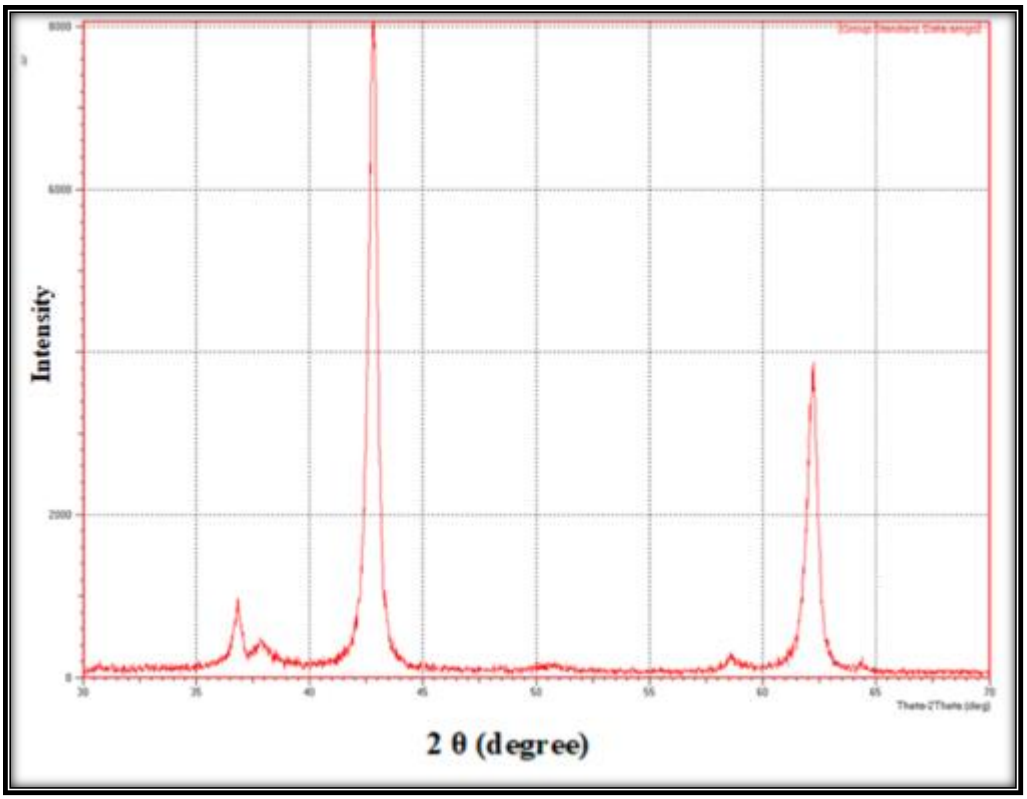

Figure 4.3: X-ray diffraction pattern of Magnesium Oxide (MgO) nanoparticles*[209]*.

The XRD pattern of the MgO NPs is shown in Figure 4.3. shows abroad peak around 2θ = 42.5^{o} and a small another at 37^{o},38 ^{o} ,58 ^{o},62.5 ^{o} .All of the reflection peaks in Figure 4.3 can be easily indexed to pure cubic phase of MgO (JCDPS No. 75- 0447).The crystallite size diameter (D) of the MgO nanoparticles has been calculated by Debye– Scherrer equation ($D = K\lambda/\beta\cos\theta$), where β FWHM (full-width at half-maximum or halfwidth) is in radian and θ is the position of the maximum of diffraction peak, K is the so-called shape factor, which usually takes a value of about 0.9, and λ is the X-ray wavelength (1.5406 Å for Cu Kα). Crystallite size of MgO has been found to be 1.75 nm.

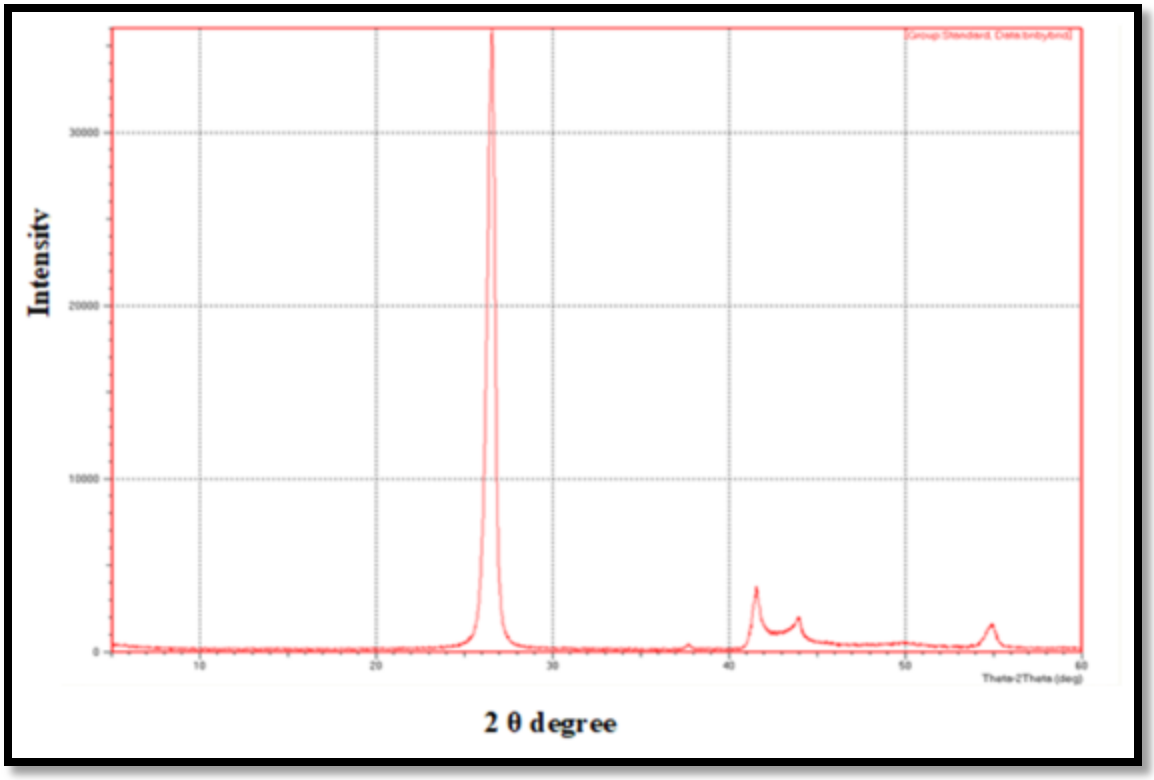

Figure 4.4:X-ray diffraction pattern of boron nitride (BN) nanoparticles[210]**.**

Structural analysis of the BN nanoparticles that it made with the x-ray diffraction (XRD) show highest peak around 2θ = 27.3 ^{o} showed in Figure.4.4 which refers to crystallinity degree of h-BN . Some of the other reflections at 2h = 41.3 ^{o} ,43.4 ^{o} and 54.6 ^{o} detected in the XRD pattern and this result correlate with the literature [210]. In addition to the grain sizes of the boron nitride nanoparticles are calculated by using Scherrer formula (D = 0:9 λ/ βcos θ), the calculated D value is 2.93 nm.

4.3 Morphological Result for Epoxy/Nanoparticals

4.3.1 AFM results

4.3.1.1 Epoxy/MgO Nanocomposite

To get further information for the effect of NP on the morphology of EP, 3D AFM images were taken and are presented in figure 4.5. Also, table 4.2(in

appendix B) shows the roughness parameters, which extracted from the 2D AFM images. Image of the pure polymer, shows that, pure epoxy is smooth with an roughness average (S_a) of 1. 5 nm, and when MgO was added, the surface topography changed and S_a increased to 2.43 nm,2.83nm,3.27nm,3.74nm for (1,3,5 and7 wt%) MgO additions, respectively. That means the final roughness increment. Similar increment (but with less extent) in the density of summits (S_{ds}), where this roughness parameter increases by MgO addition. This is due to the settling of some of MgO Nps on the epoxy surface.

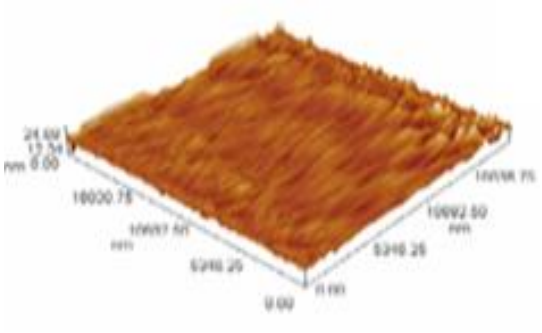

epoxy

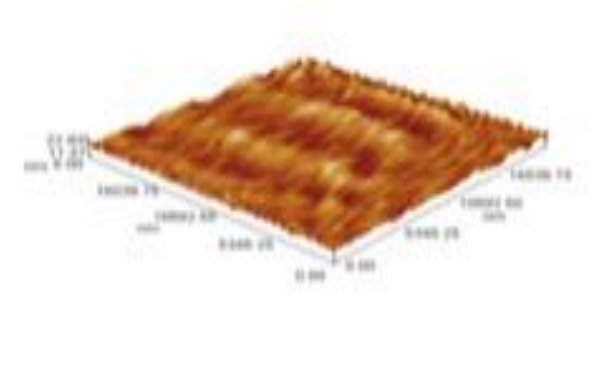

(a)

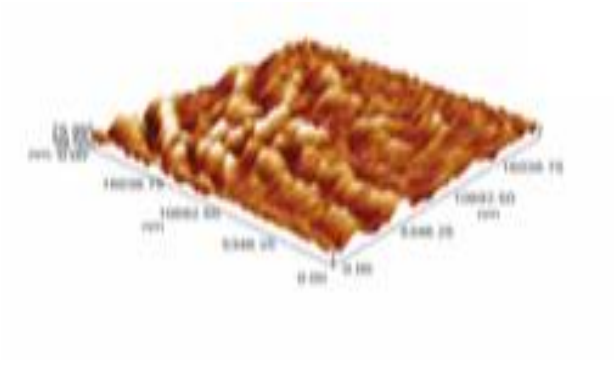

(b)

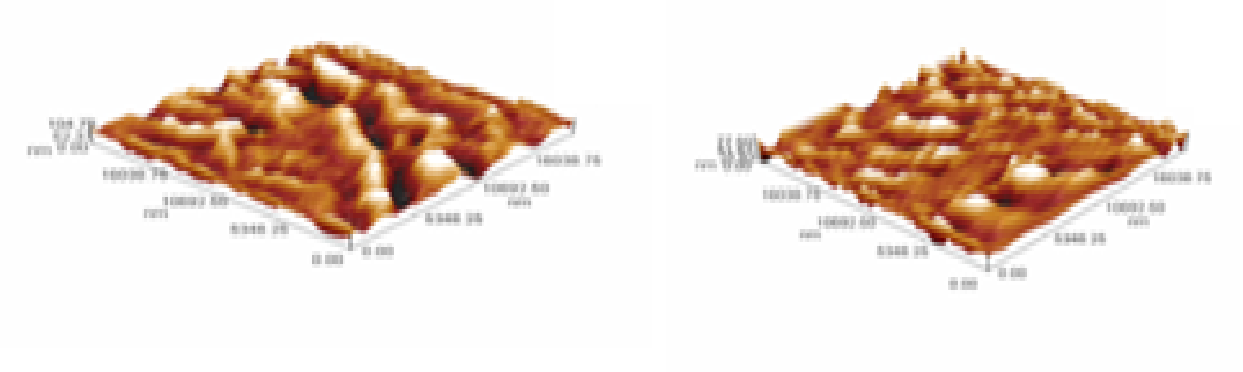

(c) (d)

Figure 4.5: AFM images of pure epoxy and (a) 1% , (b) 3 % ,(c) 5%, (d) 7 % wt)of epoxy/MgO nanocomposite.

4.3.1.2 Epoxy/BN Nanocomposite .

Figure (4.6) and Table (4.2) in appendix B show the roughness parameters of (epoxy/BN)nanocomposite the results show that pure epoxy surface is smooth with a roughness average (Sa) of 1.5 nm, and when BN Np concentration was increased the surface topography changed , Sa increased and this is applied to density of summits (S_{ds}) and surface bearing index (S_{bi})also[211].

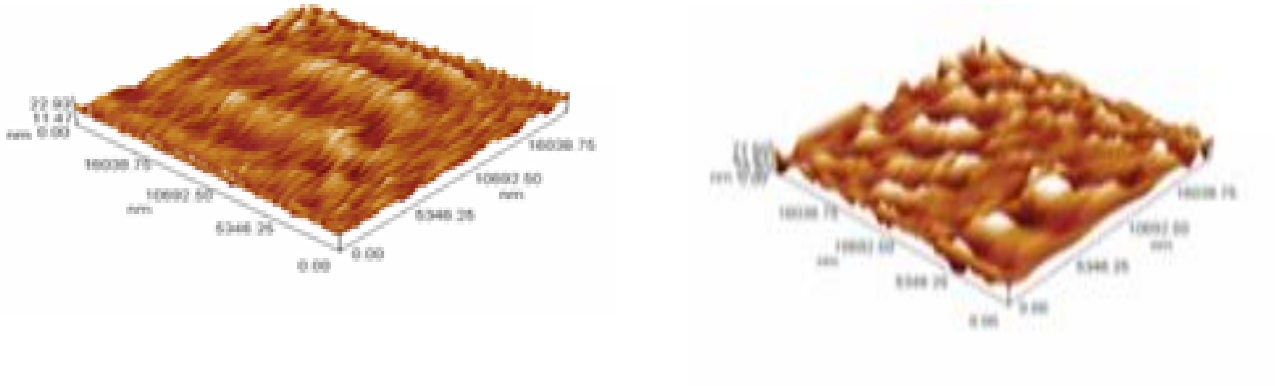

(a) (b)

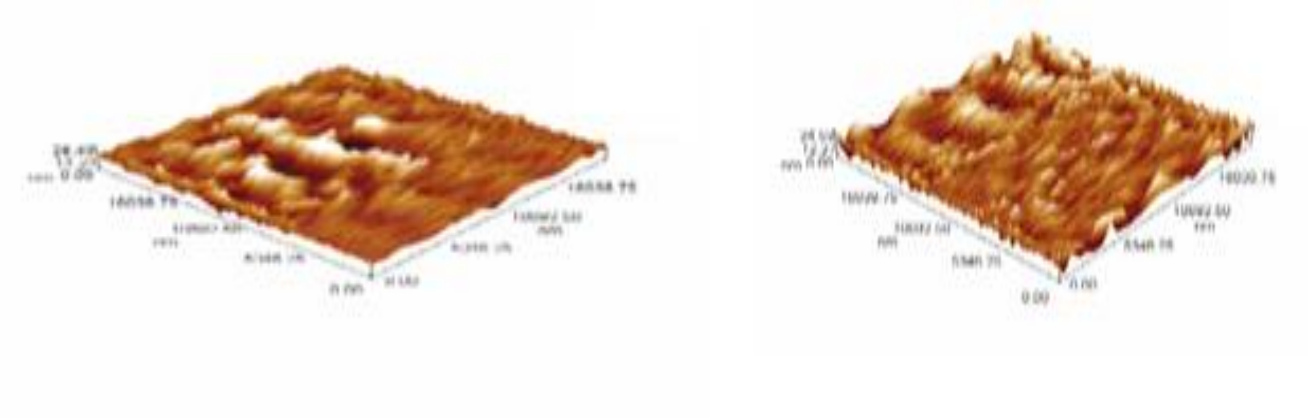

(c) (d)

Figure 4.6: AFM images of pure epoxy and (a) 1% , (b) 3 % ,(c) 5%, (d) 7 % wt)of epoxy/BN nanocomposite.

4.3.1.3 Epoxy/hybrid Nanocomposite.

The image (Figure. 4.7) and table (4.2) in appendix B demonstrate that there is good interfacial interaction between hybrid filler and epoxy matrix which may be the source of good thermal and consistent mechanical properties. The surface homogeneity is quite evident in image at pure epoxy. Also the presence of these hybrid particles (MgO and BN) results in surface roughness, Sa increased and this is applied S_{ds} and S_{bi} also.

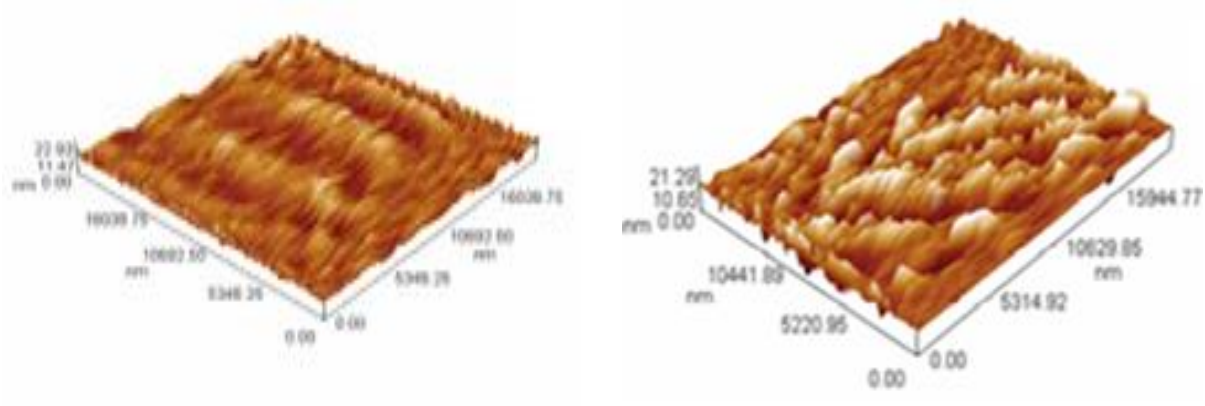

(a) (b)

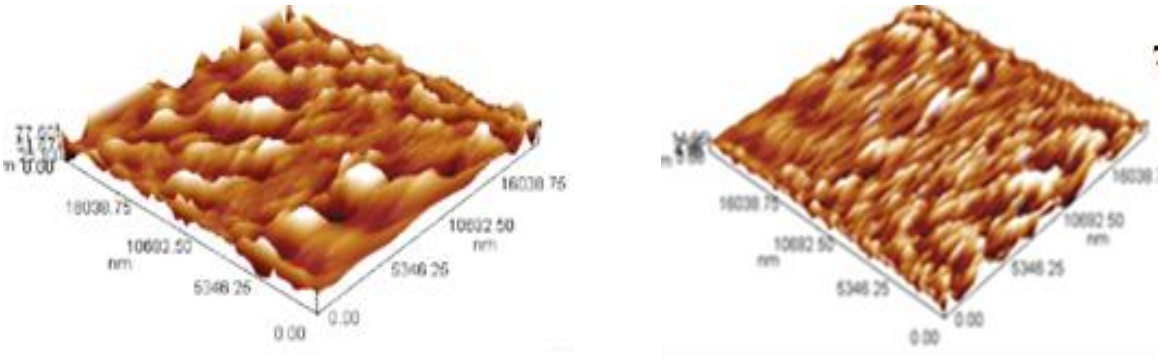

(c) (d)

Figure 4.7: AFM images of pure epoxy and (a) 1% , (b) 3 % ,(c) 5%, (d) 7 % wt)of epoxy/hybrid nanocomposite.

4.3.2 FE-SEM Results

Figures (4.8-4.11) show the field emission scanning electron micrographs (FE-SEM) images of pure epoxy, pure MgO, pure BN and their nanocomposites.

In figure (4.8) the surface of pure epoxy system shows smooth also It can be seen that nanoparticles with different shapes and sizes ,where the size of MgO particles is coarser and larger than BN that be finer size. These results show that MgO nanoparticles were obtained with an average size 74.48 nm. And BN nanoparticles were obtained with an average size about 36.54 nm. In contrast, the surfaces of epoxy /MgO , epoxy/BN and epoxy/hybrid nanocomposites in Figures (4.9,4.10 and 4.11) show rougher and coarser surfaces indicate the toughening mechanisms[212].

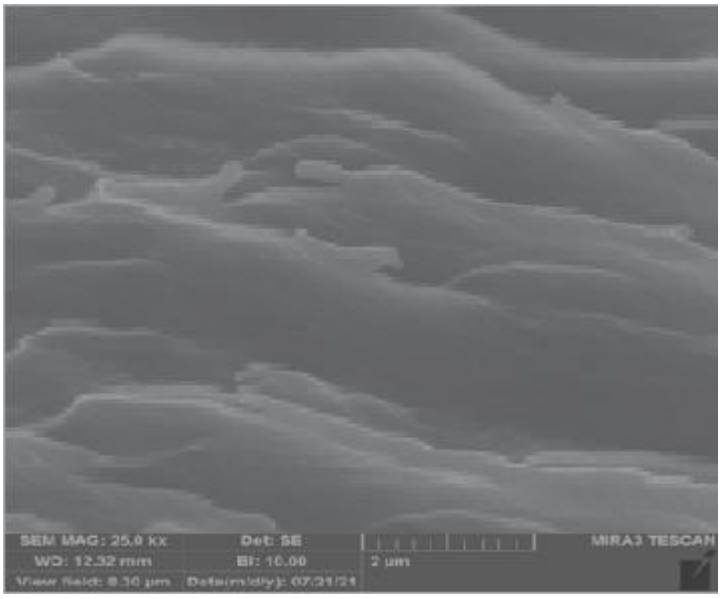
SEM MAG: 25.0 kx
Det: SE
MIRA3 TESCAN
WD: 12.32 mm
BI: 10.00
2 µm

(a)

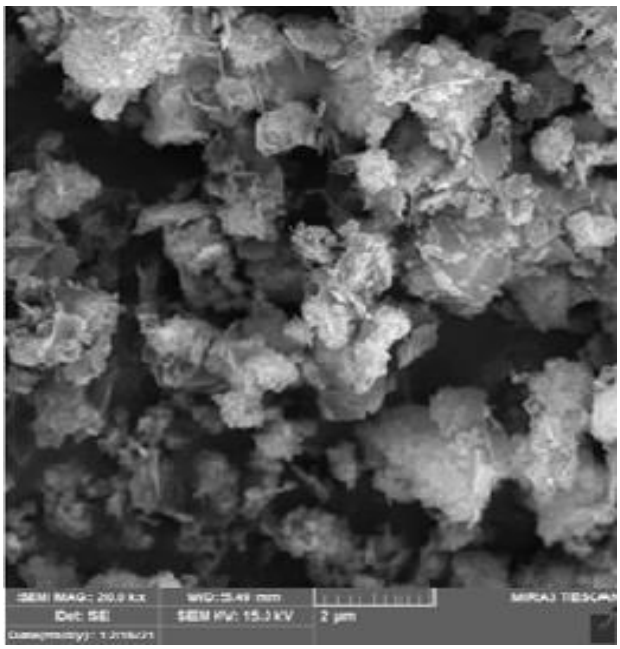

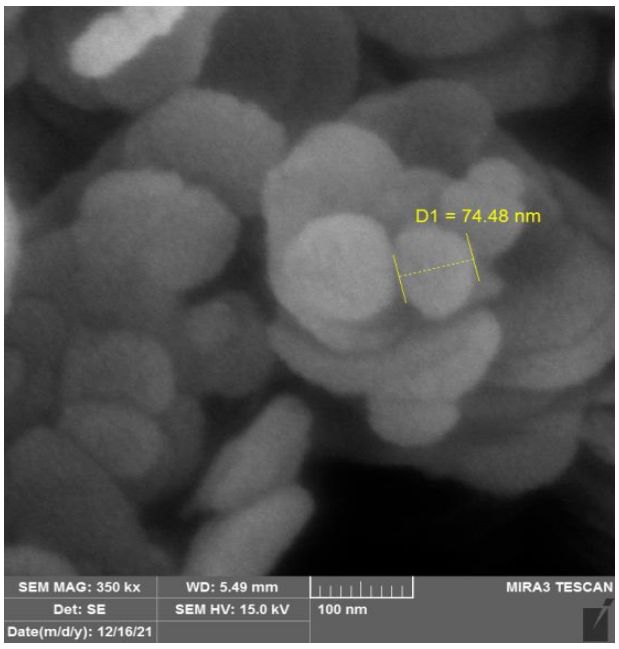
D1 = 74.48 nm
SEM MAG: 350 kx
WD: 5.49 mm
MIRA3 TESCAN
Det: SE
SEM HV: 15.0 kV
100 nm
Date(m/d/y): 12/16/21

(b)

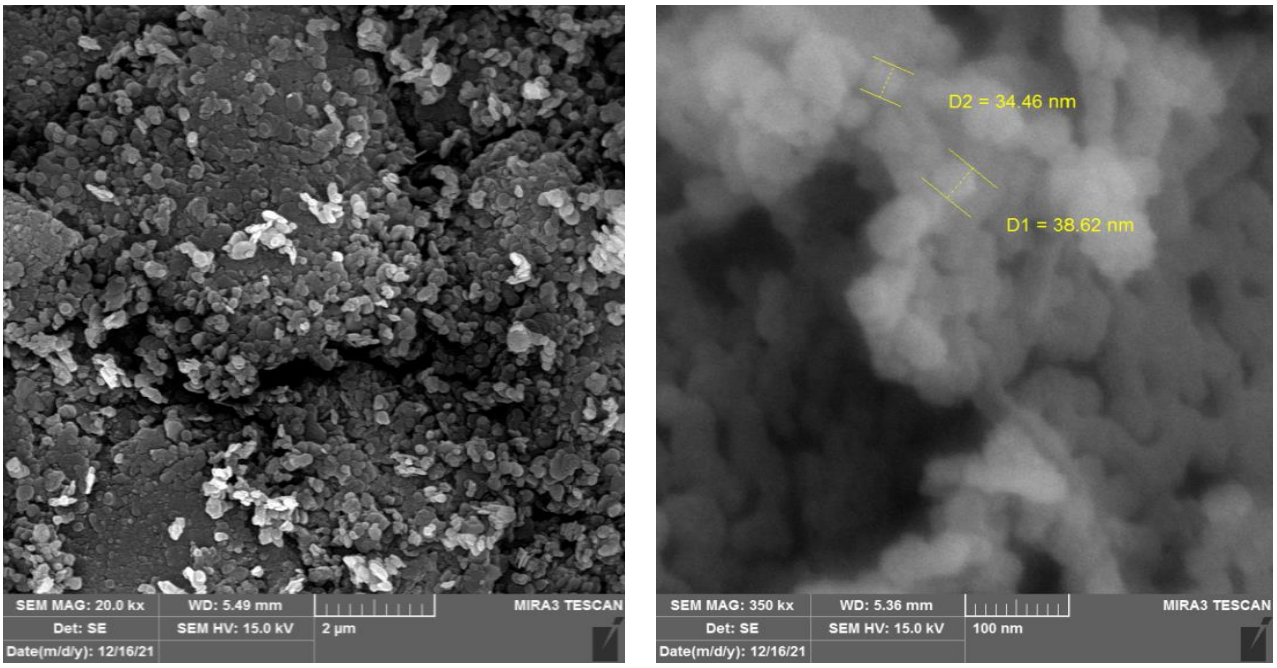

(c)

Figure 4.8: FESEM images of(a): pure epoxy, (b): pure MgO , (c) :pure BN.

It is important to discuss the effect of the nanofiller content on the structural development of the polymer matrix. Figure (4.9) shows the morphology of epoxy/MgO nanocomposites with different MgO content , The MgO nanoparticles can be observed as more brightly colored in the sample. As the doping concentration increased, the distribution density of the MgO nanoparticles gradually increased, maintaining a uniform distribution with no obvious reunion phenomenon in the early stage. The epoxy resin composite has good interfacial properties. With the increase in the doping amount of the filler, the distance between nanometer magnesium oxide particles decreases, and the surface of the composite has large protrusion, which indicates that there is roughness in the material. When the packing mass fraction reaches 5%, the composites begin to aggregate, but the degree of aggregation is relatively light. With the increase in the packing mass fraction, the aggregation became more and more obvious when the packing mass fraction reached 7%. The presence of aggregates is conducive to the

formation of the thermal conductivity network chain, which increases the thermal conductivity of epoxy resin. Compared with pure epoxy resin[213].

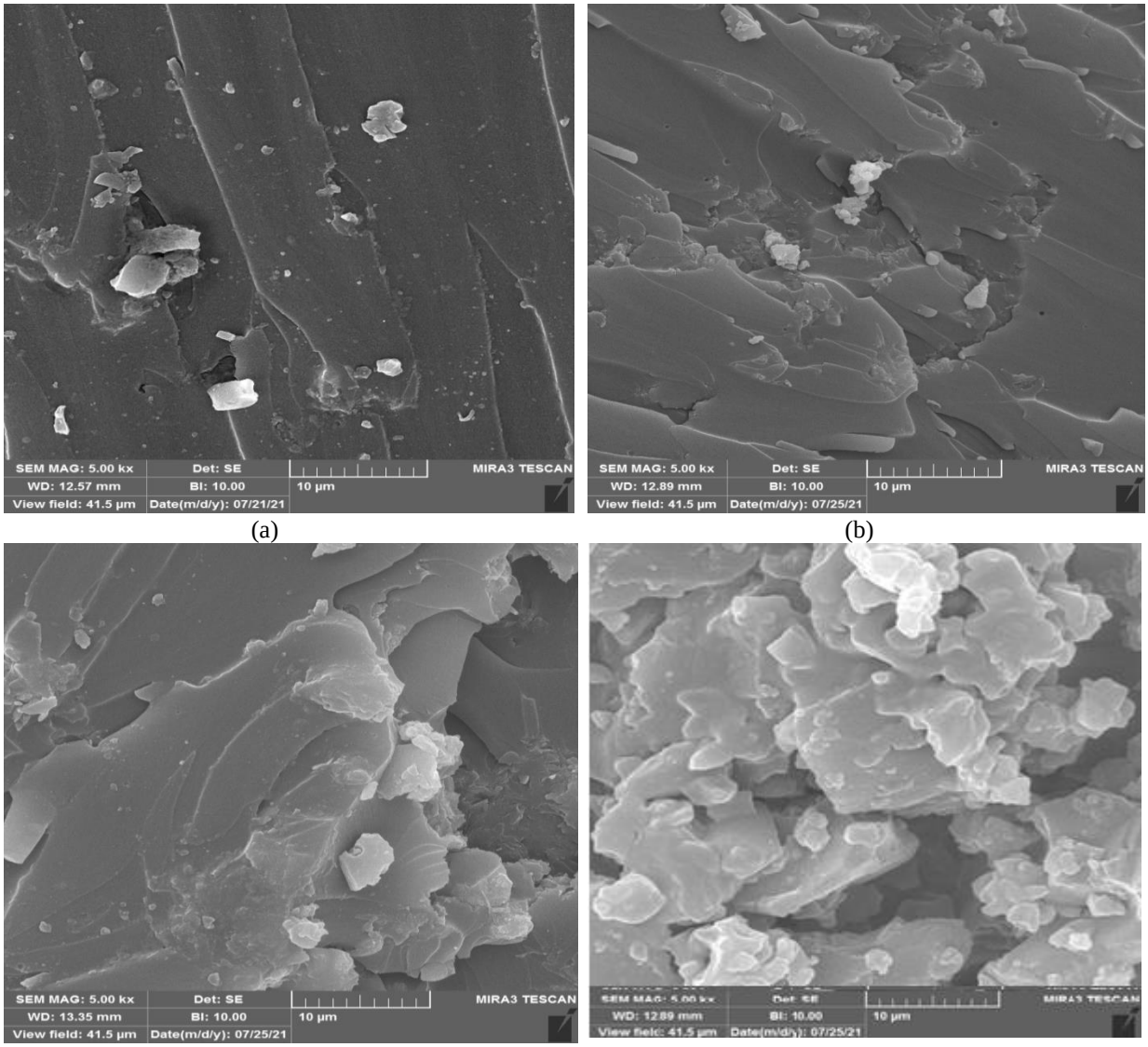

Figure 4.9: FE-SEM images of epoxy /MgO nanocomposites with various loading of mgo wt.%: (a) epoxy/MgO with 1%wt, (b) epoxy/ MgO with 3% wt, (c) epoxy/ MgO with 5% wt (d) epoxy/ MgO with 7% wt.

Figure (4.10) shows the morphology of epoxy/ BN nanocomposite with different content of BN, fractured surface of neat EP is very smooth in Figure (4.8) , As observed the roughness of the fractured surfaces increases with the increment

of BN content . due to good mixing between them leading to more roughness of nanocomposite can be seen[214].

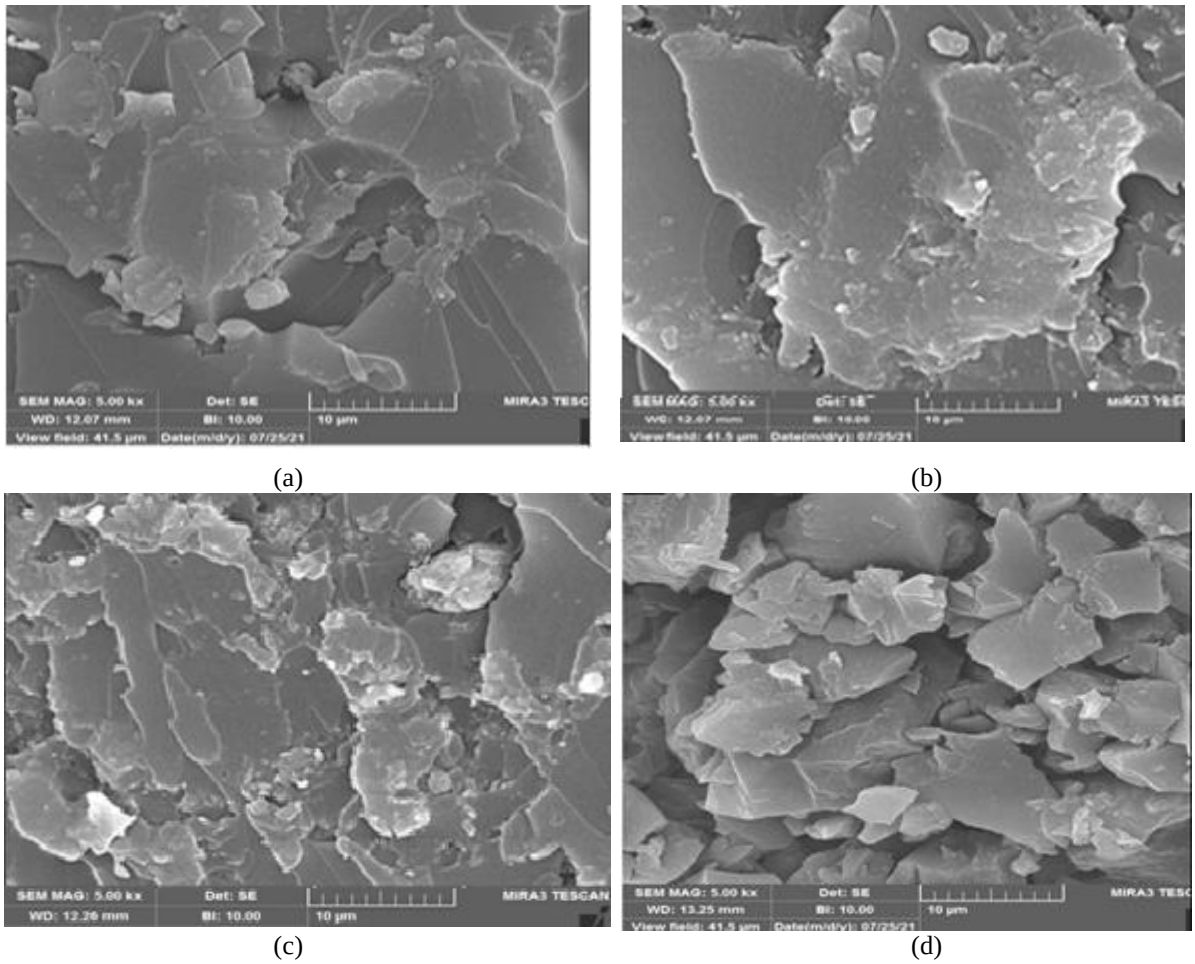

Figure 4.10: FE-SEM images of epoxy/BN nanocomposites with various loading of BN wt.% : (a) epoxy/bn with 1%wt., (b) epoxy /BN with 3% wt., (c) epoxy /BN with 5% wt (d) epoxy /BNbn with 7% wt.

Figure (4.11) shows the morphology of epoxy /hybrid with different hybrid filler content. The results show that surface roughness increases with increase filler content due to the size of NPs.

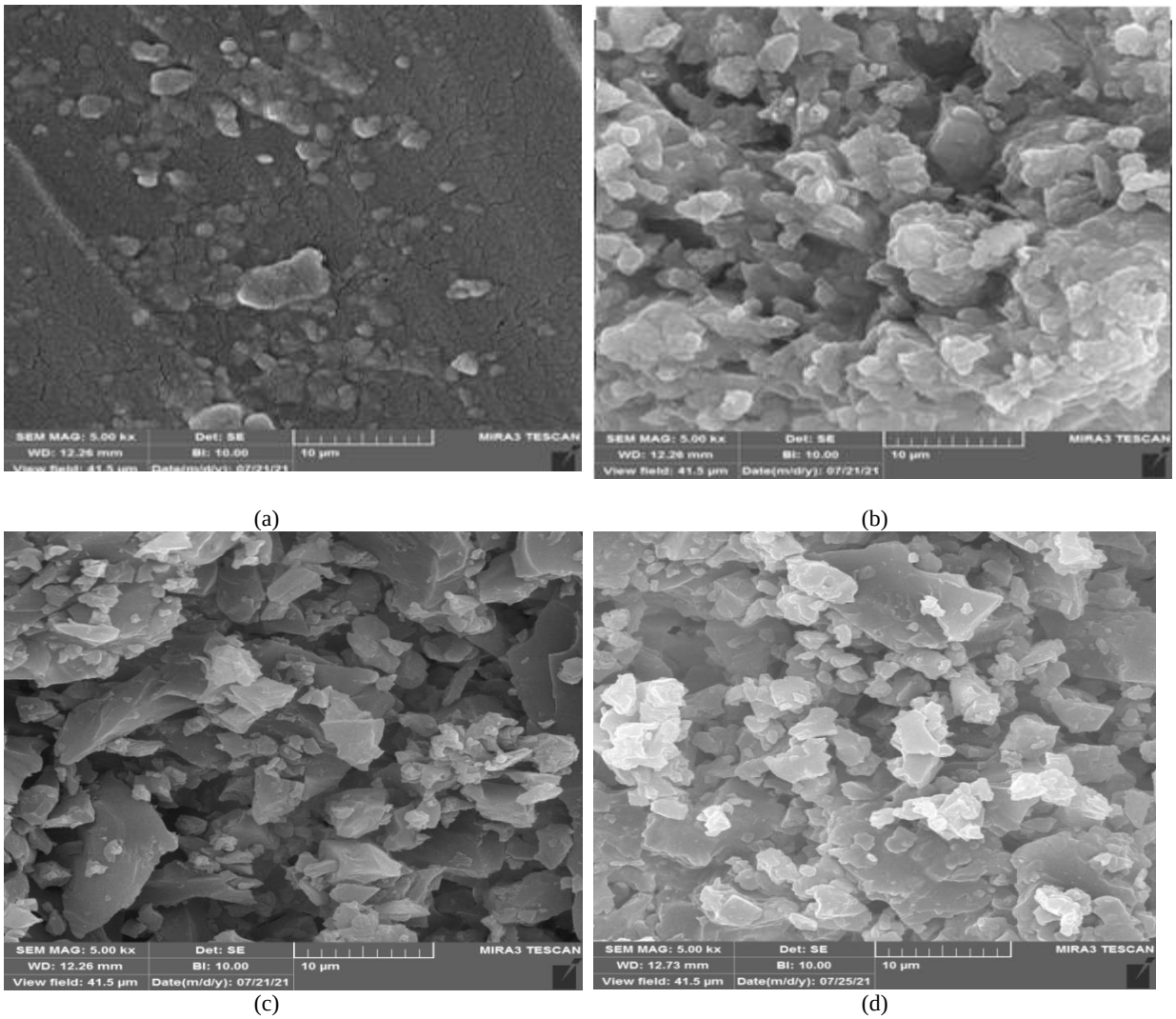

Figure 4.11:FE-SEM images of epoxy/hybrid nanocomposites with various loading of hybrid wt.%: (a) epoxy/h with 1%wt., (b) epoxy/h with 3% wt., (c) epoxy/h with 5% wt (d) epoxy/h with 7% wt

4.4 Thermal Results

4.4.1 DSC Results

Differential Scanning Calorimetry (DSC) analysis was carried out to study the thermal properties of the epoxy resin and epoxy/MgO, epoxy /BN and(1:1of MgO/ BN) hybrid nanocomposites as shown in figures (4.12, 4.13,4.14). The value of glass transition temperature(Tg) and degradation temperature(Td) was

determined from figure. 4.12 and table 4.3 (in appendix c). It is noticed that the Tg values increase linearly from 79.12 ^{o}C (for pure epoxy) up to 82.39 ^{o}C, 83.65 ^{o}C, 84.49 ^{o}C, 85.77 ^{o}C.and Td values about 308.3 ^{o}C (for pure epoxy) and (305.92 ^{o}C,305.77 ^{o}C,305.09 ^{o}C,299.60 ^{o}C) for sample with (1%,3%,5%,7% wt%) MgO NPs content respectively .This is because that MgO is a solid material and has compact structure with coarse size nanopartical as shown in FESEM image above in figure (4.6) ,and leads reduce chain mobility which leads to increase of Tg of pure epoxy and epoxy/MgO nanocomposite [215]. This increment in Tg is an indicator about the improvement of the mechanical properties of the prepared samples.

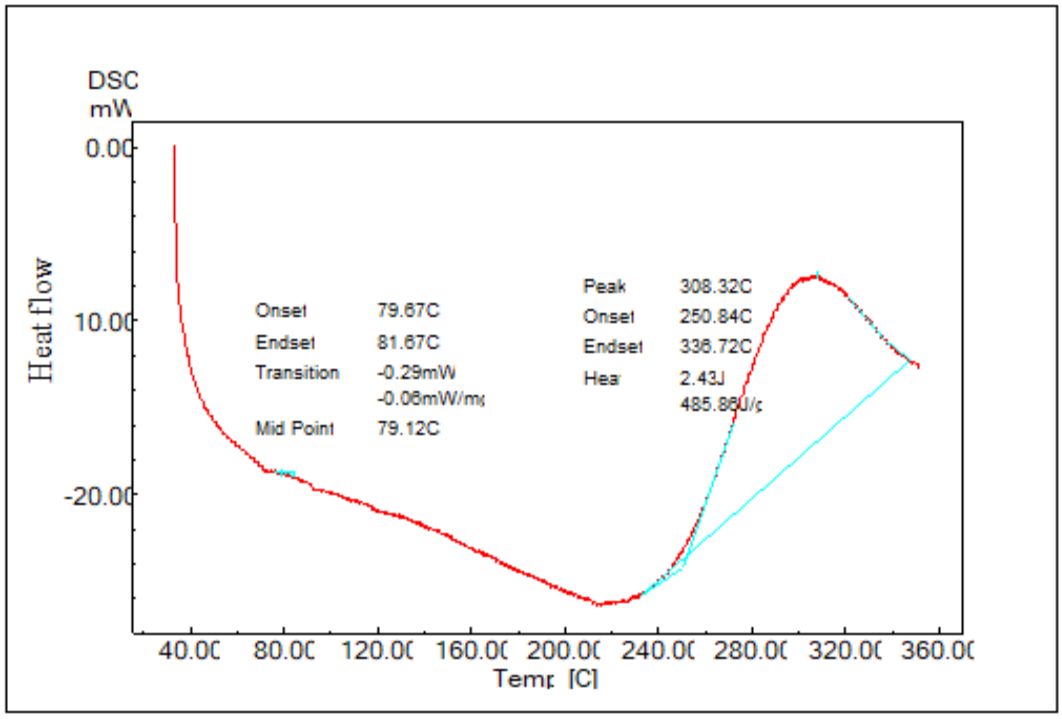

(a)

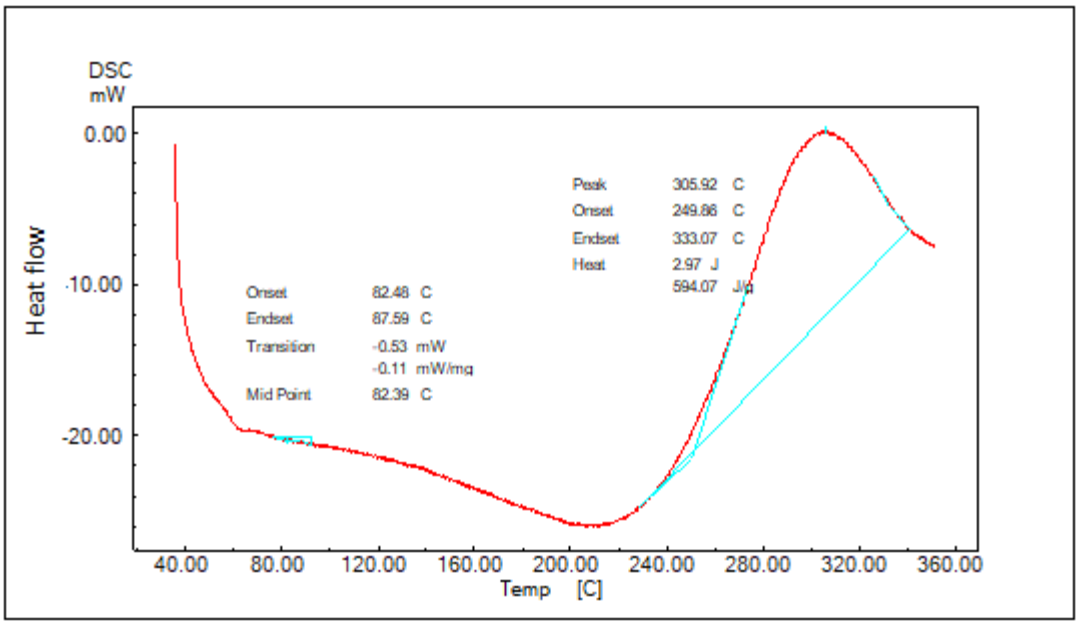
DSC
mW
0.00
-10.00
-20.00
Heat flow
Peak 305.92 C
Onset 249.86 C
Endset 333.07 C
Heat 2.97 J
594.07 J/g
Onset 82.48 C
Endset 87.59 C
Transition -0.53 mW
-0.11 mW/mg
Mid Point 82.39 C
40.00 80.00 120.00 160.00 200.00 240.00 280.00 320.00 360.00
Temp [C]

(b)

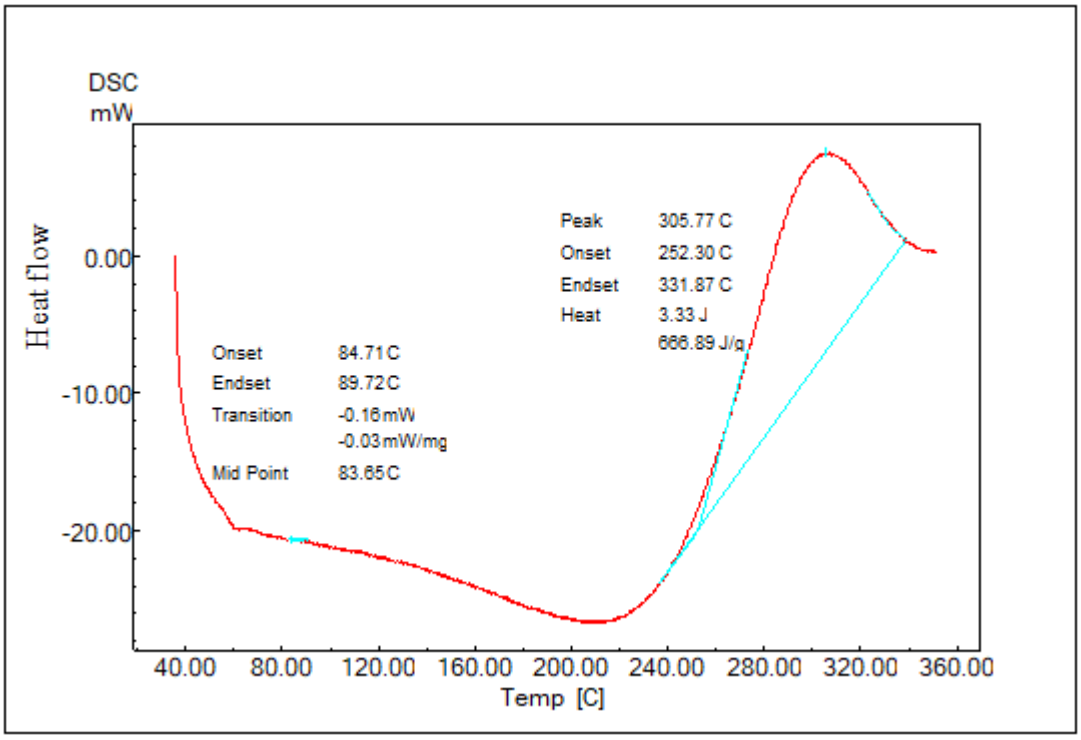
DSC
mW
0.00
-10.00
-20.00
Heat flow
Peak 305.77 C
Onset 252.30 C
Endset 331.87 C
Heat 3.33 J
666.89 J/g
Onset 84.71 C
Endset 89.72 C
Transition -0.16 mW
-0.03 mW/mg
Mid Point 83.65 C
40.00 80.00 120.00 160.00 200.00 240.00 280.00 320.00 360.00
Temp [C]

(c)

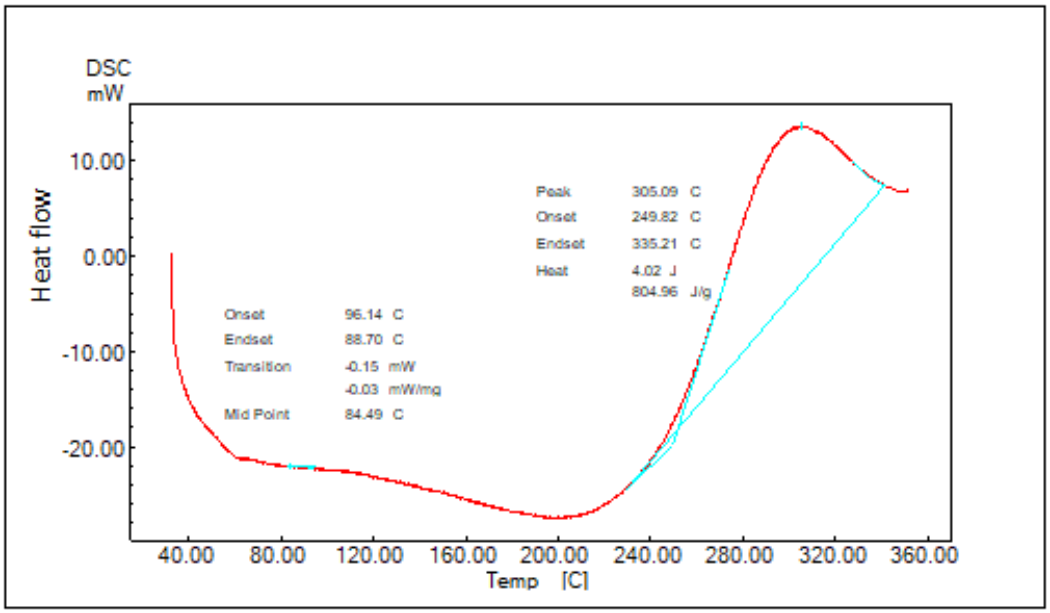

(d)

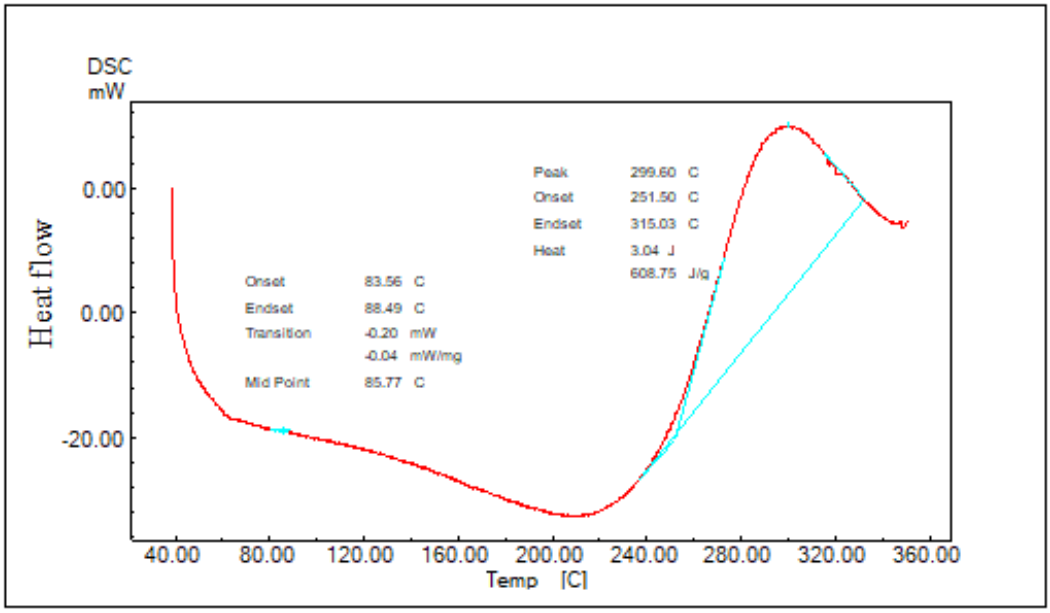

(e)

Figure 4.12: DSC of samples (a) epoxy, (b)1%,(c)3%,(d)5% ,(e) 7% of epoxy/MgO nanocomposites.

Epoxy/BN nanocomposite as shown in figure 4.13, is noticed that the glass transition temperature increases with the increase in the weight fraction of boron nitride nanoparticles from 79.12^{o}C (for pure Epoxy) up to(80.78 ^{o}C, 82.79^{o}C, 83.13 ^{o}C, 84.76 ^{o}C) ,and Td values (308.13 ^{o}C,308.32 ^{o}C,313.71 ^{o}C,300.3 ^{o}C)(for sample with 1%,3%,5%,7% wt%) BN NP ,respectively, as shown in table 4.2.

Where the addition of nanoparticles in epoxy matrix lead to reduce the mobility of the epoxy chains due to formation high immobility monolayer around each nanoparticle while the matrix chains (epoxy chains not bonded to nanoparticles)bonded to that monolayer constrained the non-contact matrix chains, so, the network of nanoparticles reduce the overall mobility of the nanocomposites system. Due to reducing free volume space occupied by the spaces at the end of chains[216].

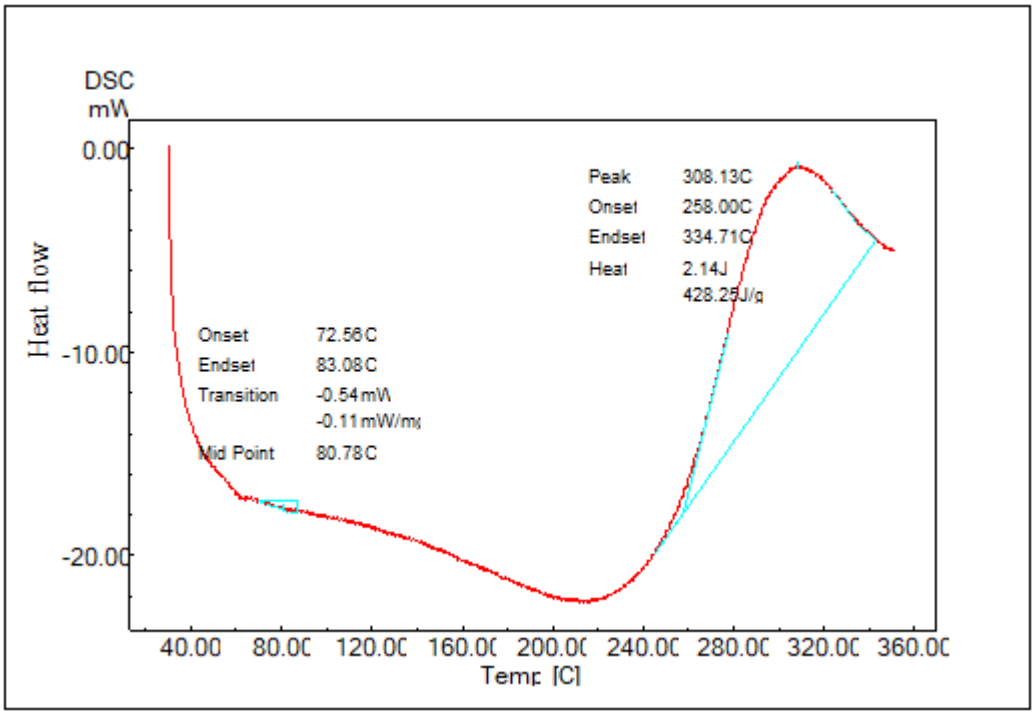

(a)

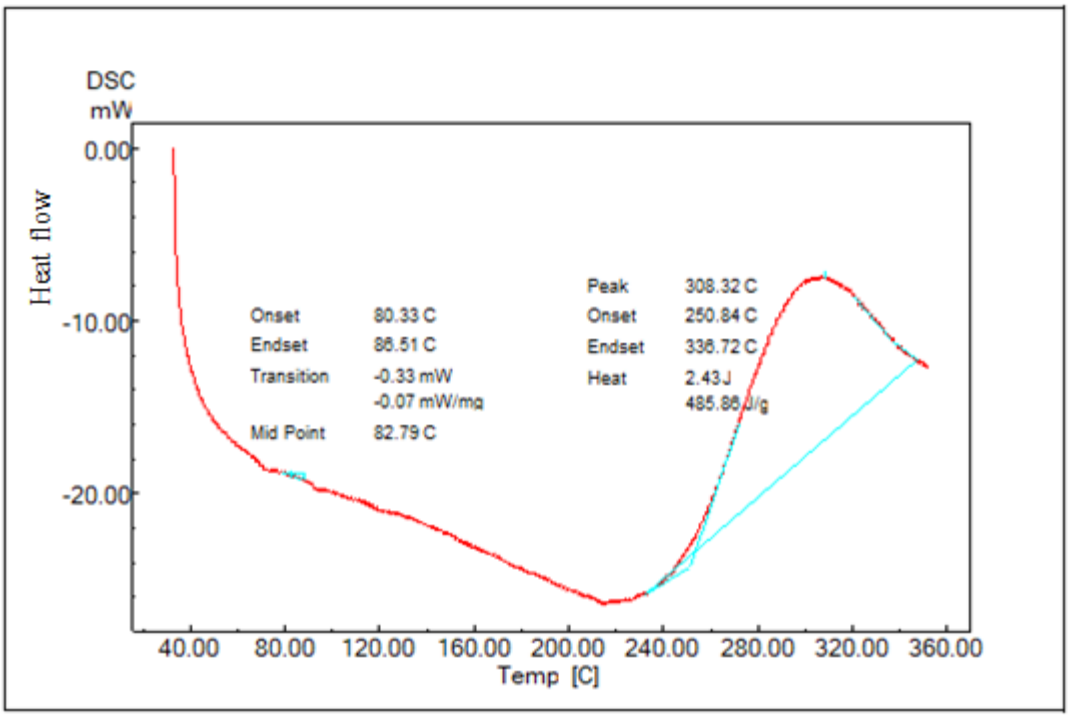
DSC
mW
0.00
-10.00
-20.00
Heat flow
Onset 80.33 C
Endset 86.51 C
Transition -0.33 mW
-0.07 mW/mg
Mid Point 82.79 C
Peak 308.32 C
Onset 250.84 C
Endset 336.72 C
Heat 2.43 J
485.86 J/g
40.00 80.00 120.00 160.00 200.00 240.00 280.00 320.00 360.00
Temp [C]

(b)

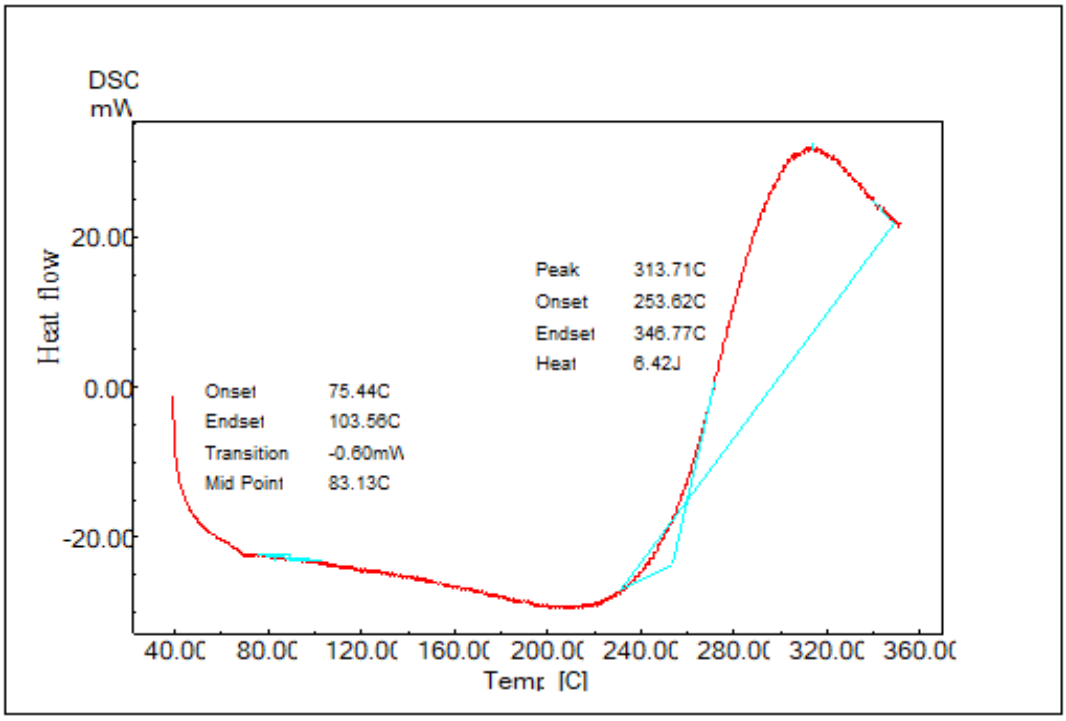
DSC
mW
20.00
0.00
-20.00
Heat flow
Peak 313.71C
Onset 253.62C
Endset 346.77C
Heat 6.42J
Onset 75.44C
Endset 103.56C
Transition -0.60mW
Mid Point 83.13C
40.00 80.00 120.00 160.00 200.00 240.00 280.00 320.00 360.00
Temp [C]

(c)

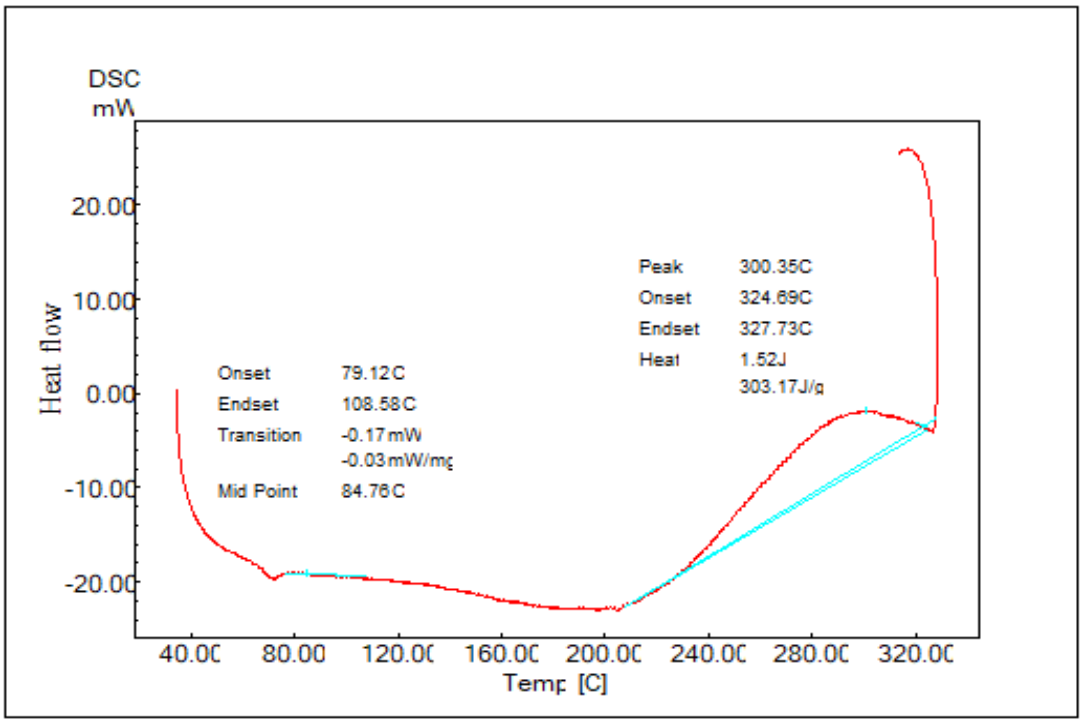

(d)

Figure 4.13: DSC of samples (a)1%,(b)3%,(c)5% ,(d) 7% of epoxy/ bn nanocomposites.

The addition of (1:1of MgO/BN)hybrid Nps in to the epoxy increases the T_g from 79.12^{o}C (for pure Epoxy) up to 80.6 ^{o}C, 84.65 ^{o}C, 86.2 ^{o}C, 92.6 ^{o}C and Td values (308.60 ^{o}C,300.85 ^{o}C,308.60 ^{o}C,297.42 ^{o}C) (for sample with 1%,3%,5%,7% wt%) hybrid NPs, respectively ,as shown in Figure (4.14) and table (4.3).

Where the mechanical mixing was effective for the uniform dispersion of nano-sized NPs [217]. which leads to increase of Tg of epoxy .

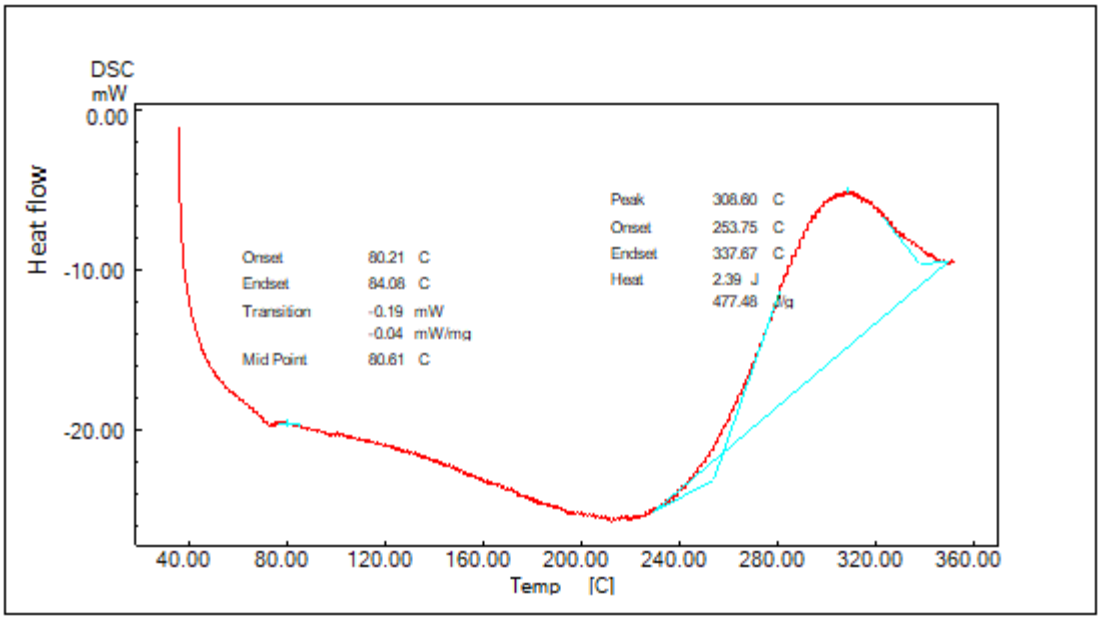
DSC
mW
0.00
-10.00
-20.00
Heat flow
Onset 80.21 C
Endset 84.08 C
Transition -0.19 mW
-0.04 mW/mg
Mid Point 80.61 C
Peak 308.60 C
Onset 253.75 C
Endset 337.67 C
Heat 2.39 J
477.48 J/g
40.00 80.00 120.00 160.00 200.00 240.00 280.00 320.00 360.00
Temp [C]

(a)

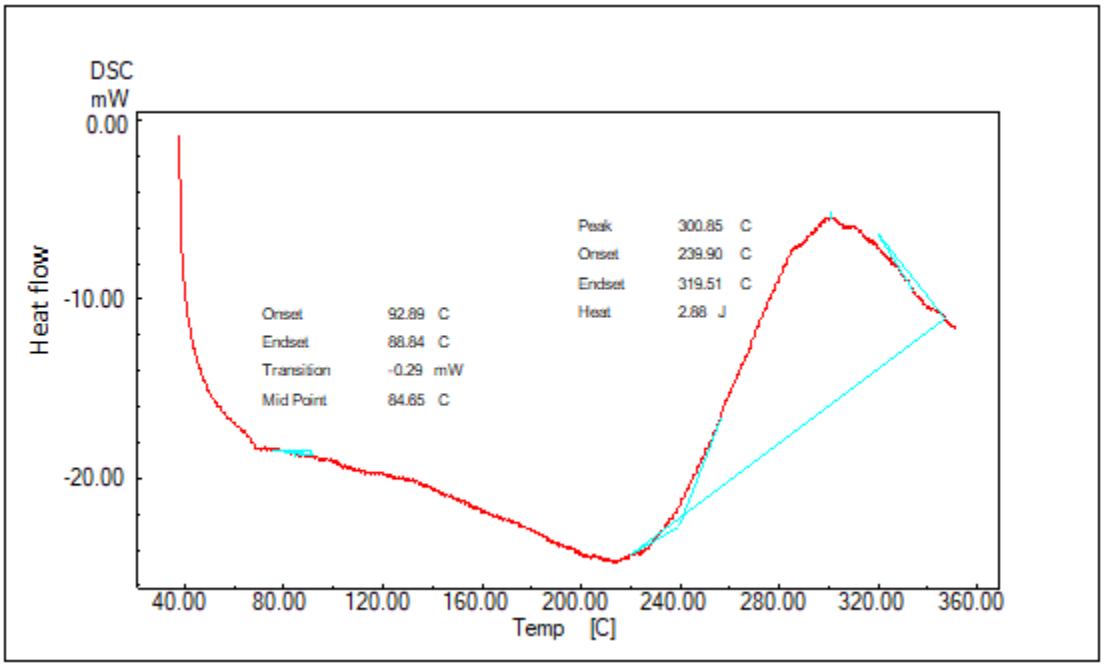
DSC
mW
0.00
-10.00
-20.00
Heat flow
Onset 92.89 C
Endset 88.84 C
Transition -0.29 mW
Mid Point 84.65 C
Peak 300.85 C
Onset 239.90 C
Endset 319.51 C
Heat 2.88 J
40.00 80.00 120.00 160.00 200.00 240.00 280.00 320.00 360.00
Temp [C]

(b)

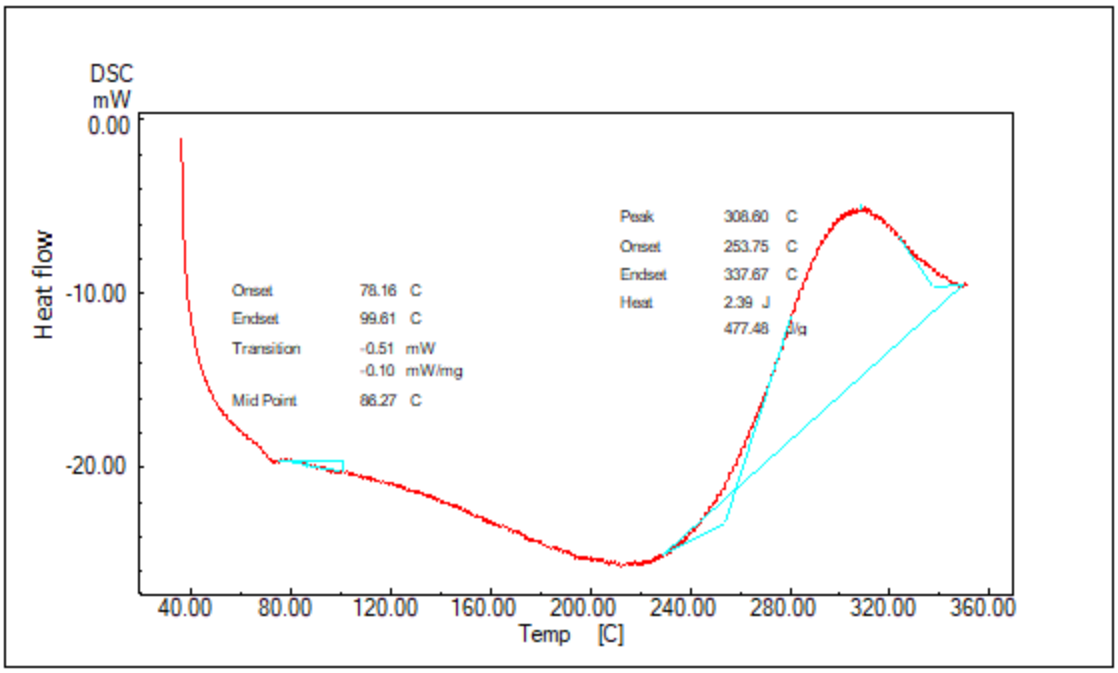

(c)

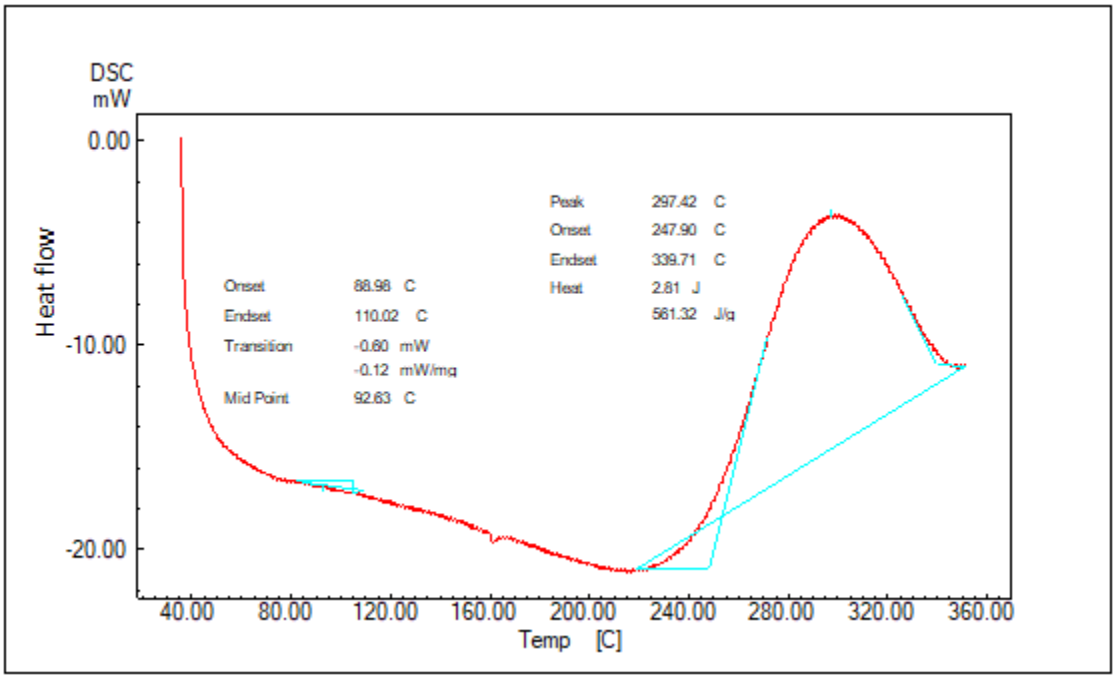

(d)

Figure 4.14: DSC of samples (a)1%,(b)3%,(c)5% ,(d) 7% of epoxy/hybrid. nanocomposites.

4.4.2.*Thermal Conductivity Results*

The main goal of this research is to improve thermal conductivity of a pure epoxy thermoset by the addition of MgO, BN and hybrid without negatively affect the electrical insulation. Different materials with increasing filler content were investigated by thermal conductivity analysis.

The thermal conductivity of the nanocomposites is controlled by the intrinsic conductivities of filler and matrix, shape and size of the filler, and the loading level of filler [218].

Figure (4.15) and table (4.3)in appendix D, show the thermal conductivity results of epoxy/MgO nanocomposite, epoxy/BN nanocomposite and (1:1 MgO/BN)hybrid nanocomposite with (1%,3%,5%,7%wt%) NPs, reaspectively.

The results reveal that when the MgO nanofiller content increases, the thermal conductivity of the composites increases which is ascribed to the MgO nanopartical thermal conductivity. At low MgO nanopartical doping ratios the composites thermal conductivity increases slowly which could be attributed to the nanoparticles independence from one another and the lack of a thermal conductive chain. The epoxy composites internal thermal conductivity was based on a tandem structure, which increased as the MgO nanoparticle content increased . At increased MgO nanoparticle levels in the matrix the nanoparticles and polymer matrix interact to form a single thermal conductive chain lowering thermal resistance and forming parallel structures resulting in the formation of a thermal conductive network [200].

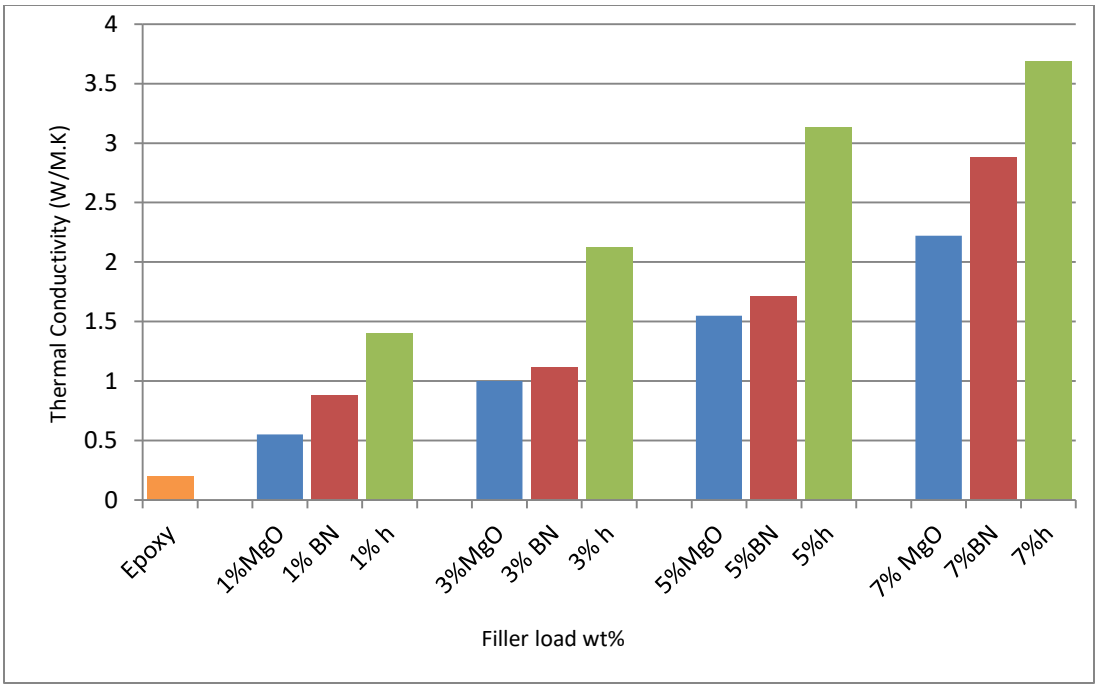

Figure 4.15: Illustrates the relation between the thermal conductivity of pure epoxy, epoxy/MgO ,epoxy/BN and epoxy/(1:1MgO/BN)hybrid nanocomposite and filler loading wt%

The results in figure (4.15) and table (4.4) in appendix D, display that the the thermal conductivity of pure epoxy significantly enhances as the BN level increases for the sample containing 7% wt of BN Nps, the thermal conductivity improved about 93% as compared to thermal conductivrty of pure epoxy.This increases due to the increase in phonon carriers and high conductive nature of boron nitride, in addition to the particles shape and size, it helps to form conductive connections that increace of thermal conductivity [219]. These results are corroborated by the FESEM pictures above in figure (4.10).

The results in figure (4.15) and table (4.4) show that the thermal conductivity of hybrid samples was more enhanced than those of pure epoxy and another nanocomposites .Where differences in particle size and shape in addition to their surface area and other factors all participate in increasing thermal

conductivity because of they form bonds that act as a bridge to transfer the phonon thus increasing the thermal conductivity, The use of hybrid size MgO and BN nanoparticles in epoxy resulted in better thermal conductivity.

The highest value of thermal conductivity was 3.69 W/M.K at 7 % wt with improvement about 95 % of epoxy /hybrid nanocomposities as compared to epoxy /MgO nanocomposities ,epoxy/BN nanocomposities and pure epoxy This behavior is attributed to the packing density and ease of formation of the conductive pathway [220] . See FESEM pictures above in figure (4.11).

It is also cited that due to the structure of hexagonal BN and cubic MgO and good mixing between two hybrid particles enhances mechanical properties and thermal conductivity of epoxy nanocomposites by (1:1of MgO/BN) hybrid filler for microelectronics packaging and another heat dissipation applications .

4.5 Electrical Result

4.5.1.The Electrical Resistivity:

Insulators are materials that do not conduct any electrical energy or currents at all. They do not allow any (or very little) electrical charge to flow through them and the thermoset's electrical resistance which quantifies the resistance to flow of current is another significant parameter in electronic fabrications[221]. The electrical resistivity of epoxy/ MgO nanocomposite, epoxy/BN nanocomposite, and epoxy/(1:1MgO/BN) hybrid nanocomposite with different filler content is shown in Figure 4.16 and tables (4.5)in appendix E.

The results show that the electrical resistivity increases linearity with increasing filler content such as MgO was used as a potential filler. The highest electrical resistivity was about 6E+15 with improvement about 60% as at 7% wt as compared to pure epoxy , this result due to of the large band gap (7.8 eV) and high electrical resistivity (10^{17} ohm.cm) of MgO NPs, it is very attractive and has

the highest resistance of any of the regularly utilized nanoscale oxide [222]. The results of increasing the electrical resistivity with increasing BN NPs content and reach the highest value about 7.2 E+15 with enhanced about 67 % at 7%wt of epoxy/BN nanocomposite as compared to pure epoxy .The results of increasing the electrical resistivity with increasing hybrid NPs in epoxy/(1:1MgO/BN) hybrid nanocomposites ,The highest value of electrical resistivety was about (8.4E+15 Ω .cm) with improvements about 71% at (7wt) hybrid NPs as compared to pure epoxy and another non hybrid nanocomposites .due to the electrical insulation nature of both nanoparticles (MgO and BN).The movement of carriers in composites enhances the resistivity due to the coulomb blocking effect [213] .This is a useful feature in the heat dissipating electronic industries such as electrical circuits or insulating protective coatings .

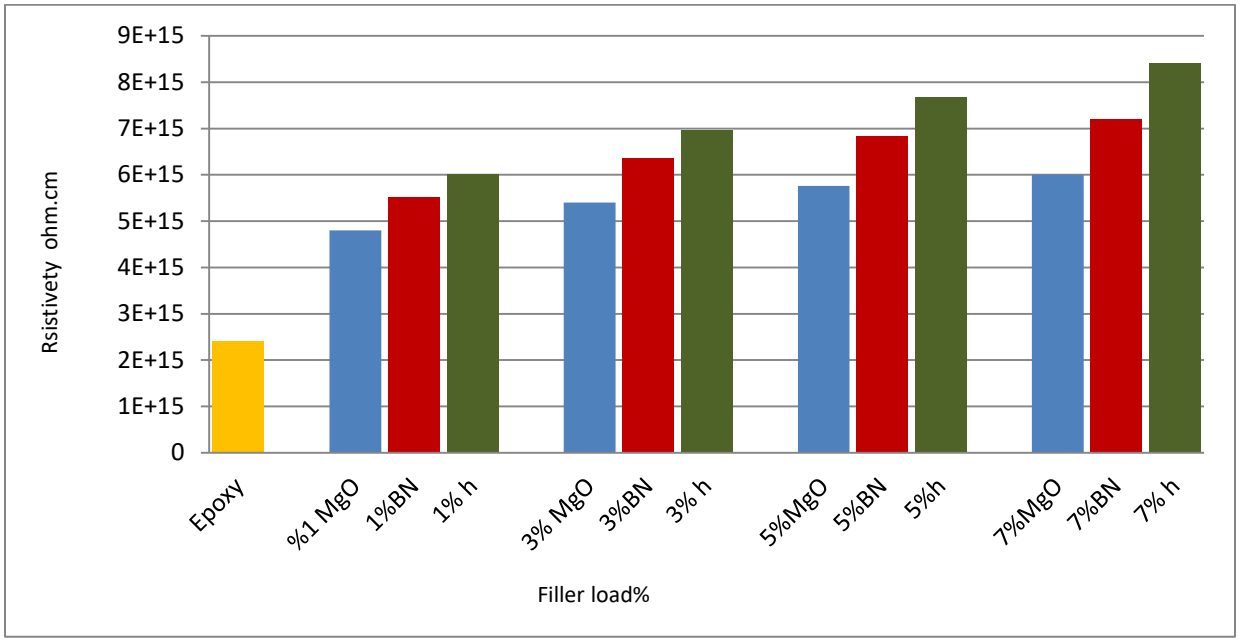

Figure 4.16: Illustrates the relation between the electrical resistivity of pure epoxy, epoxy/MgO, epoxy/BN and epoxy/(1:1 MgO /BN)hybrid nanocomposite and filler loading wt% .

4.6 Mechanical Result

4.6.1. Tensile Results :

4.6.1.1 *Tensile Strength*

Figure (4.17) and table (4.6) in appendix F.1 show the tensile strength of (epoxy/MgO) (epoxy/BN) and (epoxy/hybrid) nanocomposites at different weight percentages of nanoparticles. The results display that the tensile strength of (epoxy/MgO) and (epoxy/hybrid) nanocomposites are higher than those of pure epoxy. The addition of 7 wt % hybrid nanoparticles improved the tensile strength about 19 % as compared to pure epoxy due to the good mixing of nanoparticles within the polymer matrix can be significantly strengthened [223]. There is no big change in the tensile strength of (epoxy/BN) as the BN NP concentration increases[224]. This may be attributed to the size and nature of BN particles finer than MgO particles (See FE-SEM images above in Figure(4.8).

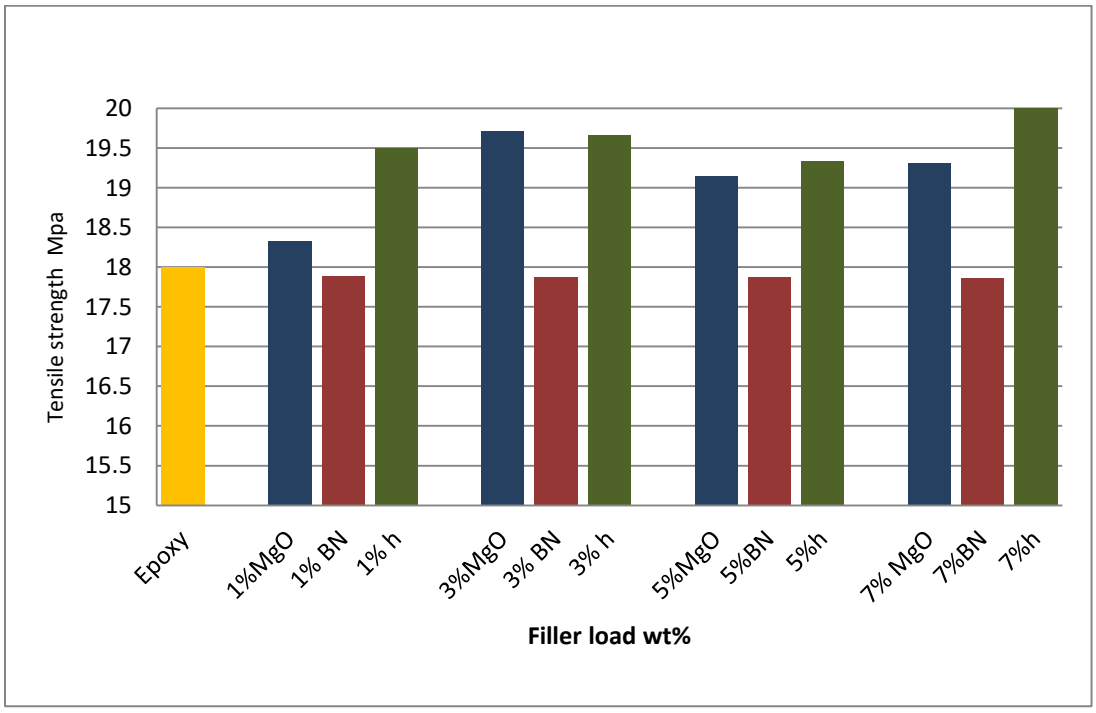

Figure 4.17: Effect of fillers content(w.t%) ,(MgO ,BN,and hybrid NPs) on the tensile strength of the epoxy matrix.

4.6.1.2 Young modulus

Figure (4.18) and table (4.6) in appendix F.1 shows the young modulus of (epoxy/MgO) (epoxy/BN) and (epoxy/hybrid) nanocomposites at different weighting percent of nanoparticles.

The results show that the young modulus of nanocomposites are greater than those of pure epoxy. young modulus is enhanced with increase MgO NP content comparison to pure epoxy because of high modulus of elasticity of MgO. The interfacial adhesion force is increased as a result the composite becomes stiffened. This result is quite comparable with previously reported work [225]. The elastic modulus is affected by shape of nanoparticles and its dispersion through polymer matrix, Figure (4.18) shows that the modulus of epoxy/BN nanocomposites increases as the BN nanoparticle concentration increases at (1,3,5,7wt %) slightly lower than epoxy/MgO nanocomposites due to good distribution of BN Np in epoxy matrix [226], as shown in table 4.6 in appendix F.1.

In Figure (4.18) displays that the modulus of epoxy/hybrid nanocomposites increase as the hybrid nanoparticle concentration increases at (1,3,5,7) wt %

The addition of 7% hybrid nanoparticles enhanced modulus of elasticity about 37 % as compared of pure epoxy and epoxy/MgO and epoxy/BN nanocomposites. Because of the good mixing between the MgO /BN nanoparticles, that giving a strong network lead to stiffening nanocomposite, where the polymer matrix and the particles further reduce the mobility of the network structure and increase of young modulus [21]. as shown in table 4.6 in appendix F.1.

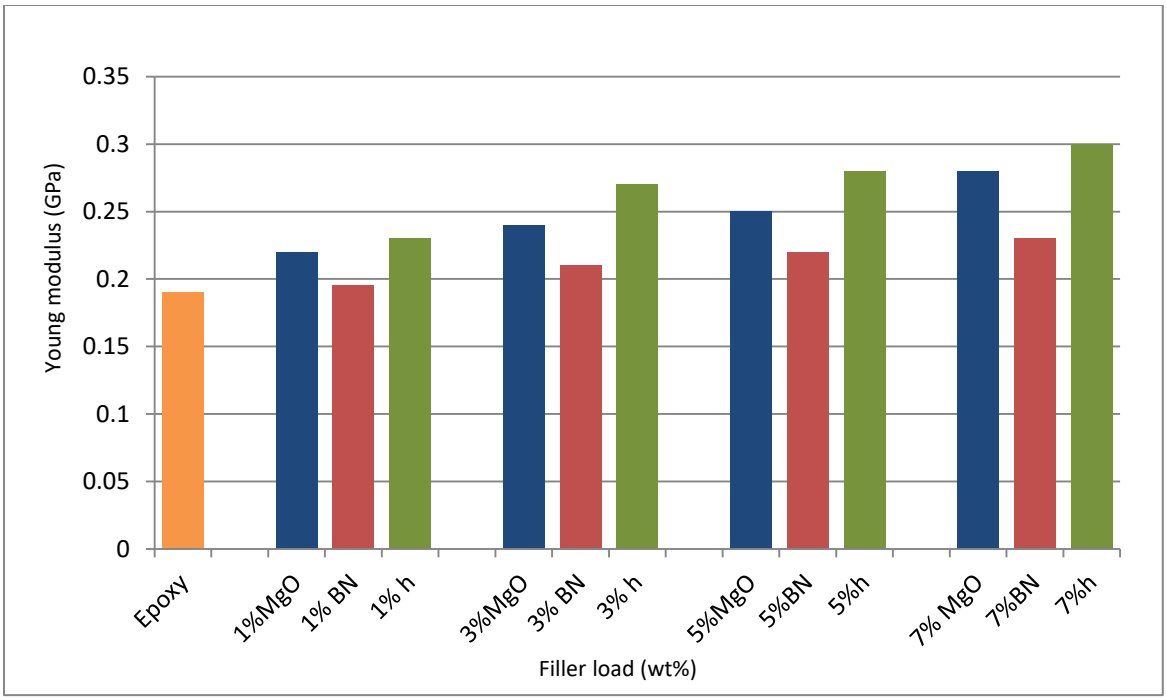

Figure 4.18: Effect of fillers content (w.t%) ,(MgO ,BN,and hybidNPs) on the elastic modulus of the epoxy matrix.

4.6.1.3 Elongation at break

Figure (4.19) shows the elongation of (epoxy/MgO) (epoxy/BN) and (epoxy/hybrid) nanocomposites at different weighting percent of nanoparticles. The results show that the elongation of epoxy/ MgO nanocomposite lower than pure epoxy [227], where the addition of nanoparticles in the epoxy matrix leads to reducing the mobility of the epoxy chains [202]. When nanoparticles amounts increased within the composite structure the steric hindrance increased so the polymeric chain restricted and cannot be sliding above each other's, which leads to reduce of elongation.

The elongation of epoxy/ BN nanocomposite lower than pure epoxy due to increase of tensile modulus .And the elongation of epoxy/hybrid nanocomposite is lower than pure epoxy, due to the high modulus of elasticity of epoxy/hybrid nanocomposite as a result of good interaction between nanoparticles and epoxy that

prevent the movement of the chain and strong structure [228], as seen in table (4.6) in appendix F.1

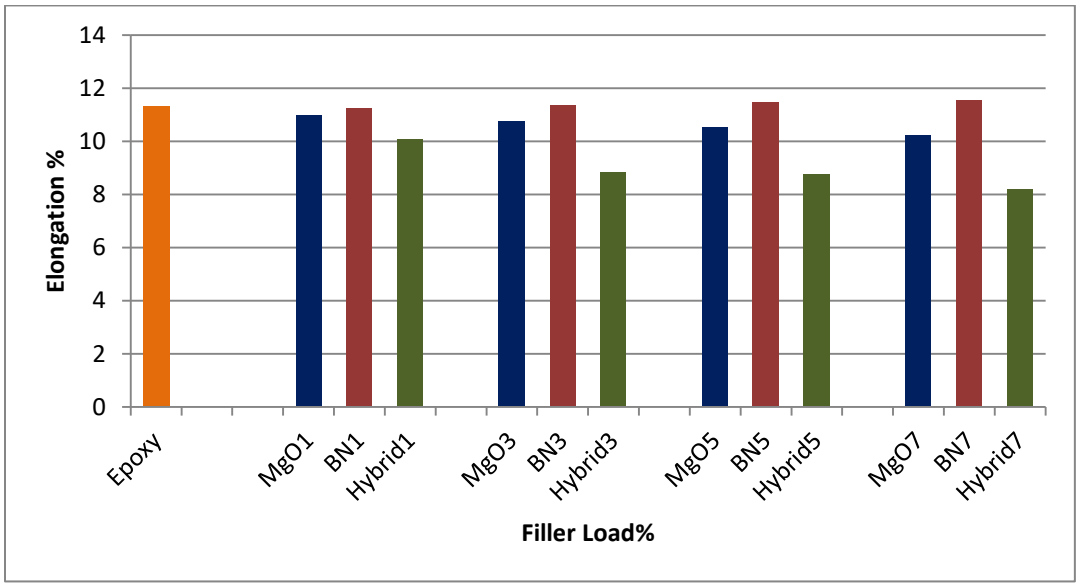

Figure 4.19: Effect of fillers content (w.t%) ,(MgO ,BN,and hybid NPs) on the elongation of the epoxy matrix.

4.6.2. Fracture Toughness Result

4.6.2.1. Compact Tention (C.T):

Figure (4.20) shows the fracture toughness (CT) of (epoxy/MgO) (epoxy/BN) and (epoxy/hybrid) nanocomposites at different weighting percent of nanoparticles.The results display that the fracture toughness (CT) of (epoxy/MgO), (epoxy/BN) and (epoxy/hybrid) nanocomposites are higher than those of pure epoxy.

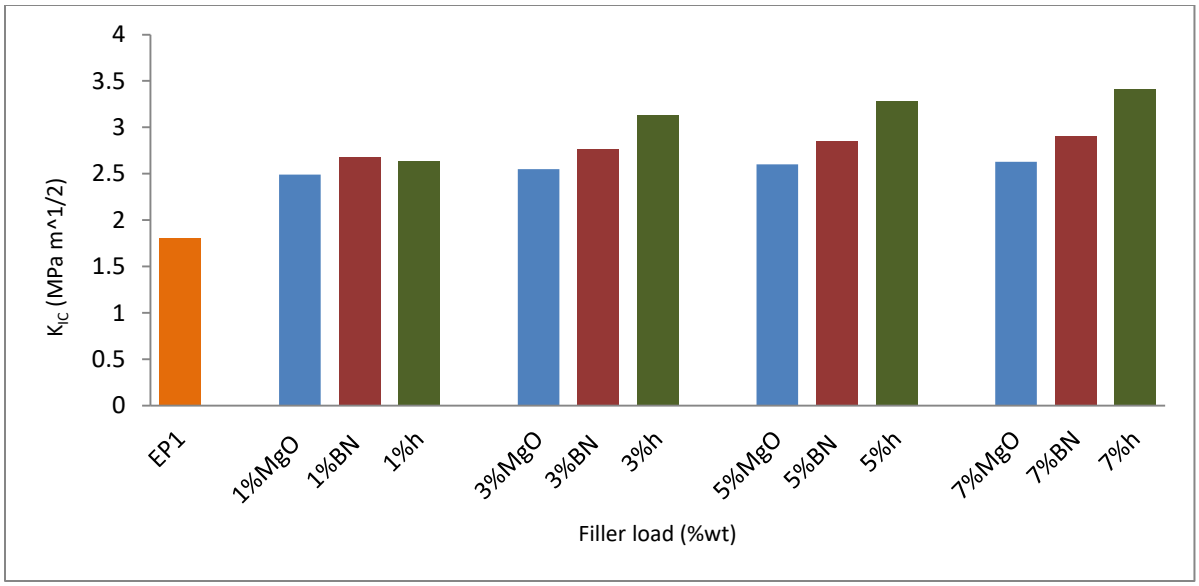

Figure 4.20: Effect of fillers content (w.t%) on the compact tension K_{IC} of the epoxy matrix.

Figure (4.21) shows the load (CT) of (epoxy/MgO) (epoxy/BN) and (epoxy/hybrid) nanocomposites at different weighting percent of nanoparticles. The results display that the load of (epoxy/MgO) ,(epoxy/BN) and (epoxy/hybrid) nanocomposites are higher than those of pure epoxy.

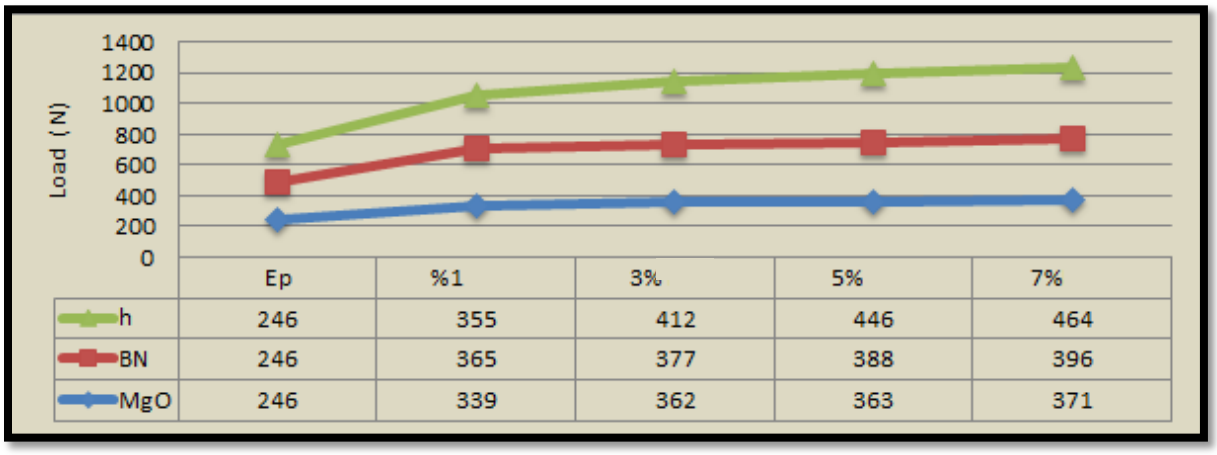

	Ep	%1	3%	5%	7%
h	246	355	412	446	464
BN	246	365	377	388	396
MgO	246	339	362	363	371

Figure 4.21: Illustrate the relationship between load and fillers content (w.t%) of epoxy/MgO,epoxy/BN and epoxy/hybrid nanocomposites.

In Figures (4.20) and (4.21), it can be observed that the fracture toughness (CT) and the load of (epoxy/MgO) nanocomposite slightly increase with

increasing MgO NP content due to the reinforcement role of the MgO NP that will be beneficial for the material resistance and its durability [21] as seen in table (4.7). While the fracture toughness (CT) and load of (epoxy/BN) nanocomposite increase with increasing BN NP content this is attributed to good dispersion of BN in the epoxy matrix leading to preventing crack propagation and needing more energy to make the crack propagate in the tension mode as shown in table(4.7) in appendix F.3. In addition, the fracture toughness (CT) and load of (epoxy/hybrid) nanocomposite increase with increasing hybrid NP content this meaning the presence of fillers enhanced the mechanical properties of nanocomposites and increasing K_{IC} where the addition of 7% hybrid nanoparticles enhanced K_{IC} about 68% **,** as shown in table (4.7) .

4.6.2.2 Single Edge Notched Bending (SENB):

Figure (4.22) shows the fracture toughness (SENB) of (epoxy/MgO) (epoxy/BN) and (epoxy/hybrid) nanocomposites at different weighting percent of nanoparticles.

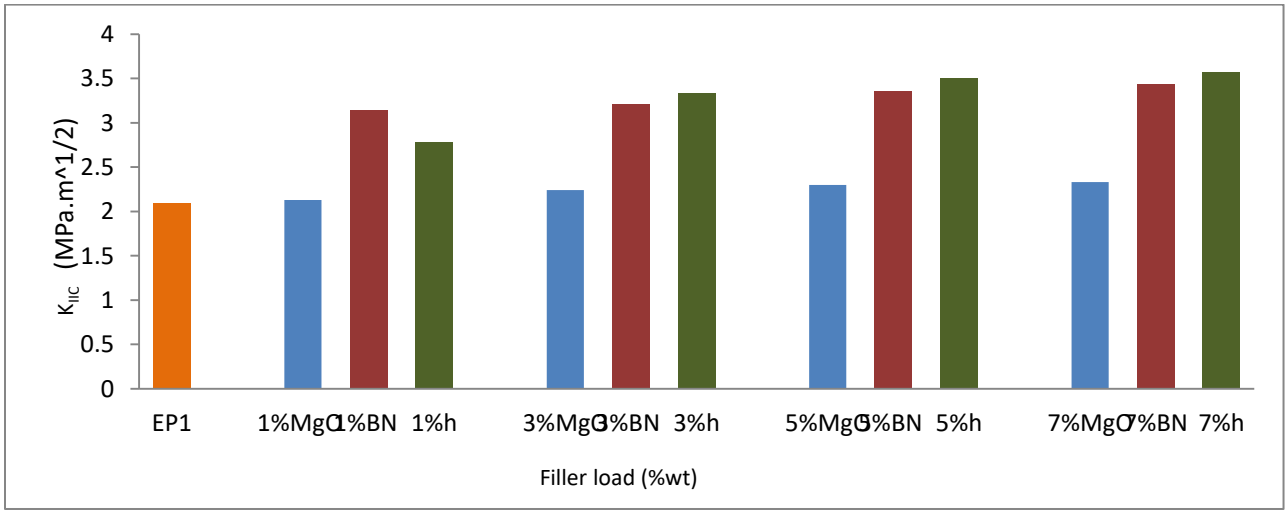

Figure 4.22: Effect of fillers content (w.t%) on the single edge notched bending K_{IIC} of the epoxy matrix.

Figures (4.23) show the load of fracture toughness (SENB) of (epoxy/MgO) (epoxy/BN) and (epoxy/hybrid) nanocomposites at different weighting percent of nanoparticles.

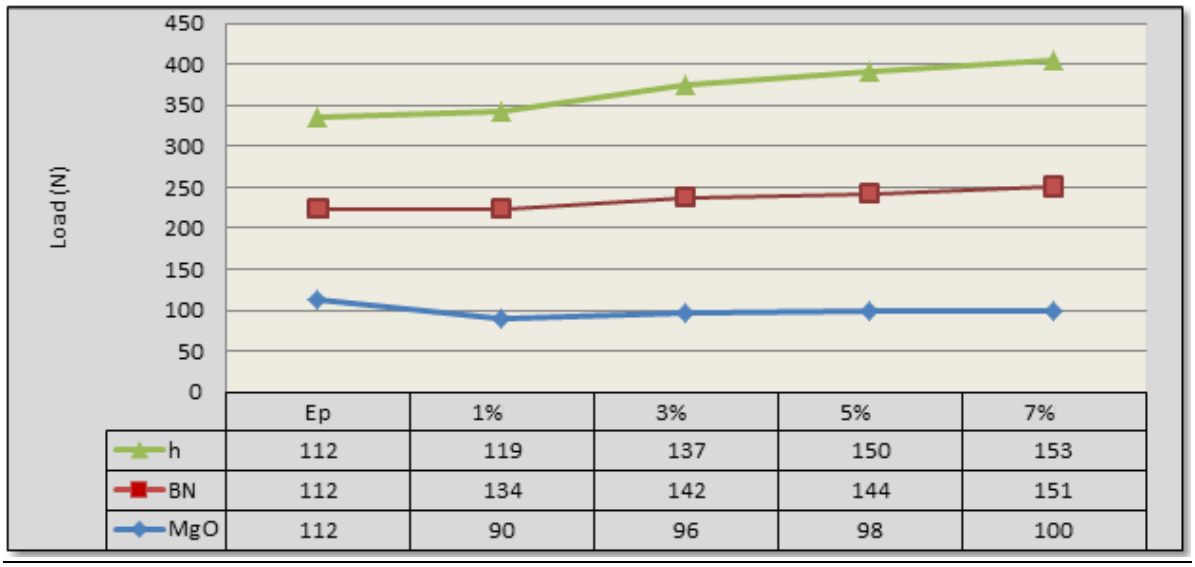

	Ep	1%	3%	5%	7%
h	112	119	137	150	153
BN	112	134	142	144	151
MgO	112	90	96	98	100

Figure 4.23: Illustrate the relation ship between load and fillers content (w.t%) of epoxy/MgO epoxy/BN and epoxy/hybrid nanocomposites.

In Figures (4.22) and (4.23) the results display that the fracture toughness (SENB) and the load of (epoxy/MgO) increase slightly as compared of pure epoxy to the same reason in previous section.

Figures (4.22) and (4.23) show the fracture toughness and the load of (epoxy/BN) and (epoxy/hybrid) nanocomposites are higher than those of pure epoxy. Where the addition of 7% hybrid nanoparticles enhanced K_{IIC} about 41% this is attributed to the same reason in previous section as seen in table (4.7) in appendix F.3

4.6.3. Hardness Results

Figure (4.24) and Table (4.8)in appendix F.4 represent the relationship between the hardness (shore D) and the percentage of addition (1, 3, 5, and 7 % wt) for epoxy/MgO ,epoxy/BN and epoxy/(1:1 MgO /BN)hybrid nanocomposites for all of the samples prepared the hardness has been represented. The results in Figure (4.24) showed that the hardness increases with the increasing of the amount of MgO the heigher value is achieved at 7% of MgO content with inhanced about (8%)This is due to compatibilization between MgO NPs and epoxy and good distribution of nanoparticals .

Since hardness is a desired property for resistance and durability of coatings [229]. It has been rated how the addition of BN NPs to the pure epoxy affects it. In figures (4.24) the hardness has been represented for all the samples prepared.The increase of BN content in the nanocomposite leads to increasing tendency of this characteristic and the heigher value is achieved at 7% of BN content with improvement about (1%) due to nature of BN has finner partical shap as compered to MgO partical shap[229].

Figure (4.24) displays the effect of (1:1 MgO and BN) hybrid NPs loading on the hardness of the epoxy nanocomposite. The results reveal that when the hybrid filler concentration increases, and the heigher value is achieved at 7% of hybrid content with improvement about (10%) due to greater epoxy chain restriction by nanoparticles [224].

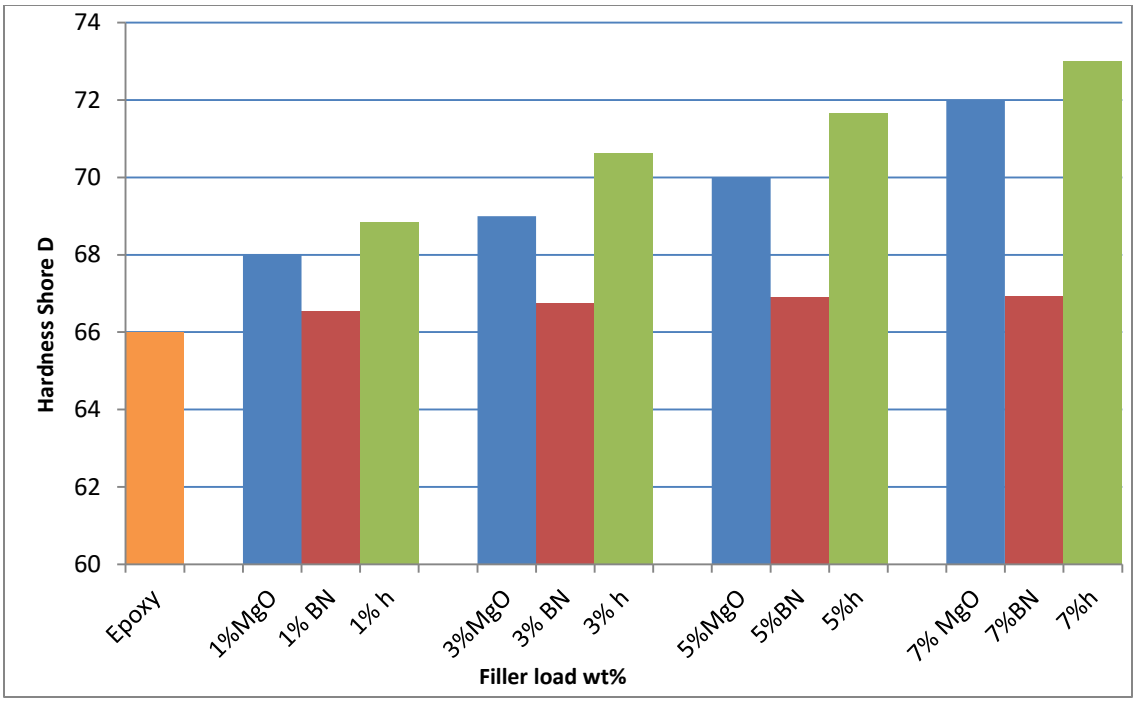

Figure 4.24: Effect of NPs (w.t%) on the hardness of the epoxy matrix.

4.6.4.The Impact Strength :

The impact strength is an indication of the ability of the composite to withstand a sudden impact [106].Figure (4.25) and Table (4.9) (in appendix F.5) show the impact strength of (epoxy/MgO) (epoxy/BN) and (epoxy/hybrid) nanocomposites at different weighting percent of nanoparticles.

The results display that the impact strength of (epoxy/MgO) (epoxy/BN) and (epoxy/hybrid) nanocomposites are greater than those of pure epoxy. The results in the figure (4.25) shows that the values of impact strength increase with MgO NP weight percentages, this could be the fact that the increasing of MgO NP content raises the quantity of absorbed energy[230]. While the values of impact strength increase with BN NP content due to good mixing of BN Np in epoxy matrix leads to enhancing the cohesive strength and making it difficult for the crack propagation [231]. In addition, the values of impact strength increase with

hybrid NP weight percentages and the heigher value is achieved at 7% of hybrid content with improvement about (125%) due to the nanoparticles work to prevent the crack propagation and then increasing the impact strength of the hybrid nanocomposites used[232].

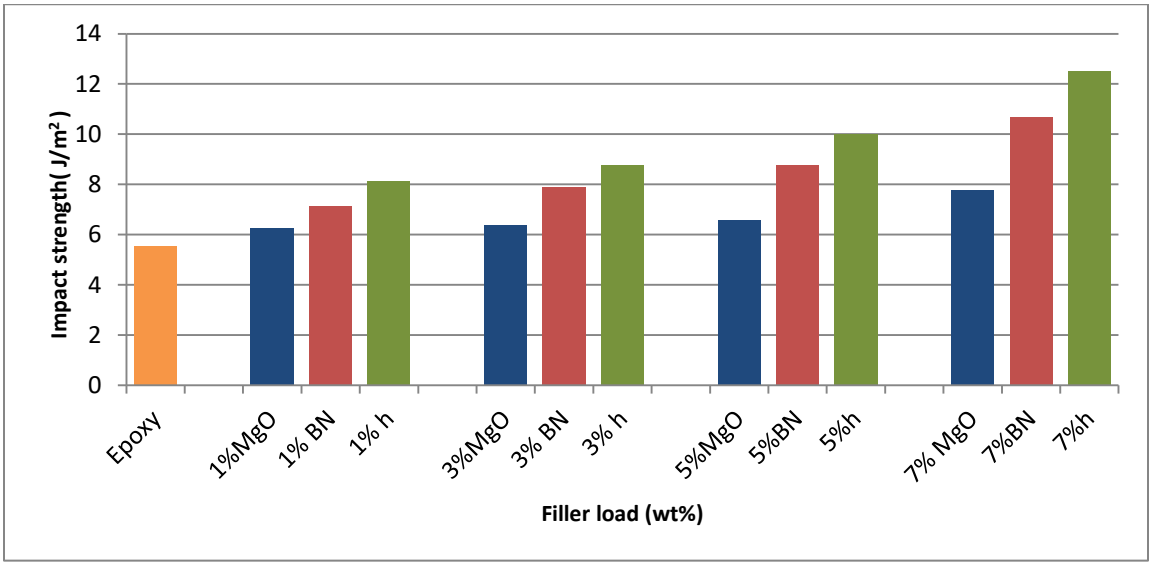

Figure 4.25: The effect of fillers content (w.t%) on the impact strength of the epoxy matrix.

4.6.5 Pull off adhesion

Figure (4.26) and table (4.10) (in appendix F.6) represent the relationship between the pull off adhesion strength and the percentage of addition of MgO, BN and hybrid nanocomposities. The addition of nanoparticles at all percentages between 1% to 7% shows greater adhesion strength than pure epoxy and the use of 7% hybrid nanoparticles enhanced pull off adhesion about 69% as compared to pure epoxy and another non hybrid nanocomposites .

This is due to high percentages of MgO, BN, and hybrid that lead to epoxy rougher when it wet the surface of substrate resulting in mechanical mixing between nanofillers and substrate surface [200] , In addition, MgO and BN np have favorable filler packing for facile heat dissipation through the composites. As

adhesives in electronic circuits not only provide heat dissipation but also mechanical support, adhesion strength is another critical parameter[233].

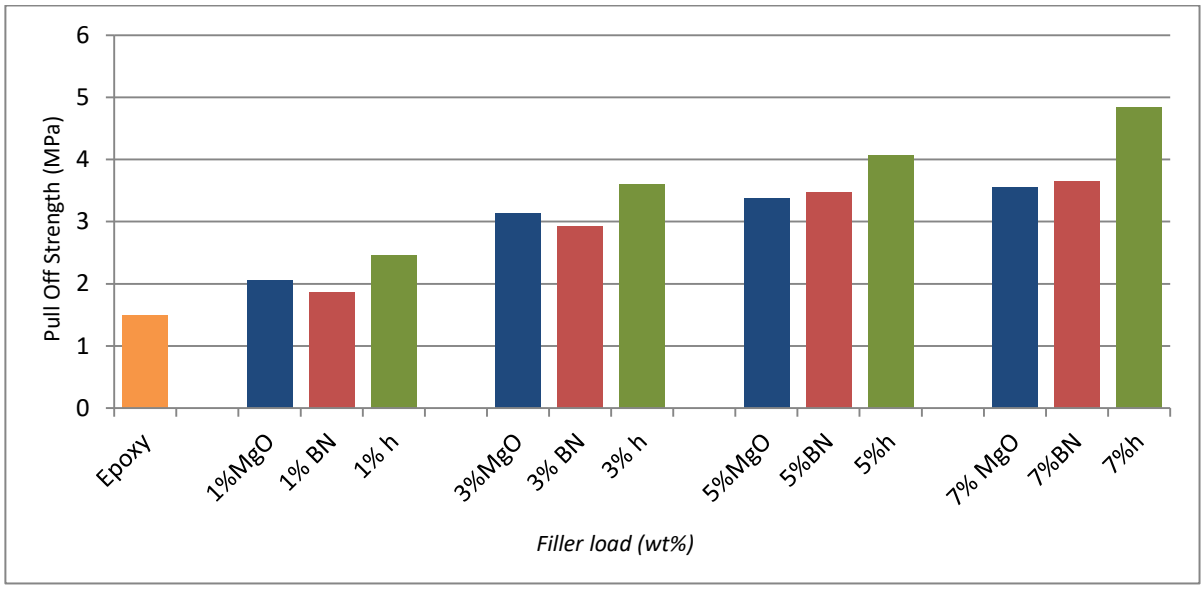

Figure 4.26 : Comparison of pull off strength of the epoxy matrix with fillers content (w.t%)

All pull off adhesion test samples show cohesive and adhesive failure as shown in figure (4.27). This is due to the cohesion force of the epoxy and MgO, BN, and hybrid nanocomposites being greater than the adhesive force between the steel and adhesive [234].

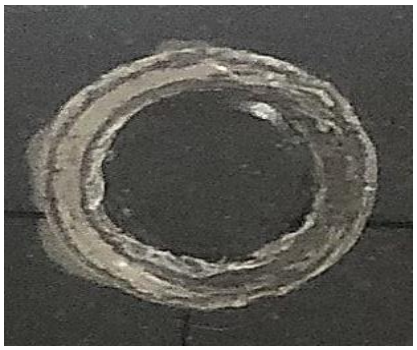

Epoxy

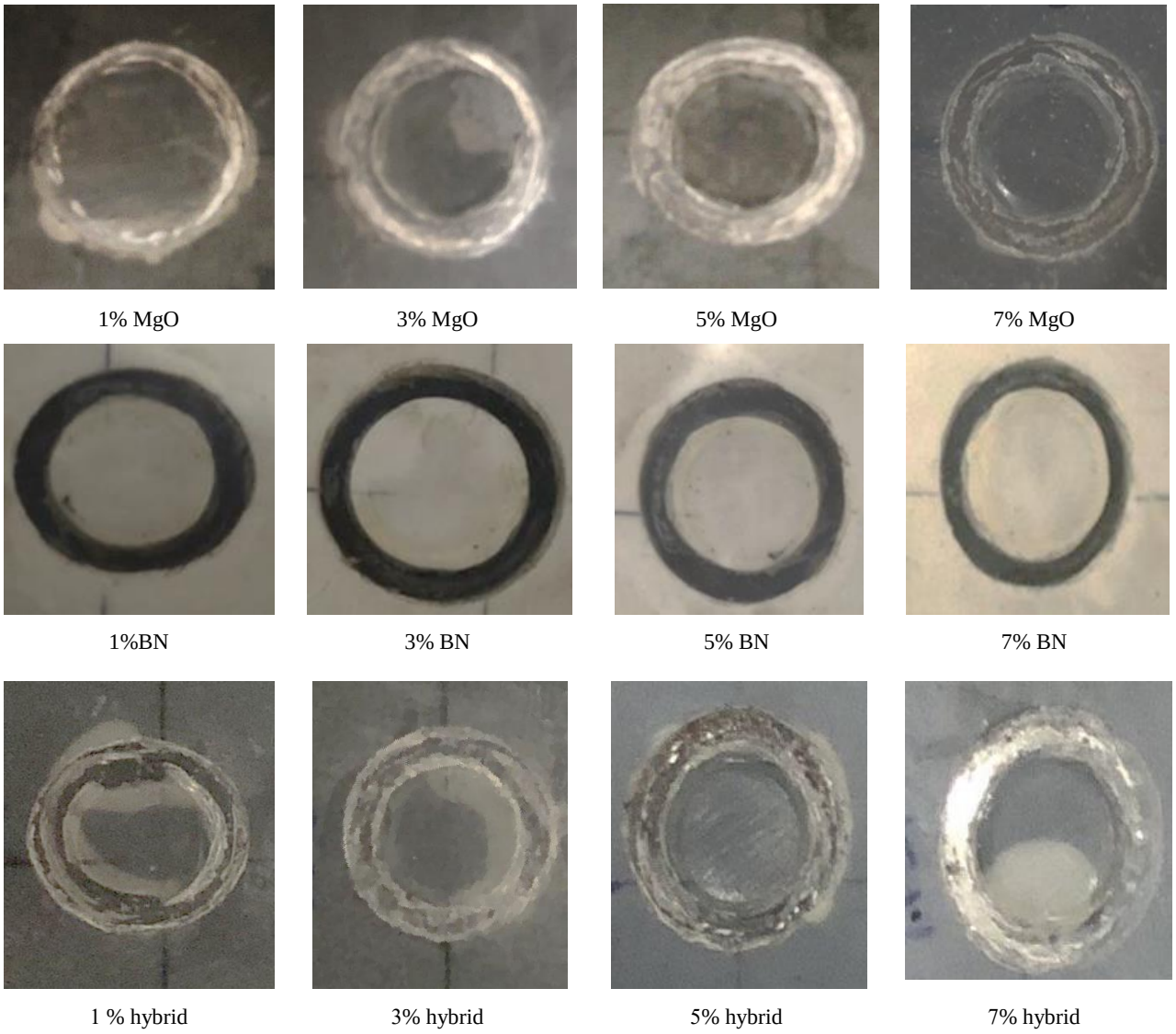

Figure 4.27: Image of adhesive failure shown on the steel substrate.

4.7. Potentiodynamic Polarization Test Results.

Potentiodynamic polarization test curves for the bare and uncoated pure epoxy and epoxy/Nps coated samples in 3.5 %NaCl solution at 25°C are depicted in figures (4.28 - 4.32). The polarization curve of substrates of the coated and uncoated steel are actually dissimilar. It can be detected that there is a noteworthy shift towards the lower current densities for coated samples compared with the uncoated samples.

The corrosion current of the epoxy coated samples are around 4.33 A/Cm^2 for the epoxy specimen compared with 8.11 A/Cm^2 for the bare specimen as shown in Figures(4.28 and 4.29) for bare and epoxy specimens, Respectively and table (4.11) .These results confirm that epoxy coating significantly reduces metal ion release for steel substrate and decreases the corrosion rate of these substrate in NaCl solution[235] , which means that the obtained pure epoxy coating was uniform and compact and its adhesion to the substrate was very good. An overall protective epoxy surface layer may ensure outstanding corrosion resistance and . These findings are in agreement with other studies which indicate that coating steel with a polymeric barrier does in fact improve corrosion resistance[236] .

It should also be pointed out that the corrosion potential of an uncoated sample is higher as compared to that of the epoxy coated one. A significant reduction was noted in the current required for the dissolution for the nanocomposite coated specimen as compared to the bare steel and pure polymer-coated specimen after inspecting the value of the current density exactly at the same polarized potentials. From Figs. (4.28-4.32) it is easy to note that for bare steel corrosion, the current density increased as the voltage increased. That increment happened rapidly up to 11.8 $*10^{-6}$ A/cm^2 .The presence of the epoxy/MgO ,epoxy/BN,epoxy/hybrid nanocomposite coating increases the corrosion resistance by decreasing the current density as compared for the bare specimen As shown in table 4.11 in appendix G.

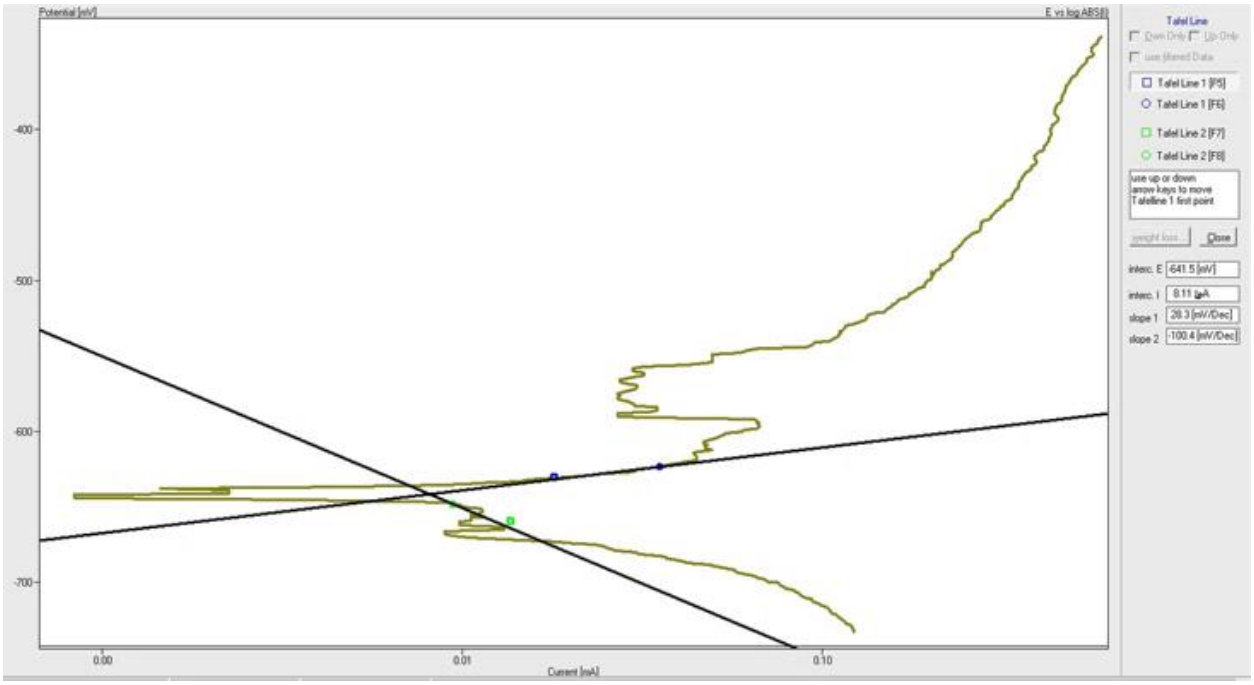

bare

Figure 4.28: Potentiodynamtic polarization for bare specimen in NaCl 3.5% solution.

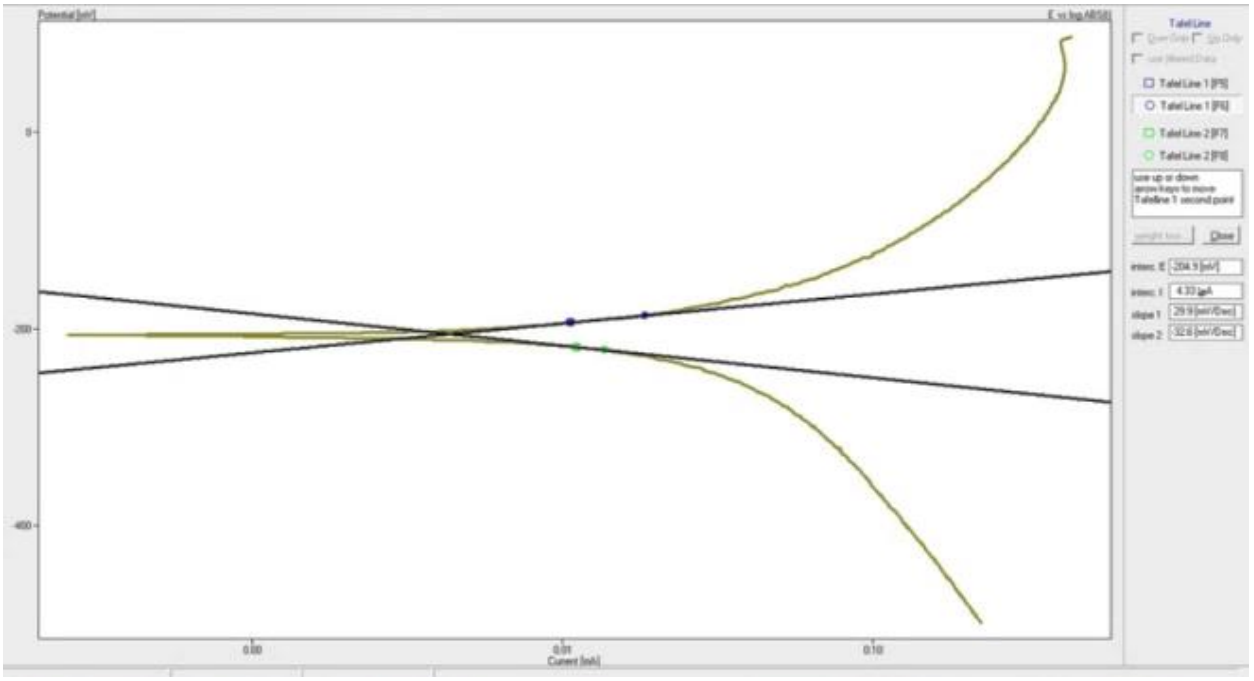

epoxy

Figure 4.29: Potentiodynamtic polarization for epoxy specimen in NaCl 3.5% solution.

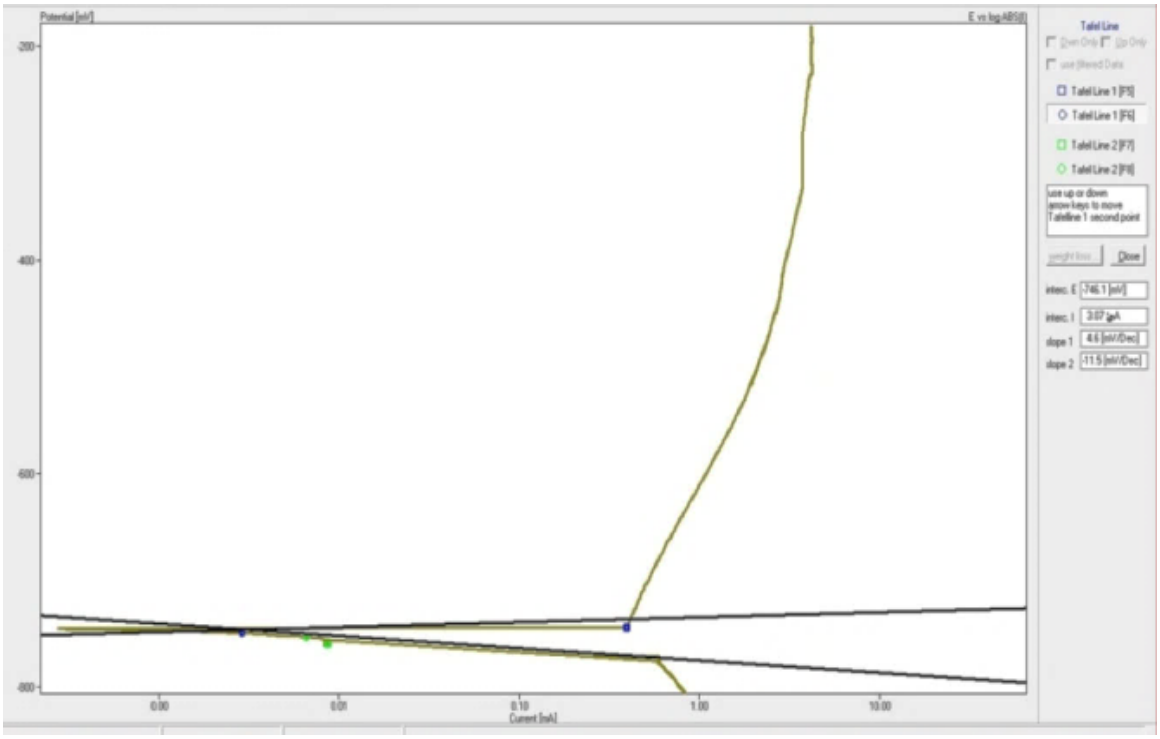

(a)

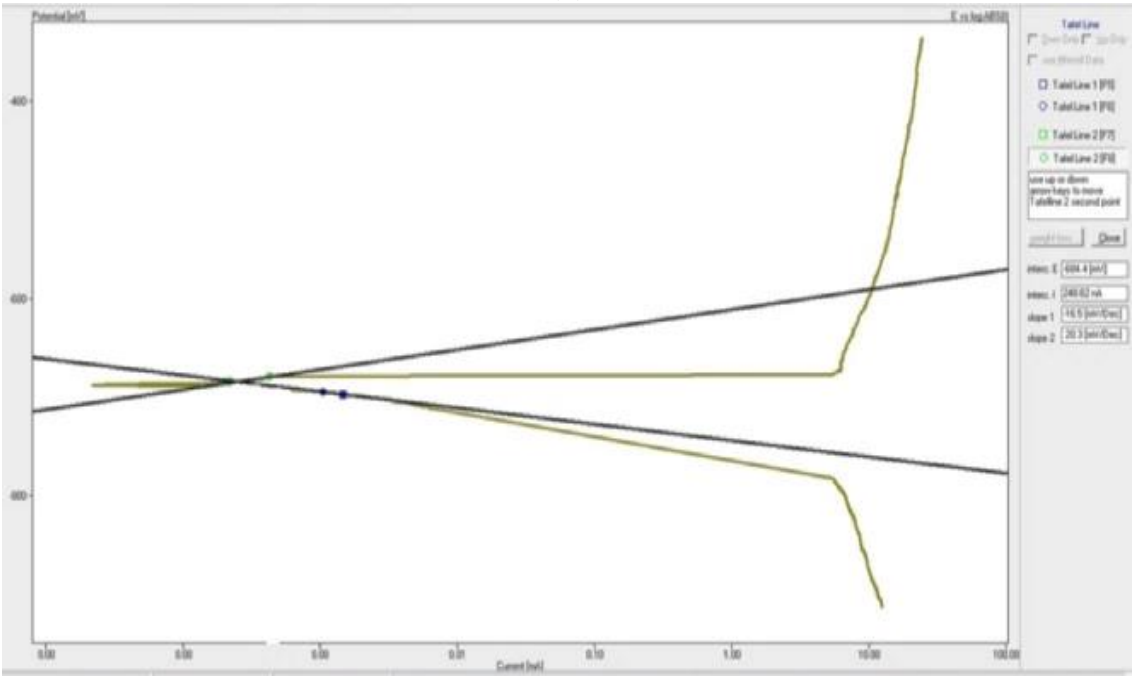

(b)

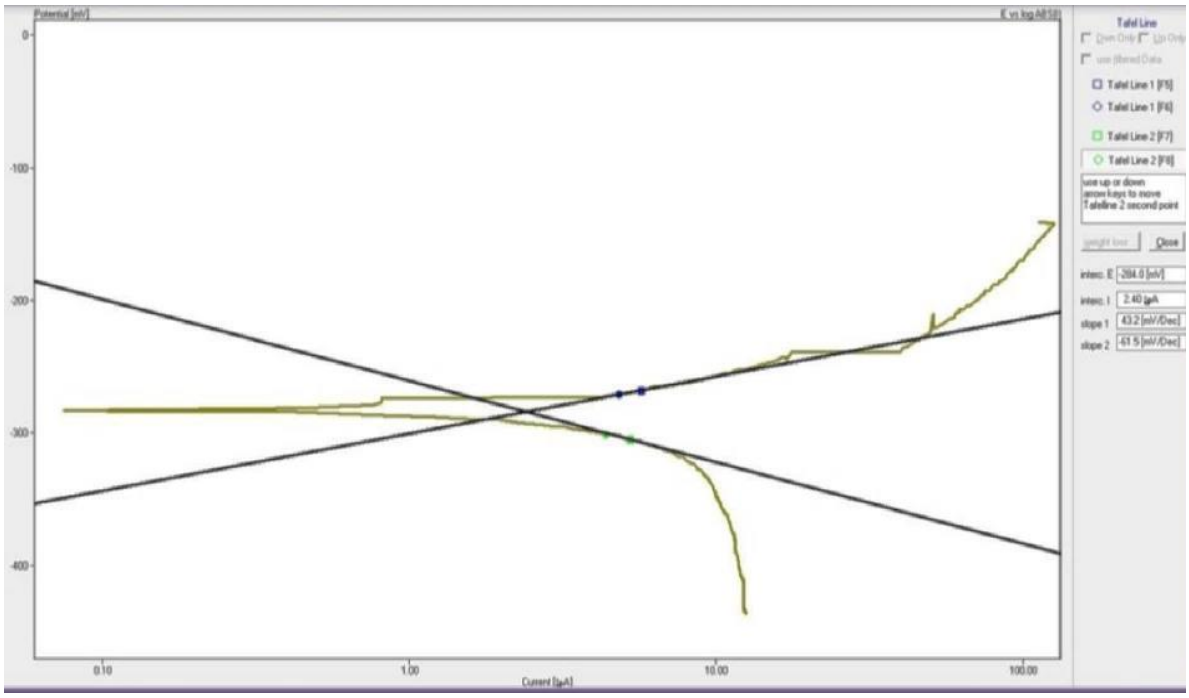

(c)

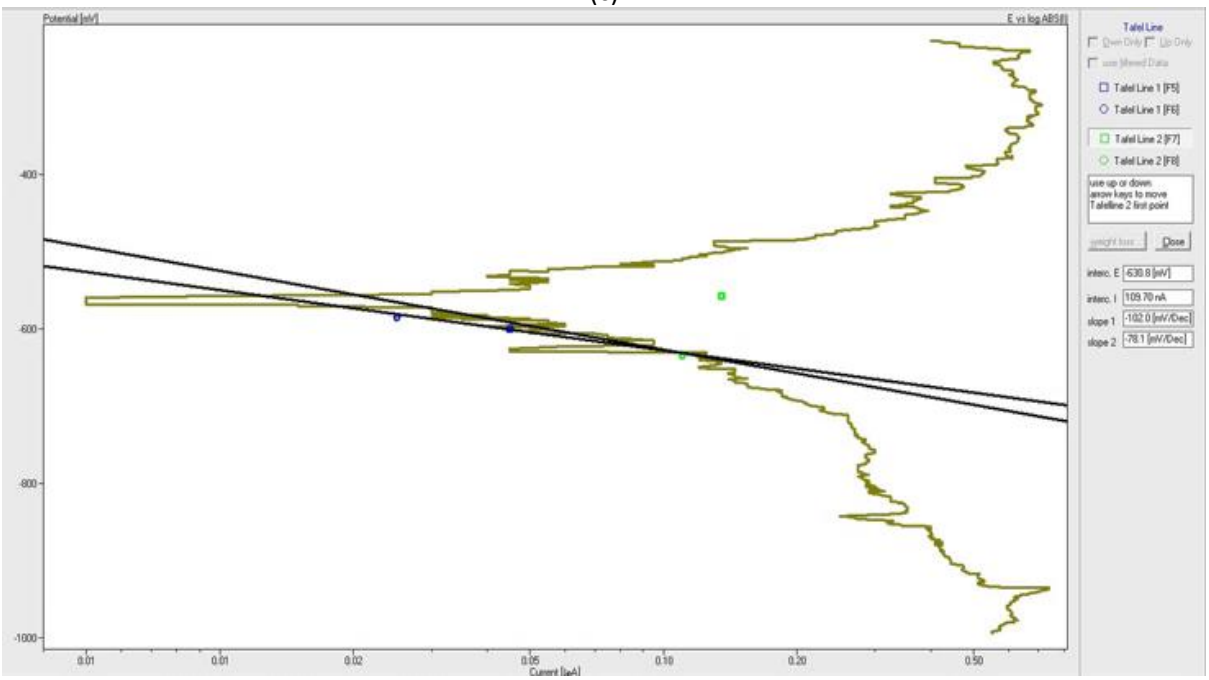

(d)

Figure 4.30 : Potentiodynamtic polarization for (a) 1% epoxy/MgO ,(b) 3% epoxy/MgO, (c)5% epoxy/MgO , and (d) 7% epoxy/MgO specimen in NaCl 3.5% solution.

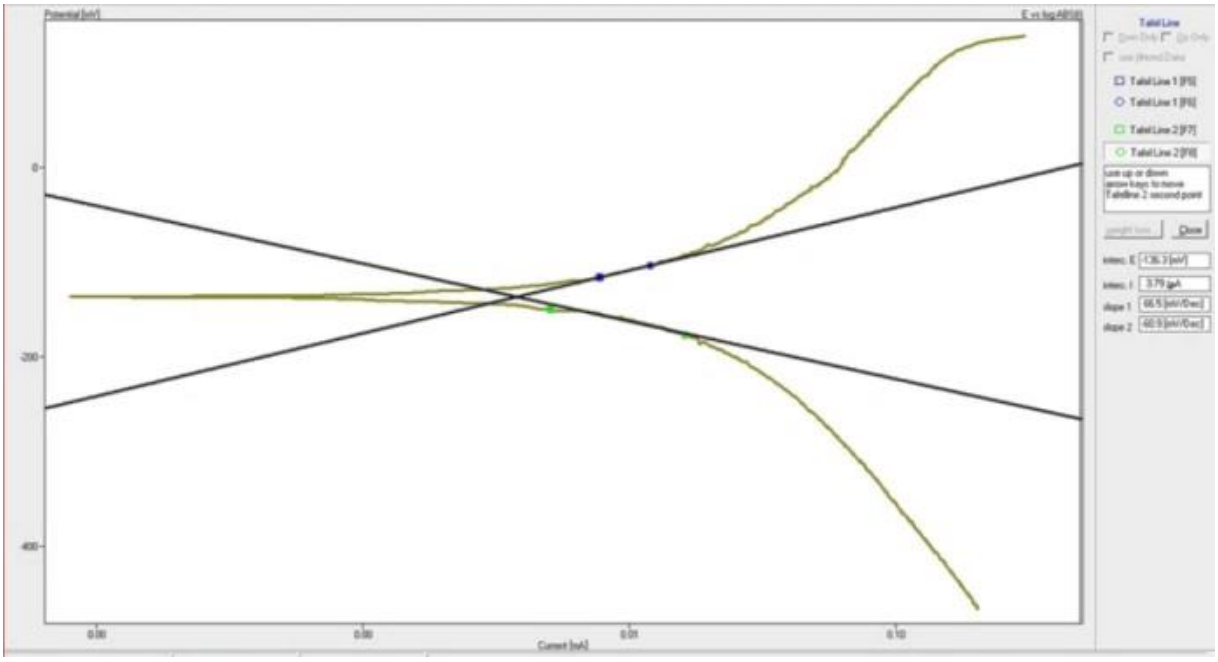

(a)

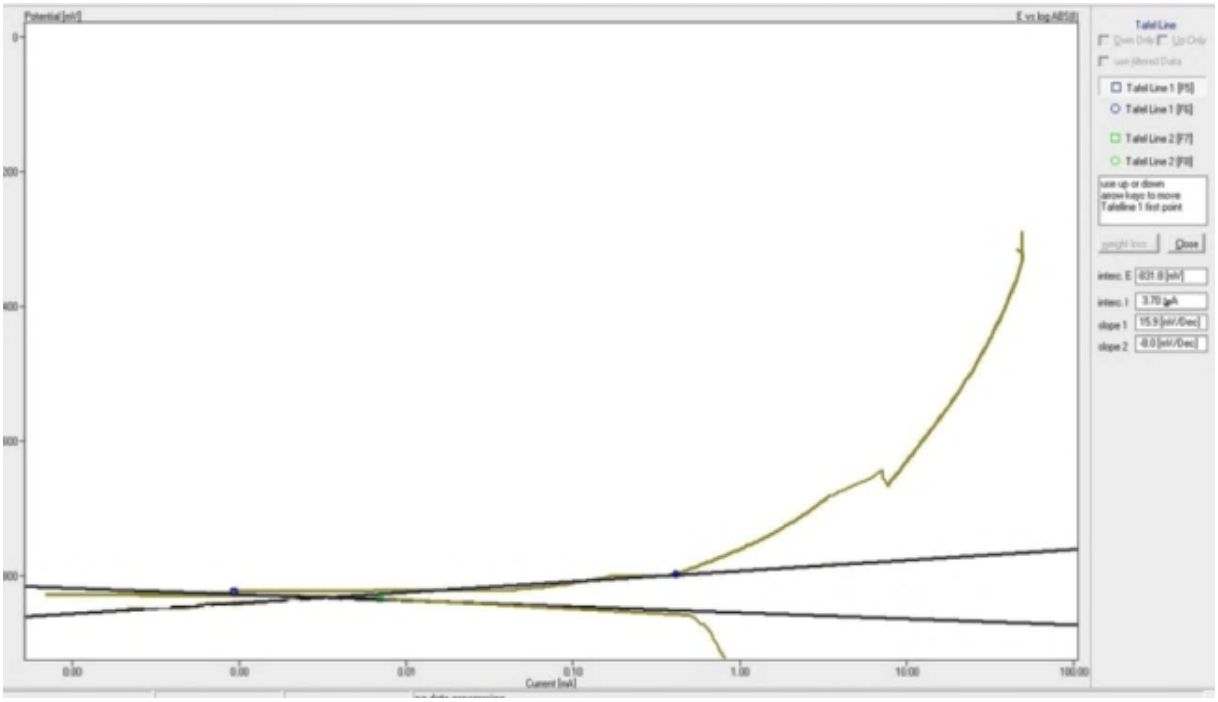

(b)

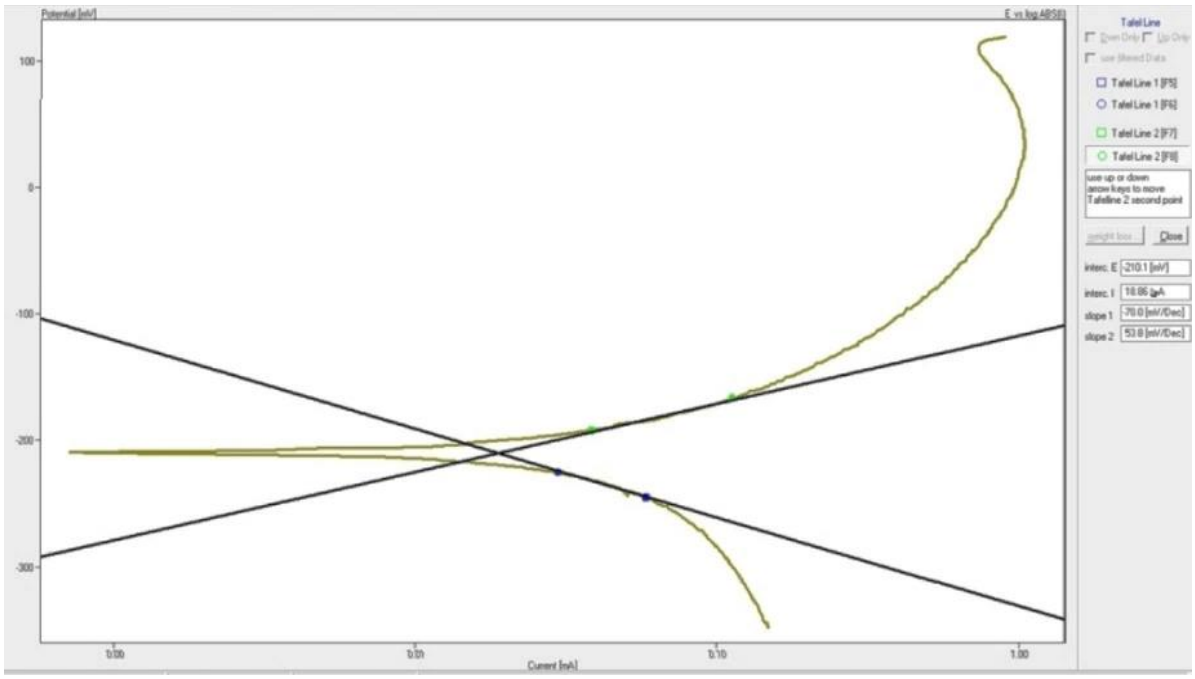

(c)

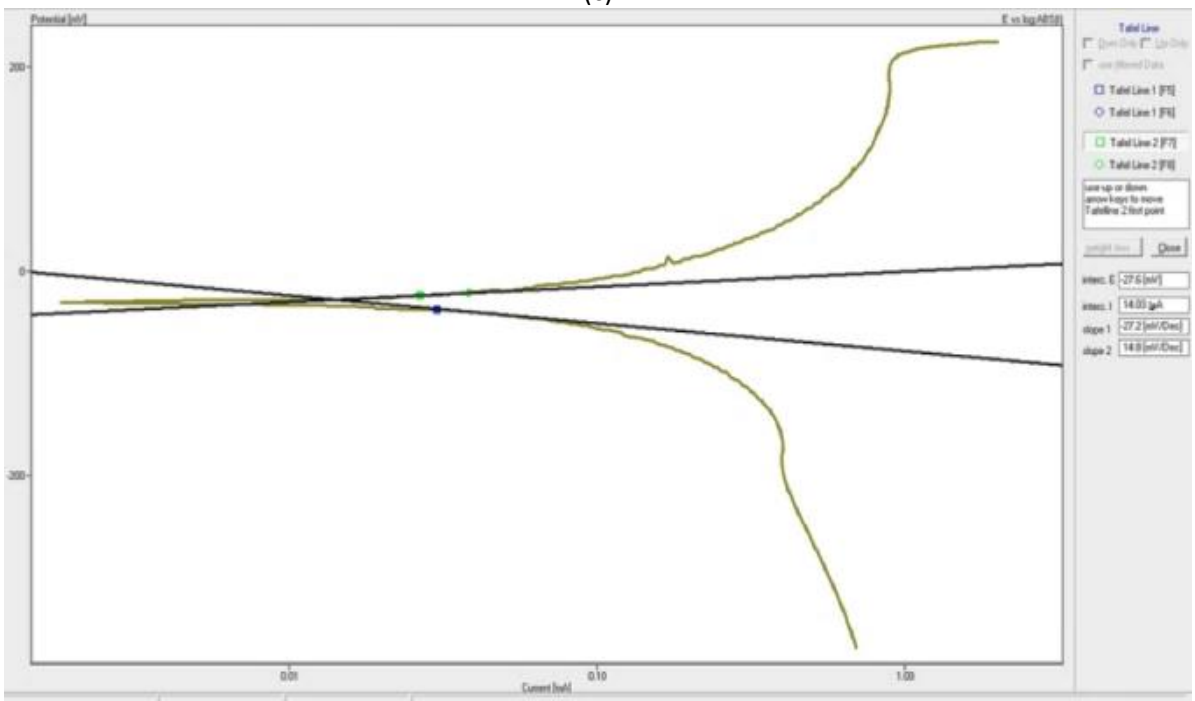

(d)

Figure 4.31: Potentiodynamtic polarization for (a) 1% epoxy/BN ,(b) 3% epoxy/BN, (c)5% epoxy/BN , and (d) 7% epoxy/BN specimen in NaCl 3.5% solution.

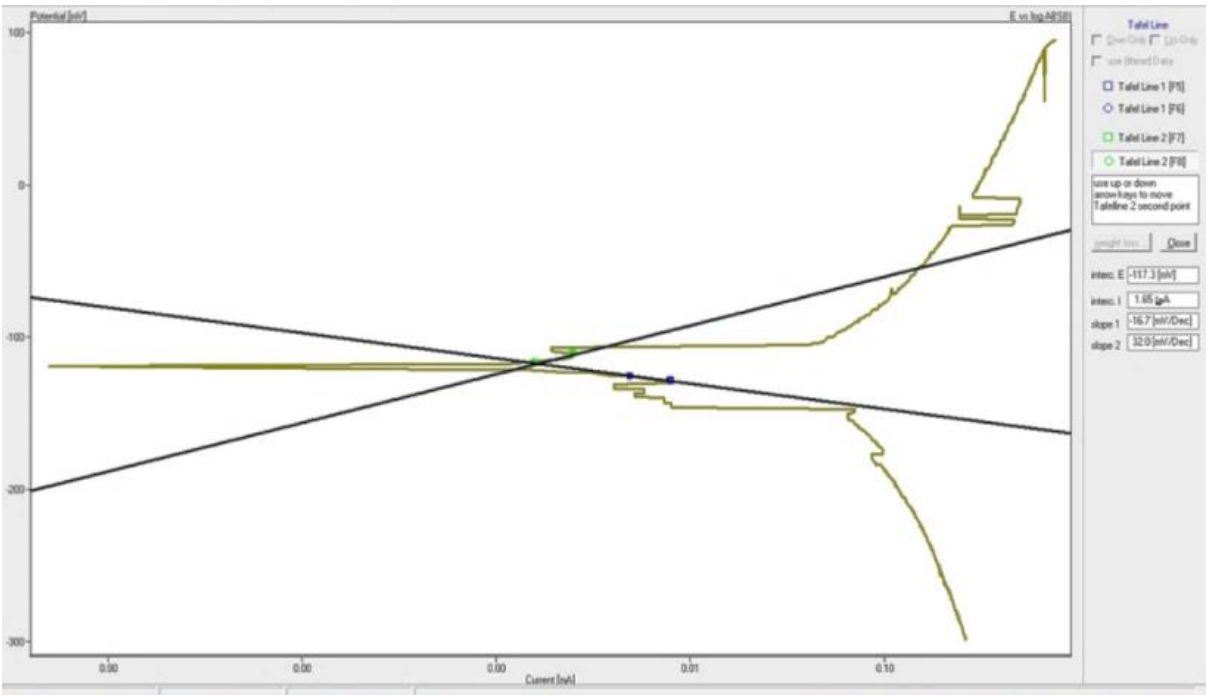
Potential [mV]
E vs log ABS(I)
Tafel Line
Tafel Line 1 [F5]
Tafel Line 1 [F6]
Tafel Line 2 [F7]
Tafel Line 2 [F8]
use up or down arrow keys to move Tafelline 2 second point
weight loss
Close
interc. E -117.3 [mV]
interc. I 1.85 µA
slope 1 -16.7 [mV/Dec]
slope 2 32.0 [mV/Dec]
100
0
-100
-200
-300
0.00
0.00
0.00
0.01
0.10
Current [mA]

(a)

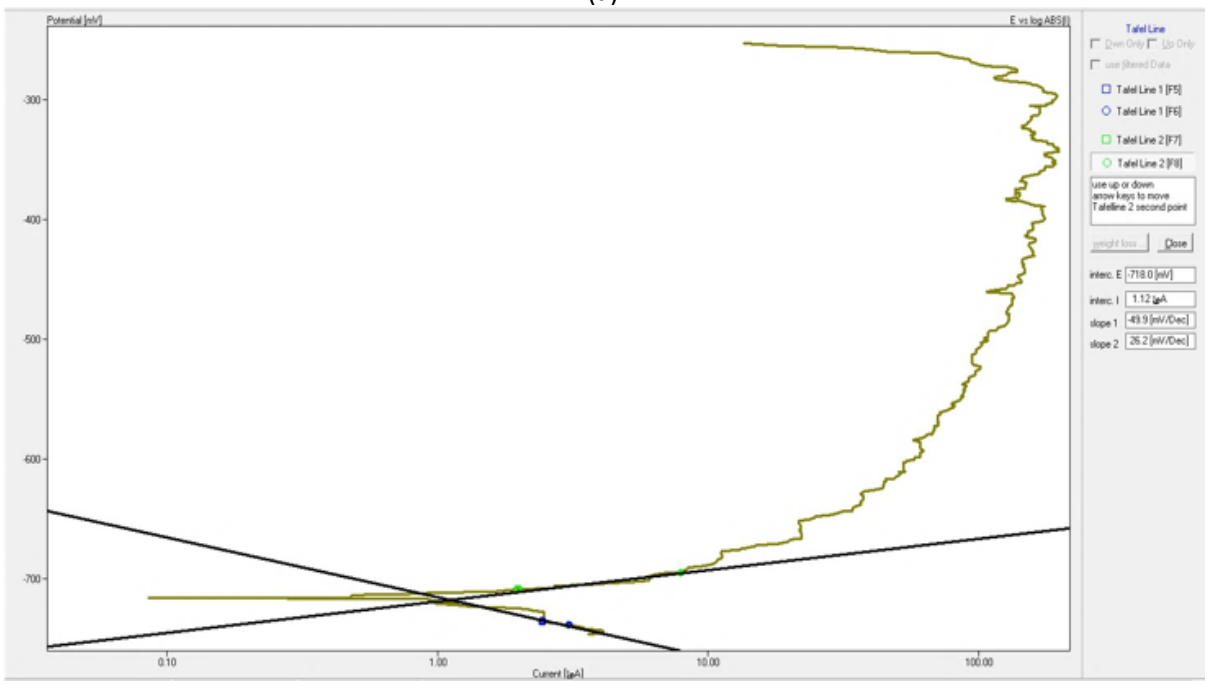
Potential [mV]
E vs log ABS(I)
Tafel Line
Tafel Line 1 [F5]
Tafel Line 1 [F6]
Tafel Line 2 [F7]
Tafel Line 2 [F8]
use up or down arrow keys to move Tafelline 2 second point
weight loss
Close
interc. E -718.0 [mV]
interc. I 1.12 µA
slope 1 -49.9 [mV/Dec]
slope 2 26.2 [mV/Dec]
-300
-400
-500
-600
-700
0.10
1.00
10.00
100.00
Current [µA]

(b)

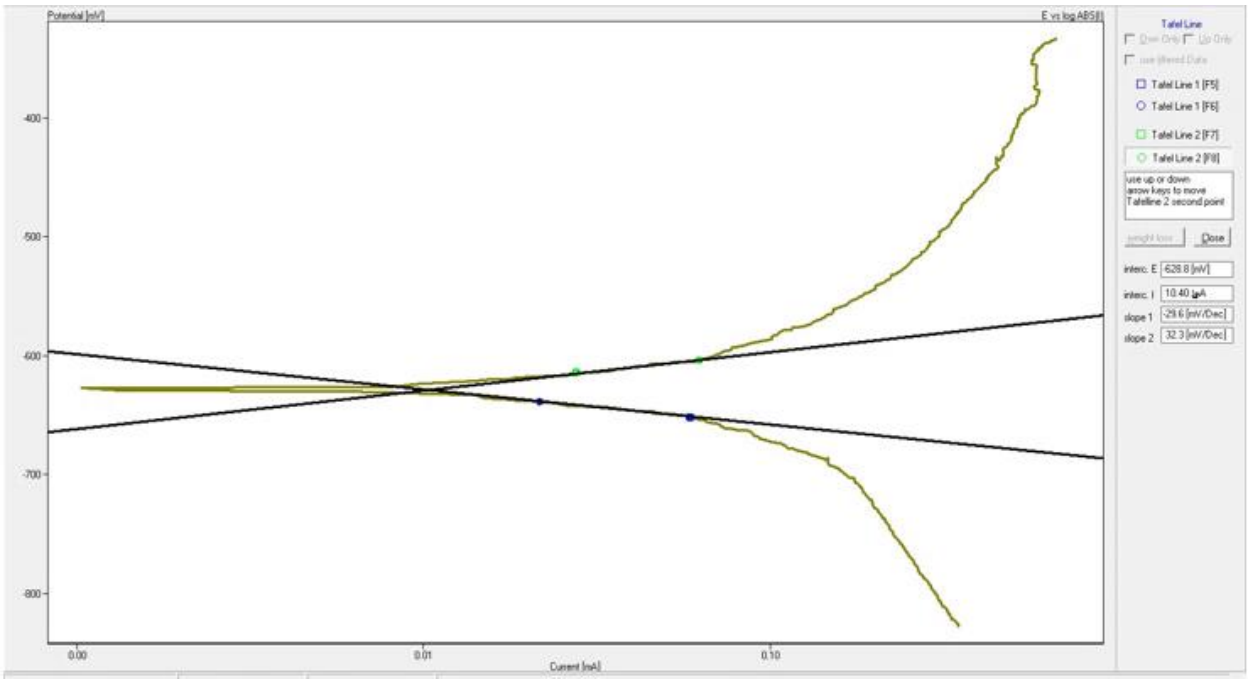

(c)

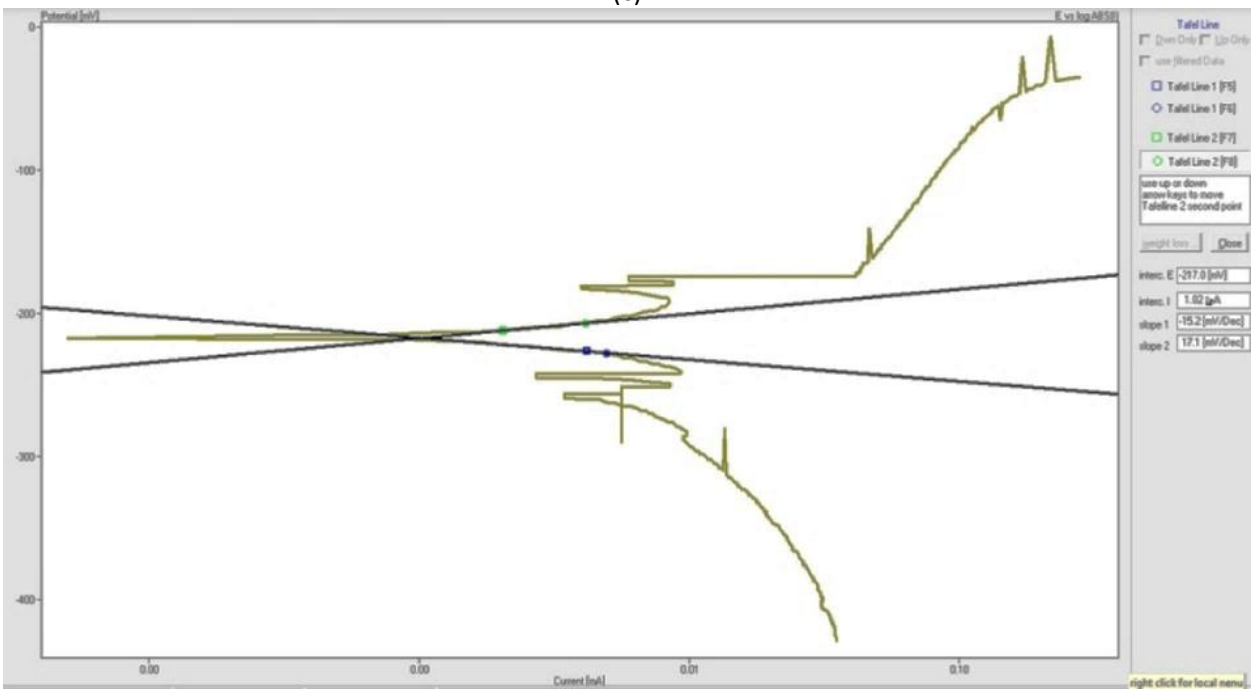

(d)

Figure 4.32: Potentiodynamtic polarization for (a) 1% epoxy/hybrid ,(b) 3% epoxy/ hybrid, (c)5% epoxy/ hybrid , and (d) 7% epoxy/ hybrid specimen in NaCl 3.5% solution.

Figures (4.33) shows the relation between the inhibition efficiency and filler content for epoxy/MgO,epoxy/BN,epoxy/hybrid nanocomposities at (1,3,5,7 wt%) filler loading.

The result show that the corrosion rate led to an increase in the inhibition efficiency with increase filler content and the addition of 7% hybrid nanoparticles enhanced the efficiency of inhibition about 87% as compared of pure epoxy and another non hybrid nanocomposites as shown in figure (4.33)and Table 4.11. Due to that barrier coating usage is essential to suppress the corrosion in a NaCl solution by controlling the diffusion of harmful ions, and electrons to the metal surface. and leads to a significant decrease in the corrosion current values in the anodic curves, which provides a high level of noticeable corrosion protection. where The coated film works as a strong and efficient passivation layer for the diffusion of ions and corrosion[237] .

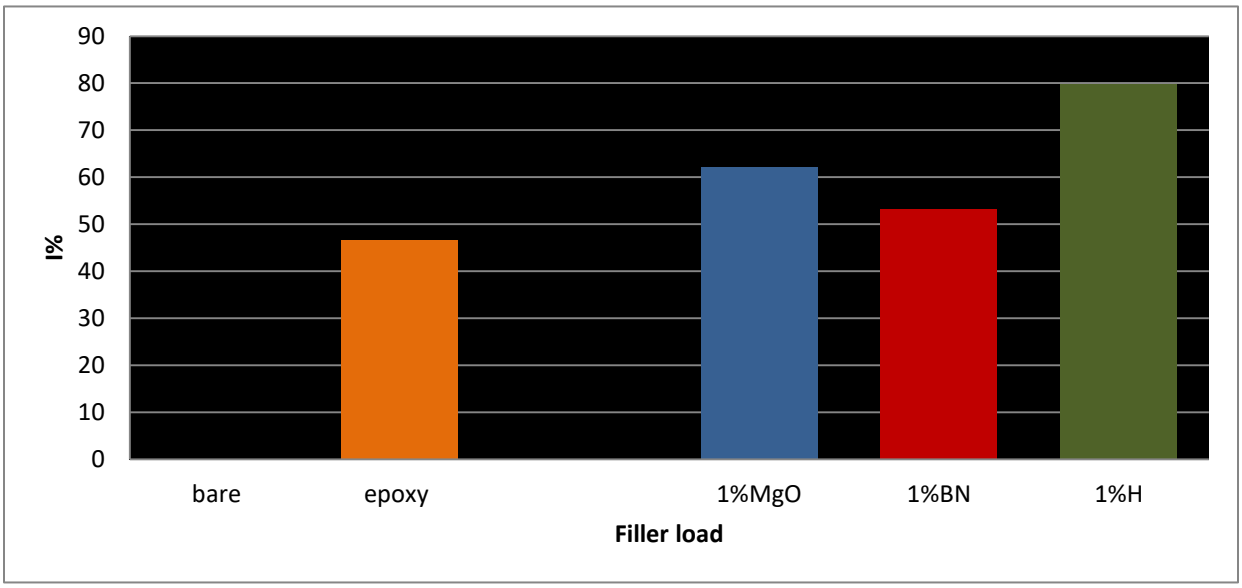

(a)

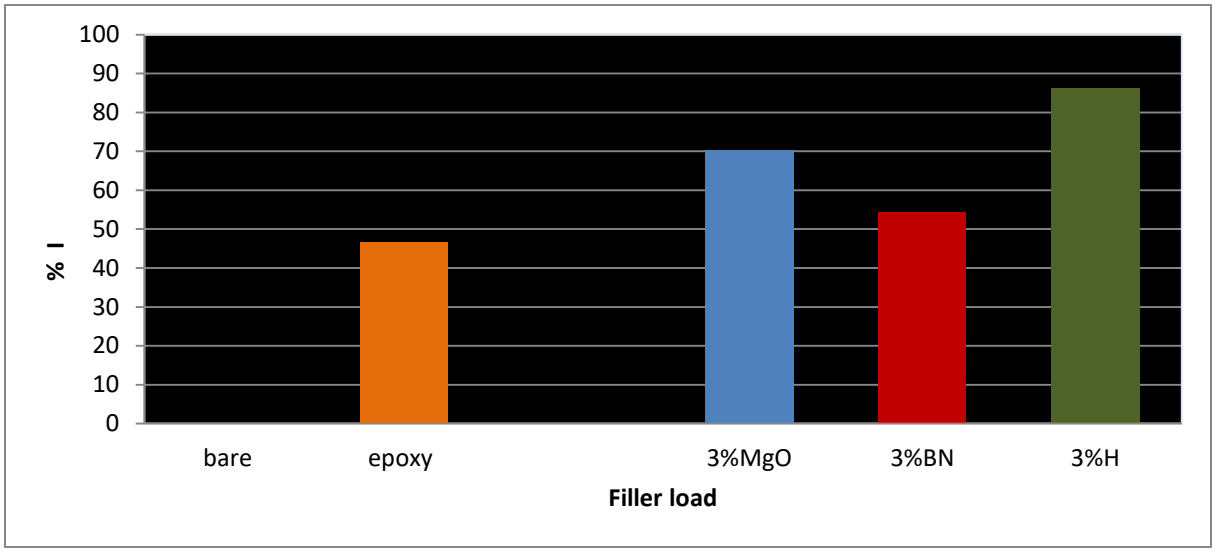
100
90
80
70
60
50
40
30
20
10
0
% I
bare
epoxy
3%MgO
3%BN
3%H
Filler load

(b)

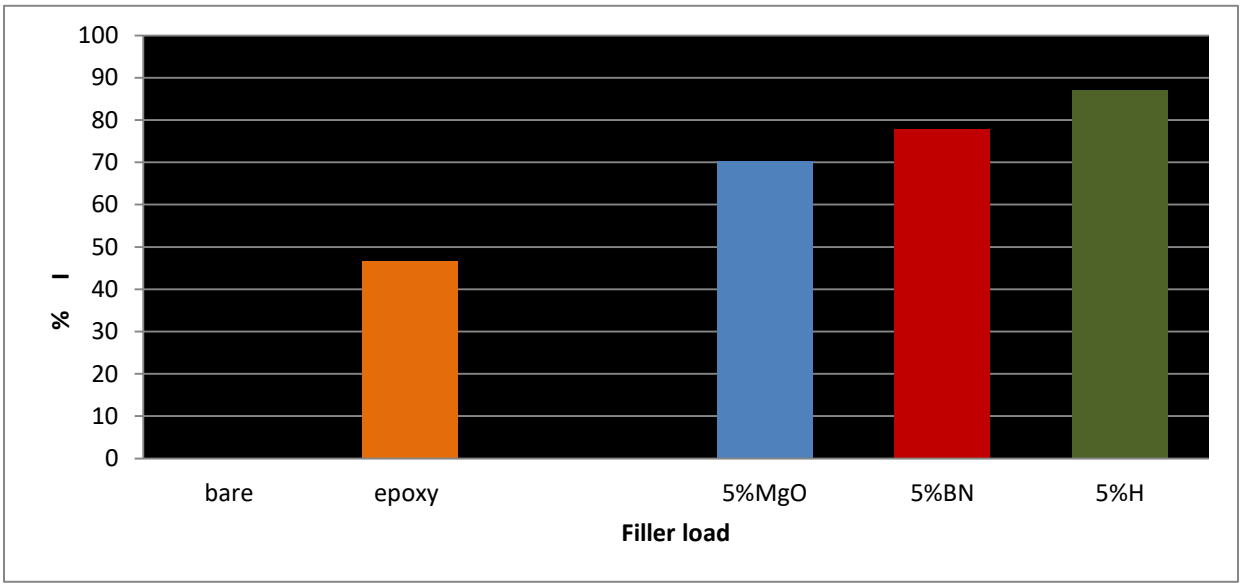
100
90
80
70
60
50
40
30
20
10
0
% I
bare
epoxy
5%MgO
5%BN
5%H
Filler load

(c)

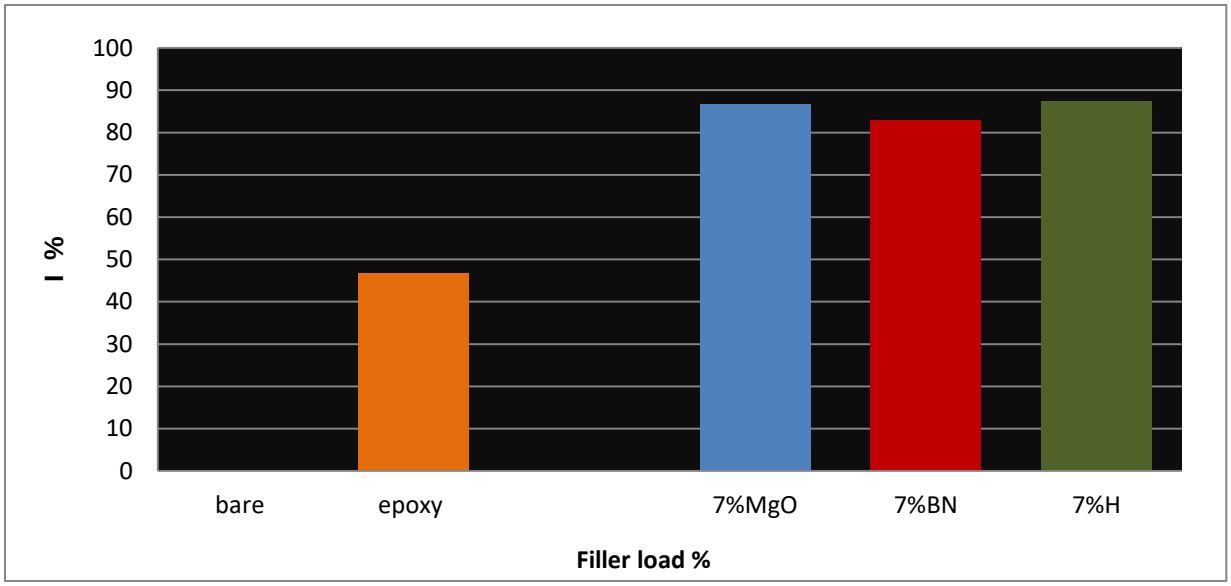

(d)

Figure 4.33: The relationship between the efficiency of inhibition (I) and filler loading of (a) 1% epoxy/MgO ,epoxy/BN and epoxy/hybrid ,(b) 3% epoxy/MgO ,epoxy/BN and epoxy/hybrid, (c)5% epoxy/MgO ,epoxy/BN and epoxy/hybrid and (d) 7% epoxy/MgO ,epoxy/BN and epoxy/hybrid.

Chapter Five
Conclusion
and
Recommendations

5.1 Conclusion

From the obtained results and their discussion in chapter four, the following conclusions can be drawn:

1. For the FT-IR results proved, there is no chemical reaction, and there is only physical interaction between the active surface of nanoparticles and the polar matrix of epoxy polymer.
2. For the XRD results proved, the reflection peaks in XRD of pure phase of MgO and pure hexagonal phase of BN.
3. DSC results proved that there is increasing in the Tg value.
4. In AFM images ,the presence of MgO Np, BN Np and hybrid Np results in surface roughness, Sa increased and this is applied to Sds and Sbi also.
5. In SEM images, MgO NP has a coarse size but BN shows a finer size.
6. The thermal conductivity of the nanocomposites increased with increasing MgO, BN, and hybrid nanoparticle concentration as compared to pure epoxy.
7. Electrical resistivity increased with increasing filler content as compared to pure epoxy.
8. Elongation of epoxyMgO, epoxy/BN and epoxy/hybrid nanocomposites decreased with the increase in the content of MgO NP, BN NP.and hybrid NP_S.
9. The tensile strength and modulus , hardness, impact strengths, fracture toughness (K_{IC},K_{IIC}), Pull off adhesion strength of nanocomposites increased with increasing MgO, BN, and hybrid nanoparticle concentration as compared to pure epoxy.

10. Current density decrease and increase the efficiency of inhibition of epoxy against steel corrosion in NaCl solution from 46.6 % of pure epoxy to 87.4 % .

5.2 Recommendations:

1. Studying another thermal testes such as flame retardancy , combustion resistance and of epoxy nanocomposites.
2. Using hybrid matrix like thermoset polyurethane, and epoxy.
3. Using different substrates like aluminum.
4. Studying the environmental conditions like UV ultraviolet, temperature for MgO ,BN and hybrid nanocomposites.
5. Using Contact Angle and wettability and Surface roughness tests for coating samples

Appendix A

Table 4.1:FTIR spectra of epoxy/MgO, (B):epoxy/BN and (C): epoxy/hybrid nanocomposities [238]**.**

Band (cm-1)	Assignment
≈ 3500	O-H stretching
3057	Stretching of C-H of the oxirane ring
2965- 2075	StretchingC-H of CH2 and CH aromatic and aliphatic
1604	Stretching C=C of aromatic rings
1509	Stretching C-C of aromatic
1459.95	C-H bending bond
1212,1033	Stretching C-O of oxirane group
925	Stretching C-O-C of ethers
831	Stretching C-O-C of oxirane group
772	Rocking CH2

Appendix B.

Table 4.2: Sa, S_{ds} ,S_{bi} and S_{ci} and AFM parameters of epoxy/MgO,epoxy/BNand epoxy/hybrid nanocomposites

Samples	roughness average (Sa) (nm)	The density of summitS (Sds)	The surface bearing index (Sbi)	The core fluid retention index (S_{ci})
EP	1. 5	0.165	0.216	1.52
1%MgO	2.43	0.169	0.298	1.53
3%MgO	2.83	0.199	0.754	1.59
5%MgO	3.27	0.217	0.864	1.62
7%MgO	3.74	0.239	1.35	1.63
1%BN	3.43	0.269	0.497	1.53
3%BN	3.83	0.299	0.553	1.57
5%BN	4.27	0.317	0.663	1.69
7%BN	3.74	0.239	1.35	1.70
1%h	3.53	0.269	0.597	1.57
3% h	3.73	0.299	0.653	1.59
5% h	4.37	0.317	0.763	1.63
7% h	4.94	0.239	1.85	1.67

Appendix C

Table 4.3: The glass transition temperature and degradation temperature of pure epoxy , EP/MgO ,EP/BN, EP/(1:1MgO/BN)hybrid nanocomposites

Nanocomposites	NPs (wt.%)	Tg (°C)	Td(°C)
Epoxy	0	79.12°C	308.3 °C
EP/MgO1	1	82.39 °C	305.92 °C
EP/MgO3	3	83.65 °C	305.77 °C
EP/MgO5	5	84.49 °C	305.09 °C
EP/MgO7	7	85.77 °C	299.60 °C
EP/BN1	1	80.78 °C	308.13 °C
EP/BN3	3	82.79°C	308.32 oC
EP/BN5	5	83.13 °C	313.71 °C
EP/BN7	7	84.76 °C	300.3 °C
EP/Hybrid1	1	80.6 °C	308.60 °C
EP/Hybrid3	3	84.65 °C	300.85 °C
EP/Hybrid5	5	86.2 °C	308.60 °C
EP/Hybrid7	7	92.6 °C	297.42 °C

Appendix D

Table 4.4: The thermal conductivity of pure epoxy , EP/MgO ,EP/BN, EP/(1:1MgO/BN) hybrid nanocomposites

Nanocomposites	NPs (wt.%)	Thermal conductivity(W/M.K)
Epoxy	0	0.20
EP/MgO1	1	0.55
EP/MgO3	3	1
EP/MgO5	5	1.55
EP/MgO7	7	2.22
EP/BN1	1	0.88
EP/BN3	3	1.11
EP/BN5	5	1.71
EP/BN7	7	2.88
EP/Hybrid1	1	1.4
EP/Hybrid3	3	2.12
EP/Hybrid5	5	3.13
EP/Hybrid7	7	3.69

Appendix E

Table 4.5: The electrical resistivity of pure epoxy , epoxy/MgO ,epoxy/BN, epoxy/(1:1MgO/BN)hybrid nanocomposites

Nanocomposites	NPs (wt.%)	Electrical Resistivity (Ω .cm)
Epoxy	0	2.4E+15
EP/MgO1	1	4.8E+15
EP/MgO3	3	5.4E+15
EP/MgO5	5	5.76E+15
EP/MgO7	7	6E+15
EP/BN1	1	5.52E+15
EP/BN3	3	6.36E+15
EP/BN5	5	6.84E+15
EP/BN7	7	7.2E+15
EP/Hybrid1	1	6E+15
EP/Hybrid3	3	6.96E+15
EP/Hybrid5	5	7.68E+15
EP/Hybrid7	7	8.4E+15

Appendix F1

Table 4.6:The tensile strength, mosulus and elongation of pure epoxy , epoxy/MgO,epoxy/BN, ep/(1:1MgO/BN) hybrid nanocomposites.

Nanocomposites	NPs (wt.%)	Tensile Strength (MPa)	Young Modulus (GPa)	Elongation (%)
Epoxy	0	18	0.19	11.3
EP/MgO1	1	18.33	0.22	10.97
EP/MgO3	3	19.71	0.24	10.73
EP/MgO5	5	19.15	0.25	10.5
EP/MgO7	7	19.31	0.28	10.2
EP/BN1	1	17.89	0.2	11.25
EP/BN3	3	17.88	0.21	11.35
EP/BN5	5	17.87	0.22	11.45
EP/BN7	7	17.86	0.23	11.52
EP/Hybrid1	1	19.5	0.23	10.06
EP/Hybrid3	3	19.66	0.27	8.82
EP/Hybrid5	5	19.34	0.28	8.76
EP/Hybrid7	7	22.33	0.3	8.2

Appendix.F2

Table appendix F2: Stress-Strain curves obtained from the tensile test of epoxy , epoxy/MgO,epoxy/ BN and epoxy/hybid nanocomposities samples for 1,3,5,7 %wt at room tempeature

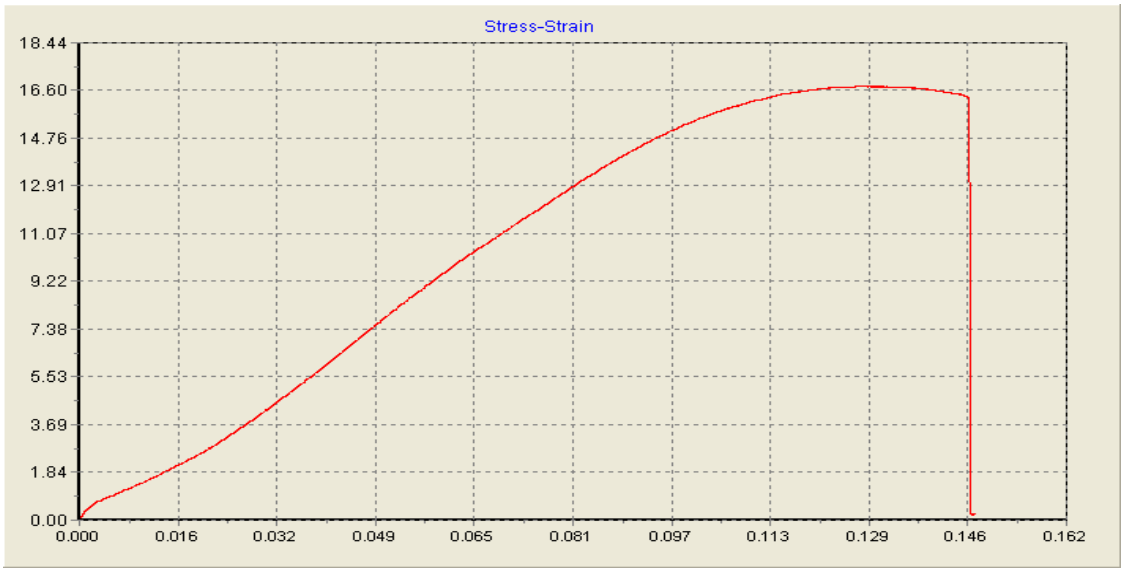

epoxy

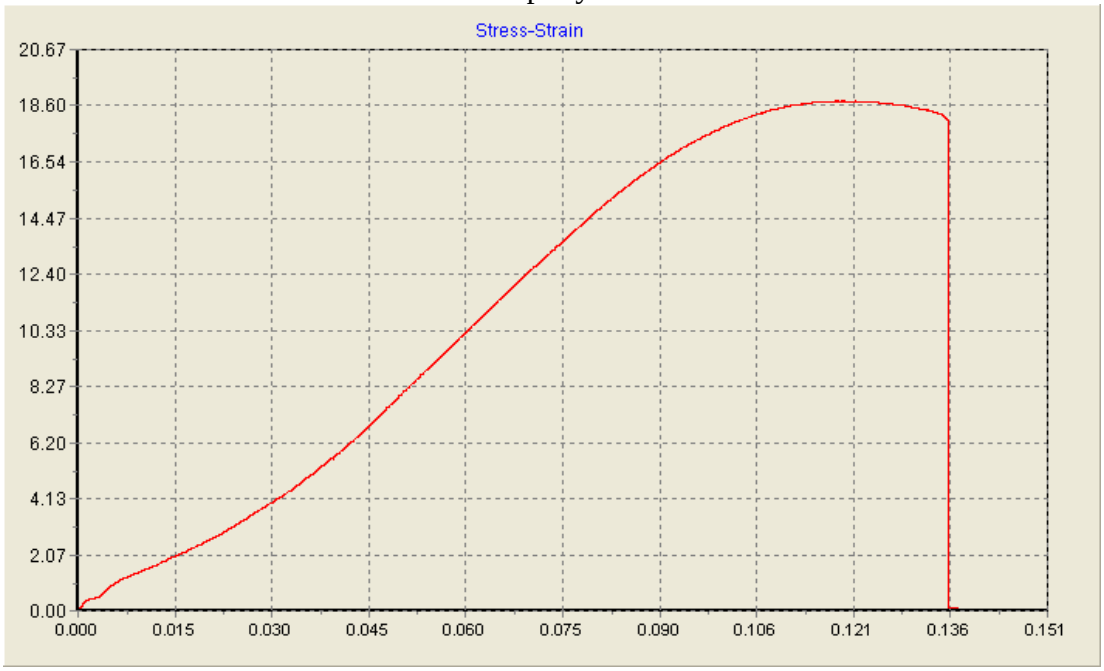

1%MgO

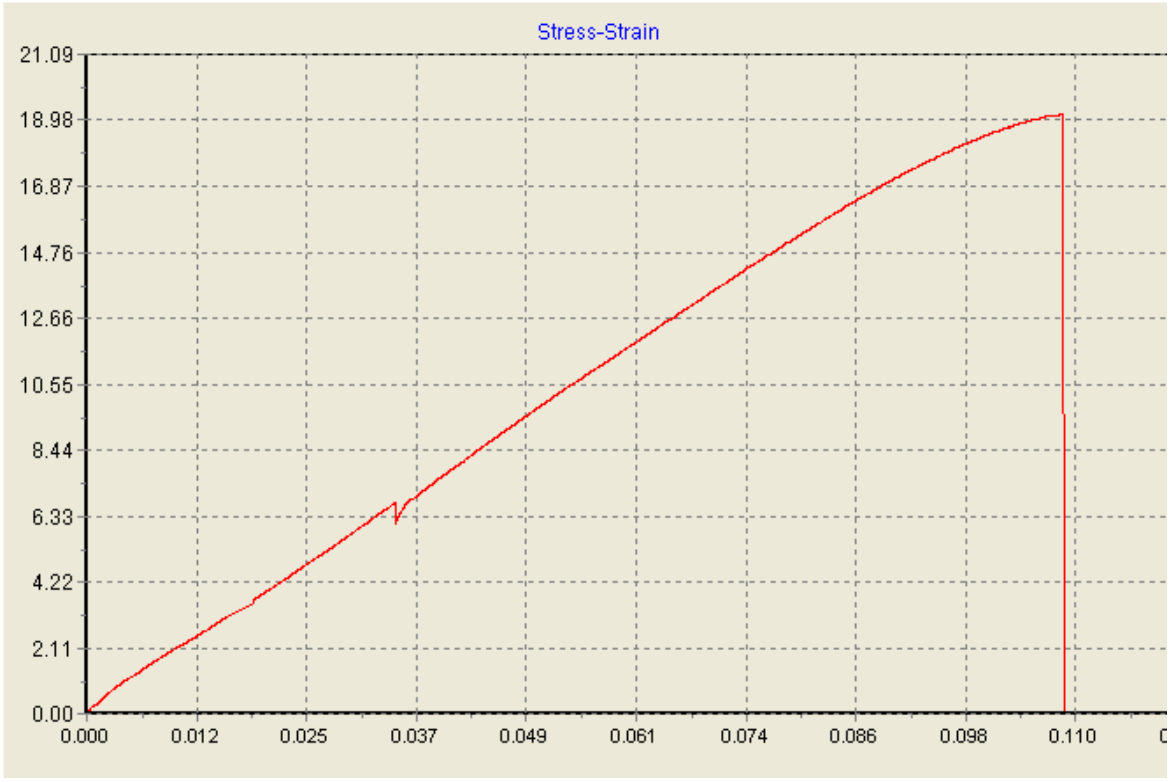
Stress-Strain
21.09
18.98
16.87
14.76
12.66
10.55
8.44
6.33
4.22
2.11
0.00
0.000
0.012
0.025
0.037
0.049
0.061
0.074
0.086
0.098
0.110

3%MgO

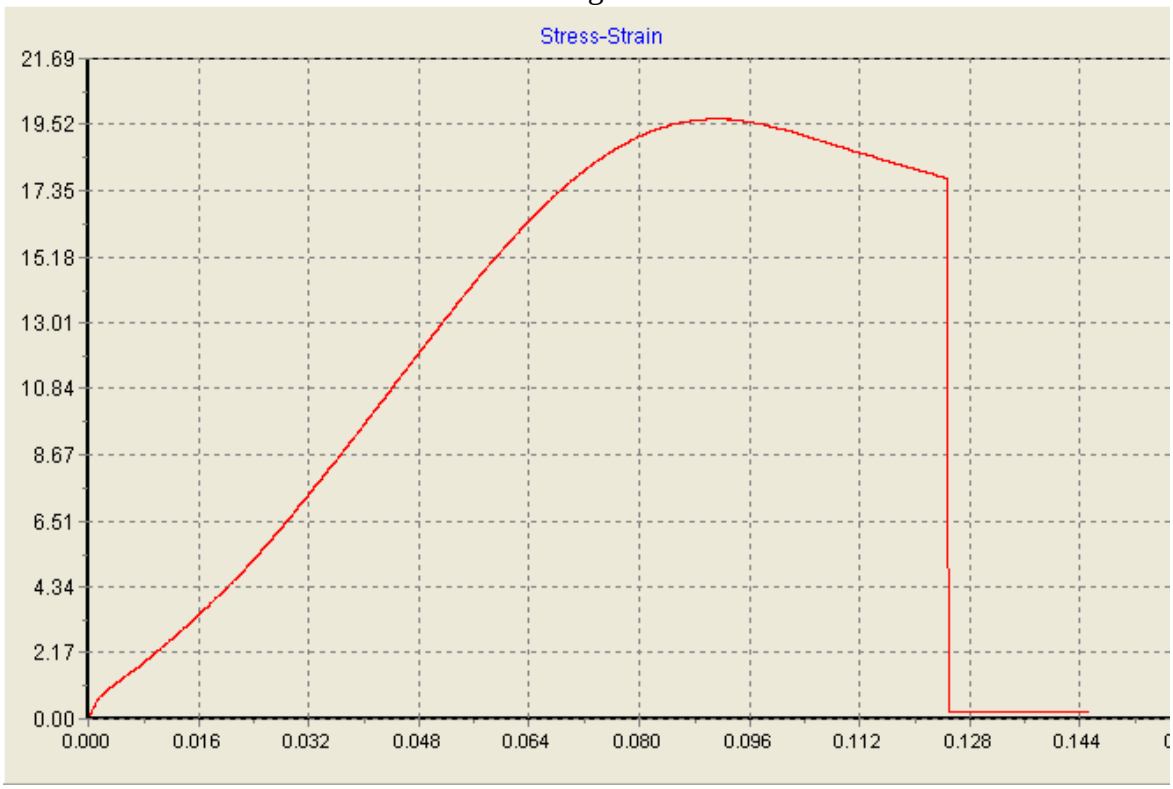
Stress-Strain
21.69
19.52
17.35
15.18
13.01
10.84
8.67
6.51
4.34
2.17
0.00
0.000
0.016
0.032
0.048
0.064
0.080
0.096
0.112
0.128
0.144

5%MgO

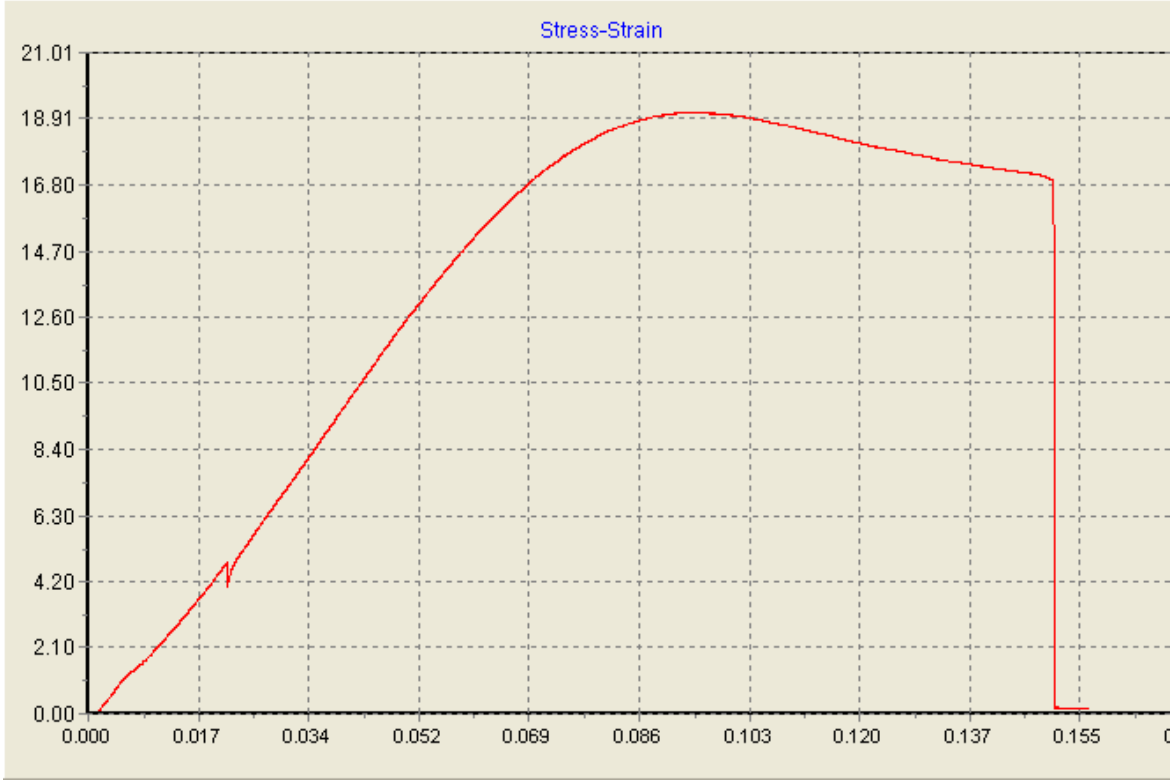
Stress-Strain
21.01
18.91
16.80
14.70
12.60
10.50
8.40
6.30
4.20
2.10
0.00
0.000
0.017
0.034
0.052
0.069
0.086
0.103
0.120
0.137
0.155

7%MgO


Stress-Strain
18.38
16.54
14.70
12.87
11.03
9.19
7.35
5.51
3.68
1.84
0.00
0.000
0.007
0.015
0.022
0.029
0.036
0.044
0.051
0.058
0.066

1%BN

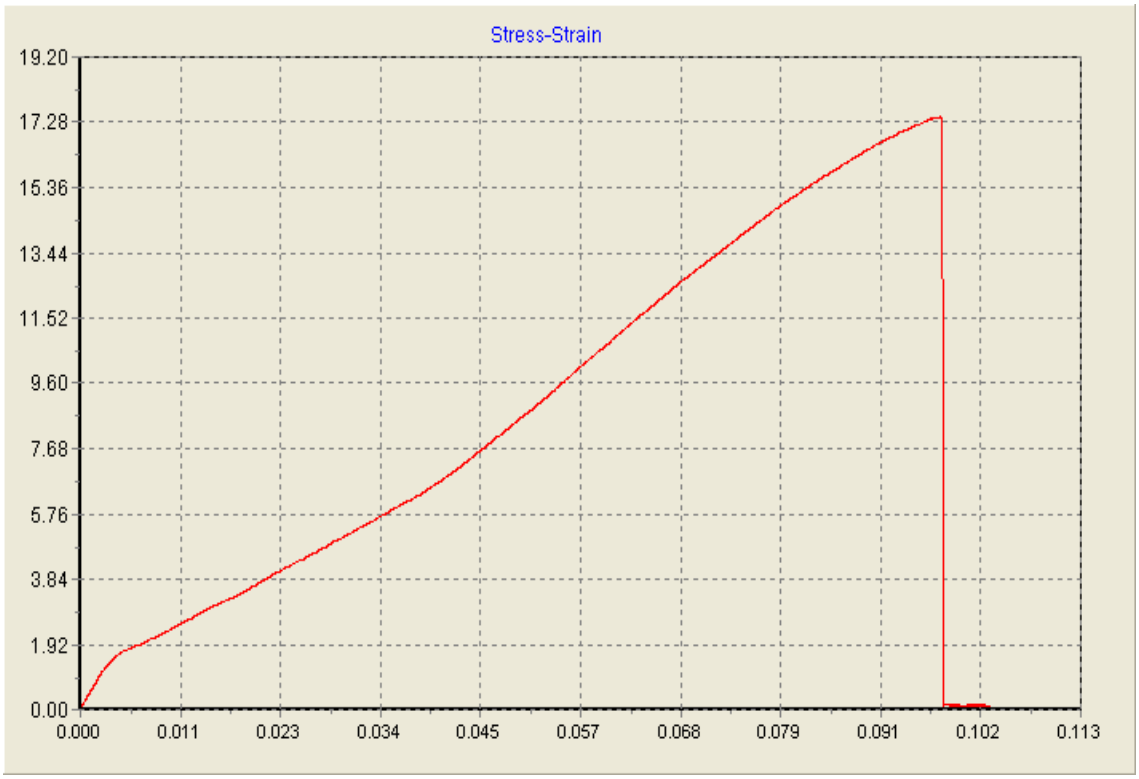
Stress-Strain
19.20
17.28
15.36
13.44
11.52
9.60
7.68
5.76
3.84
1.92
0.00
0.000
0.011
0.023
0.034
0.045
0.057
0.068
0.079
0.091
0.102
0.113

3%BN

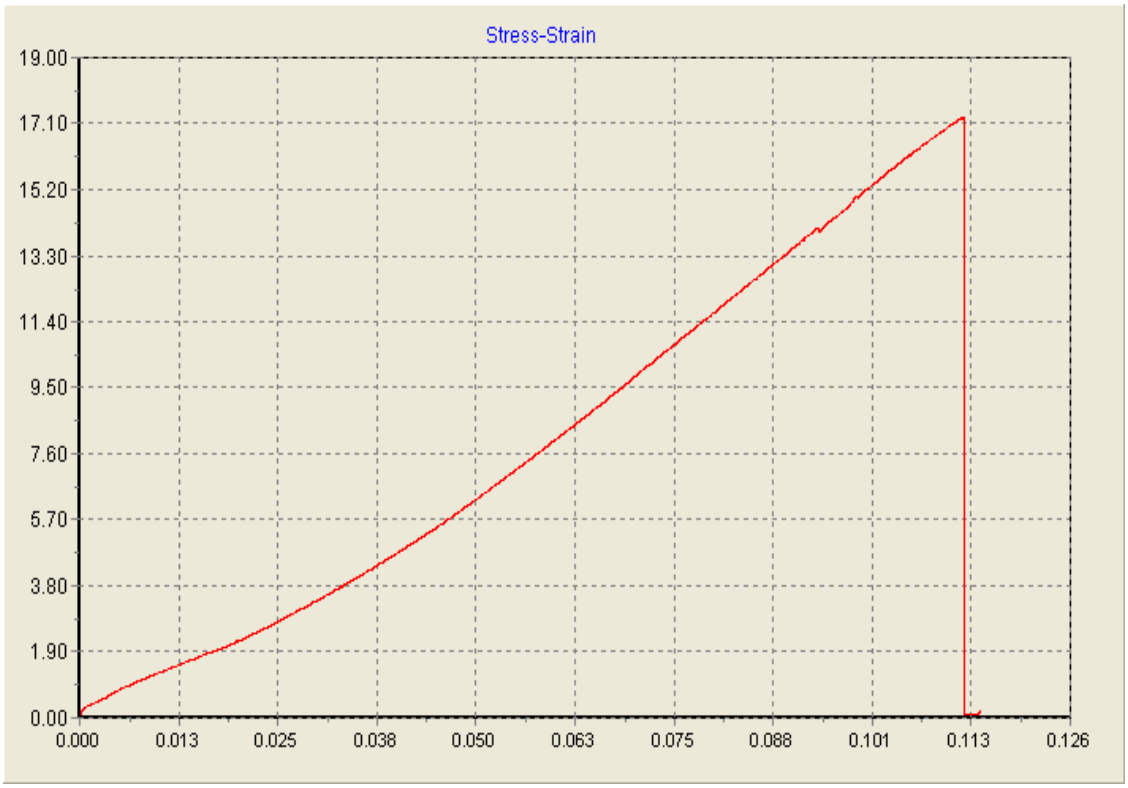
Stress-Strain
19.00
17.10
15.20
13.30
11.40
9.50
7.60
5.70
3.80
1.90
0.00
0.000
0.013
0.025
0.038
0.050
0.063
0.075
0.088
0.101
0.113
0.126

5%BN

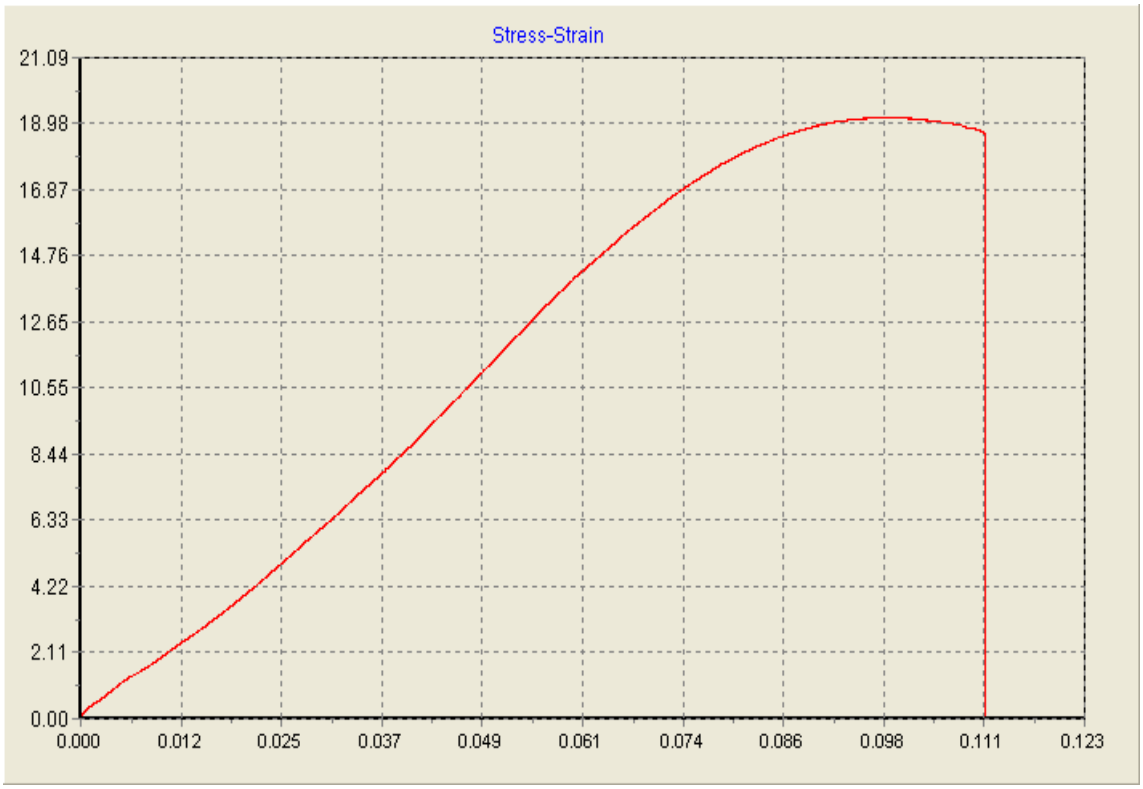
Stress-Strain
21.09
18.98
16.87
14.76
12.65
10.55
8.44
6.33
4.22
2.11
0.00
0.000
0.012
0.025
0.037
0.049
0.061
0.074
0.086
0.098
0.111
0.123

7% BN

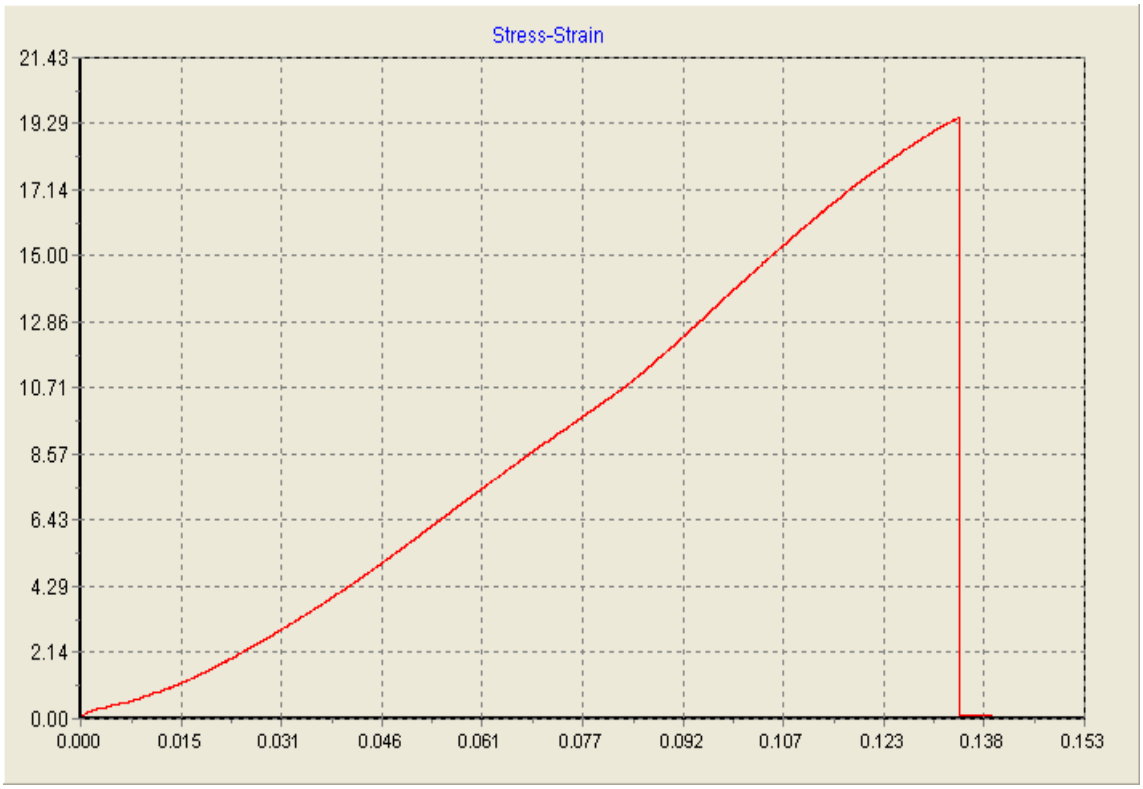
Stress-Strain
21.43
19.29
17.14
15.00
12.86
10.71
8.57
6.43
4.29
2.14
0.00
0.000
0.015
0.031
0.046
0.061
0.077
0.092
0.107
0.123
0.138
0.153

1% hybrid

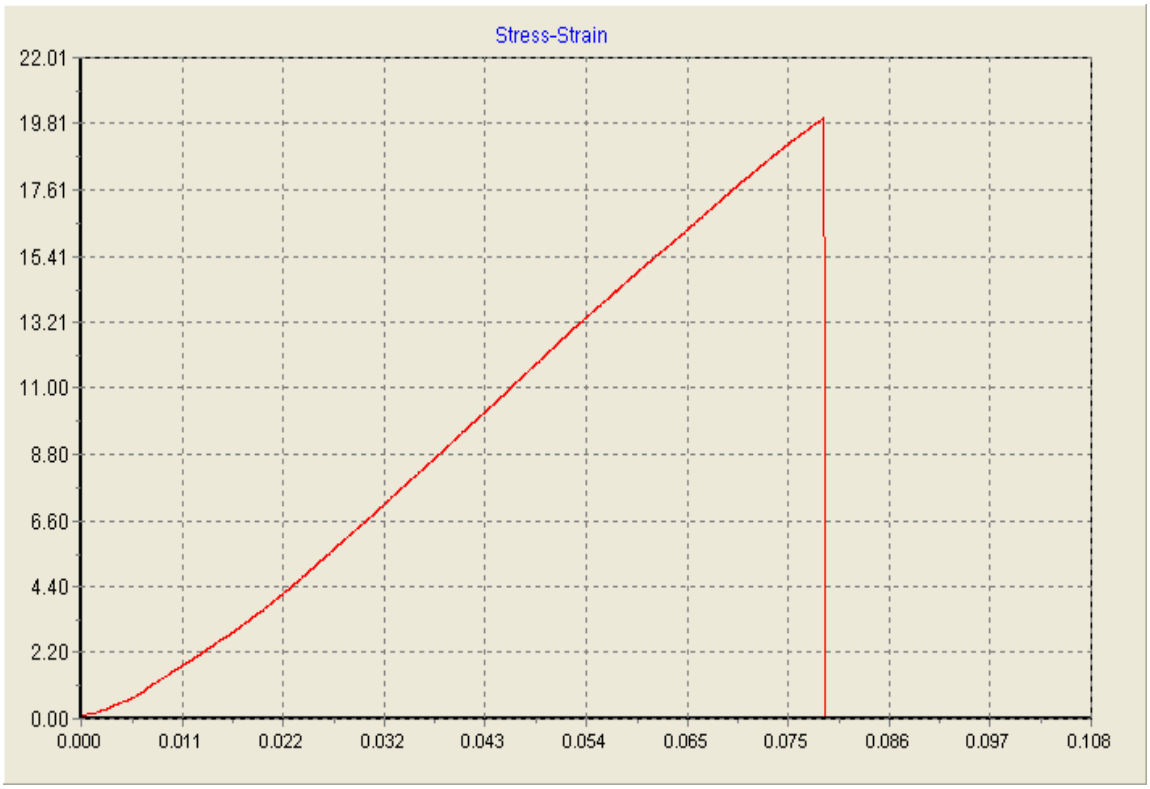

3% hybrid

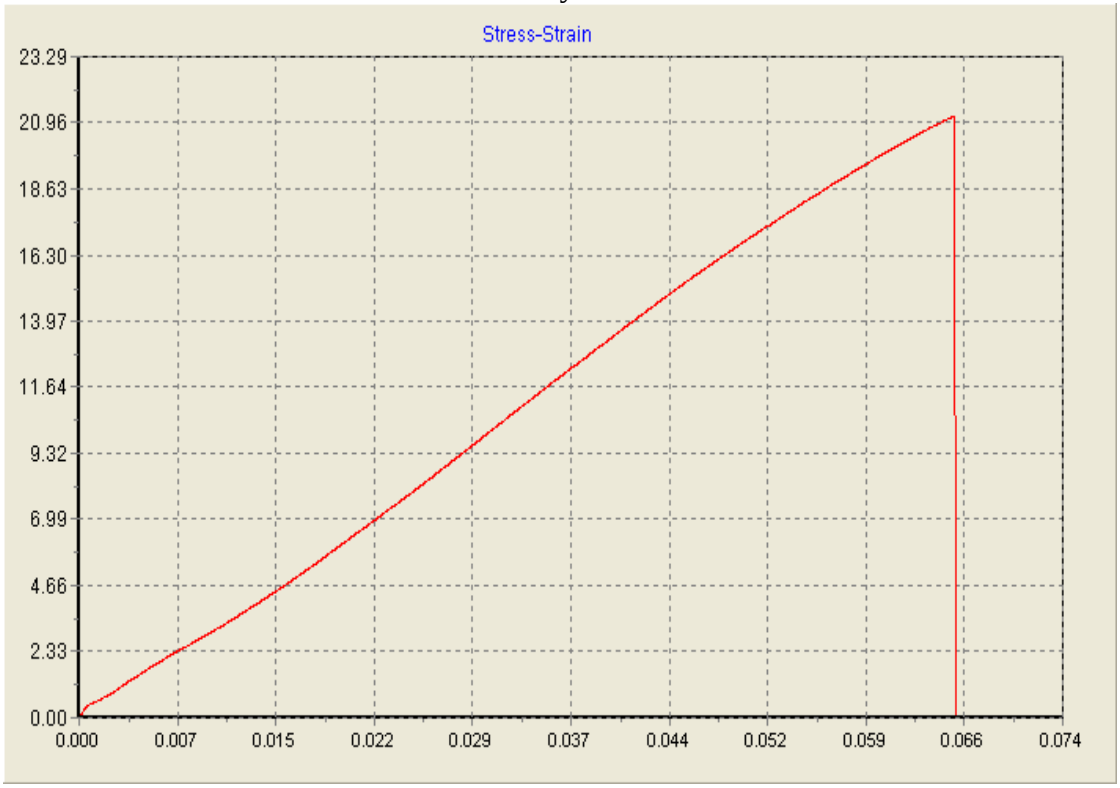

5% hybrid

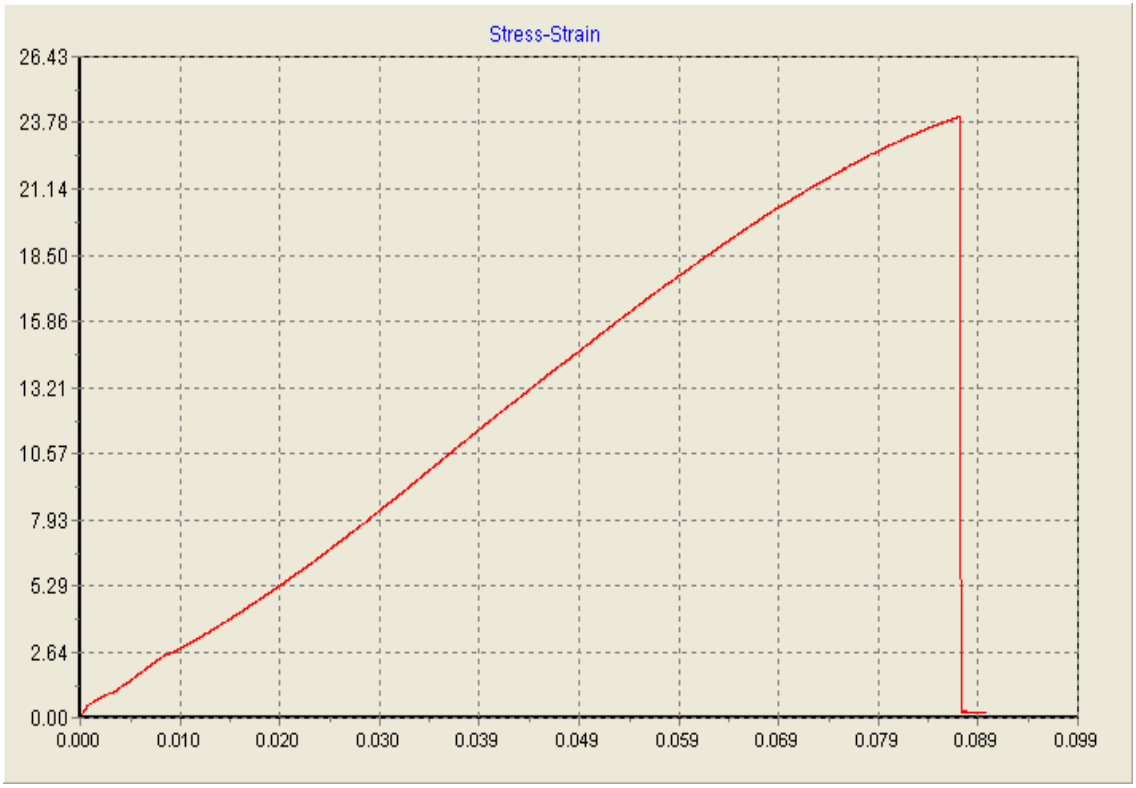
Stress-Strain
26.43
23.78
21.14
18.50
15.86
13.21
10.57
7.93
5.29
2.64
0.00
0.000
0.010
0.020
0.030
0.039
0.049
0.059
0.069
0.079
0.089
0.099

7% hybrid

Appendix F3

Table 4.7: The compact tension and single edge notched bending of pure epoxy, epoxy/MgO, epoxy/BN, epoxy/(1:1MgO/BN)hybrid nanocomposites.

Nanocomposites	NPs (wt.%)	K_{IC} (MPa. m^$^{1/2}$)	K_{IIC} (MPa.m^$^{1/2}$)
Epoxy	0	1.08	2.09
EP/MgO1	1	2.49	2.13
EP/MgO3	3	2.55	2.24
EP/MgO5	5	2.6	2.3
EP/MgO7	7	2.63	2.33
EP/BN1	1	2.68	3.14
EP/BN3	3	2.77	3.21
EP/BN5	5	2.85	3.36
EP/BN7	7	2.9	3.43
EP/Hybrid1	1	2.64	2.78
EP/Hybrid3	3	3.13	3.33
EP/Hybrid5	5	3.28	3.5
EP/Hybrid7	7	3.41	3.57

Appendix F4

Table 4.8: Hardness of pure epoxy , EP/MgO ,EP/BN, EP/(1:1MgO/BN) hybrid nanocomposites

Nanocomposites	NPs (wt.%)	Hardness(shor D)
Epoxy	0	66
EP/MgO1	1	68
EP/MgO3	3	69
EP/MgO5	5	70
EP/MgO7	7	72
EP/BN1	1	66.53
EP/BN3	3	66.76
EP/BN5	5	66.9
EP/BN7	7	66.93
EP/Hybrid1	1	68.83
EP/Hybrid3	3	70.63

EP/Hybrid5	5	71.66
EP/Hybrid7	7	73

Appendix F5

Table 4.9 : The impact strength of pure epoxy , epoxy/MgO ,epoxy/BN, epoxy/(1:1MgO/BN)hybrid nanocomposites .

Nanocomposites	NPs (wt.%)	Impact Strength(J/m^2)
Epoxy	0	5.55
EP/MgO1	1	6.24
EP/MgO3	3	6.38
EP/MgO5	5	6.56
EP/MgO7	7	7.77
EP/BN1	1	7.14
EP/BN3	3	7.9
EP/BN5	5	8.75
EP/BN7	7	10.69
EP/Hybrid1	1	8.13
EP/Hybrid3	3	8.75
EP/Hybrid5	5	10
EP/Hybrid7	7	12.5

Appendix F6

Table 4.10:The pull off strength of pure epoxy , epoxy/MgO , epoxy /BN, epoxy/(1:1MgO/BN) hybrid nanocomposites .

Nanocomposites	NPs (wt.%)	Pull Off Strength (MPa)
Epoxy	0	1. 5
EP/MgO1	1	2.05
EP/MgO3	3	3.13
EP/MgO5	5	3.38
EP/MgO7	7	3.55
EP/BN1	1	1.86
EP/BN3	3	2.92
EP/BN5	5	3.47
EP/BN7	7	3.65
EP/Hybrid1	1	2.45
EP/Hybrid3	3	3.6
EP/Hybrid5	5	4.07
EP/Hybrid7	7	4.83

Appendix G

Table 4.11: The electrochemical parameters calculated using potentiodynamic polarization technique for the corrosion of bare steel, coated with epoxy alone and coated with epoxy/MgO,epoxy/BN ,epoxy/hybrid nanocomposite in 3.5%NaCL solution at 25°C.

Sample no.	E_{Corr} mv	$I_{corr.}$ A/cm^2	I %
bare	-614	8.11	
epoxy	-204	4.33	46.6
1%MgO	-117.3	1.65	62.1
3%MgO	-718	1.12	70.2
5%MgO	-628	1.04	70.4
7%MgO	-217	1.02	86.5
1%BN	-176	3.79	53.2
3%BN	-831	3.7	54.3
5%BN	-210.1	1.8	77.8
7%BN	-276	1.4	82.7
1%H	-746	3.07	79.6
3%H	-684	2.41	86.1
5%H	-294	2.4	87.1
7%H	-630	1.09	87.4

References

[1] Kang, J.S.; Li, M.; Wu, H.; Nguyen, H.; Hu, Y. Experimental observation of high thermal conductivity in boron arsenide. Science, 361, 575–578, 2018.

[2] Song, N.; Hou, X.; Chen, L.; Cui, S.; Shi, L.; Ding, P. A Green Plastic Constructed from Cellulose and Functionalized Graphene with High Thermal Conductivity. ACS Appl. Mater. Interfaces, 9, 17914–17922, 2017.

[3] Wang, S.; Liu, Y.; Guo, Y.; Lu, Y.; Huang, Y.; Xu, H.; Wu, D.; Sun, J. Optimal analysis for thermal conductivity variation of EVA/SCF composites prepared by spatial confining forced network assembly. Mater. Today Commun, 25, 101206,. 2020.

[4] Sun, J.; Zhuang, J.; Jiang, H.; Huang, Y.; Zheng, X.; Liu, Y.; Wu, D. Thermal dissipation performance of metal-polymer composite heat exchanger with V-shape microgrooves: A numerical and experimental study. Appl. Therm. Eng, 121, 492–500, 2017.

[5] Tian, F.; Ren, Z. High Thermal Conductivity in Boron Arsenide: From Prediction to Reality. Angew. Chem. Int. Ed, 58, 5824–5831,2019.

[6] Lin, M.; Li, Y.; Xu, K.; Ou, Y.; Su, L.; Feng, X.; Li, J.; Qi, H.; Liu, D. Thermally conductive nanostructured, aramid dielectric composite films with boron nitride nanosheets. Compos. Sci. Technol,175, 85–91,2019.

[7] Zhang, S.; Tian, Y.; Gu, X.; Tangb, W.; Sun, J. Improving the flame resistance and thermal conductivity of ethylene-vinyl acetate composites by incorporating hexachlorocyclotriphosphazene-modified graphite and carbon nanotubes. Polym. Compos, 39,2018.

[8] Sun, J.; Zhuang, J.; Shi, J.; Kormakov, S.; Liu, Y.; Yang, Z.; Wu, D. Highly elastic and ultrathin nanopaper-based nanocomposites with superior electric and thermal characteristics. J. Mater. Sci, 54, 8436–8449,2019.

[9] Alim, M., Abdullah, M. Z., Aziz, M. S. A., Kamarudin, R., & Gunnasegaran, P.. Recent advances on thermally conductive adhesive in electronic packaging: a review. Polymers, 13(19), 3337,2021.

[10] Schalnat, J.. Experimental Characterisation of Short Fibre Reinforced Thermoplastic Materials for the Use in Heat Exchangers: Development of Test Setups and Methodology for Subcomponents, Coupons and Embedded Single Fibres ,2022.

[11] V. R. Burger, N.; Laachachi, A.; Ferriol, M.; Lutz, M.; Toniazzo, “Review of thermal conductivity in composites: Mechanisms, parameters and theory,” Prog. Polym. Sci, pp. 1–28 ,2016.

[12] Adnan, M. M., Tveten, E. G., Glaum, J., Ese, M. H. G., Hvidsten, S., Glomm, W., & Einarsrud, M. A. . Epoxy-Based Nanocomposites for High-Voltage Insulation: A Review. Advanced Electronic Materials, 5(2), 1800505,2019.

[13] Isarn, I., Ramis, X., Ferrando, F., & Serra, A. . Thermoconductive thermosetting composites based on boron nitride fillers and thiol-epoxy matrices. Polymers, 10(3), 277,2018.

[14] Pissis, P. "Molecular dynamics of thermoset nanocomposites." Thermoset Nanocomposites for Engineering Application; Smithers Rapra Technology Ltd.: Shawbury, UK, 143-206,2007.

[15] Kochetov, Roman. "Thermal and electrical properties of nanocomposites, including material properties." 2012.

[16] C. Z. Dmitri Golberg,* Yoshio Bando, Yang Huang, Takeshi Terao, Masanori Mitome, Chengchun Tang, “Boron nitride nanotubes and nanosheets,” vol. 4, no. 6, pp. 2979–2993, 2002.

[17] Stankovich, D. A. Dikin, GHB Dommett, KM Kohlhaas, EJ Zimney, EA Stach, RD Piner, ST Nguyen, and RS Ruoff. *Nature*, *442*, 282,2006.

[18] Hong, X., Kang, J., Zhuo, Q., Sanchez, J., Yun, H., Deng, J., & Peddi, R. , High thermal, non-electrically conductive automotive grade die attach paste: a study to evaluate the impact of filler technology. IEEE 71st Electronic Components and Technology Conference (ECTC) (pp. 1991-1997),2021.

[19] El-Shamy, A. G. New nano-composite based on carbon dots (CDots) decorated magnesium oxide (MgO) nano-particles (CDots@ MgO) sensor for

high H2S gas sensitivity performance. Sensors and Actuators B: Chemical, 329, 129154,2021.

[20] T. Andritsch, *Epoxy Based Nanodielectrics for High Voltage DC-Applications–Synthesis, Dielectric Properties and Space Charge Dynamics*, no. November, 2010.

[21] H. Wei, "Adhesion and cohesion of epoxy-based industrial composite coatings," Compos. Part B Eng., vol. 193, p. 108035, Jul. 2020.

[22] M. Tyagi and D. Tyagi, "Polymer Nanocomposites and their Applications in Electronics Industry," *Int. J. Electron. Electr. Eng.*, vol. 7, no. 6, pp. 603–608, 2014.

[23] W. S. Khan, N. N. Hamadneh, and W. A. Khan, "Science and applications of Tailored Nanostructures 50 4 Polymer nanocomposites-synthesis techniques, classification and properties Outline," pp. 50–67, 2016.

[24] W. Khan, … N. H.-S. and applications, and undefined 2016, "Polymer nanocomposites–synthesis techniques, classification and properties," *onecentralpress.com*, Accessed: Jul. 15, 2021.

[25] K. Müller ., "Review on the processing and properties of polymer nanocomposites and nanocoatings and their applications in the packaging, automotive and solar energy fields," *Nanomaterials*, vol. 7, no. 4, 2017.

[26] A. de Oliveira, C. B.- Nanocomposites-Recent, and undefined 2018, "Polymer nanocomposites with different types of nanofiller," books.google.com, Accessed: Jul. 19, 2021.

[27] Dai, X., Hou, C., Xu, Z., Yang, Y., Zhu, G., Chen, P., ... & Yan, L. T. Entropic effects in polymer nanocomposites. Entropy, 21(2), 186.2019.

[28] Verma, D., Sharma, M., & Jain, S. An introduction to high-performance advanced polymers composites, their types, processing, and applications in automotive industries. In Sustainable Biopolymer Composites (pp. 3-26). Woodhead Publishing,2022.

[29] A. Dantas de Oliveira and C. Augusto Gonçalves Beatrice, "Polymer

Nanocomposites with Different Types of Nanofiller," *Nanocomposites - Recent Evol.*, 2019.

[30] Dong, Yu. Multi-scale effects on deformation mechanisms of polymer nanocomposites: experimental characterisation and numerical study. Diss. University of Auckland, 2008.

[31] Jeon, I. Y., & Baek, J. B. Nanocomposites derived from polymers and inorganic nanoparticles. Materials, 3(6), 3654-3674,2010.

[32] D. Ponnamma, H. J. Maria, A. K. Chandra, and S. Thomas, *Rubber Nanocomposites: Latest Trends and Concepts*, no. April, 2013.

[33] Cromer, B. M., Scheel, S., Luinstra, G. A., Coughlin, E. B., & Lesser, A. J. In-situ polymerization of isotactic polypropylene-nanographite nanocomposites. Polymer, 80, 275-281,2015.

[34] Shukla, V. Review of electromagnetic interference shielding materials fabricated by iron ingredients. Nanoscale Advances, 1(5), 1640-1671,2019.

[35] N. Peddamallu ., "Understanding the electrical, thermal, and mechanical properties of epoxy magnesium oxide nanocomposites," *IET Sci. Meas. Technol.*, vol. 13, no. 5, pp. 632–639, 2019.

[36] I. Jeon, J. B.- Materials, and undefined 2010, "Nanocomposites derived from polymers and inorganic nanoparticles," *mdpi.com*, Accessed: Jul. 19, 2021.

[37] Cantarella, M., Impellizzeri, G., & Privitera, V. Functional nanomaterials for water purification. La Rivista del Nuovo Cimento, 40(12), 595-632,2017.

[38] Kaspar Albrecht"Redispersibility of Cellulose Nanofibrils"Kaspar Albrecht University of Natural Resources and Life Kaspar Albrecht University of Natural Resources and Life ,March , Thesis: Redispersibility of Cellulose Nanofibrils"2018.

[39] Kang, C., Xu, J., Niu, L., Li, C., & Fan, J. Quantitative evaluation of nanoparticle dispersion based on modeling methods and image analysis: A case study on nano-Sb2O3 filled Poly (butylene terephthalate) composites. Polymer Composites, 42(6), 30,2021.

[40] Xanthos, M. (Ed.). Functional fillers for plastics. John Wiley & Sons,2010.

[41] Balguri, P. K., Thumu, U., DG, H. S., Penki, T. R., & Chilumala, I. Manganese dioxide nanostructures reinforced epoxy nanocomposites: a study of mechanical properties. Polymer-Plastics Technology and Materials, 61(4), 441-460,2022.

[42] P. Panaitescu, D. Paven, H. Chipara, M. Chapter 1, Polymers and polymer composites. InFunctional Fillers for Plastics, 2nd ,Weinheim, Germany, pp. 1–18.55.,2010.

[43] W. Li, J. Yuan, A. Dichiara, Y. Lin and J. Bai, The use ofvertically aligned carbon nanotubes grown on SiC for insitu sensing of elastic and plastic deformation inelectrically percolative epoxy composites,Carbon, ,50(11), 4298–4301,2012.

[44] L. Yue, G. Pircheraghi, S. A. Monemian and I. M. Zloczower,Epoxy composites with carbon nanotubes and graphenenanoplatelets–dispersion and synergy effects,Carbon,78, 268–278,2014.

[45] M. Bozlar, D. He, J. Bai, Y. Chalopin, N. Mingo and S. Volz,Carbon nanotube microarchitectures for enhanced thermalconduction at ultralow mass fraction in polymercomposites,Adv. Mater,22(14), 1654–1658,2010.

[46] Y. Wu, Y. He, C. Chen, H. Li, Y. Xia and T. Zhou, MoS2-CNFscomposites to enhance the anticorrosive and mechanicalperformance of epoxy coating,Prog. Org. Coat.,128,178–186,2019.

[47] Y. Xia, Y. He, C. Chen, Y. Wu and J. Chen, MoS2nanosheetsmodi□ed SiO2to enhance the anticorrosive and mechanicalperformance of epoxy coating,Prog. Org. Coat., 132,316–327,2019.

[48] R. Stankovich, S.; Dikin, D.A.; Dommett, G.H.B.; Kohlhaas, K.M.; Zimney, E.J.; Stach, E.A.; Piner, R.D.; Nguyen, S.T.; Ruoff, “Graphene-based composite materials,, no. 442, pp. 282–286,2006.

[49] Karuppiah, A. V. Predicting the influence of weave architecture on the stress relaxation behavior of woven composite using finite element based micromechanics (Doctoral dissertation, Wichita State University),2016.

[50] G. Sims, G. B.-M. of A. Composites, and undefined 2001, "UK Polymer composites sector-competitive analysis and foresight study," *apps.dtic.mil*, Accessed: Jul. 20, 2021.

[51] C. Brazel and S. Rosen, "Fundamental principles of polymeric materials ", 2021.

[52] Liu, J., Wang, S., Peng, Y., Zhu, J., Zhao, W., & Liu, X. Advances in sustainable thermosetting resins: From renewable feedstock to high performance and recyclability. Progress in Polymer Science, 113, 101353,2021

[53] Vashchuk, A., Fainleib, A. M., Starostenko, O., & Grande, D.Application of ionic liquids in thermosetting polymers: Epoxy and cyanate ester resins. Express Polymer Letters, 12(10), 898-917,2018.

[54] J. Chen, N. Chu, M. Zhao, … F. J.-J. of A., and undefined 2020, "Synthesis and application of thermal latent initiators of epoxy resins: A review," Wiley Online Libr., vol. 137, no. 48, Dec. 2020.

[55] Suzuki, A. H., Lage, F., Oliveira, L. S., Franca, A. S., & Daniels, J. A. . Biological materials as precursors for the production of resins. Advances in Environmental Research, 49,2016.

[56] He, S., Shi, K., Bai, J., Zhang, Z., Li, L., Du, Z., & Zhang, B. Studies on the properties of epoxy resins modified with chain-extended ureas. *Polymer*, *42*(23), 9641-9647,2001.

[57] D. Ratna, G. S.- Polymer, and undefined 2001, "Thermomechanical properties and morphology of blends of a hydroxy-functionalized hyperbranched polymer and epoxy resin," *Elsevier*, Accessed: Jul. 20, 2021.

[58] S. Lu, H. Zhang, C. Zhao, and X. Wang, "New epoxy/silica-titania hybrid materials prepared by the sof-gel process," *J. Appl. Polym. Sci.*, vol. 101, no. 2, pp. 1075–1081, Jul. 2006.

[59] S. R. Lu, H. Zhang, C. Zhao, and X. Wang, "Studies on the properties of a new hybrid materials containing hyperbranched polymer and SiO2-TiO2 networks," J. Macromol. Sci. - Pure Appl. Chem., vol. 42 A, no. 12, pp.

1691–1701, Dec. 2005.

[60] S. Lu, H. Zhang, X. W.-J. of materials science, and undefined 2005, "Wear and mechanical properties of epoxy/SiO 2-TiO 2 composites," *Springer*, vol. 40, no. 11, pp. 2815–2821, Jun. 2005.

[61] S. Kang *et al.*, "Preparation and characterization of epoxy composites filled with functionalized nanosilica particles obtained via sol–gel process," *Elsevier*, Accessed: Jul. 20, 2021.

[62] S. Singha, M. T.-I. transactions on D. and, and undefined 2008, "Dielectric properties of epoxy nanocomposites", 2008 ,

[63] C. Zhang, R. Mason, G. S.-C. 2005 Annual, and undefined 2005, "Dielectric properties of alumina-polymer nanocomposites," *ieeexplore.ieee.org*, Accessed: Jul. 20, 2021.

[64] C. Zou, J. Fothergill, S. R.-I. T. on, and undefined 2008, "The effect of water absorption on the dielectric properties of epoxy nanocomposites," *ieeexplore.ieee.org*, vol. 15, no. 1, pp. 106–117, 2008.

[65] F. L. Jin, X. Li, and S. J. Park, "Synthesis and application of epoxy resins: A review," *J. Ind. Eng. Chem.*, vol. 29, pp. 1–11, Sep. 2015.

[66] Z. Zhang, E. Beatty, and C. P. Wong, "Study on the curing process and the gelation of epoxy/anhydride system for no-flow underfill for flip-chip applications," *Macromol. Mater. Eng.*, vol. 288, no. 4, pp. 365–371, Apr. 2003.

[67] I. Rafique, A. Kausar, and B. Muhammad, "Epoxy Resin Composite Reinforced with Carbon Fiber and Inorganic Filler: Overview on Preparation and Properties," *Polym. - Plast. Technol. Eng.*, vol. 55, no. 15, pp. 1653–1672, Oct. 2016.

[68] K. A. Santhi, C. Srinivas, and R. A. Kumar, "Experimental investigation of mechanical properties of Jute-Ramie fibres reinforced with epoxy hybrid composites," *Mater. Today Proc.*, vol. 39, pp. 1309–1315, Jan. 2021.

[69] M. Demir, K. Koynov, Ü. Akbey, C. Bubeck, … I. P. "Optical properties of

composites of PMMA and surface-modified zincite nanoparticles," *ACS Publ.*, vol. 40, no. 4, pp. 1089–1100, Feb. 2007.

[70] Zhang, H., Zhang, X., Fang, Z., Huang, Y., Xu, H., Liu, Y., ... & Sun, J. . Recent advances in preparation, mechanisms, and applications of thermally conductive polymer composites: A review. Journal of Composites Science, 4(4), 180,2020.

[71] J. Hornak. "Magnesium oxide nanoparticles: Dielectric properties, surface functionalization and improvement of epoxy-based composites insulating properties," *Nanomaterials*, vol. 8, no. 6, Jun. 2018.

[72] M. Shand, "The chemistry and technology of magnesia ",Accessed: Jul. 20, 2021.

[73] B. Zhang, J. Peng, L. Zhang, S. J.-M. T. 2012, and undefined 2012, "Optimization of preparation for magnesium oxide by calcination from basic magnesium carbonate using response Surface Methodology," *Springer*, Accessed: Jul. 20, 2021.

[74] A. T. Vu, S. Jiang, Y. H. Kim, and C. H. Lee, "Controlling the physical properties of magnesium oxide using a calcination method in aerogel synthesis: Its application to enhanced sorption of a sulfur Compound," *Ind. Eng. Chem. Res.*, vol. 53, no. 34, pp. 13228–13235, Aug. 2014.

[75] D. Costa, C. Chizallet, B. Ealet, J. Goniakowski, and F. Finocchi, "Water on extended and point defects at MgO surfaces," *J. Chem. Phys.*, vol. 125, no. 5, 2006.

[76] G. Sharma, R. Soni, N. J.-J. of T. U. for, and undefined 2017, "Phytoassisted synthesis of magnesium oxide nanoparticles with Swertia chirayaita," *Taylor Fr.*, vol. 11, no. 3, pp. 471–477, May 2017.

[77] M. Li, S., Meng Lin, M., Toprak, M. S., Kim, D. K., & Muhammed, "Nanocomposites of polymer and inorganic nanoparticles for optical and magnetic applications.,," Nano reviews, 2010.

[78] K. Orlovius and J. McHoul, "Effect of Two Magnesium Fertilizers on Leaf Magnesium Concentration, Yield, and Quality of Potato and Sugar Beet," *J.*

Plant Nutr., vol. 38, no. 13, pp. 2044–2054, Nov. 2015.

[79] Purwajanti, S., Zhou, L., Ahmad Nor, Y., Zhang, J., Zhang, H., Huang, X., & Yu, C. Synthesis of magnesium oxide hierarchical microspheres: a dual-functional material for water remediation. *ACS applied materials & interfaces*, *7*(38), 21278-21286,2015.

[80] S. Natarajan, V. Sivan, P. G. Tennyson, and V. R. Kiran, "Protective coatings on magnesium and its alloys: A critical review," *Corros. Prev. Control*, vol. 51, no. 4, pp. 142–163, 2004.

[81] C. Calebrese, L. Hui, L. S. Schadler, and J. K. Nelson, "A review on the importance of nanocomposite processing to enhance electrical insulation," IEEE Trans. Dielectr. Electr. Insul., vol. 18, no. 4, pp. 938–945, 2011.

[82] V. Dikshit, S. K. Bhudolia, and S. C. Joshi, "Multiscale polymer composites: A review of the interlaminar fracture toughness improvement," *Fibers*, vol. 5, no. 4, 2017.

[83] J. Hornak, P. Trnka, P. Kadlec, O. Michal, V. M.- Nanomaterials, and undefined 2018, "Magnesium oxide nanoparticles: dielectric properties, surface functionalization and improvement of epoxy-based composites insulating properties," *mdpi.com*, Accessed: Jul. 21, 2021.

[84] Kochetov, R. Thermal and electrical properties of nanocomposites, including material properties,2012.

[85] Okabe, S., Ueta, G., Nojima, K.: 'Resistance characteristics and electrification characteristics of GIS epoxy insulators under DC voltage', IEEE Trans. Dielectr. Electr. Insul., 21, pp. 1260–1267,2014.

[86] Zhou, W., Zheng, Y., Yang, S., et al.: 'Detection of intense partial discharge of epoxy insulation in SF6 insulated equipment using carbonyl sulfide', IEEE Trans. Dielectr. Electr. Insul., 23, pp. 2942–2948,2016.

[87] Tanaka, T., Montanari, G.C., Mulhaupt, R.: 'Polymer nanocomposites as dielectrics and electrical insulation-perspectives for processing technologies, material characterization and future applications', IEEE Trans. Dielectr. Electr. Insul., 11, (5),2004.

[88] Xiao, M., Du, B.X.: 'Review of high thermal conductivity polymer dielectrics for electrical insulation', High Vol., 1, (1), pp. 34–42,2016.

[89] Murakami, Y., Okazaki, T., Nagao, M., et al.: 'Space charge formation and conduction current of MgO/LDPE nanocomposite'. Annual Report on Conf. on Electrical Insulation and Dielectric Phenomena, West Lafayette, USA, pp. 556–559,2010.

[90] Q. Weng, X. Wang, X. Wang, Y. Bando and D. Golberg, Chem. Soc. Rev., 45, 3989–4012 RSC,2016.

[91] C. T. C. Z. Dmitri Golberg,* Yoshio Bando, Yang Huang, Takeshi Terao, Masanori Mitome, "Boron nitride nanotubes and nanosheets," *Online*, vol. 4, no. 6, pp. 2979–2993, 2002.

[92] D. Pacile, J. Meyer, Ç. Girit, A. Z.-A. P. Letters, and undefined 2008, "The two-dimensional phase of boron nitride: Few-atomic-layer sheets and suspended membranes," *aip.scitation.org*, vol. 92, no. 13, 2008.

[93] L. Lindsay, D. B.-P. R. B, and undefined 2011, "Enhanced thermal conductivity and isotope effect in single-layer hexagonal boron nitride," *APS*, vol. 84, no. 15, p. 155421, Oct. 2011.

[94] M. T. Alam, M. S. Bresnehan, J. A. Robinson, and M. A. Haque, "Thermal conductivity of ultra-thin chemical vapor deposited hexagonal boron nitride films," *Appl. Phys. Lett.*, vol. 104, no. 1, Jan. 2014.

[95] Sun, J.; Zhuang, J.; Shi, J.; Kormakov, S.; Liu, Y.; Yang, Z.; Wu, D. Highly elastic and ultrathin nanopaper-based nanocomposites with superior electric and thermal characteristics. J. Mater. Sci. 54, 8436–8449,2019.

[96] Zhang, H., Zhang, X., Fang, Z., Huang, Y., Xu, H., Liu, Y., ... & Sun, J.. Recent advances in preparation, mechanisms, and applications of thermally conductive polymer composites: A review. Journal of Composites Science, 4(4), 180,2020.

[97] Gutiérrez-Lezama, I., Ubrig, N., Ponomarev, E., & Morpurgo, A. F. Ionic gate spectroscopy of 2D semiconductors. *Nature Reviews Physics*, *3*(7), 508-519,2021.

[98] García-Miranda Ferrari, A., Rowley-Neale, S. J., & Banks, C. E. Recent advances in 2D hexagonal boron nitride (2D-hBN) applied as the basis of electrochemical sensing platforms. Analytical and Bioanalytical Chemistry, 413(3), 663-672,2021.

[99] Pakdel, A., Bando, Y., & Golberg, D. Nano boron nitride flatland. *Chemical Society Reviews*, *43*(3), 934-959,2014.

[100] Weng, Q., Wang, X., Wang, X., Bando, Y., & Golberg, D. Functionalized hexagonal boron nitride nanomaterials: emerging properties and applications. *Chemical Society Reviews*, *45*(14), 3989-4012,2016.

[101] Bruna, T., Maldonado-Bravo, F., Jara, P., & Caro, N. Silver nanoparticles and their antibacterial applications. International Journal of Molecular Sciences, 22(13), 7202,2021.

[102] Angizi, S., Alem, S. A. A., Azar, M. H., Shayeganfar, F., Manning, M. I., Hatamie, A., ... & Simchi, A. A comprehensive review on planar boron nitride nanomaterials: From 2D nanosheets towards 0D quantum dots. Progress in Materials Science, 124, 1,2022.

[103] Ciofani, G. Potential applications of boron nitride nanotubes as drug delivery systems. Expert opinion on drug delivery, 7(8), 889-893,2010.

[104] J. Hou, G. Li, N. Yang, L. Qin, M. E. Grami, Q. Zhang,N. Wang and X. Qu, Preparation and characterization ofsurface modifed boron nitride epoxy composites withenhanced thermal conductivity,RSC Adv., 4, 44282–44290,2014.

[105] J. Han, G. Du, W. Gao and H. Bai, An Anisotropically HighThermal Conductive Boron Nitride/Epoxy Composite Basedon Nacre-Mimetic 3D Network,Adv. Funct. Mater., 29(13), 1900412,2019.

[106] K. Wattanakul, H. Manuspiya, and N. Yanumet, “Thermal conductivity and mechanical properties of BN-filled epoxy composite: Effects of filler content, mixing conditions, and BN agglomerate size,” J. Compos. Mater., vol. 45, no. 19, pp. 1967–1980, Sep. 2011.

[107] T. L. Li and S. L. C. Hsu, “Enhanced thermal conductivity of polyimide films

via a hybrid of micro- and nano-sized boron nitride," *J. Phys. Chem. B*, vol. 114, no. 20, pp. 6825–6829, May 2010.

[108] Fotovvati, B., Namdari, N., & Dehghanghadikolaei, A. On coating techniques for surface protection: A review. Journal of Manufacturing and Materials Processing, 3(1), 28,2019.

[109] Yilbas, B. S., Al-Sharafi, A., & Ali, H. Chapter 3-Surfaces for Self-Cleaning. Self-Cleaning of Surfaces and Water Droplet Mobility; Yilbas, BS, Al-Sharafi, A., Ali, H., Eds, 45-98,2019.

[110] He, Z., Ma, M., Lan, X., Chen, F., Wang, K., Deng, H., ... & Fu, Q.Fabrication of a transparent superamphiphobic coating with improved stability. Soft Matter, 7(14), 6435-6443,2011.

[111] Brinker, C. J., & Scherer, G. W. Sol-gel science: the physics and chemistry of sol-gel processing. Academic press,2013.

[112] Sahu, N., Parija, B., & Panigrahi, S. Fundamental understanding and modeling of spin coating process: A review. Indian Journal of Physics, 83(4), 493-502,2009.

[113] Steele, A., Bayer, I., & Loth, E. Inherently superoleophobic nanocomposite coatings by spray atomization. Nano letters, 9(1), 501-505,2009.

[114] Varela, A. I. G., Aymerich, M., García, D. N., Martín, Y. C., de Beule, P. A., Álvarez, E., ... & Flores-Arias, M. T. Sol-Gel Glass Coating Synthesis for Different Applications: Active Gradient-Index Materials, Microlens Arrays and Biocompatible Channels. Recent Applications in Sol-Gel Synthesis, 231-252,2017.

[115] Rahaman, M.N. Ceramic Processing. Boca Raton: CRC Press. pp. 242–244. ISBN 978-0-8493-7285-8,2007.

[116] F. D. Bălăcianu, R. Bartoş, and A. C. Nechifor, "Organic-inorganic membrane materials," *UPB Sci. Bull. Ser. B Chem. Mater. Sci.*, vol. 71, no. 3, pp. 37–54, 2009.

[117] Quéré, David . 'FLUID COATING ON A FIBER'. Annual Review of Fluid

Mechanics. 31 (1): 347–384. doi:10.1146/annurev.fluid.31.1.347. ISSN 0066-4189,1999.

[118] A. J. Sanchez-Herencia, “Water Based Colloidal Processing of Ceramic Laminates,” Key Eng. Mater., vol. 333, no. July, pp. 39–48, 2007.

[119] Pocius, A. V. ‘Adhesion and adhesives technology: an introduction’. Carl Hanser Verlag GmbH Co KG,2012.

[120] Scheirs, J. ‘Compositional and failure analysis of polymers: a practical approach’. John Wiley & Sons,2000.

[121] Al-Maliki, H. L. R. ‘Adhesive and tribological behaviour of cold atmospheric plasma-treated polymer surfaces’. Doctoral dissertation, Ph. D. thesis, Faculty of Mechanical Engineering, Szent Istv an University,2018.

[122] Guo, Y.; Ruan, K.; Shi, X.; Yang, X.; Gu, J. Factors affecting thermal conductivities of the polymers and polymer composites: A review. Compos. Sci. Technol. 193, 108134,2020.

[123] Zhang, Y.; Heo, Y.-J.; Son, Y.-R.; In, I.; An, K.-H.; Kim, B.-J.; Park, S.-J. Recent advanced thermal interfacial materials: A review of conducting mechanisms and parameters of carbon materials. Carbon , 142, 445–460,2019.

[124] Guo, Y.; Ruan, K.; Shi, X.; Yang, X.; Gu, J. Factors affecting thermal conductivities of the polymers and polymer composites: A review. Compos. Sci. Technol, 193, 108134,2020.

[125] Guo, Y.; Lyu, Z.; Yang, X.; Lu, Y.; Ruan, K.; Wu, Y.; Kong, J.; Gu, J. Enhanced thermal conductivities and decreased thermal resistances of functionalized boron nitride/polyimide composites. Compos. Part B Eng. 164, 732–739,2019.

[126] Reiser, J., Hoffmann, A., Hain, J., Jäntsch, U., Klimenkov, M., Hohe, J., & Mrotzek, T. Thermal management materials based on molybdenum (Mo) and copper (Cu): Elucidation of the rolling-induced evolution of thermo-physical properties (eg CTE). Journal of Alloys and Compounds, 776, 387-416,2019.

[127] Liu, H.; Jian, R.; Chen, H.; Tian, X.; Sun, C.; Zhu, J.; Yang, Z.; Sun, J.; Wang, C. Application of Biodegradable and Biocompatible Nanocomposites in Electronics: Current Status and Future Directions. Nanomaterials , 9, 950,2019.

[128] Zhang, X.; Wu, K.; Liu, Y.; Yu, B.; Zhang, Q.; Chen, F.; Fu, Q. Preparation of highly thermally conductive but electrically insulating composites by constructing a segregated double network in polymer composites. Compos. Sci. Technol. 175, 135–142,2019.

[129] Zhang, F.; Feng, Y.; Qin, M.; Gao, L.; Li, Z.; Zhao, F.; Zhang, Z.; Lv, F.; Feng, W. Stress Controllability in Thermal and Electrical Conductivity of3D Elastic Graphene-Crosslinked Carbon Nanotube Sponge/Polyimide Nanocomposite. Adv. Funct. Mater. 2,2019.

[130] Huang, T.; Ma, C.; Dai, P.-B.; Zhang, J. Improvement in dielectric constant of carbon black/epoxy composites with separated structure by surface-modified hollow glass beads with reduced graphene oxide. Compos. Sci. Technol. 176, 46–53,2019.

[131] Oluwalowo, A.; Nguyen, N.; Zhang, S.; Park, J.G.; Liang, R. Electrical and thermal conductivity improvement of carbon nanotube and silver composites. Carbon . 146, 224–231,2019.

[132] Moore AL, Shi L. Emerging challenges and materials for thermal management of electronics. Mater Today,17:163-74,2014.

[133] Tong XC. Advanced materials for thermal management of electronic packaging. New York: Springer; ,pp 616 ,2011.

[134] Chen, H., Ginzburg, V. V., Yang, J., Yang, Y., Liu, W., Huang, Y., ... & Chen, B. . Thermal conductivity of polymer-based composites: Fundamentals and applications. Progress in Polymer Science, 59, 41-85,2016.

[135] L. Zhang, Li and Wu, Juntao and Jiang, “Graphene and its polymer nanocomposites,” vol. 26, no. 4, p. 560, 2014.

[136] N. Wang, Moran and Kang, Qinjun and Pan, “Thermal conductivity enhancement of carbon fiber composites,” *Appl. Therm. Eng.*, vol. 29, no. 2–

3, pp. 418--421, 2009.

[137] M. Ishimoto, K and Tanaka, T and Ohki, Y and Sekiguchi, Y and Murata, Y and Gosyowaki, "Comparison of dielectric properties of low-density polyethylene/MgO composites with different size fillers," *IEEE*, pp. 208-211, 2008.

[138] Y. Kurnianto, R and Murakami, Y and Hozumi, N and Nagao, M and Murata, "Some fundamentals on treeing breakdown in inorganic-filler/LDPE nano-composite material," *IEEE*, pp. 373--376, 2006.

[139] N. Zhou, Wenying and Qi, Shuhua and An, Qunli and Zhao, Hongzhen and Liu, "thermal conductivity of boron nitride reinforced polyethylene composites," *Mater. Res. Bull.*, vol. 42, no. 10, pp. 1863--1873, 2007.

[140] X. Hu, L. Jiang, and K. E. Goodson, "Thermal conductance enhancement of particle-filled thermal interface materials using carbon nanotube inclusions," *Thermomechanical Phenom. Electron. Syst. -Proceedings Intersoc. Conf.*, vol. 1, no. July, pp. 63–69, 2004.

[141] V. A. F. Costa and A. M. G. Lopes, "Improved radial heat sink for led lamp cooling," *Appl. Therm. Eng.*, vol. 70, no. 1, pp. 131–138, 2014.

[142] A. Moore, L. S.-M. today, and undefined 2014, "Emerging challenges and materials for thermal management of electronics," *Elsevier*, Accessed: Jul. 22, 2021.

[143] N. Haimovich, D. R. Dekel, and S. Brandon, "A Simulator for System-Level Analysis of Heat Transfer and Phase Change in Thermal Batteries," *J. Electrochem. Soc.*, vol. 156, no. 6, p. A442, 2009.

[144] H. Y. Hwang, Y. S. Chen, and J. S. Chen, "Optimizing the Heat Dissipation of an Electric Vehicle Battery Pack," *Adv. Mech. Eng.*, vol. 7, no. 1, 2015.

[145] Royne A, Dey CJ, Mills DR. Cooling of photovoltaic cells under concentrated illumination: a critical review. Sol Energy Mater Sol Cells .86:451-83,2005.

[146] Kalogirou SA, Tripanagnostopoulos Y. Hybrid PV/T solar systems for

domestic hot water and electricity production. Energy Convers Manage ,47:3368-82,2006.

[147] Kinsey GS, Edmondson KM. Spectral response and energy output of concentrator multijunction solar cells. Prog Photovoltaics ,17:279-88,2009.

[148] K. Choi, J. Lee, H. Choi, G.-W. Kim, H. Il Kim, and T. Park, "Heat dissipation effects on the stability of planar perovskite solar cells," *Energy Environ. Sci.*, vol. 13, no. 12, pp. 5059–5067, Dec. 2020.

[149] Uddin, A., Upama, M. B., Yi, H., & Duan, L. . Encapsulation of organic and perovskite solar cells: A review. Coatings, 9(2), 65,2019.

[150] M. B. Heaney, "Electrical conductivity and resistivity," *Electr. Meas. Signal Process. Displays*, vol. 1983, pp. 7-1-7–14, 2003.

[151] Lowrie, William (2007). Fundamentals of Geophysics. Cambridge University Press. pp. 254–55. ISBN 978-05-2185-902-8. Retrieved March 24, 2019.

[152] Y. Wang, C. Wang, W. Chen, and K. Xiao, 'Effect of stretching on electrical properties of LDPE/MgO nanocomposites,' IEEE Transactions on Dielectrics and Electrical Insulation, vol. 23, no. 3, pp. 1713–1722, 2016.

[153] Y. Chen and J. Wu, 'Investigation on relationship between breakdown strength enhancement of composites and dielectric characteristics of nanoparticle,' IEEE Transactions on Dielectrics and Electrical Insulation, vol. 23, no. 2, pp. 927–934, 2016.

[154] Y. Gong, W. Zhou, Y. Kou, L. Xu, H. Wu, and W. Zhao, "Heat conductive h-BN/CTPB/epoxy with enhanced dielectric properties for potential high-voltage applications," *High Volt.*, vol. 2, no. 3, pp. 172–178, 2017.

[155] S. R. Mellam, "Effect of filler concentration on the breakdown strength of epoxy nanocomposites," pp. 226–229, 2017.

[156] Li, Y., Zhang, H., Porwal, H., Huang, Z., Bilotti, E., & Peijs, T. Mechanical, electrical and thermal properties of in-situ exfoliated graphene/epoxy nanocomposites. Composites Part A: Applied Science and Manufacturing,2017.

[157] Dass, K., Chauhan, S. R., & Gaur, B. Study on the effects of nanoparticulates of SiC, Al2O3, and ZnO on the mechanical and tribological performance of epoxy-based nanocomposites. Particulate Science and Technology, 35(5), 589-606,2017.

[158] Tikhani, F., Jouyandeh, M., Jafari, S. H., Chabokrow, S., Ghahari, M., Gharanjig, K., ... & Saeb, M. R. Cure Index demonstrates curing of epoxy composites containing silica nanoparticles of variable morphology and porosity,2019.

[159] Singh, S. K., Kumar, A., & Jain, A. Improving tensile and flexural properties of SiO2-epoxy polymer nanocomposite. Materials Today: Proceedings, 5(2), 6339-6344,2018.

[160] Jen, Y. M., & Huang, J. C. Synergistic effect on the thermomechanical and electrical properties of epoxy composites with the enhancement of carbon nanotubes and graphene nano platelets. Materials, 12(2), 255,2019.

[161] Z. Xing et al., "Surface Tracking of MgO/Epoxy Nanocomposites: Effect of Surface Hydrophobicity," Appl. Sci. 2019, Vol. 9, Page 413, vol. 9, no. 3, p. 413, Jan. 2019.

[162] N. Peddamallu, G. Nagaraju K. S.-I. S., and undefined 2019, "Understanding the electrical, thermal, and mechanical properties of epoxy magnesium oxide nanocomposites," ieeexplore.ieee.org, Accessed: Jul. 23, 2021.

[163] T. Zhou et al., "The impact of polymer matrix blends on thermal and mechanical properties of boron nitride composites," J. Appl. Polym. Sci., vol. 137, no. 19, p. 48661, May 2020.

[164] Fan, J., Yang, J., Li, H., Tian, J., Wang, M., & Zhao, Y. Cryogenic mechanical properties of graphene oxide/epoxy nanocomposites: Influence of graphene oxide with different oxidation degrees. Polymer Testing, 96, 107074,2021.

[165] Mohit, H., Sanjay, M. R., Siengchin, S., Khan, A., Marwani, H. M., Dzudzevic-Cancar, H., & Asiri, A. M. Effect of TiC nanoparticles reinforcement in coir fiber based bio/synthetic epoxy hybrid composites:

mechanical and thermal characteristics,2021.

[166] Kumar, A., Saini, S., Yadav, K. L., Ghosh, P. K., & Rathi, A.Morphology and tensile performance of MWCNT/TiO2-epoxy nanocomposite. Materials Chemistry and Physics, 277, 125336,2022.

[167] Wang, J., Ren, P., Chen, Z., Sun, Z., Wu, T., & You, C. Highly thermally conductive and electrical insulating epoxy-based composites containing oriented ternary carbon/graphene/MgO hybrid network. Ceramics International,2022.

[168] Namdev, A., Telang, A., & Purohit, R. Synthesis and mechanical characterization of epoxy hybrid composites containing graphene nanoplatelets. Proceedings of the Institution of Mechanical Engineers, Part C: Journal of Mechanical Engineering Science,2022.

[169] Ali, N. H., Shihab, S. K., & Mohamed, M. T. Mechanical and physical characteristics of hybrid particles/fibers-polymer composites: A review. Materials Today: Proceedings,2022.

[170] Zhao, H., Yin, J., Liu, X., Feng, Y., Liu, Y., Li, J., ... & Zhu, C. Effect of 2-D BN on enhanced corona-resistant characteristic of PI/AlN+ BN composite investigated by quasi-in-situ technology. *Polymer Testing*, *84*, 106394,2020.

[171] Guo, H., Li, X., Li, B., Wang, J., & Wang, S. Thermal conductivity of graphene/poly (vinylidene fluoride) nanocomposite membrane. *Materials & Design*, *114*, 355-363,2017.

[172] Berro, Y., & Balat-Pichelin, M. Metal fuels production for future long-distance transportation through the carbothermal reduction of MgO and Al2O3: A review of the solar processes. Energy Conversion and Management, 251, 114951,2022.

[173] Guo, H., Li, X., Li, B., Wang, J., & Wang, S. Thermal conductivity of graphene/poly (vinylidene fluoride) nanocomposite membrane. *Materials & Design*, *114*, 355-363,2017.

[174] Yu, R., Liu, G., Wang, G., Chen, C., Xu, M., Zhou, H., ... & Zhang, L. . Ultrawide-bandgap semiconductor AlN crystals: Growth and applications,

Journal of Materials Chemistry C, 9(6), 1852-1873,2021.

[175] Wang, Z., Wang, G., Liu, X., Wang, S., Wang, T., Zhang, S., ... & Zhang, L. .Two-dimensional wide band-gap nitride semiconductor GaN and AlN materials: properties, fabrication and applications. Journal of Materials Chemistry C,2021.

[176] Arora, B., & Attri, P. Carbon nanotubes (CNTs): a potential nanomaterial for water purification. Journal of Composites Science, 4(3), 135,2020.

[177] Singh, A. K., Panda, B. P., Mohanty, S., Nayak, S. K., & Gupta, M. K.. Synergistic effect of hybrid graphene and boron nitride on the cure kinetics and thermal conductivity of epoxy adhesives. *Polymers for Advanced Technologies*, *28*(12), 1851-1864,2017.

[178] Jarosinski, L., Rybak, A., Gaska, K., Kmita, G., Porebska, R., & Kapusta, C. Enhanced thermal conductivity of graphene nanoplatelets epoxy composites. *Materials Science-Poland*, *35*(2), 382-9,2017.

[179] Uetani, K., Izakura, S., Koga, H., & Nogi, M. Thermal diffusivity modulation driven by the interfacial elastic dynamics between cellulose nanofibers. *Nanoscale Advances*, *2*(3), 1024-1030,2020.

[180] Yang, X., Yu, X., Naito, K., Ding, H., Qu, X., & Zhang, Q. Enhanced thermal conductivity of polyimide composites filled with modified h-BN and nanodiamond hybrid filler. Journal of nanoscience and nanotechnology, 18(5), 3291-3298,2018.

[181] Zhang, Y., Gao, W., Li, Y., Zhao, D., & Yin, H. Hybrid fillers of hexagonal and cubic boron nitride in epoxy composites for thermal management applications. *RSC advances*, *9*(13), 7388-7399,2019.

[182] Gu, J., Liang, C., Zhao, X., Gan, B., Qiu, H., Guo, Y., ... & Wang, D. Y. . Highly thermally conductive flame-retardant epoxy nanocomposites with reduced ignitability and excellent electrical conductivities. *Composites Science and Technology*, *139*, 83-89,2017.

[183] Chen, Y., Hou, X., Kang, R., Liang, Y., Guo, L., Dai, W., ... & Yu, J. Highly flexible biodegradable cellulose nanofiber/graphene heat-spreader films with

improved mechanical properties and enhanced thermal conductivity. *Journal of Materials Chemistry C*, *6*(46), 12739-12745,2018.

[184] K. A. A. Al-Sodani, M. Maslehuddin, O. S. B. Al-Amoudi, T. A. Saleh, and M. Shameem, "Efficiency of generic and proprietary inhibitors in mitigating Corrosion of Carbon Steel in Chloride-Sulfate Environments," *Sci. Rep.*, vol. 8, no. 1, pp. 1–13, 2018.

[185] Yahya, I., Mustaza, S. M., & Abdullah, H. Carbon nanotube-activated thin film transparent conductor applications. Transparent Conducting Films,2018.

[186] Kathiresan, S., & Meenakshisundaram, O. Effect of alkali treated and untreated cellulose fibers and human hair on FTIR and tensile properties for composite material applications. SN Applied Sciences, 4(3), 1-15,2022.

[187] Radeef, H. R., Hassan, N. A., Abidin, A. Z., Mahmud, M. Z. H., Ismail, C. R., Abbas, H. F., ... & Redha, S. Impact of ageing and moisture damage on the fracture properties of plastic waste modified asphalt. In IOP Conference Series: Earth and Envi,2022.

[188] Z. Yang, H. Peng, W. Wang, and T. Liu, "Crystallization behavior of poly(ε-caprolactone)/layered double hydroxide nanocomposites," *J. Appl. Polym. Sci.*, vol. 116, no. 5, pp. 2658–2667, 2010.

[189] Mazen, A., McClanahan, B., & Weaver, J. M. Factors affecting ultimate tensile strength and impact toughness of 3D printed parts using fractional factorial design. The International Journal of Advanced Manufacturing Technology, 1-13,2022.

[190] N. N. Bhiwankar and R. A. Weiss, "Melt intercalation/exfoliation of polystyrene-sodium-montmorillonite nanocomposites using sulfonated polystyrene ionomer compatibilizers," Polymer (Guildf)., vol. 47, no. 19, pp. 6684–6691, 2006.

[191] K. Wattanakul, H. Manuspiya, and N. Yanumet, 'Thermal conductivity and mechanical properties of BN-filled epoxy composite: Effects of filler content, mixing conditions, and BN agglomerate size,' J. Compos. Mater., vol. 45, no. 19, pp. 1967–1980, Sep. 2011.

[192] Pham, T. H. N., Tran, N. P. D., Tran, T. K., Nguyen, T. T., Vo, X. T., Tran, N. T., ... & Hoang, V. H. Effect of PC Percentages on Hardness and Notched Impact Strength of PBT/PC Blends. In Solid State Phenomena (Vol. 329, pp. 17-22,2022.

[193] Albozahid, M., & Mateab, S. Study the effect of adding mwcnts on the hardness, impact strength, and structural properties of composite materials based on epoxy polymer. Egyptian Journal of Chemistry, 65(3), 1-2,2022.

[194] Kumar, B. S., Londe, V. N., Lokesha, M., Anilas, M., & Surendranathan, A. O. Experimental investigation on Mode-I fracture toughness of Carbon-Carbon composites fabricated by preformed yarn method. Materials Today: Proceedings, 46, 2431-2435,2021.

[195] Subramanya, R., Reddy, D. S., & Sathyanarayana, P. S. Tensile, impact and fracture toughness properties of banana fibre-reinforced polymer composites. Advances in Materials and Processing Technologies, 6(4), 661-668,2020.

[196] Y. Yang, C. Lu, X. Su, and X. Wang, "Effects of emulsion sizing with nano-SiO2 on interfacial properties of carbon fibers/epoxy composites," J. Mater. Sci., vol. 42, no. 15, pp. 6347–6352, 2007.

[197] Standard, A. S. T. M. D5045-14,'. Standard Test Methods for Plane-Strain Fracture Toughness and Strain Energy Release Rate of Plastic Materials'. Ann. BookASTM Stand. Part, 99, 1-9,2014.

[198] Erukhimovich and M. O. de la Cruz, 'Phase equilibria and charge fractionation in polydisperse polyelectrolyte solutions,' pp. 1466–1473, 2004.

[199] Fan, X. J., Qu, R. T., & Zhang, Z. F. Remarkably high fracture toughness of HfNbTaTiZr refractory high-entropy alloy. Journal of Materials Science & Technology,2022.

[200] I. Isarn, F. Gamardella, L. Massagués, X. Fernàndez-Francos, À. Serra, and F. Ferrando, "New epoxy composite thermosets with enhanced thermal conductivity and high Tg obtained by cationic homopolymerization," *Polym. Compos.*, vol. 39, pp. E1760–E1769, 2018.

[201] D. S. Rickerby, "A review of the methods for the measurement of coating-

substrate adhesion," *Surf. Coatings Technol.*, vol. 36, no. 1–2, pp. 541–557, 1988.

[202] Yu, Q., Yang, X., Dong, W., Wang, Q., Zhang, F., & Gu, X. Layer-by-layer investigation of the multilayer corrosion products for different Ni content weathering steel via a novel Pull-off testing. Corrosion Science, 195, 109988,2022.

[203] Sugawara, A., Akashi, T., Takahashi, Y., & Tanigaki, T. Magnetic imaging using ultra-high-voltage cold-field-emission microscopes. Journal of Magnetism and Magnetic Materials, 542, 168593,2022.

[204] Ramanaiah, K., Sanaka, S. P., Prasad, A. R., & Reddy, K. H. Measurement of Thermal Conductivity of Natural Fiber Composites. Sustainable Natural Fiber Composites, 122, 199-208,2022.

[205] Goh, C. F., Hadgraft, J., & Lane, M. E. Thermal analysis of mammalian stratum corneum using differential scanning calorimetry for advancing skin research and drug delivery. International Journal of Pharmaceutics, 121447,2022.

[206] Isarn, I., Massagués, L., Ramis, X., Serra, À., & Ferrando, F. New BN-epoxy composites obtained by thermal latent cationic curing with enhanced thermal conductivity. *Composites Part A: Applied Science and Manufacturing*, *103*, 35-47,2017.

[207] P. Wan., "Synthesis of PDA-BN@f-Al2O3 hybrid for nanocomposite epoxy coating with superior corrosion protective properties," *Prog. Org. Coatings*, vol. 146, no. April, p. 105713, 2020.

[208] N. M. D. Asra Ali HUSSEIN1* and and A. E. AL-KAWAZ1, "Corrosion protection of 316L stainless steel by (PVDF/HA) Technique, coating using a spinning coating," *Mater. Sci. Nanotechnol.*, vol. 69, no. 2, 2021.

[209] J. Safaei-ghomi, "MgO Nanoparticles : an Efficient , Green and Reusable Catalyst for the One- pot Syntheses of 2 , 6-Dicyanoanilines and 1 , 3-Diarylpropyl Malononitriles under Different Conditions MgO Nanoparticles : an Efficient , Green and Reusable Catalyst for the One-," no. June, 2015.

[210] M. Ac, “Synthesis , characterization and cytotoxicity of boron nitride nanoparticles : emphasis on toxicogenomics,” vol. 8, 2019.

[211] Nayak, S. K., Mohanty, S., & Nayak, S. K. Mechanical properties and thermal conductivity of epoxy composites enhanced by h-BN/RGO and mh-BN/GO hybrid filler for microelectronics packaging application. SN Applied Sciences, 1(4), 1-15,2019.

[212] S. Singh, V. K. Srivastava, and R. Prakash, ‘Influences of carbon nanofillers on 9 mechanical performance of epoxy resin polymer,’ Appl. Nanosci., vol. 5, no. 3, pp. 10 11 305–313, 2015.

[213] G. Ge, Y. Tang, Y. Li, and L. Huang, “Effect of Environmental Temperature on the Insulating Performance of Epoxy/MgO Nanocomposites,” *Appl. Sci. 2020, Vol. 10, Page 7018*, vol. 10, no. 20, p. 7018, Oct. 2020.

[214] Patki, A. M., & Goyal, R. K. High performance polyetherketone-hexagonal boron nitride nanocomposites for electronic applications. Journal of Materials Science: Materials in Electronics, 30(4), 3899-3908,2019.

[215] K. Mori, N. Hirai, Y. Ohki, Y. Otake, T. Umemoto, and H. Muto, “Effects of interaction between filler and resin on the glass transition and dielectric properties of epoxy resin nanocomposites,” *IET Nanodielectrics*, vol. 2, no. 3, pp. 92–96, 2019.

[216] A. A. Thamer, H. A. Yusr, and N. J. Jubier, “TGA, DSC, DTG properties of epoxy polymer nanocomposites by adding Hexagonal Boron Nitride Nanoparticles,” *J. Eng. Appl. Sci.*, vol. 14, no. 2, pp. 567–574, 2019.

[217] A. A. Thamer, H. A. Yusr, and N. J. Jubier, “TGA, DSC, DTG properties of epoxy polymer nanocomposites by adding Hexagonal Boron Nitride Nanoparticles,” *J. Eng. Appl. Sci.*, vol. 14, no. 2, pp. 567–574, 2019.

[218] S. K. Ng, H. Y., Lu, X., & Lau, “Thermal conductivity of boron nitride-filled thermoplastics: effect of filler characteristics and composite processing conditions.,” Polym. Compos., vol. 26, no. 6, pp. 778-790.,2005.

[219] S. Kemaloglu, G. Ozkoc, and A. Aytac, ‘Properties of thermally conductive micro and nano size boron nitride reinforced silicon rubber composites,’

Thermochim. Acta, vol. 499, no. 1–2, pp. 40–47, 2010.

[220] S. Kemaloglu, G. Ozkoc, and A. Aytac, “Properties of thermally conductive micro and nano size boron nitride reinforced silicon rubber composites,” *Thermochim. Acta*, vol. 499, no. 1–2, pp. 40–47, 2010.

[221] G. Ge, Y. Tang, Y. Li, and L. Huang, “Effect of Environmental Temperature on the Insulating Performance of Epoxy/MgO Nanocomposites,” Appl. Sci. 2020, Vol. 10, Page 7018, vol. 10, no. 20, p. 7018, Oct. 2020.

[222] Ghaleb, A. M., Munef, R. A., & Mohammed, S. F. First principles study the effect of Zn doped MgO on the energy band gap using GGA approximation. Journal of Ovonic Research, 18(1),2022.

[223] Akhtar, M. W., Kim, J. S., Memon, M. A., Khan, M. Y., & Baloch, M. M. . Surface modification of magnesium oxide/epoxy composites with significantly improved mechanical and thermal properties. Journal of Materials Science: Materials in Electronics, 32(11), 15307-15316,2021.

[224] Thamir, A. A. Enhanced Mechanical, Electrical Properties of the Epoxy Polymer by Adding Hexagonal Boron Nitride Nanoparticles. Indian Journal of Natural Sciences Vol. 8 / Issue 49 /August 2018.

[225] M. W. Akhtar, J. S. Kim, M. A. Memon, M. Y. Khan, and M. M. Baloch, “Surface modification of magnesium oxide/epoxy composites with significantly improved mechanical and thermal properties,” J. Mater. Sci. Mater. Electron. 2021 3211, vol. 32, no. 11, pp. 15307–15316, May 2021.

[226] Huang, T., Zeng, X.L., Yao, Y.M., et al.: ‘Boron nitride@graphene oxide hybrids for epoxy composites with enhanced thermal conductivity[J]’, Rsc Adv., 6, (42), pp. 35847–35854,2016.

[227] Fan, J., Wang, Z., Yang, J., Yin, X., & Zhao, Y. Applying alternating ‘rigid-and-soft’ interphase into functionalized graphene oxide/epoxy nanocomposites toward enhanced mechanical properties. Applied Surface Science, 585, 152702,2022.

[228] Gong, Y., Zhou, W., Kou, Y., Xu, L., Wu, H., & Zhao, W. Heat conductive h-BN/CTPB/epoxy with enhanced dielectric properties for potential high-

voltage applications. High Voltage, 2(3), 172-178,2017.

[229] I. Isarn, X. Ramis, F. Ferrando, and A. Serra, “Thermoconductive thermosetting composites based on boron nitride fillers and thiol-epoxy matrices,” Polymers (Basel)., vol. 10, no. 3, 2018.

[230] Naveen, J., Babu, M. S., & Sarathi, R. Impact of MgO nanofiller-addition on electrical and mechanical properties of glass fiber reinforced epoxy nanocomposites. Journal of Polymer Research, 28(10), 1-13,2021.

[231] Aradhana R, Mohanty S, Nayak SK. High performance epoxy nanocomposite adhesive: effect of nanofillers on adhesive strength, curing and degradation kinetics. Int J Adhesion Adhes 2018.

[232] Demirci, İ., & Avcı, A. Effects of seawater corrosion environment on the impact behavior of multi-walled carbon nanotube and SiO2 reinforced basalt/epoxy hybrid nanocomposites. Journal of Composite Materials,2021.

[233] Wei, H., Xia, J., Zhou, W., Zhou, L., Hussain, G., Li, Q., & Ostrikov, K. K. Adhesion and cohesion of epoxy-based industrial composite coatings. Composites Part B: Engineering, 193, 108035,2020.

[234] F. Isarn, I., Massagués, L., Ramis, X., Serra, À., & Ferrando, “New BN-epoxy composites obtained by thermal latent cationic curing with enhanced thermal conductivity. ,” Appl. Sci. Manuf. , no. 103, pp. 35-47,2017.

[235] R. Raja, S. Jannet, and M.A. Thampy, ‘Synthesis and characterization of AA5083 and AA2024 reinforced with SiO2 particles’, Bull. Pol. Acad. Sci. Tech. Sci. 66(2), 127–132 ,2018.

[236] F. Gebhardt, S. Seuss, M.C. Turhan, H. Hornberger, S. Virtanen, and A.R. Boccaccini, ‘Characterization of electrophoretic chitosan coatings on stainless steel’, Mater. Lett. 66, 302–304, 2012.

[237] E. Husain, A. Abdel Nazeer, J. Alsarraf, K. Al-Awadi, M. Murad, and A. Al-Naqi, A. Shekeban,Corrosion behavior of AISI 316 stainless steel coated with modified fluoropolymer in marine condition, J. Coat. Technol. Res. 302–304, 2018.

[238] M. G. González, J. C. Cabanelas, and J. Baselga, “Applications of FTIR on Epoxy Resins – Identification , Monitoring the Curing Process , Phase Separation and Water Uptake,” vol. 2, 1988.

الخلاصـــة

تعتبر المواد المركبة القائمة على الايبوكسي مواد عازلة مفضلة للعديد من التطبيقات الكهربائية ، مثل لوحات الدوائر المطبوعة وأنظمة عزل الجدار الأرضي للمولد ومحولات الراتينج المصبوب ، على الرغم من أن راتنجات الإيبوكسي هي مواد ذات قيمة عالية في تطبيقات الطلاء والالتصاق ، إلا أن التوصيل الحراري لهذا البوليمر تكون في النطاق المنخفض تتراوح من 0.1 إلى 0.3 واط م · كلفن.ممايجعل الايبوكسي غير مناسب لتطبيقات تبديد الحرارة , يمكن أن تؤدي إضافة دقائق التقوية غير العضوية إلى مادة الإيبوكسي إلى تحسين التوصيل الحراري بشكل كبير ويمكن أن تؤثر أيضًا على الخصائص الميكانيكية للمواد المركبة.

يضيف هذا البحث إلى فهمنا لكيفية صنع طلاء من مواد مركبة متناهية الصغر موصل حراريًا وعازلًا للكهرباء مع الحد الأدنى من محتوى التحميل لتحقيق موصلية حرارية عالية وعزل كهربائي فائق ، وقد أوصي بالطلاء الهجين الذي يشتمل على نوعين من الدقائق بأشكال وأحجام مختلفة. نظرًا لقدرة مزيج من الدقائق الموصلة الحرارية على زيادة كثافة التعبئة ، مما يسمح للدقائق الصغيرة باحتلال الفراغ بين الدقائق الكبيرة المجاورة ، يمكن إنشاء شبكات موصلة حراريًا ذات مقاومة حرارية منخفضة باستخدام نسب حشو أقل. في هذه الدراسة ، تم تطوير طلاء جديد واقي من التآكل مع خصائص التبديد للحرارة والعزل الكهربائي الذي يمكن استخدامه لحماية التوربينات في السيارات أو السفن أو الطائرات ، وكذلك في الصناعة الكهربائية والتطبيقات الإلكترونية المتمثلة بوحدة المعالجة المركزية للمركبات ECUs ، ويتم مقارنتها بالخواص الميكانيكية , الحرارية , والكهربائية والاستقطاب الديناميكي الفعال لمواد الطلاء باستخدام الايبوكسي كطور اساس والدقائق النانوية الغير عضوية كطور تقوية . تم توفير خصائص التبديد للحرارة والعزل الكهربائي بواسطة استخدام أوكسيد المغنيسيوم (MgO) ونتريد البورون السداسي (h-BN) ، حيث يوفر MgO عددًا من الخصائص الجذابة ، بما في ذلك العزل الكهربائي ، فضلاً عن كونها منخفضة التكلفة وغير ضارة. وفي الوقت نفسه ، يبدو أن BN على وشك تطوير مواد لاصقة موصلة بدرجة حرارة عالية لتطبيقات الطلاء المبدد للحرارة وعازل للكهرباء أفضل من دقائق الجرافين النانوية.

تم تحضير المواد المركبة النانوية والطلاءات النانوية باستخدام طلاء الغمر بالمحلول واستخدام تركيزات مختلفة من الدقائق النانوية (MgO) ، (BN) والدقائق الهجينة (بنسبة 1: 1) مع نسبة الوزن (3, 1, 0 wt% 7, 5,).تم فحص خصائص المواد المركبة النانوية باستخدام((FTIR) (XRD) ، (FESEM) ،

(AFM) والفحوصات الحرارية والكهربائية بالإضافة الى الفحوصات الميكانيكية (اختبار الشد ، اختبار الصدم ، اختبار متانة الكسر ، صلادة Shor D ، اختبار التصاق الانسحاب) واختبار الاستقطاب الديناميكي الفعال, وفحص سمك الطلاء .

أظهرت النتائج أن نتائج (FTIR) قد أثبتت عدم وجود تفاعل كيميائي ، وهناك تفاعل فيزيائي فقط بين الدقائق النانوية و بوليمر الايبوكسي. أثبتت نتائج DSC أن هناك زيادة في قيمة Tg وتعزز بنحو 15 ٪ عند 7 ٪ من الدقائق النانوية الهجينة مقارنة بالإيبوكسي النقي ومركبات نانوية أخرى غير هجينة ، مما يشير إلى تحسن في الاستقرار الحراري والخصائص الميكانيكية.في صور AFM ، أظهرت النتائج عند زيادة محتوى التقوية تزداد خشونة المواد المركبة النانوية .وجد أنه تم الحصول على تحسن كبير في الخصائص الحرارية دون تأثير سلبي على الخواص الكهربائية عند إضافة دقائق MgO و BN والدقائق النانوية الهجينة إلى بوليمر الايبوكسي حيث عززت إضافة7 ٪ بالوزن من الدقائق النانوية الهجينة, الموصلية الحرارية بحوالي 95٪ وتحسنت المقاومة الكهربائية حوالي 71٪ مقارنة بالدقائق النانوية غير الهجينة والأيبوكسي النقي.

إضافة 7٪ بالوزن من الدقائق النانوية الهجينة حسنت كل من (قوة الشد ،معامل المرونة ، صلادة Shor D، قوة الصدم ، متانة كسر الشد المضغوط K_{IC} ،متانة الحافة المفردة المنحنية K_{IIC} ، قوة سحب الالتصاق حوالي (19٪ ،37٪،10٪ ، 56٪ ، 68٪ ، 41٪ و 69) ٪) على التوالي ، بالمقارنة مع الايبوكسي النقي و المواد المركبة النانوية الأخرى غير الهجينة.أدت إضافة 7٪بالوزن من الدقائق النانوية الهجينة إلى تعزيز كفاءة التثبيط بحوالي 87٪ مقارنة بالإيبوكسي النقي والمركبات الناوية الاخرى الغير هجينة. في صور FESEM ، تحتوي دقائق MgO النانوية على حجم حبيبي خشن لكن دقائق BN النانوية تظهر حجمًا حبيبي أدق ، كما تم إثبات أن الدقائق النانوية الهجينة قادرة على توفير آليات تقوية فعالة في المواد المركبة الايبوكسية كما هو موضح بواسطة الصور المجهرية FESEM.

جمهورية العراق

وزارة التعليم العالي والبحث العلمي

جامعة بابل

كلية هندسة المواد

قسم هندسة البوليمرات والصناعات البتروكيمياوية

تحضير ودراسة تأثير مواد مضافة هجينة على الخصائص الحرارية والكهربائية لطلاء الايبوكسي

اطروحـــــــــة

مقدمة الى كلية هندسة المواد/ جامعة بابل وهي جزء من متطلبات نيل درجة فلسفة الدكتوراه في هندسة المواد/البوليمر

من قبل

انـــوار قــاسم ســـعيد جودي

بإشراف

أ.د. ذو الفقار كريم مزعل

هـ1444 2022م